Cardiff School of Pharmacy and Pharmaceutical Sciences
Cardiff University

Chemical and Physical Strategies Promoting Nanoparticle Permeation through Intestinal Mucus Barrier

A thesis submitted *in accordance with the conditions governing candidates* for the degree of

Philosophiae Doctor in Cardiff University

Muthanna Abdulkarim Albaldawi

Supervisor: Prof. Mark Gumbleton

December 2015

DECLARATION

This work has not been submitted in substance for any other degree or award at this or any other university or place of learning, nor is being submitted concurrently in candidature for any degree or other award.

Signed (candidate) Date: 04/05/2016

STATEMENT 1

This thesis is being submitted in partial fulfillment of the requirements for the degree of PhD.

Signed (candidate) Date: 04/05/2016

STATEMENT 2

This thesis is the result of my own independent work/investigation, except where otherwise stated.

Other sources are acknowledged by explicit references. The views expressed are my own.

Signed (candidate) Date 04/05/2016

STATEMENT 3: PREVIOUSLY APPROVED BAR ON ACCESS

I hereby give consent for my thesis, if accepted, to be available online in the University's Open Access repository and for inter-library loans **after expiry of a bar on access previously approved by the Academic Standards & Quality Committee.**

Signed (candidate) Date: 04/05/2016

Acknowledgements

First of all, I would like to thank my supervisor, Prof. Mark Gumbleton for his guidance, support and continuous encouragement. Without his valuable input, this work would have never been completed. Special thanks go to my colleagues and friends in lab 1.38, Robert Gutteridge, Jack Sim, Chiara Moriconi, Daniel Price and Ghaith Aljayyoussi who were my second family, without their support, I would not be able to finish my work, their friendship is the priceless achievement I have had last few years.

My sincere thanks also go to my colleagues in the Cardiff school of pharmacy and pharmaceutical science: Dr Mathew Smith, Dr Edward Sayers, Dr Fabrizio Pertusati, Dr Michaela Serpi and Valentina Ferrari for sacrificing extra hours to help me to do my work. I am thankful also for all the staff and colleagues in the school who were very helpful, kind and supportive. Also I would like to express my gratitude to Prof Salvador Borros and the staff in his lab, Dr Victor Ramos, Sejin Oh and Dr Miguel Lázaro for guiding me on RAFT polymerization and letting me use the facilities in the lab. Personal thanks go to my friends Suhaib Mohammad and Qutaiba Karwi who were always there for me when I was ready to give up and needed true friends.

My closing thanks go to my dad (Fawzi), my mum (Nawal), my sister (Nagham) and my brother (Zaid), Although 6,000 kilometres away, they were with me all the time giving me all the support. Without them, I would not be what I am today. Finally, there is no words describe my gratitude to my wife, Asraa, and my beloved children, Dania and Harith, who were always waiting for their late father. I can not imagine that anybody else in the world will withstand all the obstacles we face together. I am very thankful for all the sacrifices.

Lastly, I would like to thank Cardiff school of pharmacy and pharmaceutical science for the financial support and for give me the chance to pursue my PhD study, I am very proud for doing my PhD in this great school.

Abstract

Orally administered therapeutic agents need to cross the mucosal epithelial membrane in the intestine to reach the systemic circulation. This intestinal epithelial membrane is covered by a biopolymer barrier, namely, mucus which protects the underlying layer through trapping or degrading of foreign particles and macromolecules. Thus, mucus can restrict the systemic absorption of some therapeutic agents such as peptides by enzymatic degradation. Nanoparticles (NPs) could serve as a carrier for these peptides to protect them from environmental conditions in the mucus and to increase their bioavailability. However, these NPs can be trapped themselves by the mucus, hence, a proper nano-strategy should be selected to deliver these peptides orally. NPs delivery through intestinal mucus barrier has been studied extensively, where various *in vitro* tests and mucus models were investigated to mimic the *in vivo* test. In this thesis, two mucus models were assessed for their suitability as intestinal mucus barrier through which NPs diffusion can be studied. Also, multiple particle tracking (MPT) technique was exploited to study the diffusion and interaction of nanoparticles through pig intestinal mucus barrier. This technique (MPT) was used to understand the factors affecting the diffusion through mucus of NPs representing various nano-strategies such as PEGylated NPs and mucolytic NPs. Based on data obtained for the diffusion of NPs, we adopted a nano-strategy mimicking the capsid shell virus in which the NPs surfaces are densely covered with oppositely charged groups but with overall neutral charge. To do so, polyelectrolyte (PEC) NPs based on the self-assembly of (+) chitosan and (-) polyacrylic acid (PAA) were synthesized and the diffusion of these densely charged NPs was studied. After proving the concept, RAFT technique was used to synthesize zwitterionic densely charged NPs in which butyl methcrylate (BMA) was used as the lipophilic core and sulfobetaine as the shell of NPs.

Native mucus prepared by our group was found to be a proper model to study NPs diffusion through it by the MPT technique. Study of diffusion of NPs representing various nano-strategies through mucus revealed the impact of various properties of these NPs on their diffusion. For example, particle size, zeta potential, type and molecular weight of the polymer, type and concentration of the diffusion enhancer and method of synthesis of NPs were detected to affect the diffusion of these NPs. For PEC NPs, the data obtained showed a relation between the zeta potential of NPs and their diffusivities through the mucus, where the highest diffusivity was obtained for the neutrally charged PEC NPs. Accordingly, sulfobetaine NPs were highly efficient NPs in term of their stability, charge density, particle size and importantly their diffusivities through the mucus barrier which was significantly higher as compared with all other tested NPs and related to the ratio of the sulfobetaine polymer in the NPs. This indicates that densely charged viral like NPs can be promising carriers to improve the mucus permeation of some therapeutic agents.

PUBLICATIONS FROM THIS THESIS

Refereed Journal Articles

J. Rohrer, A. Partenhauser, S. Hauptstein, C.M. Gallati, B. Matuszczak, **Muthanna Abdulkarim**, M Gumbleton, A Bernkop-Schnürch, Mucus permeating thiolated self-emulsifying drug delivery systems, Eur. J. Pharm. Biopharm. 98 (2016) 90–97. doi:10.1016/j.ejpb.2015.11.004.

Muthanna Abdulkarim, N Agulló, B Cattoz, P Griffiths, A Bernkop-Schnürch, S Borros, M Gumbleton. Nanoparticle diffusion within intestinal mucus: Three-dimensional response analysis dissecting the impact of particle surface charge, size and heterogeneity across polyelectrolyte, pegylated and viral particles, Eur. J. Pharm. Biopharm. 97 (2015) 230–238. doi:10.1016/j.ejpb.2015.01.023.

J Grießinger, S Dünnhaupt, B Cattoz, P Griffiths, S Oh, S Gómez, M Wilcox, J Pearson, M Gumbleton, **Muthanna Abdulkarim**, I de Sousa, A Bernkop-Schnürch. Methods to determine the interactions of micro- and nanoparticles with mucus, Eur. J. Pharm. Biopharm. 96 (2015) 464–476. doi:10.1016/j.ejpb.2015.01.005.

Refereed Journal Articles (in preparation)

Muthanna Abdulkarim, Victor Ramos, Salvador Gomes Borros, Mark Gumbleton. Use of RAFT technique to synthesize sulfobetaine muco-inert nanoparticles (on going).

Muthanna Abdulkarim, et al. Comparative study on the diffusion coefficient through intestinal mucus barrier of NPs representing various nano-strategies by using of the MPT technique (on going).

S Oh, **Muthanna Abdulkarim**, M Gumbleton, A Bernkop-Schürch, Salvador Borrós. Enhanced mucus permeability and transfection of poly(β-amino ester)s/pDNA complexes coated with poly(acrylic acid)-bromelain (On going).

Patents

Muco-inert sulfobetaine NPs (on going).

Conference Presentations

Muthanna Abdulkarim, N Agulló, B Cattoz, S Borros, P Griffiths, A Bernkop-Schnürch, M Gumbleton. NPs diffusion through the pig intestinal mucus barrier: Study of the effect of surface charge and particle size. Crossing Biological Barriers - Advances in Nanocarrier Design for Targeted Drug Delivery, Dechema. November 2016 (Poster).

Abbreviations

α	Exponential anomalous
δ	Phase angle
η	Water viscosity
π	Pi
-N=N-	Azo compound
-O-O-	Peroxide
σ	Tracking resolution
aa	Amino acids
AD5	Adenovirus
AFM	Atomic force microscopy
AIBN	2,2′-Azobis(2-methyl propionitrile)
ATRP	Atomic transfer radical polymerization
BMA	Butyl methyl methacrylate
°C	Centigrade
C*	overlap concentration
CDCL3	Deuterated Chloroform
cm	Centimetre
CPR	Control radical polymerization
CTA	Chain transfer agent
D°	Absolute diffusion
DDW	Distilled deionised water
Deff	Effective diffusion coefficient
<Deff>	Ensemble effective diffusion
DF	Diffusivity factor
DMAEMA	N,N-Dimethylaminoethyl Metha- crylate
DMSO	Dimethyl sulfoxide
DMSO-d6	Deuterated DMSO
EE%	Entrapment efficiency
EM	Electron Microscopy
FRAP	Fluorescence Recovery after Photo Bleaching
FTIR	Fourier transform infrared spectroscopy

g	Gravitational force
G’	Storage modulus
G’’	Loss modulus
GIT	Gastrointestinal tract
gm	Gram
GPC	Gel Permeation Chromatography
HCL	Hydrochloric acid
^{1}H-NMR	NMR proton analysis
IEP	Isoelectric point
IR	Infrared
κ	Boltzmann constant
k_a	Addition constant
K_{-a}	Degrade back constant
KCl	Potassium chloride
kDa	Kilo Dalton
k_f	Fragmentation constant
K_{-f}	De-fragmentation constant
KHz	Kilo hertz
KH2PO4	Potassium dihydrogen phosphate
K_i	Initiation constant
K_p	Propagation constant
K_t	Termination constant
LD%	Loading capacity
LR	Lumogen Red 305
m	Meter
M	Molarity
mg	Milligram
MHz	Mega hertz
min	Minutes
ml	Millilitre
µl	Microliter
µm	Micrometre

Mn	Aimed molecular weight of the polymer
Mna	Number average molecular weight
ms	Millisecond
mol monomer/mol CTA	Molar ratio of monomer to the CTA agent
MSD	Mean square displacement
<MSD>	Ensemble mean square displacement
MPT	Multiple particle tracking
mV	Millivolt
MW	Molecular weight
Mwa	Average weight molecular weight
MWCO	Molecular weight cut off
NaCl	Sodium chloride
Na2HPO4	Disodium hydrogen phosphate
NaOH	Sodium hydroxide
nm	Nanometer
NMR	Nuclear magnetic resonance
NP(s)	Nanoparticle(s)
p	P value
PAA	Polyacrylic acid
(PAM)	Poly(allylamine)
PBS	Phosphate buffer saline
PDI	Poly dispersity index
PEC NPs	Polyelectrolyte Nanoparticles
PEG-NP	PEGylated nanoparticles
PGM	Porcine gastric mucin
PGSE-NMR	Pulsed-gradient spin-echo NMR
PLGA	Poly(lactic-co-glycolic acid)
$Pm^{\cdot}$	Propagating radical
$Pn^{\cdot}$	Propagating radical
ppm	Part per million
PTS	Proline, Threonine and Serine
r	Radius of Nanoparticles

$R^{\cdot}$	Radical
RAFT	Reversible addition fragmentation chain transfer
$Rm^{\cdot}$	Propagating radical
RP	Radical polymerization
rpm	Revolution per minute
SANS	Small angle neutron spectroscopy
SD	Square Displacement
s.d.	Standard deviation
SEA domain	Sea-urchin sperm protein, Enterokinase and Agrin
Sec	Second
s.e.m	Standard error of mean
SMEDD	Self microemulsion drug delivery
t	Time interval
T	Absolute temperature
Δt	Time interval
TFE	2,2,2-Trifluoroethanol
THF	Tetrahydrofuran
$^{w}/_{v}$	Weight per volume

Table of Contents

List of Figures

List of Tables

CHAPTER ONE

GENERAL INTRODUCTION: INTESTINAL MUCUS BARRIER

1. INTRODUCTION

1.a The Mucus Barrier in the Gastrointestinal tract

Generally, a drug molecule exerts its systemic therapeutic effect only after reaching into the systemic circulation. If the injection route is not applicable, then drug molecules should be administered either trans-dermally, meaning that the molecules have to cross the epidermis, or they may be administered by other routes where the drug molecules need to cross the mucosal epithelium layer. The mucosal epithelium layer is covered with a biological barrier, namely, mucus which drug molecule need to permeate through before crossing the epithelial membrane. For example, therapeutic agent needs to permeate the mucus barrier covering the epithelial membranes in the gastrointestinal tract (GIT), urogenital tract, pulmonary system, oral cavity or nasal cavity. The thickness of this barrier varies depending on the site in the body. For example, it is 0.578 μm thick in the eye [1], 0.1–50 μm in the trachea [2] and 15-150 μm in the colon [3].

Functionally, the main roles of mucus are lubricating, hydrating and protecting against mechanical stress of the underlying epithelial membrane [4,5]. Moreover, mucus represents the body's first line of defence against harmful particles such as pathogens and microorganisms [6,7]. This defensive mechanism, however, extends to include all types of foreign particles including therapeutic macromolecules and nanoparticles (NPs), meaning that mucus is the key limiting barrier preventing the delivery of various macromolecular therapeutic agents [8].

In the respiratory system and the middle ear, mucus plays the major regulatory role of water balance, ion exchange and clearance of foreign particles, while in saliva, mucus

served as an anti-microbial layer [9]. Mucus in the cervical system has additional functions include being a reservoir and transporting medium for sperm [9].

In the GIT, mucus can be found as either a gel layer or a viscous slippery fluid depending on the location within the GIT [10]. The GIT is the part of the body where most types of microorganisms and foreign particles are in contact with. Hence, mucus in the GIT is thicker and has higher mechanical strength [11,12] compared to other mucus barriers in the body, this helps to prevent the passage of any foreign particles [13]. The thicker GIT mucus is not only important to avoid the permeation of foreign particles but works together with the bicarbonate buffering system of the GIT mucus to protect the underlying epithelial membrane against the high acidity in the lumen [14,15]. Additionally, mucus avoids the permeation of pepsin enzyme that is secreted to digest food, hence, by this mean, mucus protects gastric epithelial membrane from auto-digestion [16].

Thus, mucus in the GIT serves as a semipermeable membrane that allows nutrients and small drug molecules to be absorbed provided these molecules are not affected by the GIT environment, such as pH and enzymes [17]. So, therapeutic agents that are small enough to permeate through mucus, should not be hydrolysed in the GIT environment; otherwise they need to be protected from this environment. This mostly happens by incorporating drugs into a colloidal system, like NPs, which in turn will have to cross the mucus barrier. Due to their degradation in the GIT environment, peptides and genes are the main therapeutic agents that need to be encapsulated into a proper nano-delivery system when they are delivered orally [18]. Although these NPs will protect peptides from the GIT environment, they will, however, themselves be trapped by the intestinal mucus [19]. Difficulties involved with diffusion of macromolecules and NPs through the intestinal mucus barrier has been described in many review articles [20–22].

Since the trapping mechanism of mucus is mainly correlated to the composition of the mucus barrier; it is important to study the composition of mucus in order to arrive at a better understanding of how the mucus trapping mechanism might be circumvented.

GIT Mucus Composition

Generally, mucus contains 90-95% water regardless of its location in the body, with various ratios of glycoprotein, electrolytes, lipids, DNA, sloughed epithelial membrane and bacteria [23,24]. In most parts of the body, mucus contains around 0.5–5% of glycoprotein and lipids, around 1% of mineral salts and 1% of free protein [9]. Although the water content usually doesn't change in response to diseases or position in the body, the other components are highly affected by the location and healthiness of the mucus [25]. Larhed et al. (1998) [26] found that dry pig intestinal mucus (mucus was dried prior to the measurement) encompasses 5% glycoprotein, 37% lipids, 39% proteins and 6% DNA.

The high DNA content was linked to the high rate of slaughtering of epithelial cells into the intestinal mucus. The high DNA content (4%) in the intestinal mucus has also been reported in another study [27]. Accordingly, high lipid content was attributed to the release of the lipid after the digestion of food. This intestinal lipid is removed when mucus is purified by various extraction and separation methods leaving the purified mucin in lack of this ingredient [28]. Lipid content plays a major role in the permeation of lipophilic drugs. Larhed et al. (1997) [29] studied this correlation by comparing the permeation of lipophilic drugs in a native pig intestinal mucus model and in a purified pig intestinal mucin model. In contrast to the native mucus which showed direct correlation, purified mucin showed no relation between drug lipophilicity and permeation through the mucus. Other sites in the body possess different ratios of mucus constituents which are supposed to exhibit different influences on drug permeation. For

example, the dry content of human ocular mucus comprises 29% protein, 53% carbohydrate and 12% lipid; bovine submaxillary glands have 31% protein, 58% carbohydrate and 11% lipid, while ovine submaxillary glands exhibit 33% protein, 53% carbohydrate and 14% lipid [9].

Even with the important role that other ingredients of mucus have, the key element in mucus is the glycoprotein content. In the 1960s, researchers agreed to refer to the glycoprotein units in mucus as mucin and to identify mucin as the building block of the mucus [30]. Mucin fibres are responsible for the formation of the mucus viscoelastic structure through the protein and the glycosidic residues of these units. The protein parts are responsible for the formation of the network and the glycosidic parts are responsible for the swelling of this network [31,32]. Understanding the chemical composition and physical properties of mucin is, therefore, the only way to understand the whole physicochemical properties of mucus barrier.

2. Mucin Structure and Composition

Mucin macromolecule is a large glycoprotein with an average molecular weight of 2000-10000 kDa [33,34]. In electron microscopy (EM), purified mucin units are appeared curvilinear fibres with an average diameter of about 5–7 nm and a length of about 200 to 4000 nm [35,36]. The purification process involves extraction and separation step to remove other components adsorbed into mucin fibres. The diameter of non-purified freshly collected mucin fibre is appeared thicker in EM, with a diameter range of 30-100 nm due to the adsorption of various mucus components such as lysozyme [37]. At high concentrations mucin (20-40 mg/ml), a mucus gel network is formed by interconnection of mucin macromolecules via various types of interactions [38].

Mucin macromolecule is formed from 3-4 mucin monomers, each has a molecular weight of 3-5 x 10^5 Da [16]. Each of these subunits, or monomers, consists of glycosylated and non-glycosylated protein domains in consequent order (Figure 1.1). The glycosylated domains are composed of polypeptide backbones rich with threonine, serine and proline (PTS) amino acids (aa) [39] and are densely coated with glycosylated side chains (Figure 1.1). These glycosylated protein domains are separated by non-glycosylated protein regions (Figure 1.1) which are rich with cysteine aa. These naked protein regions are responsible for linking glycosylated domains by means of intramolecular disulphide bonds [34]. Functionally, the densely glycosylated regions are resistant to proteolytic enzyme, while the naked protein regions are susceptible to proteolysis due to the absence of the protective glyosidic side chain [40,41].

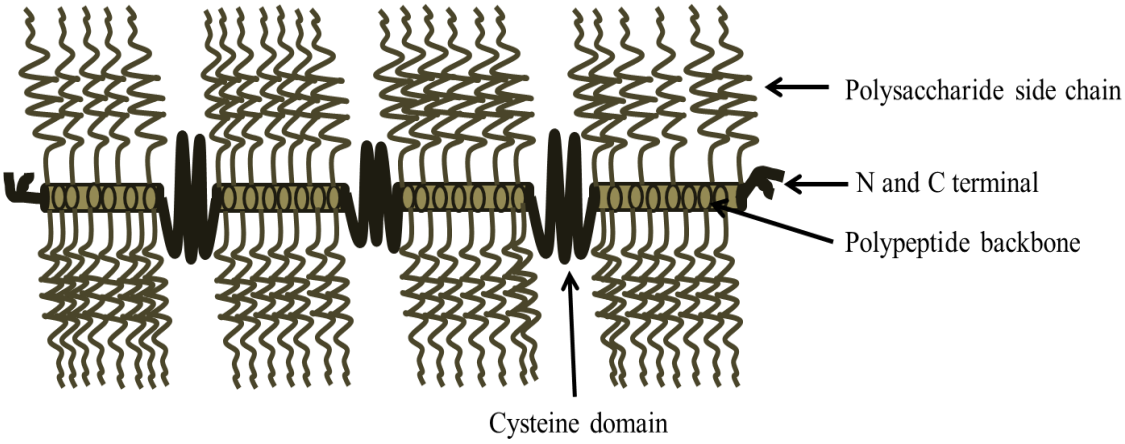

Figure 1.1: Structure of mucin subunit showing the glycosylated domain and the naked protein region (Cysteine domains).

Structurally, each polysaccharide side chain is linked to the polypeptide core through an O-glyosidic linkage between the α -1 position of the N-acetylgalactosamine and the hydroxyl groups of the serine or threonine units [42,43]. The glycoprotein structure of mucin is unique in the body, with its polypeptide backbone that is predominantly formed of the hydroxyl containing aa (Serine and Threonine) and the O-glyosidic linkage between the peptide chain and the glycosylated side chains [44]. Moreover,

mucin is also unique in terms of the degree of glycosylation, where the polysaccharides consist 80% of the total weight of mucin and each glycosylated region is covered with around 160-200 glyosidic side chains [20].

Besides the secreted mucin, there is another mucin type, known as cell associated mucin (Figure 1.2). This type of mucin has a transmembrane region which is responsible for fixing of mucin into the epithelial surface. The extracellular part of this mucin type possesses a unique region, namely, the SEA domain (sea-urchin sperm protein, enterokinase and agrin). This unique domain is responsible for splitting the extracellular mucin from the transmembrane part in response to any mechanical stress or auto-proteolysis process without affecting the membrane [45]. The extracellular part of the cell-associated mucin is similar to other secreted mucin types in having a high PTS content. This extracellular part is projected 100 nm from the epithelial surface with around 5000 aa along the polypeptide backbone.

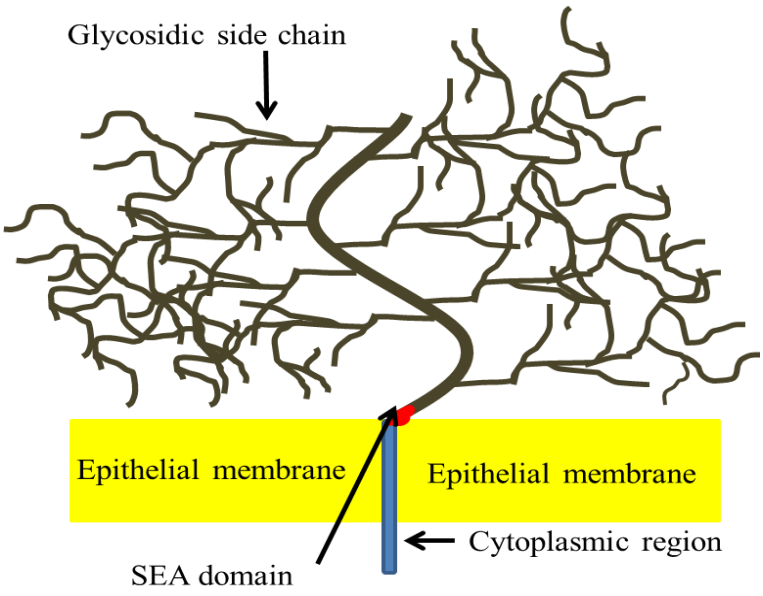

Figure 1.2: Cell associated mucin containing the cytoplasmic region, SEA domain and the glycosylated polypeptide extracellular region.

Also, mucin can be classified depending on the encoding genes, which are known as MUC genes. Each mucin type is named after the same encoding gene, i.e. MUC1 is named after the MUC gene 1. These MUCs share almost the same structural PTS backbone. Up to date, various MUC gene types have been isolated and identified, for example: MUC1, MUC2, MUC3A, MUC3B, MUC4, MUC5AC, MUC5B, MUC6, MUC7, MUC8, MUC11, MUC12, MUC13 and MUC16 [46,47]. In human, MUC1 and MUC4 have been identified as the MUC gene for the cell associated mucin type [48,49]. Accordingly, regarding secreted mucin in the GIT, MUC genes are expressed as follows: (i) MUC5b, MUC7, MUC19 are highly expressed in the oral cavity, (ii) MUC5b is highly expressed in the oesophagus, (iii) MUC5ac and MUC6 are the predominant type in the stomach, (iiii) MUC2 is the main gene in the small intestine and MUC2, MUC5b, MUC6 are the main genes in the large intestine [27].

MUC2 was found to be the predominant mucin type in the small intestine of human [50], rats [51], mice [52] and pigs [53]. Although some studies showed minor levels of MUC11 and MUC6 in the small intestine, MUC2, which is secreted by goblet cells, still has the major influence on the properties of the intestinal mucus including the barrier properties against the absorption of therapeutic agents [54].

The polypeptide backbone of each MUC2 subunit consists of 5100 aa (Figure 1.3), which are divided into glycosylated and non-glycosylated regions and C and N terminals [55]. In MUC2, there are two main glycosylated regions that are separated by a 148 aa Cysteine rich domain [56]. The glycosylated regions can be imagined like a bottle brush shape, with the polysaccharide side chains being concentrated in the middle of the polypeptide core leaving both ends of the core un-glycosylated (Figure 1.3). In regards to the first glycosylated region, the polypeptide backbone mainly consists of up to 100 repetitive blocks. Each block consists of 23 aa in which the predominant aa,

threonine, is linked to N-galactoseamine unit through an O-glycosidic linkage. Each of these polysaccharide side chains contains up to 15 sugar units, making them a densely packed shield around the polypeptide backbone. Accordingly, the protein core of the other glycosylated domain contains 347 aa, which is rich with serine and proline, as well as being densely coated with polysaccharides [57].

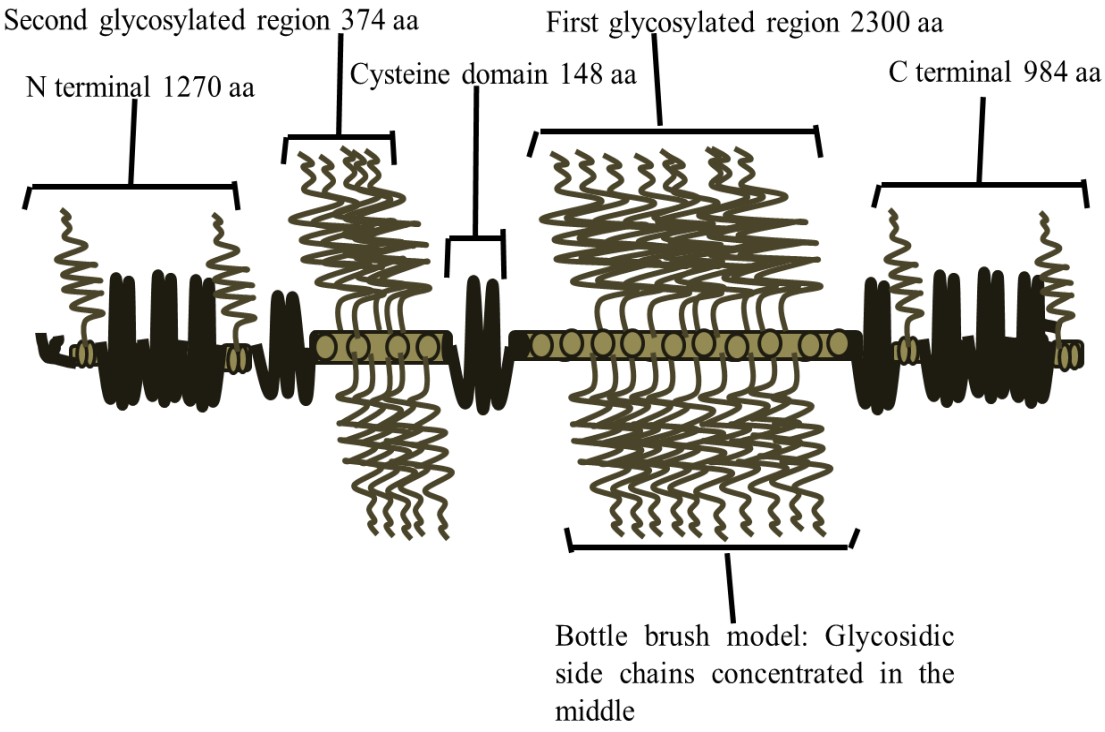

Figure 1.3: MUC2 structure, the main constituent of intestinal mucus. The Figure shows the main two glycosylated regions, the cysteine non-glycosylated region and the C and N terminal.

The carboxyl terminal (Figure 1.3) is composed of 984 aa in which there is a glycosylated peptide subdomain consisting of 139 aa and a cysteine rich subdomain of 845 aa. The N terminal, meanwhile, contains a cysteine subdomain of 700 aa and another glycosylated polypeptide subdomain of 570 aa [58]. The C and N terminals are responsible for the end to end oligomerization of mucin subunits through intermolecular sulphide bonds to form a long linear chain. The protein core of mucin fibres represents around 20% of the total mucin fibres.

Conformation of Mucin in the Aqueous Phase

Generally, there are three types of polymer solutions: dilute, semi-dilute and concentrated [59]. Similarly, mucin in solution can form the same three main systems. Identification of these systems depends on an important factor called the critical overlap concentration (C*), which is the concentration at which polymer molecules overlap to each other [60]. The dilute system is characterised by a polymer concentration less than the overlap concentration ($c << C^*$), where the polymer molecules are separated from each other. At the Simi-dilute system, polymer concentration is equal to the C* and intermolecular interactions are existed among mucin fibres, at the concentrated system, polymer concentration is much higher than the overlap concentration ($c >> C^*$) and entanglement of the polymer network is observed [61].

A dilute mucin solution can be generated, in laboratory, by hydrolysing mucin macromolecules into subunits and dispersing these subunits in water [62]. These linear and non-branched mucin subunits are swollen in solution due to the interaction of glycosidic chains with water [63]. Accordingly, the mucin unit, the whole mucin fibre, has an extended random coil conformation in water [64,65]. However, this conformation varies depending on the pH of the media, that is, at $pH > 4$, negatively charged groups in the sugar units and positively charged amino group in the non-glycosylated cysteine rich domain are interacted resulting in a coiled conformation [66]. Oppositely, at $pH < 4$, sugar carboxylate groups are protonated and the electrostatic interactions are broken inducing an extended conformation for mucin [67]. Accordingly, coiled conformation of mucin is resulted from folding and rotating of mucin fibre in the un-glycosylated region only, i.e. rotating of mucin fibres in the glycosylated domain is not possible due to the rigidity provided by the glycosylated side chains [46].

Globally, the approved model of mucin macromolecule conformation is the Carlstedt model [64], which describes mucin macromolecule as a flexible extended linear filament consisting of 4-5 subunits linked together by disulphide bridges between the cysteine rich domains of the C and N terminals. While the glycosidic domains are described as swollen regions, the un-glycosylated lipophilic cysteine domains were also reported to have unique globular conformations (Figure 1.4), i.e. un-glycosylated domains are arranged just like pearls in the mucin string [68–70]. These lipophilic globular regions play major role in the formation of the mucin network gel.

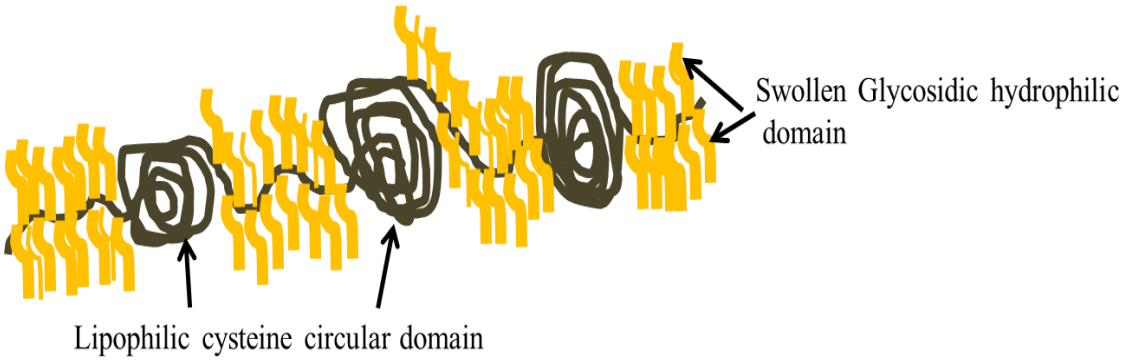

Figure 1.4: Mucin macromolecular conformation.

Formation of Mucin Network (Gel Formation)

As was described earlier, mucin is a very high molecular weight polymer, and this means that the overlapping concentration C* is very low for these units, indeed, Bansil et al. (1995) [71] reported mucin gel can be formed at an average concentration of 2 mg/ml. Accordingly, Bromberg has shown that purified human tracheobronchial mucin can aggregate to form a gel structure at a concentration of 15 mg/ml [72]. This overlapping concentration is much lower than the physiological mucin concentration (50 mg/ml). Hence, mucin fibres tend to be highly aggregated and entangled at their physiological concentration [73]. Moreover, mucin gelation and aggregation was found to be happened at relatively lower concentrations when pH is less than 4 than that at

neutral pH [74]. Imaging of mucin by atomic force microscopy (AFM) at different pH value showed the transformation of mucin from separated filamentous molecules at pH 6 to an aggregate at pH 4 which followed by formation of clusters at pH 2 [75].

The mucin network which is the building structure of the mucus gel was found to be constructed depending on the formation of disulphide bridges among cysteine rich domains [76]. Rheological studies, meanwhile, showed that the electrostatic interactions among glycosidic and polypeptide chains, are the main cross-linking interactions responsible for the formation of gel at low pH [76,77]. In these studies, it was found that the increase of the ionic strength in which mucin fibres are dispersed and introducing of thiol reduction agents restricted the formation of mucin gel at low pH levels. This finding is in agreement with other studies which showed that the disulphide bridges among the cysteine rich domains are the main cross-linking building blocks in the mucin gel at any pH conditions [64,78].

Besides the covalent disulphide bonds, entanglement of glycosidic side chains is an essential factor for the formation of mucus gel [79]. McCullagh et al. (1996) showed a parallel correlation between the length of the glycosidic side chains and the formation of the mucin gel [80]. Another study showed that the interdigitating of the glycosidic side chains is another reason for the formation of a stable three-dimensional network through the formation of a cohesive intermolecular physical interaction [81]. This was confirmed by another study which showed that the destruction of the mucin network by proteolytic enzymes did not change the mechanical properties of mucus gel, indicating the essential role of the interdigitated glycosidic side chains in the formation of mucus gel [82].

Physicochemical Properties of Mucin

Like any other polymer, the physicochemical properties of mucin are driven by its chemical compositions which are the polysaccharide side chains, the cysteine rich domains and the disulphide bridges. Firstly, mucin has a negative charge due to the negative nature of the polysaccharide side chains. These are full with sialic acid and galactose sulphate ester units which are responsible for the negative charge of mucin [83]. Sialic acid has a pKa of 2.6, so it is supposed to be totally charged at the physiological pH 7 [84]. In the GIT, mucin is expected to be fully charged in the intestine and colon but to be neutral or weakly positively charged in the stomach. On the other hand, apart from the glycosidic chain, the presence of aspartic acid and glutamic acid in the polypeptide chain is another reason for the negativity of the mucin macromolecules [85].

Secondly, the high lipophilicity of the cysteine-rich domains in the protein core exerts a lipophilic nature on the mucin macromolecules [86]. Also, methyl groups at equatorial positions of the fucose units in the polysaccharide side chain are also additional lipophilic areas within the mucin macromolecules [87]. This structural feature of mucin represented by lipophilic cores and a highly charged glycosidic cover indicates structural similarity to the highly lipophilic polyelectrolyte particle. Hence, it is also affected in the same way by the environmental conditions, such as the ionic strength and the pH of the media [88].

Thirdly, disulphide bridges are responsible for the mechanical properties of mucus since these bridges are the building block of the mucin network which gives the known viscoelastic property of mucus. However, mucin can form either hard gel mucus or weak viscous mucus depending on the ratios of the aa in the polypeptide cores and the length of the polysaccharide side chains [89]. Hence, other aa within the protein core

can affect the physical properties of mucin network. Figure 1.5 shows the structures of the main chemical moieties within mucus that are responsible for its physicochemical properties.

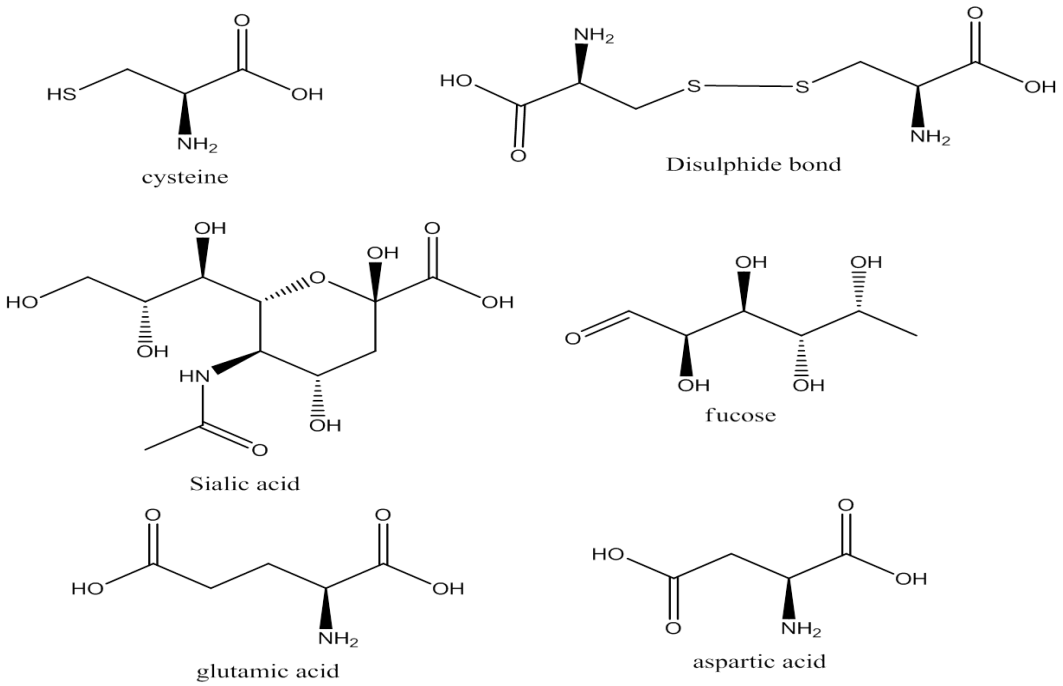

Figure 1.5: Structures of Cysteine, disulphide bond, sialic acid, fucose, glutamic acid and aspartic acid.

3. Aspects of Intestinal Mucus

Besides the physicochemical properties of mucus, there are some other important aspects of mucus in the GIT. Studying these aspects makes it easier to understand the mechanism through which GIT mucus works as a barrier for the absorption of macromolecules. These are as follows:

Multi-Layered Nature of the Intestinal Mucus

Early studies on GIT mucus identified the presence of more than one layer within the GIT mucus. This concept was based on the analysis of the gastric scraped mucus which showed that 22% of mucin was water soluble and up to 80% was insoluble [90]. The same researchers observed breaking down the insoluble mucin units into the same

subunits of soluble mucin when treated with pronase enzyme indicating that both layers are composed of the same subunits but with different molecular weights and solubility [91]. Indeed, the enzyme pronase is able to hydrolyse the mucin network by breaking the peptide chains, thus leading to smaller mucin units. Later, examination of the colonic mucus in the mouse revealed its two layered nature, with MUC2 being the main building block of both layers [55]. These layers were classified as inner and outer layer, where the inner layer is adherent to the epithelial membrane, densely packed and impermeable to bacteria, conversely, the outer layer is loosely packed, colonized with bacteria and continuously moving down through the GIT [92,93].

Some studies showed the existence of the two layered mucus only in colon but not in the small intestine, these studies interpreted the existence of only a loose layer in the small intestine to allow the absorption of nutrients [94,95]. Based on this concept, the antibacterial defence mechanism of the small intestine was attributed to the secretion of antibacterial agents [96]. This concept has been contradicted by other studies which have showed the presence of an adherent mucus gel layer with variable thickness along the small intestine [97,98]. Since this layer is unstirred and adhered to the epithelial membrane, it is either called adherent or unstirred layer [99].

It is believed that this layer adheres to the intestinal epithelial membrane through the entanglement of mucin with the cell associated mucin anchored into the cell membrane [100,101]. The cell associated mucin fibres with some of the entangled adherent layer form a densely packed layer called glyocalyx. This layer is densely packed with a thickness range of 0.1-0.5 μm [102,103]. Glycocalyx is not only a physical barrier or a hook to clasp the adherent layer but is highly responsible for the hydrolysis of orally administered peptide due to the high enzymatic content [104].

Researchers have studied the difference in the compositions and functions of each mucus layer in the small intestine. Since both layers consist mainly of MUC2, gradual hydrolysis and dilution of MUC2 as moving away from the secretion sites has been proposed as an explanation for the difference between the two layers [105]. Accordingly, the presence of high levels of bacteria in the loose layer is argued to be responsible for the degradation of mucin by secreting glycosidase enzymes [106]. Degradation of glycosidic side chain works together with proteolytic enzymes to break down the mucin network producing weaker mucus in the loose layer. The hydrolysed mucus in the loose layer is further diluted and weakened by the chyme containing water in the intestinal lumen [107].

Thus, the function of each layer is related to the mechanical strength of this layer. So, the unstirred inner layer is maintained intact in order to prevent any permeation of pathogens and digestive enzymes [108]. Accordingly, the loose layer, meanwhile, is continuously moving in order to wipe and clear bacteria and foreign particles. This lubricating effect is essential in order to prevent any quick growth of bacteria in the intestinal lumen [109]. Figure 1.6 shows how both mucus layers in the intestine work together as a defensive mechanism to prevent the reaching of bacteria and foreign particles to the intestinal epithelial membrane. In the eye, for example, where there is no adherent mucus layer, fast clearance of mucus is the main defensive mechanism [110]. Similarly, the high rate of clearance of the nasal mucus protects the lower respiratory tract [111]. Moving on, it is important to understand the rheological behaviour mucus so as to realize how the two distinct mucus layers are dynamically retained.

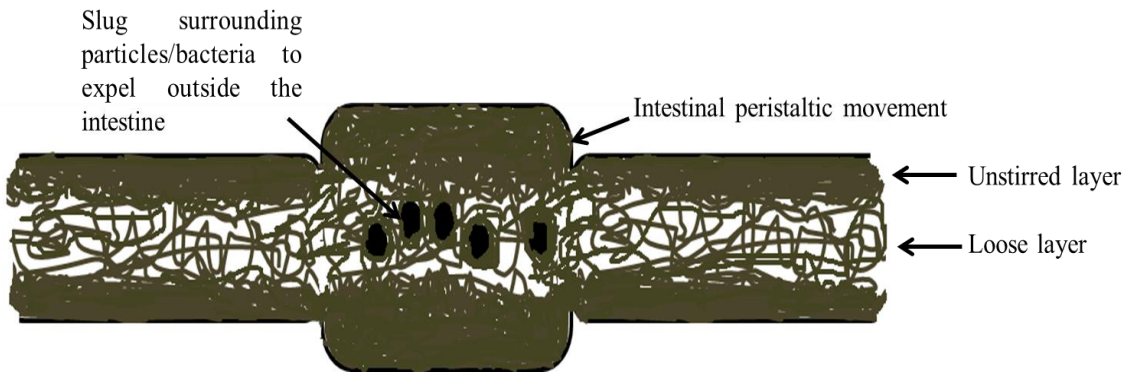

Figure 1.6: Defence mechanism of intestinal mucus to prevent permeation of bacteria and other particles into the intestinal epithelium by moving the particles away with the loose layer.

Rheological and Mechanical Properties of Intestinal Mucus

As was described in the previous section, lubricating effect of the intestinal loose mucus layer is important to keep the body safe. This lubricating effect is directly correlated to the general rheological and mechanical properties of the mucus. Generally, mucus is characterised by a shear thinning behaviour in response to high physiological stress like swallowing and coughing [112]. Upon the passage of food or particles, two processes occur concurrently. First, mucus forms a very sticky slug (Figure 1.5) around the particles due to the formation of many low affinity bonds between various lipophilic and hydrophilic domains of mucin network and particles [113]. These bonds are continuously deformed and reformed between the flexible mucin fibres and the particles so as to keep sticking to the particles. Concurrently, passage of particles exerts a shear force onto the planes of the loose mucus layer that is in contact with the particle resulting in a shear thinning response and reduction of viscosity [10]. This lower viscosity allows the loose layers to slide over each other to form a slippage plane to lubricate the movement of the slugged particles.

The other important rheological property of mucus is its viscoelastic behaviour which gives mucus the flexibility to adhere to moving particles [114,115]. Thus, at small shear stresses, mucin fibres stretch rather than split apart, followed by spring back. This elasticity and flexibility is very important in helping the mucin fibres to rearrange around the particles, which in turn keeps the particles stuck in the mucin slug [101]. Mucus viscoelasticity is controlled by water and ion content [116], as well as the lipid content [117].

Thickness of Intestinal Mucus

The thickness of each of the mucus layers varies throughout the whole GIT system [118]. Mucus thickness at each site in the body is a consequence of the function of mucus at that site as well as the rate of turnover. Mucus is secreted and removed continuously either by digestion, recycling or by shedding with a short lifetime [119]. For example, mucus in the pulmonary system is exchanged in less than 20 minutes (min) to ensure quick movement of any harmful particles [120]. Indeed, continuous mucus secretion is the origin of the defensive mechanism against irritants since it is the source for the shedding of the loose layer and replacement of the unstirred layer. Accordingly, it has been found that goblet cells increase their mucus secretion in response to intestinal inflammation [121].

Generally, 1 litre of mucus is secreted into the GIT every day with variable turnover times of up to few hours (hr) [122]. In the stomach, secretion should be fast enough to avoid the permeation of pepsin enzyme into the epithelial membrane [15]. Lehr et al. (1991) [123] measured the rate of mucus secretion and turnover in the rat intestine, showing the rate of secretion to be 0.16 µl min^{-1} cm^{-1}, the volume of adherent mucus to be 7.7 µl cm^{-1}, and the rate of turnover to be between 47 to 240 min. Accordingly, a comparative study between the rate of turnover of mucus in the jejunum and proximal

colon of rats showed that mucus turnover in the small intestine is 2.2 times higher than in the colon, with turnover rates of 1.1 and 0.5 μg min^{-1} cm^{-1}, respectively [124].

The thickness of mucus within the GIT has been studied extensively. It is well known that gastric adherent mucus layer is the thickest in the GIT system with an average of 180 μm and a range of 50–450 μm in the human stomach [125]. The adherent mucus is thinner in the small intestine with an average thickness of 28 and 93 μm in the duodenum and jejunum of rat, respectively [126]. Accordingly, the thickness of the colonic mucus in the mouse was found to be 150 μm, with the adherent layer being around 50 μm and the loose layer to be 100 μm [93].

Although many studies have been carried out to measure thickness of intestinal mucus, Atuma et al. (2001) [127] study on the GIT of the rat is the most often referred to in most review articles discussing this subject. Figure 1.7 was modified from Atuma et al. (2001) which shows the thickness of each mucus layer in the GIT rat model. This Figure illustrates the thickness of the unstirred layer, which is 154 μm in the stomach, 15-29 μm in the small intestine and 116 μm in the colon. On the other hand, the loose layer is shown to be 120 μm in the stomach, 108-447 μm in the small intestine and 715 μm in the colon [127].

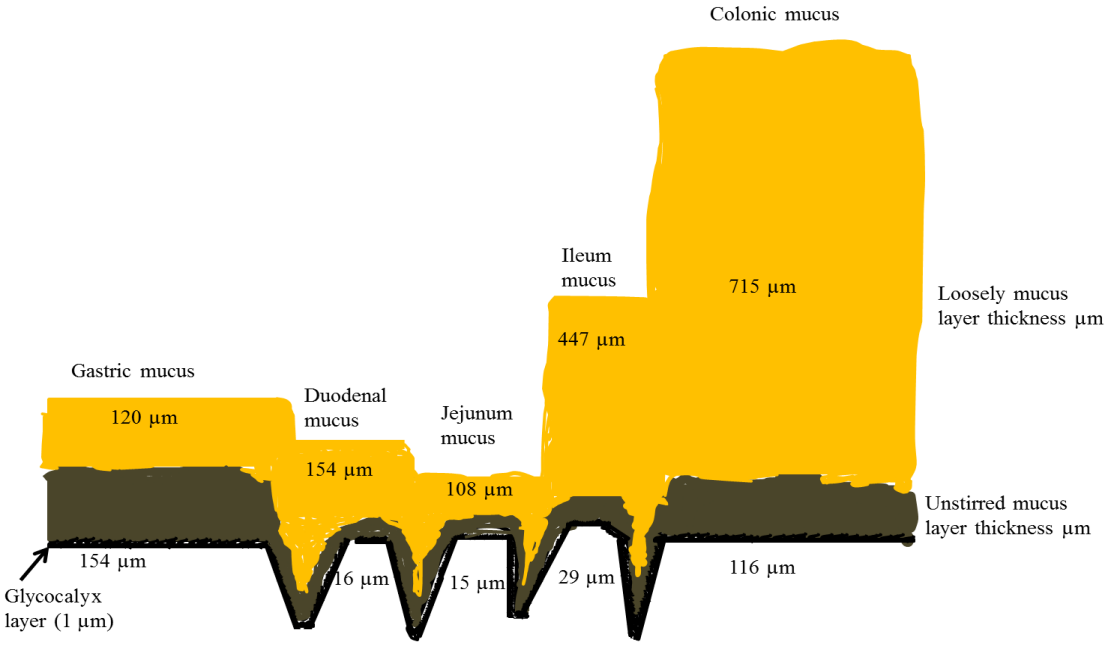

Figure 1.7: Thickness of the mucus along the GIT tract. Yellow area represents the loose mucus layer, brown area is the unstirred layer and black area is the glycocalyx layer. This Figure is modified from Atuma et al. (2001).

Intestinal Mucus pH

As was explained earlier in this chapter, pH plays a role in the aggregation and gelation of mucus [10]. The pH varies from site to site along the GIT specifically, intestinal pH changes from the lumen up to the mucus attaching the epithelial membrane where it reaches the neutrality [128]. Trials to detect the pH of the intestinal mucus were initially conducted by sacrificing the animal (dog) and collecting the mucus from the GIT to measure the pH [129]. Average pH in the sacrificed dog was found to be 3.68 in the stomach, 5.9 in the duodenum, 6 in the Jejunum, 6.3 in the ileum, 6.5 in the cecum and 6.8 in the colon. Talley et al. (1992) used the pH microelectrode technique to measure the pH in the stomach and to identify the gradient change in the pH of mucus from the gastric lumen to the mucosal epithelial membrane [130]. In Talley's experiment, pH microelectrode was inserted endoscopically into human volunteers' stomach, where the pH difference between the gastric lumen and mucosal membrane was found to be 5.3

indicating the bicarbonate neutralization mechanism to prevent self-digestion of the stomach.

In the small intestine, reaching of the chyme to the duodenum is accompanied by a sharp reduction in the neutral luminal pH [131], thus, luminal pH in the duodenum can be reduced down to 2 before being quickly neutralized by mixing with the bicarbonate secretions in the duodenum [98]. The large intestine, however, is too distant to be affected by the high acidity of the stomach contents. For example, in the large intestine of the guinea pig, the pH was found to be neutral [132].

Evans et al. (1988) [133] used pH sensitive radiotelemetry capsules to measure the pH at each site within the GIT of 66 normal humans. The pH was found to be highly acidic in the stomach, with a range of 1 to 2.5, neutral in the small intestine, with an average of 6.6 in the more proximal part of the intestine and 7.5 in the ileum. The pH was reduced in the caecum to 6.4 and raised again in the colon to 7.0 [133]. The same technique was used to measure the pH in the GIT of 14 normal children. In the stomach, the pH was found to be 1.5, rising to 6.4 in the duodenum and 7.4 in the ileum, the pH was reduced in the caecum to 5.9 but increased again to 6.5 in the rectum [134].

4. Barrier Properties of Intestinal Mucus

As was described above, mucus completely covers the intestinal epithelial membrane. Mucus forms an efficient barrier based on its physical and chemical nature. Physically, the mucin network works as a size-based exclusion barrier that prevents the diffusion of particles by steric repulsion. Chemically, the defensive mechanism of mucin is based on its lipo- and hydro-philic regions, which form low affinity bonds with any particulates that come in contact with it, so as to immobilize their movements [135]. Mucus allows the free permeation of nutrients and small drug molecules. Early study, however,

showed that permeation of some drugs could be highly restricted through the intestinal mucus barrier as compared to their permeation in the PBS. This restriction was found to be 45% for phenylalanine, 37% for a-methyl-glucoside, 38% for aminopyrine, 40% for antipyrine, 46% for benzoic acid and 51% for urea [136].

Olmsted et al. (2001) [137] used the fluorescent recovery after photo-bleaching technique (FRAP) to study the correlation of protein particle sizes to their diffusion through the mucus. The Olmsted's study revealed the following: (i) peptides as small as 4.1 nm, exemplified by chicken lysozyme, and 4.5 nm, exemplified by porcine pepsin, showed almost 100% diffusion in the mucus. (ii) Human immunoglobulin G and A, with particle sizes of 11 nm, showed free diffusion in mucus. (iii) Norwalk and human papilloma viruses, which have particle sizes of 38 and 55 nm respectively, had also free diffusion. (iv) However, human lysozyme (3.5 nm) and cholera toxin B subunit (5.4 nm) exhibited diffusions of 74% and 68% respectively indicating a non-specific cut off particle size and the importance of the surface chemistry of particles in their permeation through the mucus [137].

Accordingly, using of chamber model to examine the diffusion of a protein with a molecular weight range of 126-186000 Da through porcine gastric mucus showed no cut off limit, even though a reduction of diffusion was prominent at a molecular weight of 30000 Da and above [138]. A similar study in which the permeation through the intestinal mucus of peptides with molecular weight range of 3.4 to 66 kDa was studied using various peptides such as bovine serum albumin, myoglobin, lysozyme, cytochrome c and aprotinin [139]. This study showed that diffusion was only around 1% for all peptides molecular weight ranges between 12.4 to 66 KDa, while peptides with molecular weight of 3.4 and 6.5 kDa had relatively higher diffusion through the mucus (2% and 3% respectively).

The trapping of particles has been linked to the multi interactive nature of mucus [140]. On this basis, the immobilized diffusion of Herpes simplex virus, having a size of 180 nm, was explained on the basis of the interaction of the mucus lipophilic domains with the lipophilic envelope of the viruses rather than the steric trapping [141]. Comparison of mucus permeation of hydrophilic and lipophilic drug models revealed the high tendency of pig intestinal mucus to trap lipophilic agents [142]. Thus, the lipophilic molecule, testosterone, showed a 6.8 fold reduction in permeability through caco-2 cells covered with mucus compared to cells covered with PBS. The same study showed a varied reduction in permeability of hydrophilic agents, with a maximum reduction of three times for the biggest hydrophilic macromolecules. The retardation of lipophilic agents permeability through the mucus secreting cells (HT29) has also been reported in many other studies [143,144].

Accordingly, Larhed et al. (1997) [29] finding is consistent with previous studies on the permeability of hydrophilic and lipophilic drugs through the pig intestinal mucus. Larhed found that the lipophilicity of drugs is the crucial factor in limiting drug permeability through intestinal mucus, while the retardation of hydrophilic agents' permeability through mucus was more apparent for the very high molecular weight large peptides. Similarly, Boegh et al. (2015) tested the permeability of various lipophilic and hydrophilic drugs through a bio-similar mucus model consisting of reconstituted gastric pig mucin containing cholesterol, linoleic acid and BSA [145]. This study showed that the lipophilicity and the ability to form H bonds were the reducing factors for the permeability of lipophilic drugs, while for the hydrophilic peptides, cationic groups was found to be the reductive factor on their permeability [145]. The limitation of the permeability of lipophilic drugs through mucus was also reported by Meaney et al. [146].

The first evidence that NPs (submicron in size) can diffuse through the mucus barrier was shown by Saltzman et al. (1994) [147], who reported muco-diffusive antibodies and particulates in the size range of 30-60 nm. Subsequently, Frey et al. (1996) [103] showed that cholera toxin (CTB)-fluorescein isothiocyanate NPs with a size of 6.4 nm can penetrate the mucus layer and adhere to the enterocytes of both an *in vitro* (Caco-2) cell line model and within an *in vivo* intestinal model. In the same study, 28 nm gold NPs conjugated with CTB lacked the ability to cross the thick mucus barrier indicating the trapping of these relatively small particles by the mucus barrier. Sanders et al. [148] demonstrated steric hindrance of the intestinal mucus barrier to the permeation of NPs, a hindrance which was dependant on the size of the particles. They found that 520 nm polystyrene NPs were totally trapped by the 220 μm thick cystic fibrosis (CF) sputum layer, however the same type of particles but at a smaller size of 124 nm were found to readily cross the same barrier.

The abovementioned outcomes have been used as the basis for the design of nano-strategies to overcome the mucus barrier (Chapter Three). Thus, the inert surface is identified as the hydrophilic surface that is completely covering the internal lipophilic core of the particle, so as to prevent any lipophilic interaction of the particles and cysteine domains of the mucus. Also, the hydrophilic surface should not form any H-bonds or electrostatic interactions with the glyosidic domain of the mucin network [149]. Particles that are densely covered with a PEGylated shell have been studied extensively. The first such study, conducted by the John Hopkins University, revealed a very high permeability through the mucus barrier [150]. PEGylated NP have shown a high mucus permeability through cervicovaginal mucus [141], CF sputum (pulmonary unhealthy mucus) [151], pulmonary mucus (healthy mucus) [152] and through various other mucus barriers [153]. In addition to PEG, other surface chemistries were

examined for the ability to form an inert surface that does not form lipophilic, electrostatic or H-bond interactions.

5. Techniques to Measure Particle Diffusion through the Mucus Barrier

The measurement of particle diffusion through a dynamically active biological fluid such as mucus is challenging. Studies should be planned carefully in order to avoid misleading permeation data. In this thesis, a multiple particle technique (MPT) will be used to measure the diffusion of NPs through the intestinal mucus barrier. Other widely used techniques that are very often reported to measure particle diffusion will be briefly described.

Transwell Chamber Technique

This outdated technique is still the most widely used method to measure particle permeation across a static mucus layer. This method involves a donor and receptor compartments arranged in parallel or vertically to each other and separated by a layer of mucus sandwiched between two membranes. Drugs or particles are applied in the donor compartment and the amount of drug that crosses the mucus layer is measured in the receptor compartment which is filled with a suitable buffer [138,154]. As well as being an easy method, mucus components can be easily altered during the experiment to mimic various physiological and pathological conditions [9]. For example, Boegh et al. (2015) modified a technique in which the caco-2 cell layer is grown on the membrane separating two transwell vertical compartments, then, mucus or bio-similar mucus gel consisting of pig gastric mucin is added onto the cell layer and drug permeation through this mucosal membrane was measured [140,145].

This method, however, measures only the average permeation of the bulk sample without measuring the behavioural movement and interaction of particles in the mucus

[9]. It is also a time consuming method since samples need a long time to cross the mucus layer which could be enough time to change the mucus integrity by enzymatic degradation or by dilution resulting in clogging of filters or leaking of mucus contents into the receptor compartment [8].

Fluorescence Recovery after Photo-Bleaching (FRAP)

This method is widely used to measure particle diffusion through highly concentrated solutions and bio-gel samples like mucus [155]. In this method, fluorescently labelled particles are added into the mucus sample and placed under fluorescence microscopy. A confined area of the mucus sample is bleached by exposing to a high intensity laser beam which bleaches the fluorescently labelled particles. Then, the unbleached fluorescently labelled particles start to move to the previously bleached area, resulting in the recovery of the fluorescent intensity of that area. The diffusion of particles through mucus is measured from the time at which fluorescent recovery happens [156]. Olmsted et al. (2001) used the FRAP technique to measure the diffusion of the fluorescently labelled viruses and polypeptides through mucus [137]. Similarly, Saltzman et al. (1994) [147] used this technique to measure the diffusion of antibodies through the cervical mucus.

The FRAP technique was also used to study the effect of mucin on particles' aggregation. According to Afdhal's concept [157], the increase in the sizes of cholesterol vesicles was attributed to the interaction with mucin, resulting in particle aggregation. Other techniques like Pulsed-gradient spin-echo NMR (PGSE-NMR) and small angle neutron spectroscopy (SANS) have also been reported to measure particles diffusion through mucus barrier [158,159].

MPT Technique to Measure Particles' Permeation through the Intestinal Mucus

MPT involves the video microscopy and post-acquisition analysis of time-resolved particle trajectories within the particular matrix under study, e.g. cell cytoplasm, mucus, etc. As a technique, it allows for the dynamic measurement of the movement of individual particles within a heterogeneous matrix [160], and as such, contrasts to static techniques which quantify only the bulk movement of particles [161]. MPT is not only capable of the accurate assessment of the diffusion for hundreds of particles both individually and simultaneously [162] but also provides 'behavioural' or qualitative information for hundreds of particles both individually and simultaneously about the environment in which the particles are moving. In particular, it can reveal information about particle-matrix interactions e.g. interactions of particles with mucin fibers or the steric trapping of particles within the mucus mesh network [163]. Such qualitative information is obtained through the more in-depth analysis of the time-resolved particle trajectories to determine the different modes of particle diffusion [164] (see also below).

The Hanes group have been prominent early pioneers in using MPT to assess particle diffusion through heterogeneous matrices [165]. The group subsequently applied the technique to understand and quantify particles, including NPs, to transport them through a range of heterogeneous biological samples [160,161]. For example, the group used MPT to study the transport of amine and carboxylated modified polystyrene NPs through the sputum of cystic fibrosis patients and related the respected transport to the micro-viscosity and macro-viscosity characteristics of the sputum [166]. The group has also used MPT to quantify, for example, the intracellular transport of non-viral polyethylene-imine/DNA nano-sized polyplexes [167].

MPT involves the simultaneous capture of the movement of hundreds of individual particles within a particular matrix, the basic principles of which include:

- Labeling of the particles with a fluorescent dye whose physicochemical properties are appropriate for the particle under study, and which will provide a high signal to noise ratio in the biological matrix under investigation. Issues such as high background auto-fluorescence of the matrix itself can compromise image quality and particle tracking [168]. Although not essential, a confocal microscopy platform may allow for an improved signal to capture noise data as more defined excitation and emission sources can be selected (see below).
- Inoculation of particles within the matrix. Clearly the pre-experimental preparation of the matrix will impact on the efficiency and effective distribution of particle inoculation. Similarly, the concentration of the particle inoculum itself can cause particle aggregation within the matrix [150]. In mucus samples (0.5 g) it was found an inoculum of a 25 µl 0.002% NP suspension to consistently lack aggregation problems. Particle distribution within the matrix also requires a period of equilibration following inoculation and prior to the video capture of the experiment. Typically, mucus samples are equilibrated with particles at 37°C for 2 hr prior to experimentation.
- Video-microscopy capture of particles' movement within the matrix. This will involve the maintenance of the matrix under the appropriate physiological conditions, e.g. 37^{o}C, and the use of a high speed camera to capture the particle movements. Typically, camera speeds of at least 30 frames per second are used with videos of generally 10-20 seconds in length; the short collection periods are sufficient to collect robust data and help to minimise sample degradation issues, e.g. as discussed for mucus [9].
- The microscope itself may be either a standard wide-field Epifluorescence or a confocal type. Nevertheless, for mucus samples, particle movement is most

commonly captured in 2-dimensions (X-Y), principally due to the isotropic nature of the matrix, i.e. particle movement in X=Y=Z. Furthermore, 2-dimensional capture avoids inaccuracies in subsequent data and trajectory analysis that may be introduced by the process of Z-sectioning through the sample.

The basic principles involved the post-acquisition analysis of particle movement and particle trajectories include:

- Use of appropriate software, e.g. Fiji Image J, which can track the video movements of the particles at resolutions as high as 4 nm [169]. The software converts the movement of each particle as captured by high-speed video microscopy into individual particle trajectories. Appropriate rules need to be applied to the analyses e.g. videos capturing particle movement in 2-dimensions should show that any single particle eligible for analysis must remain within the same X-Y plane throughout all the frames of the entire video capture period.
- The movement of particles is translated into individual particle trajectories which are initially represented as numeric pixel data. This data is then converted from pixels into metric distance based on the microscope and video capture settings. From this, the inter-frame distances moved by each particle in the X-Y plane are expressed as a squared displacement (SD). The mean square displacement (MSD) of one particle represents the geometric mean of the sum of all of that particle's square displacements throughout its transport trajectory [170]. Typically, in a single experiment, MSD data is calculated for at least 120 particles of each NP species under study, and the average of these MSD values (ca. 120 values) represents an "ensemble mean square displacement" defined by <MSD>. The ensemble Effective Diffusion Coefficient <Deff> of a particular NP species can then be determined by

<Deff> = <MSD>/(4*frame rate), where 4 is a constant relating to a 2-dimensional mode of video capture and the frame rate relates to the speed of video capture [151].

The MPT technique tracks the change in movement of each single particle as a function of time. Unlike particle diffusion in water, which is non-restrictive and unchangeable with time, particles will undergo varying degrees of hindrance during their diffusion through a polymeric gel matrix such as mucus. Here the mucin fibres are undergoing continuous association and disassociation and the network as a whole undergoes elastic behaviour resulting in the formation and collapse of aqueous cages surrounded by mucin fibres [101]. As such, there will be significant potential for particle-gel interactions within mucus, the probability of which increases as a function of time [171]. Accordingly, how the diffusion of individual particle changes with time not only provides information on the kinetics of movement but also the nature of movement, e.g. changes in time from unrestricted to restricted movement, e.g. the "pearl on string trajectory", may be indicative of the successive binding-unbinding of particles to the mucin network [172]. Such interactions captured by MPT have helped to reveal information on the structure of the mucus mesh network [141] as well as on the mucus micro-rheology [173].

The analysis underpinning studies on the nature or mode of particle diffusion can be undertaken by calculating the <MSD> for each particle over successive time scales, with a change <MSD> over this time period revealing the mode of particle motion which is represented in the literature by an exponential anomalous (α) [174]. Particle transport in water is described as 'freely diffusive' and α is equal to 1, while in an accelerated mixing environment α can be greater than 1 with the movement described then as 'active diffusion'. Particle diffusion in mucus is often restricted and the α value is less than 1 with diffusion then generally described as 'sub-diffusive' [175] and where

α values are between 0.2 and 0.9, it reflects varying degrees of hindrance to particle movement [150]; particles with an α value of less than 0.2 are then considered to be completely immobilized. A nuance building on such an analysis of individual particle behaviour is profiling the distribution of diffusive properties for the entire population of particles studied. Such information can provide a unique assessment of the heterogeneity of particle movement and the presence of outlier sub-populations indicative of distinctive pathways of diffusion through the matrix [176].

In summary, MPT allows the dynamic measurement of the movement of individual particles and sub-populations within heterogeneous biological and non-biological matrices. The information it provides complements that obtained by static approaches to assess particle diffusion. The main technical challenge for any investigator wishing to use the approach will be their ability to undertake high-speed fluorescent video microscopy.

Dynamic Light Scattering for Measurement of Particle Sizes

Throughout this thesis, Malvern Nano ZS was used to measure particle sizes of NPs which is based on the principles of dynamic light scattering (DLS). In this technique, a laser light beam is passed through a suspension of NPs and the intensities of the scattered light by particles are detected by an image detector which processes the data to determine and record the particle size. That is, the intensity of the scattered light corresponds to the velocity of particle movement in the suspension, i.e, the diffusion coefficient of these particles in the suspension. Particle size is measured by using the Stock-Einstein equation (Chapter 2). The limit of detection of this technique is ranged between 10 nm to 1 μm [177].

The instrument determines the change in the intensity of scattered light over time rather than the intensity itself. This is driven by the fact that the intensity of the scattered light is fluctuates over time depending on how fast the particle is diffusing. For the Malvern instrument, a digital auto correlator device is used to correlate the intensity of the scattered light of same particles at sequential time scales. This correlation is presented as an autocorrelation curve (correlogram) for which the correlation within time decays faster as the particle diffusion speed increases. Thus, the time at which the correlation is decayed is proportional to the size of the particle measured.

6. Aim and Overview of the Studies in this Thesis

This study was performed in collaboration with the Alexander European Consortium aiming to produce muco-diffusive nano-particulate system that can improve the diffusion through the intestinal mucus barrier of some therapeutic agents like peptides. Alexander is a large collaborative group within the 7th European Framework programme. This group is responsible for research upon mucus permeating nanoparticulates. It includes 14 industrial and academic partners within Europe that have expertise in chemistry, biochemistry, pharmacy, chemical engineering, pharmaceutical technology, molecular physiology, biopharmaceutics, toxicology, drug development and project management.

This thesis can be divided into two main parts. In the first part (chapter 2 and 3), we run a validation and comparison studies on the interaction to and diffusion through the intestinal mucus barrier of various nano-particulate systems that synthesized by the partners in the Alexander consortium. Thus this part involves the studying of:

(i) Physicochemical properties of the intestinal mucus and how these properties are changed in response to the processing procedures and how these changes affect the barrier properties of intestinal mucus.

(ii) NPs diffusion by the MPT technique including the validation and assessment of this technique to be used for the dynamic analysis of the transport through the intestinal mucus of NPs synthesized by the Consortium.

(iii) The factors affecting the diffusion and interaction of NPs through the intestinal mucus.

Based on the findings in the first part, the second part of this thesis (chapter 4 and 5) involves the synthesis of novel NPs having high diffusivity through the intestinal

mucus barrier so as to be the nano-carrier for the oral delivery of certain therapeutic agents.

The overall objectives of this work can be summarized in four main objectives:

- Identification of a suitable pig intestinal mucus model to be used as a barrier to study particles interaction and diffusion through it.
- Use MPT to study particle diffusion/interaction through the pig intestinal mucus barrier.
- To study the diffusion of NPs representing various nano-strategies through the pig intestinal mucus model to identify the factors and properties enabling high diffusivity of NPs through the intestinal mucus barrier.
- Based on data acquired from objective three, is to synthesize a novel NP with certain physicochemical properties enabling the high diffusivity through the pig intestinal mucus barrier.

7. Reference

[1] S.-W. Moon, J.-H. Hwang, S.-H. Chung, K.-H. Nam, The impact of artificial tears containing hydroxypropyl guar on mucous layer., Cornea. 29 (2010) 1430–1435. doi:10.1097/ICO.0b013e3181ca636b.

[2] D.E. Sims, M.M. Horne, Heterogeneity of the composition and thickness of tracheal mucus in rats., Am. J. Physiol. 273 (1997) L1036–L1041.

[3] G. Ponchel, J.M. Irache, Specific and non-specific bioadhesive particulate systems for oral delivery to the gastrointestinal tract, Adv. Drug Deliv. Rev. 34 (1998) 191–219. doi:10.1016/S0169-409X(98)00040-4.

[4] K. Miyake, T. Tanaka, P.L. McNeil, Disruption-induced mucus secretion: Repair and protection, PLoS Biol. 4 (2006) 1525–1531. doi:10.1371/journal. pbio. 0040276.

[5] B. Button, R.C. Boucher, Role of mechanical stress in regulating airway surface hydration and mucus clearance rates, Respir. Physiol. Neurobiol. 163 (2008) 189–201. doi:10.1016/j.resp.2008.04.020.

[6] M.R. Knowles, R.C. Boucher, Mucus clearance as a primary innate defense mechanism for mammalian airways, J. Clin. Invest. 109 (2002) 571–577. doi:10.1172/JCI200215217.

[7] S.K. Linden, P. Sutton, N.G. Karlsson, V. Korolik, M. a McGuckin, Mucins in the mucosal barrier to infection., Mucosal Immunol. 1 (2008) 183–197. doi:10.1038/mi.2008.5.

[8] N.N. Sanders, S.C. De Smedt, J. Demeester, The physical properties of biogels and their permeability for macromolecular drugs and colloidal drug carriers, J. Pharm. Sci. 89 (2000) 835–849. doi:10.1002/1520-6017(200007)89:7<835::AID-JPS1>3.0.CO;2-6.

[9] K. Khanvilkar, M.D. Donovan, D.R. Flanagan, Drug transfer through mucus., Adv. Drug Deliv. Rev. 48 (2001) 173–93.

[10] J.P. Celli, B.S. Turner, N.H. Afdhal, R.H. Ewoldt, G.H. McKinley, R. Bansil, et al., Rheology of gastric mucin exhibits a pH-dependent sol-gel transition, Biomacromolecules. 8 (2007) 1580–1586. doi:10.1021/bm0609691.

[11] B. Sandzén, H. Blom, S. Dahlgren, Gastric mucus gel layer thickness measured by direct light microscopy. An experimental study in the rat., Scand. J. Gastroenterol. 23 (1988) 1160–1164. doi:10.3109/00365528809090185.

[12] J.D. Kaunitz, Barrier function of gastric mucus, Keio J. Med. 48 (1999) 63–68. doi:10.2302/kjm.48.63.

[13] S.Z. Hasnain, D.J. Thornton, R.K. Grencis, Changes in the mucosal barrier during acute and chronic Trichuris muris infection, Parasite Immunol. 33 (2011) 45–55. doi:10.1111/j.1365-3024.2010.01258.x.

[14] E. Engel, P.H. Guth, Y. Nishizaki, J.D. Kaunitz, Barrier function of the gastric mucus gel, Am. J. Physiol. Gastrointest. Liver Physiol. 269 (1995) G994–G999.

[15] a Allen, a Garner, Mucus and bicarbonate secretion in the stomach and their possible role in mucosal protection., Gut. 21 (1980) 249–262.doi:10.1136 /gut.21.3.249.

[16] T. Ichikawa, K. Ishihara, Protective Effects of Gastric Mucus, in: Paola Tonino (Ed.), Gastritis Gastric Cancer - New Insights Gastroprotection, Diagnosis Treat., intechopen.com, 2011: pp. 1–24. doi:10.5772/23951.

[17] S.C. Bischoff, G. Barbara, W. Buurman, T. Ockhuizen, J.-D. Schulzke, M. Serino, et al., Intestinal permeability ¿ a new target for disease prevention and therapy., BMC Gastroenterol. 14 (2014) 189–214. doi:10.1186/s12876-014-0189-7.

[18] A. des Rieux, V. Fievez, M. Garinot, Y.J. Schneider, V. Préat, Nanoparticles as potential oral delivery systems of proteins and vaccines: A mechanistic approach, J. Control. Release. 116 (2006) 1–27. doi:10.1016/j.jconrel.2006.08.013.

[19] T. Jung, W. Kamm, a. Breitenbach, E. Kaiserling, J.X. Xiao, T. Kissel, Biodegradable nanoparticles for oral delivery of peptides: Is there a role for polymers to affect mucosal uptake?, Eur. J. Pharm. Biopharm. 50 (2000) 147–160. doi:10.1016/S0939-6411(00)00084-9.

[20] a. MacAdam, The effect of gastro-intestinal mucus on drug absorption, Adv. Drug Deliv. Rev. 11 (1993) 201–220. doi:10.1016/0169-409X(93)90010-2.

[21] P.G. Bhat, D.R. Flanagan, M.D. Donovan, Drug binding to gastric mucus glycoproteins, Int. J. Pharm. 134 (1996) 15–25. doi:10.1016/0378-5173(95) 04333-0.

[22] D. a. Norris, N. Puri, P.J. Sinko, The effect of physical barriers and properties on the oral absorption of particulates, Adv. Drug Deliv. Rev. 34 (1998) 135–154. doi:10.1016/S0169-409X(98)00037-4.

[23] J.M. Creeth, Constituents of mucus and their separation., Br. Med. Bull. 34 (1978) 17–24.

[24] W.N. Wong WM, Poulsom R, Trefoil peptides, Gut. 44 (1999) 890–895. doi:10. 1136/gut.44.6.890.

[25] T.D. Brogan, H.C. Ryley, L. Allen, H. Hutt, Relation between sputum sol phase composition and diagnosis in chronic chest diseases, Thorax. 26 (1971) 418–423. doi:10.1136/thx.26.4.418.

[26] A.W. Larhed, P. Artursson, E. Björk, The influence of intestinal mucus components on the diffusion of drugs, Pharm. Res. 15 (1998) 66–71. doi:10. 1023/A:1011948703571.

[27] a. R. MacKie, a. N. Round, N.M. Rigby, a. MacIerzanka, The Role of the Mucus Barrier in Digestion, Food Dig. 3 (2012) 8–15. doi:10.1007/s13228-012-0021-1.

[28] H. Witas, J. Sarosiek, M. Aono, V.L.N. Murty, A. Slomiany, B.L. Slomiany, Lipids associated with rat small-intestinal mucus glycoprotein, Carbohydr. Res. 120 (1983) 67–76. doi:10.1016/0008-6215(83)88007-0.

[29] A.W. Larhed, P. Artursson, J. Gråsjö, E. Björk, Diffusion of drugs in native and purified gastrointestinal mucus, J. Pharm. Sci. 86 (1997) 660–665. doi:10.1021 /js960503w.

[30] K. Hotta, "Gastric Mucus", a Mysterious and Interesting Substance., Trends Glycosci. Glycotechnol. 12 (2000) 59–68. doi:10.4052/tigg.12.59.

[31] N.F. Tabachnik, P. Blackburn, a. Cerami, Biochemical and rheological characterization of sputum mucins from a patient with cystic fibrosis, J. Biol. Chem. 256 (1981) 7161–7165.

[32] S. Rossi, M.C. Bonferoni, G. Lippoli, M. Bertoni, F. Ferrari, C. Caramella, et al., Influence of mucin type on polymer-mucin rheological interactions., Biomaterials. 16 (1995) 1073–1079. doi:10.1016/0142-9612(95)98903-R.

[33] R.D. Specian, M.G. Oliver, Functional biology of intestinal goblet cells., Am. J. Physiol. 260 (1991) C183–C193.

[34] A. Allen, J.P. Pearson, Mucus glycoproteins of the normal gastrointestinal tract, Eur. J. Gastroenterol. Hepatol. 5 (1993) 193–199. doi:10.1097/00042737-199 304000-00002.

[35] J.K. Sheehan, K. Oates, I. Carlstedt, Electron microscopy of cervical, gastric and bronchial mucus glycoproteins., Biochem. J. 239 (1986) 147–153.

[36] H.S. Slayter, J.K. Wold, T. Midtvedt, Intestinal mucin of germ-free rats. Biochemical and electron-microscopic characterization, Carbohydr. Res. 222 (1991) 1–9. doi:10.1016/0008-6215(91)89001-V.

[37] A.I. Yudin, F.W. Hanson, D.F. Katz, Human cervical mucus and its interaction with sperm: a fine-structural view., Biol. Reprod. 40 (1989) 661–671. doi:10. 1095/biolreprod40.3.661.

[38] L. Ashton, P.D. a Pudney, E.W. Blanch, G.E. Yakubov, Understanding glycoprotein behaviours using Raman and Raman optical activity spectroscopies: Characterising the entanglement induced conformational changes in oligosaccharide chains of mucin, Adv. Colloid Interface Sci. 199-200 (2013) 66–77. doi:10.1016/j.cis.2013.06.005.

[39] J. Dekker, W.M. Van Beurden-Lamers, a Oprins, G.J. Strous, Isolation and structural analysis of rat gastric mucus glycoprotein suggests a homogeneous protein backbone., Biochem. J. 260 (1989) 717–723.

[40] I. Brockhausen, H. Schachter, P. Stanley, O-GalNAc Glycans, in: Essentials Glycobiol., 2009: pp. 1–16. doi:NBK1896 [bookaccession].

[41] D. Moncada, K. Keller, K. Chadee, Entamoeba histolytica -Secreted Products Degrade Colonic Mucin Oligosaccharides, Infect. Immun. 73 (2005) 3790–3793. doi:10.1128/IAI.73.6.3790.

[42] T. Shirazi, R.J. Longman, A.P. Corfield, C.S. Probert, Mucins and inflammatory bowel disease., Postgrad. Med. J. 76 (2000) 473–478. doi:10.1136/pmj. 76. 898. 473.

[43] R. Xu, S.R. Hanson, Z. Zhang, Y.-Y. Yang, P.G. Schultz, C.-H. Wong, Site-specific incorporation of the mucin-type N-acetylgalactosamine-alpha-O-threonine into protein in Escherichia coli., J. Am. Chem. Soc. 126 (2004) 15654–15655. doi:10.1021/ja044711z.

[44] L. Reid, J.R. Clamp, The biochemical and histochemical nomenclature of mucus., Br. Med. Bull. 34 (1978) 5–8.

[45] B. Macao, D.G. a Johansson, G.C. Hansson, T. Härd, Autoproteolysis coupled to protein folding in the SEA domain of the membrane-bound MUC1 mucin., Nat. Struct. Mol. Biol. 13 (2006) 71–76. doi:10.1038/nsmb1035.

[46] J. Ferez-Vilar, R.L. Hill, The structure and assembly of secreted mucins, J. Biol. Chem. 274 (1999) 31751–31754. doi:10.1074/jbc.274.45.31751.

[47] J. Dekker, J.W. a Rossen, H. a. Büller, a. W.C. Einerhand, The MUC family: An obituary, Trends Biochem. Sci. 27 (2002) 126–131. doi:10.1016/S0968-0004(01)02052-7.

[48] S.J. Gendler, C. a. Lancaster, J. Taylor-Papadimitriou, T. Duhig, N. Peat, J. Burchell, et al., Molecular cloning and expression of human tumor-associated polymorphic epithelial mucin, J. Biol. Chem. 265 (1990) 15286–15293.

[49] N. Moniaux, S. Nollet, N. Porchet, P. Degand, A. Laine, J.P. Aubert, Complete sequence of the human mucin MUC4: a putative cell membrane-associated mucin., Biochem. J. 338 (Pt 2 (1999) 325–333. doi:10.1042/0264-6021: 338 0325.

[50] B.J. Van Klinken, K.M. Tytgat, H. a Büller, a W. Einerhand, J. Dekker, Biosynthesis of intestinal mucins: MUC1, MUC2, MUC3 and more., Biochem. Soc. Trans. 23 (1995) 814–818.

[51] N.G. Karlsson, A. Herrmann, H. Karlsson, M.E. V Johansson, I. Carlstedt, G.C. Hansson, The glycosylation of rat intestinal Muc2 mucin varies between rat strains and the small and large intestine. A study of O-linked oligosaccharides by

a mass spectrometric approach, J. Biol. Chem. 272 (1997) 27025–27034. doi:10.1074/jbc.272.43.27025.

[52] J.M. Holmén Larsson, K. a Thomsson, A.M. Rodríguez-Piñeiro, H. Karlsson, G.C. Hansson, Studies of mucus in mouse stomach, small intestine, and colon. III. Gastrointestinal Muc5ac and Muc2 mucin O-glycan patterns reveal a regiospecific distribution., Am. J. Physiol. Gastrointest. Liver Physiol. 305 (2013) G357–63. doi:10.1152/ajpgi.00048.2013.

[53] P.J. Puiman, M. Jensen, B. Stoll, I.B. Renes, A.C.J.M. de Bruijn, K. Dorst, et al., Intestinal threonine utilization for protein and mucin synthesis is decreased in formula-fed preterm pigs., J. Nutr. 141 (2011) 1306–1311. doi:10.3945/ jn.110.135145.

[54] M. a McGuckin, S.K. Lindén, P. Sutton, T.H. Florin, Mucin dynamics and enteric pathogens., Nat. Rev. Microbiol. 9 (2011) 265–278. doi:10.1038/nrmicro2538.

[55] J.R. Gum, J.W. Hicks, N.W. Toribara, B. Siddiki, Y.S. Kim, Molecular Cloning of Human Intestinal Mucin (MUC2) cDNA: Identification of the Amino Terminus and Overall Sequence Similarity to Prepro-Von Willebrand Factor, J. Biol. Chem. 269 (1994) 2440–2446.

[56] M. Scawen, a Allen, The action of proteolytic enzymes on the glycoprotein from pig gastric mucus., Biochem. J. 163 (1977) 363–368.

[57] A. Allen, D. a. Hutton, J.P. Pearson, The MUC2 gene product: A human intestinal mucin, Int. J. Biochem. Cell Biol. 30 (1998) 797–801. doi:10.1016/S1357-2725(98)00028-4.

[58] J.R. Gum, J.W. Hicks, N.W. Toribara, E.M. Rothe, R.E. Lagace, Y.S. Kim, The human MUC2 intestinal mucin has cysteine-rich subdomains located both upstream and downstream of its central repetitive region, J. Biol. Chem. 267 (1992) 21375–21383.

[59] S.S. Patel, K.M. Takahashi, Polymer dynamics in dilute and semidilute solutions, Macromolecules. 25 (1992) 4382–4391. doi:10.1021/ma00043a022.

[60] C. Clasen, J.P. Plog, W.-M. Kulicke, M. Owens, C. Macosko, L.E. Scriven, et al., How dilute are dilute solutions in extensional flows?, J. Rheol. (N. Y. N. Y). 50 (2006) 849. doi:10.1122/1.2357595.

[61] N. Kozer, Y.Y. Kuttner, G. Haran, G. Schreiber, Protein-protein association in polymer solutions: from dilute to semidilute to concentrated., Biophys. J. 92 (2007) 2139–2149. doi:10.1529/biophysj.106.097717.

[62] J.E. Herr, T.M. Winegard, M.J. O'Donnell, P.H. Yancey, D.S. Fudge, Stabilization and swelling of hagfish slime mucin vesicles., J. Exp. Biol. 213 (2010) 1092–1099. doi:10.1242/jeb.038992.

[63] T.J. McMaster, M. Berry, a P. Corfield, M.J. Miles, Atomic force microscopy of the submolecular architecture of hydrated ocular mucins., Biophys. J. 77 (1999) 533–541. doi:10.1016/S0006-3495(99)76910-9.

[64] I. Carlstedt, H. Lindgren, J.K. Sheehan, The macromolecular structure of human cervical-mucus glycoproteins. Studies on fragments obtained after reduction of disulphide bridges and after subsequent trypsin digestion., Biochem. J. 213 (1983) 427–435.

[65] K. Jumel, F.J.J. Fogg, D. a. Hutton, J.P. Pearson, A. Allen, S.E. Harding, A polydisperse linear random coil model for the quaternary structure of pig colonic mucin, Eur. Biophys. J. 25 (1997) 477–480. doi:10.1007/s002490050063.

[66] B. Barz, B.S. Turner, R. Bansil, B. Urbanc, Folding of pig gastric mucin non-glycosylated domains: A discrete molecular dynamics study, J. Biol. Phys. 38 (2012) 681–703. doi:10.1007/s10867-012-9280-x.

[67] A. Maleki, G. Lafitte, A.L. Kjøniksen, K. Thuresson, B. Nyström, Effect of pH on the association behavior in aqueous solutions of pig gastric mucin, Carbohydr. Res. 343 (2008) 328–340. doi:10.1016/j.carres.2007.10.005.

[68] N. Jentoft, Why are proteins O-glycosylated?, Trends Biochem. Sci. 15 (1990) 291–294. doi:10.1016/0968-0004(90)90014-3.

[69] M. Fritzy, M. Radmacher, J.P. Cleveland, M.W. Allersma, R.J. Stewart, R. Gieselmann, et al., Imaging Globular and Filamentous Proteins in Physiological Buffer Solutions with Tapping Mode Atomic Force Microscopy d j, Langmuir. (1995) 3529–3535. doi:10.1021/la00009a040.

[70] A.N. Round, M. Berry, T.J. McMaster, A.P. Corfield, M.J. Miles, Glycopolymer charge density determines conformation in human ocular mucin gene products: An atomic force microscope study, J. Struct. Biol. 145 (2004) 246–253. doi:10.1016/j.jsb.2003.10.029.

[71] R. Bansil, E. Stanley, J.T. LaMont, Mucin biophysics., Annu. Rev. Physiol. 57 (1995) 635–657. doi:10.1146/annurev.physiol.57.1.635.

[72] L.E. Bromberg, D.P. Barr, Self-association of mucin., Biomacromolecules. 1 (2000) 325–334. doi:10.1021/bm005532m.

[73] R. Bansil, B.S. Turner, Mucin structure, aggregation, physiological functions and biomedical applications, Curr. Opin. Colloid Interface Sci. 11 (2006) 164–170. doi:10.1016/j.cocis.2005.11.001.

[74] X. Cao, R. Bansil, K.R. Bhaskar, B.S. Turner, J.T. LaMont, N. Niu, et al., pH-dependent conformational change of gastric mucin leads to sol-gel transition., Biophys. J. 76 (1999) 1250–1258. doi:10.1016/S0006-3495(99)77288-7.

[75] Z. Hong, B. Chasan, R. Bansil, B.S. Turner, K.R. Bhaskar, N.H. Afdhal, Atomic force microscopy reveals aggregation of gastric mucin at low pH., Biomacromolecules. 6 (2005) 3458–66. doi:10.1021/bm0505843.

[76] K.R. Bhaskar, D.H. Gong, R. Bansil, S. Pajevic, J. a Hamilton, B.S. Turner, et al., Profound increase in viscosity and aggregation of pig gastric mucin at low pH., Am. J. Physiol. 261 (1991) G827–G832.

[77] J. Kočevar-Nared, J. Kristl, J. Šmid-Korbar, Comparative theological investigation of crude gastric mucin and natural gastric mucus, Biomaterials. 18 (1997) 677–681. doi:10.1016/S0142-9612(96)00180-9.

[78] R.L. Shogren, a. M. Jamieson, J. Blackwell, N. Jentoft, The thermal depolymerization of porcine submaxillary mucin, J. Biol. Chem. 259 (1984) 14657–14662.

[79] E.R. Morris, D. a Rees, Principles of biopolymer gelation. Possible models for mucus gel structure., Br. Med. Bull. 34 (1978) 49–53.

[80] C.M. McCullagh, R. Gupta, a. M. Jamieson, J. Blackwell, Gelation of fractionated canine submaxillary mucin in a chaotropic solvent, Int. J. Biol. Macromol. 18 (1996) 247–253. doi:10.1016/0141-8130(95)01086-6.

[81] A.E. Bell, A. Allen, E.R. Morris, S.B. Ross-Murphy, Functional interactions of gastric mucus glycoprotein, Int. J. Biol. Macromol. 6 (1984) 309–315. doi:10.1016/0141-8130(84)90015-1.

[82] L.A. Sellers, A. Allen, E.R. Morris, S.B. Ross-Murphy, Mucus glycoprotein gels. Role of glycoprotein polymeric structure and carbohydrate side-chains in gel-formation., Carbohydr. Res. 178 (1988) 93–110. doi:10.1016/0008-6215(88)80104-6.

[83] V.L. Pereira-Chioccola, a Acosta-Serrano, I. Correia de Almeida, M. a Ferguson, T. Souto-Padron, M.M. Rodrigues, et al., Mucin-like molecules form a negatively charged coat that protects Trypanosoma cruzi trypomastigotes from killing by human anti-alpha-galactosyl antibodies., J. Cell Sci. 113 (Pt 7 (2000) 1299–1307.

[84] E.R. Vimr, K. a Kalivoda, E.L. Deszo, S.M. Steenbergen, Diversity of microbial sialic acid metabolism., Microbiol. Mol. Biol. Rev. 68 (2004) 132–153. doi:10.1128/MMBR.68.1.132.

[85] a. E. Eckhardt, C.S. Timpte, J.L. Abernethy, a. Toumadje, W.C. Johnson, R.L. Hill, Structural properties of porcine submaxillary gland apomucin., J. Biol. Chem. 262 (1987) 11339–11344.

[86] H.H. Sigurdsson, J. Kirch, C.M. Lehr, Mucus as a barrier to lipophilic drugs, Int. J. Pharm. 453 (2013) 56–64. doi:10.1016/j.ijpharm.2013.05.040.

[87] R. Sommer, T.E. Exner, A. Titz, A Biophysical Study with Carbohydrate Derivatives Explains the Molecular Basis of Monosaccharide Selectivity of the

Pseudomonas aeruginosa Lectin LecB., PLoS One. 9 (2014) e112822. doi:10.1371/journal.pone.0112822.

[88] S.E. Harding, The macrostructure of mucus glycoproteins in solution., Adv. Carbohydr. Chem. Biochem. 47 (1989) 345–381.

[89] G.J. Strous, J. Dekker, Mucin-type glycoproteins., Crit. Rev. Biochem. Mol. Biol. 27 (1992) 57–92. doi:10.3109/10409239209082559.

[90] D. Snary, a Allen, Studies on gastric mucoproteins. The production of radioactive mucoproteins by pig gastric mucosal scrapings in vitro., Biochem. J. 127 (1972) 577–587.

[91] a Allen, D. Snary, The structure and function of gastric mucus., Gut. 13 (1972) 666–672. doi:10.1136/gut.13.8.666.

[92] M.E. V. Johansson, M. Phillipson, J. Petersson, A. Velcich, L. Holm, G.C. Hansson, The inner of the two Muc2 mucin-dependent mucus layers in colon is devoid of bacteria, Proc. Natl. Acad. Sci. U. S. A. 105 (2008) 15064–9. doi:10.4161/gmic.1.1.10470.

[93] M.E. V Johansson, J.M.H. Larsson, G.C. Hansson, The two mucus layers of colon are organized by the MUC2 mucin, whereas the outer layer is a legislator of host-microbial interactions., Proc. Natl. Acad. Sci. U. S. A. 108 Suppl (2011) 4659–4665. doi:10.1073/pnas.1006451107.

[94] A. Ermund, A. Schütte, M.E. V Johansson, J.K. Gustafsson, G.C. Hansson, A. Schuette, Gastrointestinal mucus layers have different properties depending on location - 1. Studies of mucus in mouse stomach, small intestine, Peyer's patches and colon., Am. J. Physiol. Gastrointest. Liver Physiol. 305 (2013) G341–G347. doi:10.1152/ajpgi.00046.2013.

[95] M.E. V Johansson, H. Sjövall, G.C. Hansson, The gastrointestinal mucus system in health and disease., Nat. Rev. Gastroenterol. Hepatol. 10 (2013) 352–61. doi:10.1038/nrgastro.2013.35.

[96] S. Vaishnava, M. Yamamoto, K.M. Severson, K. a Ruhn, X. Yu, O. Koren, et al., The Antibacterial Lectin RegIIIg Promotes the Spatial Segregation of Microbiota and Host in the Intestine, server2.phys.uniroma1.it. 334 (2011) 255–258.

[97] S. McQueen, D. Hutton, a Allen, a Garner, Gastric and duodenal surface mucus gel thickness in rat: effects of prostaglandins and damaging agents., Am. J. Physiol. 245 (1983) G388–G393.

[98] A. Allen, G. Flemström, Gastroduodenal mucus bicarbonate barrier: protection against acid and pepsin., Am. J. Physiol. Cell Physiol. 288 (2005) C1–C19. doi:10.1152/ajpcell.00102.2004.

[99] S.M. Sharpe, X. Qin, Q. Lu, E. Feketeova, D.C. Palange, W. Dong, et al., Loss of the intestinal mucus layer in the normal rat causes gut injury but not toxic

mesenteric lymph nor lung injury., Shock. 34 (2010) 475–81. doi:10.1097/ SHK. 0b013e3181dc3ff5.

[100] a Allen, J.P. Pearson, The gastrointestinal adherent mucous gel barrier., Methods Mol. Biol. 125 (2000) 57–64. doi:10.1385/1-59259-048-9:057.

[101] R. a Cone, Barrier properties of mucus., Adv. Drug Deliv. Rev. 61 (2009) 75–85. doi:10.1016/j.addr.2008.09.008.

[102] J. Maury, C. Nicoletti, L. Guzzo-Chambraud, S. Maroux, The filamentous brush border glycocalyx, a mucin-like marker of enterocyte hyper-polarization, Eur. J. Biochem. 228 (1995) 323–331. doi:10.1111/j.1432-1033.1995.tb20267.x.

[103] A. Frey, K.T. Giannasca, R. Weltzin, P.J. Giannasca, H. Reggio, W.I. Lencer, et al., Role of the glycocalyx in regulating access of microparticles to apical plasma membranes of intestinal epithelial cells: implications for microbial attachment and oral vaccine targeting., J. Exp. Med. 184 (1996) 1045–1059. doi:10.1084/ jem.184.3.1045.

[104] Y. Aoki, M. Morishita, K. Asai, B. Akikusa, S. Hosoda, K. Takayama, Region-dependent role of the mucous/glycocalyx layers in insulin permeation across rat small intestinal membrane, Pharm. Res. 22 (2005) 1854–1862. doi:10.1007 /s11095-005-6137-z.

[105] L.C. Hoskins, M. Agustines, W.B. McKee, E.T. Boulding, M. Kriaris, G. Niedermeyer, Mucin degradation in human colon ecosystems. Isolation and properties of fecal strains that degrade ABH- blood group antigens and oligosaccharides from mucin glycoproteins, J. Clin. Invest. 75 (1985) 944–953. doi:10.1172/JCI111795.

[106] G. Larson, P. Falk, L.C. Hoskins, Degradation of human intestinal glycosphingolipids by extracellular glycosidases from mucin-degrading bacteria of the human fecal flora, J. Biol. Chem. 263 (1988) 10790–10798.

[107] W.O.J.A.B. Aranowski, UV−VIS Spectra of Intestinal Mucins with Change in Solution Concentration and pH, Adv. Clin. Exp. Med. 15 (2006) 253–258.

[108] A. Swidsinski, V. Loening-Baucke, F. Theissig, H. Engelhardt, S. Bengmark, S. Koch, et al., Comparative study of the intestinal mucus barrier in normal and inflamed colon., Gut. 56 (2007) 343–350. doi:10.1136/gut.2006.098160.

[109] M.E. V Johansson, D. Ambort, T. Pelaseyed, A. Schütte, J.K. Gustafsson, A. Ermund, et al., Composition and functional role of the mucus layers in the intestine, Cell. Mol. Life Sci. 68 (2011) 3635–3641. doi:10.1007/s00018-011-0822-3.

[110] J.L. Greaves, C.G. Wilson, Treatment of diseases of the eye with mucoadhesive delivery systems, Adv. Drug Deliv. Rev. 11 (1993) 349–383. doi:10.1016/0169-409X(93)90016-W.

[111] J. Yadav, A. Verma, J. Singh, Study on Nasal Mucous Clearance in Patients of Perennial Allergic Rhinitis, 17 (2003) 89–91.

[112] M. King, Experimental models for studying mucociliary clearance, Eur. Respir. J. 11 (1998) 222–228. doi:10.1183/09031936.98.11010222.

[113] R. Cone, Mucus, in: L.M. Jiri Mestecky, Michael E. Lamm, Pearay L. Ogra, Warren Strober, John Bienenstock, Jerry R. McGhee (Ed.), Mucosal Immunol., 3rd ed., Elsevier Academic Press, London, 2005: pp. 49–72.

[114] L.A. Sellers, A. Allen, E.R. Morris, S.B. Ross-Murphy, Mucus glycoprotein gels. Role of glycoprotein polymeric structure and carbohydrate side-chains in gel-formation., Carbohydr. Res. 178 (1988) 93–110. doi:10.1016/0008-6215(88) 80104-6.

[115] F. Balzola, C. Bernstein, Intestinal mucus barrier in normal and inflamed colon: Commentary, Inflamm. Bowel Dis. Monit. 10 (2009) 18–19. doi:10.1097/ MPG. 0b013e3181a117ea.

[116] L.M. Ensign, R. Cone, J. Hanes, Oral drug delivery with polymeric nanoparticles: The gastrointestinal mucus barriers, Adv. Drug Deliv. Rev. 64 (2012) 557–570. doi:10.1016/j.addr.2011.12.009.

[117] B.L. Slomiany, V.L. Murty, S.R. Carter, a Slomiany, Effect of covalently bound fatty acids and associated lipids on the viscosity of gastric mucus glycoprotein in cystic fibrosis., Digestion. 34 (1986) 275–280. doi:10.1159/000199341.

[118] N. Jordan, J. Newton, J. Pearson, a Allen, A novel method for the visualization of the in situ mucus layer in rat and man., Clin. Sci. (Lond). 95 (1998) 97–106. doi:10.1042/CS19980081.

[119] S.K. Lai, Y.Y. Wang, J. Hanes, Mucus-penetrating nanoparticles for drug and gene delivery to mucosal tissues, Adv. Drug Deliv. Rev. 61 (2009) 158–171. doi: 10.1016/j.addr.2008.11.002.

[120] M.S. Ali, J.P. Pearson, Upper airway mucin gene expression: a review., Laryngoscope. 117 (2007) 932–938. doi:10.1097/MLG.0b013e3180383651.

[121] J. Kim, W. Khan, Goblet Cells and Mucins: Role in Innate Defense in Enteric Infections, Pathogens. 2 (2013) 55–70. doi:10.3390/pathogens2010055.

[122] P. Gruber, a Rubinstein, V.H. Li, P. Bass, J.R. Robinson, Gastric emptying of nondigestible solids in the fasted dog., J. Pharm. Sci. 76 (1987) 117–122.

[123] C.-M. Lehr, F.G.J. Poelma, H.E. Junginger, J.J. Tukker, An estimate of turnover time of intestinal mucus gel layer in the rat in situ loop, Int. J. Pharm. 70 (1991) 235–240. doi:10.1016/0378-5173(91)90287-X.

[124] A. Rubinstein, B. Tirosh, Mucus gel thickness and turnover in the gastrointestinal tract of the rat: Response to cholinergic stimulus and implication for mucoadhesion, Pharm. Res. 11 (1994) 794–799. doi:10.1023/A:1018961204325.

[125] M. Copeman, J. Matuz, A.J. Leonard, J.P. Pearson, P.W. Dettmar, A. Allen, The gastroduodenal mucus barrier and its role in protection against luminal pepsins: the effect of 16,16 dimethyl prostaglandin E2, carbopol-polyacrylate, sucralfate and bismuth subsalicylate., J. Gastroenterol. Hepatol. 9 Suppl 1 (1994) S55–S59. doi:10.1111/j.1440-1746.1994.tb01303.x.

[126] L. Szentkuti, K. Lorenz, The thickness of the mucus layer in different segments of the rat intestine., Histochem. J. 27 (1995) 466–472. doi:10.1007/BF02388803.

[127] C. Atuma, V. Strugala, a Allen, L. Holm, The adherent gastrointestinal mucus gel layer: thickness and physical state in vivo., Am. J. Physiol. Gastrointest. Liver Physiol. 280 (2001) G922–G929.

[128] S. Schreiber, P. Scheid, Gastric mucus of the guinea pig: proton carrier and diffusion barrier., Am. J. Physiol. 272 (1997) G63–G70.

[129] D.M. Grayzel, J. Miller, Edgar G., The pH of the Contents of the Gastrointestinal Tract in Dogs, in Relation to Diet and Rickets, J. Biol. Chem. 76 (1928) 423–436. http://www.jbc.org/cgi/content/long/76/2/423 (accessed May 21, 2015).

[130] N.J. Talley, J.E. Ormand, C.A. Frie, A.R. Zinsmeister, Stability of pH gradients in vivo across the stomach in Helicobacter pylori gastritis, dyspepsia, and health., Am. J. Gastroenterol. 87 (1992) 590–594.

[131] M. Sjöblom, Duodenal epithelial sensing of luminal acid: Role of carbonic anhydrases, Acta Physiol. 201 (2011) 85–95. doi:10.1111/j.1748-1716. 2010 .02166.x.

[132] R. Busche, W. Von Engelhardt, pH gradients and a mirco-pore filter at the luminal surface affect fluxes of propionic acid across guinea pig large intestine, J. Comp. Physiol. B Biochem. Syst. Environ. Physiol. 177 (2007) 821–831. doi:10. 1007/s00360-007-0182-3.

[133] D.F. Evans, G. Pye, R. Bramley, a G. Clark, T.J. Dyson, J.D. Hardcastle, Measurement of gastrointestinal pH profiles in normal ambulant human subjects., Gut. 29 (1988) 1035–1041. doi:10.1136/gut.29.8.1035.

[134] J. Fallingborg, L.A. Christensen, M. Ingeman-Nielsen, B.A. Jacobsen, K. Abildgaard, H.H. Rasmussen, et al., Measurement of gastrointestinal pH and regional transit times in normal children., J. Pediatr. Gastroenterol. Nutr. 11 (1990) 211–214. doi:10.1097/00005176-199008000-00010.

[135] O. Lieleg, K. Ribbeck, Biological hydrogels as selective diffusion barriers, Trends Cell Biol. 21 (2011) 543–551. doi:10.1016/j.tcb.2011.06.002.

[136] D. Winne, W. Verheyen, Diffusion coefficient in native mucus gel of rat small intestine., J. Pharm. Pharmacol. 42 (1990) 517–519.

[137] S.S. Olmsted, J.L. Padgett, a I. Yudin, K.J. Whaley, T.R. Moench, R. a Cone, Diffusion of macromolecules and virus-like particles in human cervical mucus., Biophys. J. 81 (2001) 1930–7. doi:10.1016/S0006-3495(01)75844-4.

[138] M. a Desai, M. Mutlu, P. Vadgama, A study of macromolecular diffusion throug native porcine mucus., Experientia. 48 (1992) 22–26. doi:10.1007 /BF 01923598.

[139] a Bernkop-Schnurch, R. Fragner, Investigations into the diffusion behaviour of polypeptides in native intestinal mucus with regard to their peroral administration, Pharm. Sci. 2 (1996) 361–363.

[140] M. Boegh, H.M. Nielsen, Mucus as a Barrier to Drug Delivery - Understanding and Mimicking the Barrier Properties, Basic Clin. Pharmacol. Toxicol. 116 (2015) 179–186. doi:10.1111/bcpt.12342.

[141] Y. Wang, K. Hida, R. Cone, M. Sanson, Y. Vengrenyuk, J. Liu, et al., Nanoparticles reveal that human cervicovaginal mucus is riddled with pores larger than viruses, Proc. Natl. Acad. Sci. 108 (2011) 14371–14371. doi:10. 1073 /pnas.1111693108.

[142] M. Boegh, S.G. Baldursdóttir, A. Müllertz, H.M. Nielsen, Property profiling of biosimilar mucus in a novel mucus-containing in vitro model for assessment of intestinal drug absorption, Eur. J. Pharm. Biopharm. 87 (2014) 227–235. doi:10. 1016/j.ejpb.2014.01.001.

[143] a. Wikman, J. Karlsson, I. Carlstedt, P. Artursson, A drug absorption model based on the mucus layer producing human intestinal goblet cell line HT29-H, Pharm. Res. 10 (1993) 843–852. doi:10.1023/A:1018905109971.

[144] I. Behrens, P. Stenberg, P. Artursson, T. Kissel, Transport of lipophilic drug molecules in a new mucus-secreting cell culture model based on HT29-MTX cells, Pharm. Res. 18 (2001) 1138–1145. doi:10.1023/A:1010974909998.

[145] M. Boegh, M. García-Díaz, A. Müllertz, H.M. Nielsen, Steric and interactive barrier properties of intestinal mucus elucidated by particle diffusion and peptide permeation, Eur. J. Pharm. Biopharm. (2015) 1–8. doi:10.1016/ j.ejpb.2015 .01.014.

[146] C. Meaney, C. O'Driscoll, Mucus as a barrier to the permeability of hydrophilic and lipophilic compounds in the absence and presence of sodium taurocholate micellar systems using cell culture models, Eur. J. Pharm. Sci. 8 (1999) 167–175. doi:10.1016/S0928-0987(99)00007-X.

[147] W.M. Saltzman, M.L. Radomsky, K.J. Whaley, R. a Cone, Antibody diffusion in human cervical mucus., Biophys. J. 66 (1994) 508–515. doi:10.1016/S0006-3495(94)80802-1.

[148] N.N. Sanders, S.C. De Smedt, E. Van Rompaey, P. Simoens, F. De Baets, J. Demeester, Cystic fibrosis sputum: A barrier to the transport of nanospheres, Am. J. Respir. Crit. Care Med. 162 (2000) 1905–1911. doi:10.1164/ ajrccm. 162.5.9909009.

[149] Y. Wang, S.K. Lai, J.S. Suk, A. Pace, R. Cone, J. Hanes, Addressing the PEG mucoadhesivity paradox to engineer nanoparticles that "slip" through the human mucus barrier., Angew. Chem. Int. Ed. Engl. 47 (2008) 9726–9. doi:10.1002 /anie.200803526.

[150] S.K. Lai, D.E. O'Hanlon, S. Harrold, S.T. Man, Y.-Y. Wang, R. Cone, et al., Rapid transport of large polymeric nanoparticles in fresh undiluted human mucus., Proc. Natl. Acad. Sci. U. S. A. 104 (2007) 1482–7. doi:10.1073/pnas.06 08611104.

[151] J.S. Suk, S.K. Lai, Y.-Y. Wang, L.M. Ensign, P.L. Zeitlin, M.P. Boyle, et al., The penetration of fresh undiluted sputum expectorated by cystic fibrosis patients by non-adhesive polymer nanoparticles., Biomaterials. 30 (2009) 2591–7. doi:10. 1016/j.biomaterials.2008.12.076.

[152] B.S. Schuster, J.S. Suk, G.F. Woodworth, J. Hanes, Nanoparticle diffusion in respiratory mucus from humans without lung disease, Biomaterials. 34 (2013) 3439–3446. doi:10.1016/j.biomaterials.2013.01.064.

[153] A.J. Kim, N.J. Boylan, J.S. Suk, M. Hwangbo, T. Yu, B.S. Schuster, et al., Use of single-site-functionalized PEG dendrons to prepare gene vectors that penetrate human mucus barriers, Angew. Chemie - Int. Ed. 52 (2013) 3985–3988. doi:10. 1002/anie.201208556.

[154] P.G. Bhat, D.R. Flanagan, M.D. Donovan, Drug diffusion through cystic fibrotic mucus: Steady-state permeation, rheologic properties, and glycoprotein morphology, J. Pharm. Sci. 85 (1996) 624–630. doi:10.1021/js950381s.

[155] S.C. De Smedt, A. Lauwers, J. Demeester, Y. Engelborghs, G. De Mey, M. Du, Structural information on hyaluronic acid solutions as studied by probe diffusion experiments, Macromolecules. 27 (1994) 141–146. doi:10.1021/ma00079a021.

[156] T.K.L. Meyvis, S.C. De Smedt, P. Van Oostveldt, J. Demeester, Fluorescence recovery after photobleaching: A versatile tool for mobility and interaction measurements in pharmaceutical research, Pharm. Res. 16 (1999) 1153–1162. doi:10.1023/A:1011924909138.

[157] N.H. Afdhal, X. Cao, R. Bansil, Z. Hong, C. Thompson, B. Brown, et al., Interaction of mucin with cholesterol enriched vesicles: Role of mucin structural domains, Biomacromolecules. 5 (2004) 269–275. doi:10.1021/bm0341733.

[158] P. Occhipinti, P.C. Griffiths, Quantifying diffusion in mucosal systems by pulsed-gradient spin-echo NMR, Adv. Drug Deliv. Rev. 60 (2008) 1570–1582. doi:10.1016/j.addr.2008.08.006.

[159] P.C. Griffiths, P. Occhipinti, C. Morris, R.K. Heenan, S.M. King, M. Gumbleton, PGSE-NMR and SANS studies of the interaction of model polymer therapeutics with mucin, Biomacromolecules. 11 (2010) 120–125. doi:10.1021/bm9009667.

[160] S.K. Lai, J. Hanes, Real-time multiple particle tracking of gene nanocarriers in complex biological environments., in: Methods Mol. Biol., 2008: pp. 81–97. doi:10.1007/978-1-60327-248-36.

[161] S.K. Lai, Y.-Y. Wang, J. Hanes, Mucus-penetrating nanoparticles for drug and gene delivery to mucosal tissues., Adv. Drug Deliv. Rev. 61 (2009) 158–71. doi:10.1016/j.addr.2008.11.002.

[162] J. Suh, M. Dawson, J. Hanes, Real-time multiple-particle tracking: applications to drug and gene delivery., Adv. Drug Deliv. Rev. 57 (2005) 63–78. doi:10.10 16/j.addr.2004.06.001.

[163] Y.-Y. Wang, S.K. Lai, C. So, C. Schneider, R. Cone, J. Hanes, Mucoadhesive nanoparticles may disrupt the protective human mucus barrier by altering its microstructure., PLoS One. 6 (2011) e21547. doi:10.1371/journal.pone.0021547.

[164] B.S. Schuster, J.S. Suk, G.F. Woodworth, J. Hanes, Nanoparticle diffusion in respiratory mucus from humans without lung disease., Biomaterials. 34 (2013) 3439–46. doi:10.1016/j.biomaterials.2013.01.064.

[165] M.T. Valentine, P.D. Kaplan, D. Thota, J.C. Crocker, T. Gisler, R.K. Prud'homme, et al., Investigating the microenvironments of inhomogeneous soft materials with multiple particle tracking., Phys. Rev. E. Stat. Nonlin. Soft Matter Phys. 64 (2001) 061506.

[166] M. Dawson, D. Wirtz, J. Hanes, Enhanced viscoelasticity of human cystic fibrotic sputum correlates with increasing microheterogeneity in particle transport., J. Biol. Chem. 278 (2003) 50393–401. doi:10.1074/jbc.M309026200.

[167] J. Suh, D. Wirtz, J. Hanes, Efficient active transport of gene nanocarriers to the cell nucleus., Proc. Natl. Acad. Sci. U. S. A. 100 (2003) 3878–82. doi:10.1073/ pnas.0636277100.

[168] J.S. Suk, A.J. Kim, K. Trehan, C.S. Schneider, L. Cebotaru, O.M. Woodward, et al., Lung gene therapy with highly compacted DNA nanoparticles that overcome the mucus barrier., J. Control. Release. 178 (2014) 8–17. doi:10.1016/j. jconrel. 2014.01.007.

[169] J. Apgar, Y. Tseng, E. Fedorov, M.B. Herwig, S.C. Almo, D. Wirtz, Multiple-particle tracking measurements of heterogeneities in solutions of actin filaments and actin bundles., Biophys. J. 79 (2000) 1095–106. doi:10.1016/S0006-3495(00)76363-6.

[170] A. Macierzanka, A.R. Mackie, B.H. Bajka, N.M. Rigby, F. Nau, D. Dupont, Transport of particles in intestinal mucus under simulated infant and adult

physiological conditions: impact of mucus structure and extracellular DNA., PLoS One. 9 (2014) e95274. doi:10.1371/journal.pone.0095274.

[171] N. Fatin-Rouge, K. Starchev, J. Buffle, Size effects on diffusion processes within agarose gels., Biophys. J. 86 (2004) 2710–9. doi:10.1016/S0006-3495(04)74325-8.

[172] J. Suh, D. Wirtz, J. Hanes, Real-time intracellular transport of gene nanocarriers studied by multiple particle tracking, Biotechnol. Prog. 20 (2004) 598–602. doi: 10.1021/bp034251y.

[173] P. Georgiades, P.D. a Pudney, D.J. Thornton, T. a. Waigh, Particle tracking microrheology of purified gastrointestinal mucins, Biopolymers. 101 (2014) 366–377. doi:10.1002/bip.22372.

[174] D.S. Martin, M.B. Forstner, J. a Käs, Apparent subdiffusion inherent to single particle tracking., Biophys. J. 83 (2002) 2109–17. doi:10.1016/S0006-3495 (02)73971-4.

[175] M.J. Saxton, K. Jacobson, Single-particle tracking: applications to membrane dynamics., Annu. Rev. Biophys. Biomol. Struct. 26 (1997) 373–99. doi:10.1146/ annurev.biophys.26.1.373.

[176] J.S. Suk, S.K. Lai, N.J. Boylan, M.R. Dawson, M.P. Boyle, J. Hanes, Rapid transport of muco-inert nanoparticles in cystic fibrosis sputum treated with N-acetyl cysteine., Nanomedicine (Lond). 6 (2011) 365–75. doi:10.1016/j.

[177] W. Anderson, D. Kozak, V.A. Coleman, , M. Trau, A comparative study of submicron particle sizing platforms: Accuracy, precision and resolution analysis of polydisperse particle size distributions, J. Colloid Interface Sci. 405 (2013) 322–330. doi:10.1016/j.jcis.2013.02.030.

CHAPTER TWO

INTESTINAL MUCUS MODELS: CHARACTERIZATION OF MUCUS MODELS, VALIDATION OF MPT TECHNIQUE AND MEASUREMENT OF PARTICLES DIFFUSION THROUGH MUCUS

1 INTRODUCTION

1.a Mucus Models

As was described in Chapter 1, mucus is a biopolymer lining the intestinal epithelial membrane which serves as a barrier to limit the permeation of macromolecules from the intestinal lumen into the blood circulation. Hence, the permeation of macromolecules through the intestinal mucosal membrane needs to be studied in the context of their permeation through mucus. Intestinal mucus has always been described as a gel barrier due to the structural nature of the mucin network [1]. The properties of the mucus gel varies between different regions in the intestine depending on the main MUC gene product that constitutes the respective mucin network [2,3]. To this end one of the most common models is to use the purified mucin itself isolated from the intestine.

Among commercially available mucins, dried porcine gastric mucin (PGM) from Sigma Aldrich has been widely used [4–6]. This has been rationalised on the basis of similarities between the pig and human intestinal mucin, where both types are MUC 2 tetramer structures [7] and possess the same amino acid sequences [8]. The dried PGM can simply be re-suspended in an aqueous phase to form a gel representative to some extent of the native intestinal mucus. However, it was found that some physicochemical properties of natural intestinal mucus gel cannot be reproduced by gel formed from re-suspending of the sigma PGM. For example, Kocevar-Nared et al. (1997) [9] showed that the rheological properties of natural intestinal mucus gel are different from that of the re-suspended gel-Sigma´s dried PGM. This was attributed to the degradation of the commercially available mucin fibres during the initial isolation step which damaged the disulfide-bridges crosslinking the mucin subunits. Despite concerns over reconstituted mucin, various models of either a reconstituted mucin gel or a native mucus sample

have been used to study the permeation of NPs through the 'intestinal mucus barrier' [10,11].

1.b Biophysical Properties of Mucus

Mucus is a complex biological polymer with unique properties that provides a rich material for biophysical and biochemical analyses, which extend from the dynamic and chemical properties of the mucin basic unit to the rheological and structural properties of the mucus gel itself [12]. For example, the physical appearance of gastric, cervical and bronchial mucin macromolecules in diluted solutions was studied by electron microscopy revealing these units have linear conformations with a diameter of ca. 5 nm and length of ca. 5000 nm [13]. Electron microscopy has also been used to measure the size of mucin subunits revealing an average length of 400 nm [14]. While electron microscopy has allowed researchers to build up a comprehensive picture of mucin morphology, light scattering techniques have informed the molecular weight of mucin units, subunits and domains [15,16]. Chemically, the polypeptide and polysaccharide content of mucus has been examined by the nuclear magnetic resonance (NMR) technique [17,18].

In this chapter, AFM and rheology will be used to study the biophysical properties of intestinal mucus:

Rheological Studies on Mucus

Rheology is the study of the deformation and/or flow-ability of material when stress is applied. Rheological testing is used to classify material into a solid, semisolid or fluid according to its flow-ability in response to the applied rheological stress [19]. The most important rheological system is the semi-solid which is a system that possesses the characteristics of both solid and fluid systems [20]. In other words, this system

although defined as a fluid contains solid components which build structure to deliver properties consistent with a solid material. As an example, a gel is a semisolid system where the polymer concentration in the fluid is high enough to build a structured network to behave like a solid. When the gel sample is subjected to shear stress, the gel structure will change in response to the level of shear stress. These changes can be expressed in terms of the degree of fluidity ("loss modulus") versus degree of solidity ("storage modulus") [21]. Since mucus is a gel system, rheological analysis is of significance in the study of its structure. Moreover, rheology is important in terms of delivery of agents through mucus as it can reveal the effect of variables such as mucus components and the interaction of mucus with particles [22].

A decade ago, the rheological properties of native pig gastric mucus and purified mucin gel was reported by the Taylor group [23]. Both of these models have shown shear-hardening behaviour, where viscosity increases as the applied stress is increased up to a particular level ("low stress level"). When the applied stress is further increased, these mucus models flowed and behaved as shear thinning systems [23]. This shear-thickening behaviour of the mucus might explain the resistance of mucus to the small mechanical strength like stresses applied through intestinal motility. Although recently, Nordgård and Draget (2015) [24] showed the shear-hardening behaviour of pig intestinal mucus in response to levels of mechanical stress encountered in the intestine. In their study a stress of 1 Pascal, which is the same as the stress applied by the gut wall, was applied to native intestinal mucus and a hardening response was obtained.

Moreover, rheological tests have the capacity to show the effect of NP interactions on mucus structure. For example, in the study the interaction of muco-adhesive polymers with gastric homogenised mucus, Madsen et al. (1998) [25] showed that the mixture of mucus and muco-adhesive polymer has a higher mechanical strength than that of mucus

alone indicating the formation of an entangled cross-linked gel between the mucus network and the polymer network. This interaction of muco-adhesive polymer with mucus resulted in what is termed ‘rheological synergism’, where the resistance to the shear stress is much higher for the mucus-polymer mixture than the resistance of both systems measured separately [26]. However, another study showed that muco-adhesive modified polystyrene NPs has no effect on the bulk rheological behaviour of mucus [27]. The concept of no effect of NP on the bulk rheology of the mucus was used to indicate the free permeation of particles through the mucus [28].

AFM Studies to Examine Mucus Structure

Electron microscopy techniques for imaging biological samples involve destructive procedures such as sample drying. In contrast, AFM provides a non-destructive procedure where the biological sample can be imaged in its hydrated form and with a resolution at the sub-nanometer level [29]. Unlike other microscopy techniques which depend on visualising a fixed sample, AFM depends on sensing the surface architecture and anomalies of samples through a sharp tip ‘stylus’ which is attached to a flexible cantilever. The sharp tip stylus scans the sample surface either through direct contact, non-contact or tapping mode. The movement of this stylus are transmitted via the flexible cantilever leading to specific bending profile of the cantilever that is related to the structural properties of the sample. Through the laser deflection technique, this bending profile can be expressed as an image of the sample [30].

The late 1990s witnessed the use of AFM to image the molecular structure of hydrated ocular mucin. Mucin was collected from human conjunctiva, and then purified and hydrated in a physiological pH buffer [31]. This early study showed that hydrated mucin has a variable range of lengths from a 100 nm up to a few microns. Accordingly, purified gastric mucin, dispersed in 0.1 M sodium acetate buffer, showed a long linear

filamentous structure when observed by AFM [32]. Deacon et al. (2000) [32] also used AFM to indicate the muco-adhesive properties of chitosan when it is mixed with mucin, where the aggregation of chitosan-mucin was imaged by the AFM. Similarly, AFM was used to identify the muco-adhesive properties of pectin polymer when it is mixed with mucin dispersed in deionized water [33].

Moreover, the effect of environmental pH on the structural behaviour of the porcine gastric mucin was studied by the AFM [34]. It was found that both of the diluted and concentrated gastric mucin aqueous solutions at pH 2 showed as big as 3000 nm^2 clustered aggregations. The same study used AFM to image human gastric mucus collected by endoscopy which appeared as a 'pearl and necklace' in which the pearl size is similar to that of the clustered aggregates which was observed in the dispersed gastric mucin (3000 nm^2). This finding is in accordance with the suggested aggregation behaviour of mucin in low pH media.

Processed Intestinal Mucus "Consortium Mucus Gel" Model

The work in this thesis was supported by the FP7 Alexander European Consortium. The mucus gel model introduced by the Alexander European Consortium as the groups' principle model aimed to mimic the intestinal mucus barrier in term of its rheological gel structure. This model was designed to form a gel layer with high mechanical strength to study NP permeation, and in particular NP permeation across the intestinal mucus gel that had been coated upon Transwell semi-permeable membrane filter-chambers. This mucus model was obtained by squeezing ('milking') the luminal content from longitudinally intact pig intestine sections (cut cross-sectionally into 25 cm length pieces). Given the method of collection, the harvested product contained not only the mucin and other mucus constituents but also food debris and significant water content. The mucus model was processed to remove any food debris and as much excess water

as deemed appropriate in order to form a more compacted structural product. The processing procedures included multiple washing and high speed centrifugation of the harvested intestinal luminal content followed by removal of the supernatant. This centrifugation step resulted in a gel with high mechanical strength that formed an intact layer in the Transwell semi-permeable membrane filter-chambers.

There were two main drivers for the centrifugation of mucus in this model. First, is to form a stiff gel layer of mucus for the Transwell experiments. Second, is to retain the other structural features of mucus such as a mucin mesh spacing involving physical cross-linking of the mucin network, but with cross-linking that is capable of forming reversible attaching/detaching interactions [35] involving electrostatic interactions [36], hydrophobic interactions [37] and/or calcium interactions [38]. Such reversible viscoelastic properties should enable the mucus to retain its other features by re-annealing upon removing of the applied stress [39]. However, the Yudin and co-workers (1989) [40] demonstrated that imposing upon mucus any physical stretching such as centrifugation results in a change in the mucus mesh spacing (network's microstructural properties). As such, retaining the native mesh properties of mucus that has been subjected to high speed centrifugation is questionable. In this chapter, the effect of processing on the physicochemical properties of mucus will be studied extensively.

Native Pig Intestinal Mucus "Cardiff Native Mucus" Model

The Cardiff team introduced another mucus model to the consortium which simply comprised freshly isolated mucus gently scraped from pig intestine without any significant processing procedures such as centrifugation [10]. This model was introduced to represent the native intestinal mucus as close as possible in terms of mesh spacing and the content of water, lipid, and protein. The collection of the native mucus

involved gentle scraping of the mucus layer lining the epithelial membrane after removing of any food debris. This mucus should retain the same network structure of the mucus in the intestine [10]. This mucus model was used by our group to compare the biophysical properties of various mucus models and to study the dynamic permeation of NP by the MPT technique.

1.c Aim of the Study

The aim of this chapter was to characterise an appropriate intestinal mucus model that closely mimics the *in vivo* mucus system, and one that afforded the conduct of multiple particle tracking (MPT) for the analysis of NP diffusion.

The objectives of this study are as follows:

- Preparation of various pig intestinal mucus models the "Consortium mucus-gel model" and the "Cardiff native mucus model' and assess the suitability of these models for MPT analysis of NP diffusion. In particular this chapter focused on the use of some standard NPs of Poly(lactic-co-glycolic acid) (PLGA) and PEG- PLGA NPs.
- Assess each of the mucus models in terms of mechanical strength, microscopical structure and water content, and characterise these properties such as to allow their use in future (later chapters) interpretations of NP permeation.

2. MATERIALS AND METHODS

2.a Materials

Glass bottom imaging dishes (35 mm diameter dish with a glass coverslip at 1.5 mm thick and 10mm diameter) were from MatTek Corporation (USA). Other standard chemicals such as NaCl, KCl, Na2HPO4, KH2PO4, NaOH and HCL were from Fisher scientific (Loughborough, UK). Poly(lactic-co-glycolic acid) (PLGA) and polyethylene glycol (PEG)-PLGA NPs encapsulated with Lumogen red 305 were supplied by Nanomi, Netherland as part of the FP7 Alexander Consortium.

2.b Collection of Mucus Models

Native Pig Intestinal Mucus "Cardiff Native Mucus" Model

Freshly isolated pig intestinal ileum (2 m in length from proximal region) was obtained from a local abattoir (Cardiff) and kept in ice-cold oxygenated phosphate buffered saline (PBS) (no longer than 1 hr) prior to sample processing. The ileum was processed into 25 cm lengths with each length cut longitudinally to allow intestinal food and other waste debris to be gently rinsed away from the intestinal surface using ice-cold PBS. The mucus was then harvested by an approach described previously [41], and one recognised to optimise the yield of not only the loose mucus layer but critically also a high content of the adherent mucus layer. Simply, it involved gentle scraping of the mucus from the intestinal surface using a wooden spatula while at the same time avoiding the shedding of significant intestinal epithelial tissue. The mucus collected was divided into aliquots (0.5 gm) and kept at -20 °C prior to experimentation [42].

Processed Intestinal Mucus "Consortium Mucus Gel" Model

Freshly isolated pig intestine was collected and cross-sectionally cut into 25 cm length pieces. The intestinal content from each of the 25 cm intestinal pieces was squeezed or

'milked' into a container. This sample of intestinal content was then mixed with 0.1 M NaCL (saline) at a ratio of 1 gm to 5 ml saline, and the mixture was gently stirred for one hr at 4 °C afterwhich it was centrifuged at 10,400 g at 4 °C for one hr. The supernantant was discarded and the granular material (food debris) removed from the bottom of the tube. The process of washing and centrifugation was repeated once more and the supernantant and any residual food debris were removed again. The remaining mucus was divided into aliqouts and kept at -20 °C for further analysis.

2.c Measurement of pH of Mucus

The pH of both the mucus models was measured in triplicate using a pH meter (Orion 410A, USA). For the 'mucus gel' model, the pH was measured before the last centrifugation step since the immersion of the pH probe into the mucus sample was not possible after the final centrifugation step due to the stiffness of this sample.

2.d Measurement of Water Content of Mucus

The water content was measured in triplicate for the both mucus samples. Simply, 0.5 gram of each mucus sample was weighed and freeze-dried (Scanvac, Denmark) for three days. The weight of the sample was measured again after lyophilisation and the difference in weights (pre- vs post- freeze-drying) was expressed as a %loss representing the original water content of the sample.

2.e AFM Imaging of Mucus

This study was carried out by the group of Dr Polina Prokopovich at Cardiff School of Pharmacy and Pharmaceutical sciences. AFM imaging (XE-100 Advanced Scanning Probe Microscope, Park Systems, Korea) was used to measure the pore size of the mucin network and to define the surface morphology of the mucus sample. Three mucus samples of each model type were scanned by the AFM non-contact mode [43].

10 images were acquired from 10 different regions within the samples so as to cover the whole mucus sample. Images were obtained at different formats, these are: large format of 25x25 µm, medium format 15x15 µm and small formats 5x5 µm and 2 x 2 µm. A total of 100 pores were measured for each mucus sample and the overall distribution of pore diameters was plotted. XEI analysis software was used to measure the pore diameter within each image.

2.f Rheological Studies on Mucus

The strain sweep test was conducted by measuring the elastic modulus ('Storage modulus') and the viscous modulus ('Loss modulus') in triplicate using an IR550 rheometer (TA Instruments, USA) (experiments were conducted at the University Ramon Llull, Barcelona, Spain). In this experiment, a 1 gram mucus sample accurately weighed and placed between the parallel plates' chamber in which the plate diameter is 40 mm and the gap width is 1 mm. An oscillating amplitude mode was applied at up to 95% strain in which the plateau stress curve is obtained and the Loss (G´´) and Storage (G´) moduli were recorded in Pascal. The phase angle (δ) was calculated by the equation: tan δ= (G´´/ G´) [44].

2.g. Measurement of NP Diffusion in Mucus by the MPT Technique

For NPs received from the Consortium partners they were provided either as freeze-dried powders or dispersed particles in an aqueous phase. Freeze-dried powder samples were re-suspended in the aqueous phase that was originally used by the partner. Simply, powder was weighed and dispersed in the aqueous phase to the concentration suitable to run the MPT experiment. Samples were dispersed either by vortex, sonication, magnetic stirrer or probe sonicator depending on the protocol for particles dispersion recommended by the respective partner. The PLGA and PEG-PLGA NPs received from our partner in the consortium were fluorescently labelled with Lumogen red by the

encapsulation method (0.1% w/w). NPs diffusion through intestinal mucus was assessed by the MPT technique [45] using both the 'consortium model mucus gel' and the 'Cardiff native mucus model'. Due to the varying properties of the two mucus models a number of methods were explored to disperse the NPs into the mucus matrices:

(i) Method 1. The fluorescently-labelled NPs were inoculated onto the surface of mucus. Specifically, a 25 µl aliquot of the 0.002% NP suspension was added to the surface of a 0.5 gm mucus sample (or 10 µl for 0.2 gm mucus). This dilution of NP suspension was confirmed to reproducibly avoid particles aggregation at the point of NP inoculation. To ensure effective particle distribution throughout the mucus matrix, the inoculation was immediately followed by a 2 hr period of equilibration at 37^0 C prior to capturing the movement of the NPs by MPT video-microscopy. We found this approach suitable for the Cardiff mucus model.

(ii) Method 2. - The fluorescently-labelled NPs were inoculated directly into the core of the mucus sample. This was explored as a way to distribute particles into the Consortium mucus model, where the surface addition approach described above was simply not successful. However, following analysis of the outcome for the Consortium model, an additional 'mixing' step was then added which involved a centrifugation step at 10,400 g for 15 min and removal of the supernatant corresponding to the NP loading volume of 25 µl.

Prior to the use with the Consortium model, some validation tests were performed using the Cardiff mucus model but with inoculation Method 2. Video capture involved 2-dimensional imaging on a Leica DM IRB wide-field Epifluorescence microscope (X 63 magnification oil immersion lens) using a high speed camera with a 20x digital magnification system (Allied Vision Technologies, UK) running at a frame rate of 33

ms, i.e. capturing 30 frames sec^{-1}; each completed video film comprised 300 frames. For each mucus sample approximately 120 NPs were simultaneously tracked and their movements captured. For any distinct NP species three distinct mucus samples were analysed, i.e. minimum of 360 individual NP trajectories assessed. Moreover, these triplicates measurement was repeated on three different days so as to ensure the reproducibility of the data.

Videos were imported into Fiji Image J software to convert the movement of each NP into individual NP trajectories across the full duration of the 10 sec videos. Then the movements of each particle within sequential 30 frame segments (corresponding to 1 sec intervals) were tracked throughout the 10 sec video. That is, the displacement of each particle was measured over consecutive 1 sec intervals, i.e. during the 1 sec continuous presence of the particle in the X-Y plane throughout the 10 sec video. The measurement of particles diffusion at 1 sec interval limits the impact of mucin movement upon the particle diffusion calculations [46]. The individual particle trajectories were converted into numeric pixel data (Mosaic Particle Tracker within Fiji Image J) which, based on the microscope and video capture settings, was converted into metric distance. The distances moved by each particle over a selected time interval (Δt) in the X-Y trajectory were then expressed as a squared displacement (SD). The mean square displacement (MSD) of one particle represents the geometric mean of the particle's squared displacements throughout its entire 30-frame trajectory.

MSD was determined as follows [47]:

$$MSD_{(\Delta t)} = (X_{\Delta t})^2 + (Y_{\Delta t})^2 \qquad \text{Equation 2.1}$$

In any single mucus sample experiment an MSD was calculated for at least 120 individual particles with the experiment replicated a further two times for any particle

type, i.e. at least 360 particles studied in total. For each NP type under study an "ensemble mean square displacement" (defined by <MSD>) was then determined for each of the three replicate studies. The Ensemble Effective Diffusion Coefficient (<Deff>) for a particular NP type was then calculated by:

$$\langle Deff \rangle = \langle MSD \rangle / (4 * \Delta t) \qquad \text{Equation 2.2}$$

Where 4 is a constant relating to the 2-dimensional mode of video capture and Δt is the selected time interval.

The 'tracking resolution' (σ) was measured for each NP species by gluing (cyanoacrylate-based glue) the particles to a glass bottom imaging dish followed by drying and setting of the glue matrix. Videos were captured and particles trajectories were tracked similar to the abovementioned. The σ was then calculated by two approaches: (i) independently determining X- and Y-direction displacements followed by calculating of geometric mean of the data; (ii) Calculation of the square root of MSD.

In order to provide a comparison for the respective mucus diffusion data, the determination of NP diffusion in water made. The NP diffusion coefficient (D°) in water was calculated by the Stokes-Einstein equation at a temperature of 37 C° [48]:

$$[D^\circ = \kappa T / 6\pi\eta r] \qquad \text{Equation 2.3}$$

Where κ is Boltzmann constant, T is absolute temperature, η is water viscosity and r is radius of the particle. The diffusions of all particles were also expressed as the parameter, %ratio <Deff> / [D°].

Statistical Analysis: T test was used to compare the two mucus models for their pH and water content, the same t test was used to compare the % ratio <Deff>/D° of NPs added into the mucus by method 1 and 2 with significant value of $p < 0.05$.

3. RESULTS AND DISCUSSION

In this chapter, two pig intestinal mucus models were assessed for their capacity to study NP diffusion by the MPT technique. The first model, "Consortium model" seems to fits the requirement to study the permeation of particles by the transwell chamber model since a mucus barrier with sufficient mechanical strength is needed to separate the donor and receptor compartments in the transwell chamber system. In this model, the centrifugation at high speed should form this physical gel barrier. However, suitability of this mucus gel model to study particles transport by other dynamic methods like MPT technique is doubted for many reasons.

First, centrifugation at high speed is expected to reduce the water content of this mucus model. This is an important factor that can affect particles diffusion through the mucus since the dynamic movement of particles through the mucus is carried out through the spaces filled with water in the mucin network [49]. Wine reported that reduction of water content can dramatically reduce the movement of particles through the mucus [50]. Moreover, the other effect coming from water content is the viscoelastic properties of the mucus since water content affect the elasticity of the systems under stress [51]. Regarding this point, this consortium mucus model was introduced as a gel model having the general viscoelastic characteristics of gel system; however, the less water content should have an impact on these viscoelastic properties. Lastly, processing of this mucus model could change the structure of the mucin network. To be more specific, centrifugation step involved in the preparation of this model can induce structural changing on the mucus network due to the bundling of mucin fibres [41]. For all the above mentioned, the water content, pore sizes and viscoelasticity were measured to assess the effect of processing steps on the properties of this mucus gel model.

On the other hand, the native intestinal mucus model was used in this study as a standard model representing the pig intestinal mucus [11]. What is more important, is the suitability of the native mucus model for the MPT analysis which was revealed by Crater and Carrier (2010) [52]. In their literature about studying of particles' diffusion by the MPT technique, Crater and Carrier (2010) showed a high correlation between the chemical properties of the assessed NPs and the diffusion in the native pig intestinal mucus, whereas they found no correlation between the particles' chemical properties and diffusion in the purified mucin sample (PGM) [52]. Hence, this native mucus was used to extrapolate the relation between the physicochemical properties of tested nanoparticles and their diffusion coefficients through the mucus. Also, this mucus model was assessed for its water content, viscoelasticity and e pore sizes.

3.a Measurement of pH of Mucus

This study was carried out to confirm the pH of the mucus models were within the range of pH values to be expected from the small intestine, i.e. 6.5 to 7.5 [53]. The pH of the "Consortium mucus gel" model was 6.50 (±0.05) and for the "Cardiff native mucus" model was 6.70 (±0.12) (Table 2.1). This range of pH values is in agreement with the pH range of the mucus collected from pig small intestine [47]. As described in Chapter 1, the pH of intestine is usually reported in a range rather than a specific value due to the high variability seen between studies. The non-significant difference (ca. 0.2 pH units) in the pH values between the "Consortium model" and the native mucus model may be due to the varying methods of collection and processing, i.e. the processing of the "Consortium mucus gel" model involving a 'milking' of the intestinal contents (food debris) should affect the final pH of the system.

Table 2.1: Water content and pH of the two mucus models. N = measurements taken from three separate experiments. (The difference in the data from each mucus model was compared by T test).

Biophysical test	Consortium model Mean (±s.d)	Cardiff model Mean (±s.d)	**T test** comparison of pH and water content of the two mucus models (p value)
pH	6.5 (±0.05)	6.7 (±0.12)	Non-significant (0.0561)
Water content	81.2 (±1.4)	91.4 (±0.51)	Significant (0.0003)

3.b Measurement of Water Content of Mucus

One of the main concerns about the processing strategy for the "Consortium mucus-gel" is the potential water loss due to the centrifugation and the impact of this step upon the structure of the mucin network. As is shown in Table 2.1, the water content of the "Consortium mucus-gel" was determined at 81.2 ±1.4%, while for the "Cardiff native mucus" model it was 91.4 ±0.51%. The significant difference of 10% lower water content of the processed "Consortium mucus-gel" may be expected due to the centrifugation of the intestinal mucus followed by the supernatant from which was then discarded. In contrast, the water content of the "Cardiff native mucus model" was as expected higher, essentially due to the minimal processing of the material. Indeed the water content of the "Cardiff native mucus model" is consistent with previous studies [54–56] which reported the water content of more than 90% in mucus.

The difference in water content between the two models is also reflected in their contrasting physical appearance. Figure 2.1 shows the physical appearance of the "Consortium mucus-gel" model (left) and the "Cardiff native mucus" model (right). The "Consortium mucus-gel" model appears considerably desiccated compared to the "Cardiff native mucus" model. The high water loss of the "Consortium mucus-gel" model would also likely indicate a change in the mucin network structure following centrifugation; therefore, structural analysis was explored by AFM below.

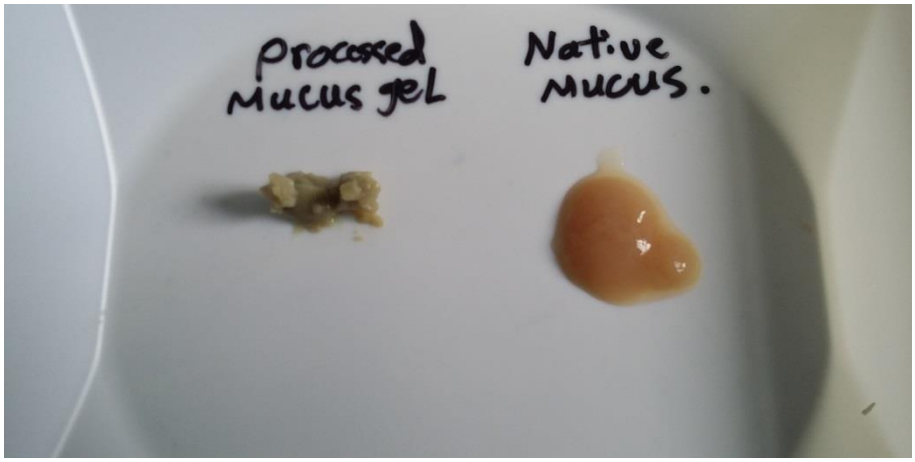

Figure 2.1: Imaging of the processed mucus gel model (left) and the native mucus model (right) showing the watery nature of the native mucus model and dried nature of the processed mucus gel model.

3.c AFM Imaging of Mucus

AFM was used to detect the morphology of the mucin fibre mesh within each of the two mucus models. AFM imaging involves less sample processing compared to electron-microscopy techniques and has resolving power to the nanometre range [57]. Figure 2.2A shows the surface morphology and the pores within the mucin network of the "Cardiff native mucus" model displayed as large-field (25x25 µm), medium-field (15x15 µm) and small-field (5x5 µm) AFM images. Figure 2.2B shows a histogram of the size distribution of these pores determined from over 98% of all of the pores within imaged by the AFM.

The data shown in Figures 2.2A and 2.2B show the pore population to be comparatively heterogeneous with an approximate 7-fold range in the pore size (diameter) between 60 nm to 400 nm, but with a distribution defined by more than 50% of pore size below 200 nm and a mode of 300 nm. Moreover, it can be seen that 33% of the pores sizes are between 300 to 400 nm. The large macro-porous spaces (above 400 nm) comprised ca. 2% of the total size distribution. The heterogeneity is isotropic within all the areas of

this mucus model which has also been reported previously where the system has been defined as symmetrically heterogeneous [58,59].

As described in chapter 1, the pore characteristics in the Cardiff native mucus model are consistent with other mucus model in term of average pore sizes (ca. 200 nm) and the presence of small ratio of large pores sizes [40,60]. This may not be that surprising as the mucus harvesting approach adopted for the Cardiff model is one recognised to contain some of the loose layer and the adherent mucus layer [41,61] and as such, our approach will naturally lead to a heterogeneous but realistic data.

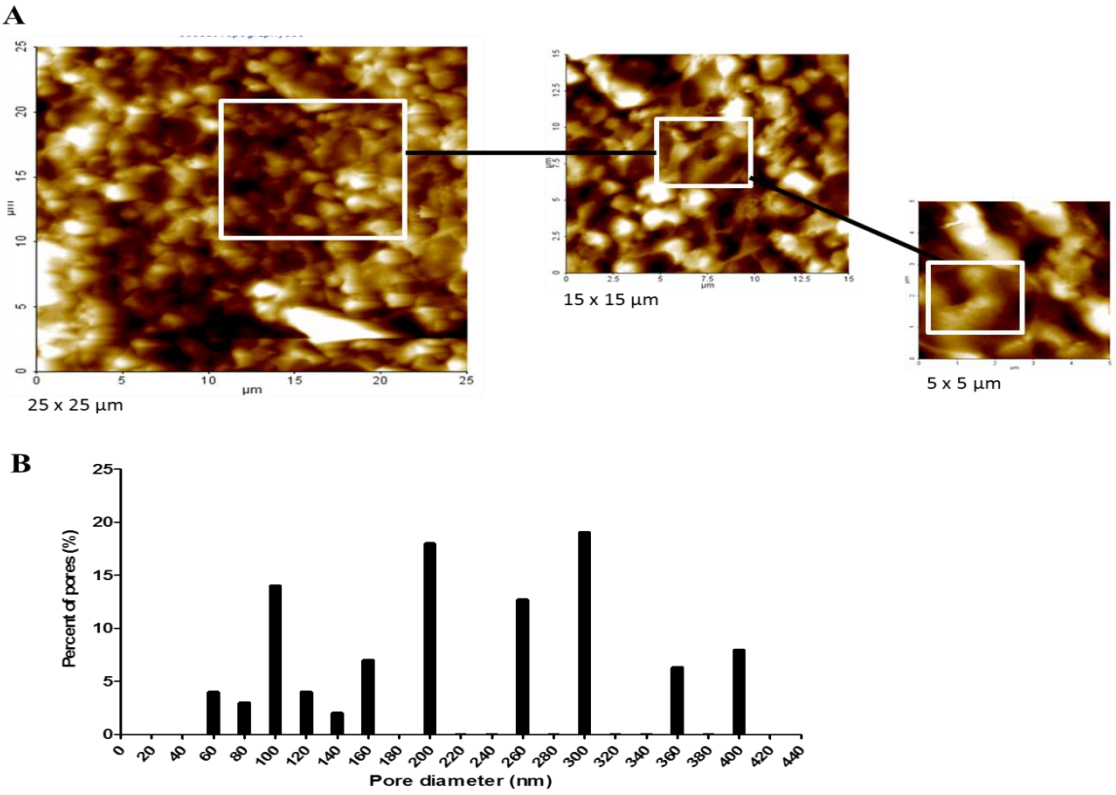

Figure 2.2: AFM imaging of the "Cardiff native mucus" model. (A) AFM surface morphology of the mucus with large (25x25 µm), medium (15x15 µm) and small (5x5 µm) field images of the network of pores; (B) size distribution of over 98% of all visible pores within the mucus.

In comparison AFM imaging of the "Consortium mucus gel model" (Figures 2.3, 2.4, 2.5) revealed the impact of the processing steps on the mucin network. The figures illustrate the mucus gel model to be anisotropic system with different morphologies

within different sites in the mucin network. To be specific, three different morphologies were detected within the "Consortium mucus gel model". Firstly, Figures 2.3A and 2.3B show two different areas within the mucus gel at 10 x10 µm and 25 x 25 µm frames, respectively. These figures highlight areas within the "Consortium mucus gel model" in which very large pores in the mucin network are seen to dominate, with the size of these voids reaching up to 5 µm and 8 µm respectively. Figure 2.3 also shows large mucin aggregates surrounding the large pores. These aggregates may play an important role in the physicochemical properties of the mucus-gel.

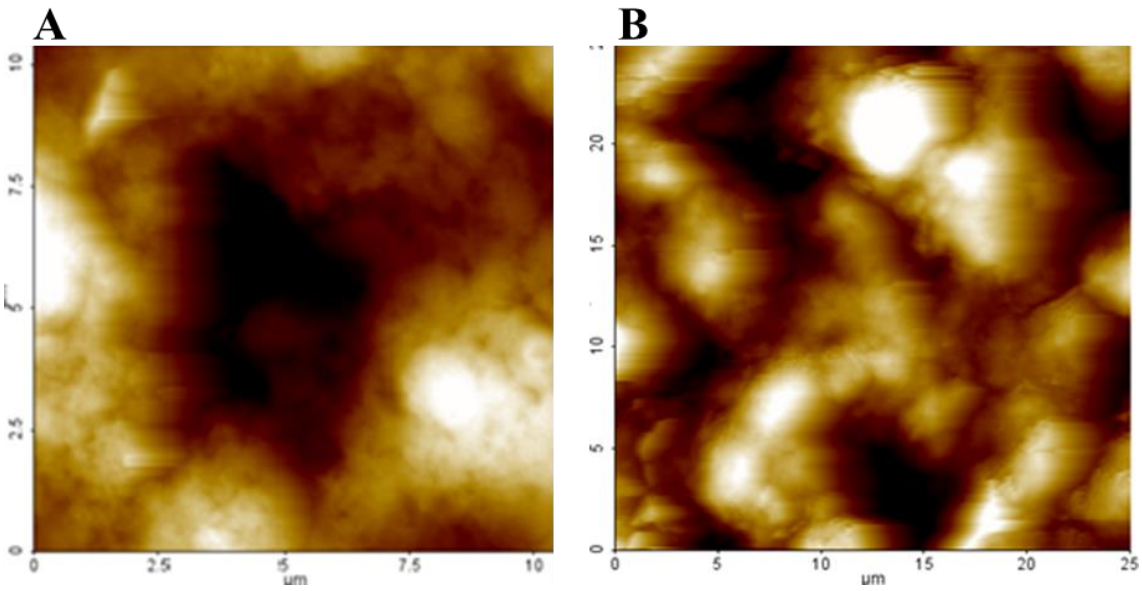

Figure 2.3: AFM imaging of the "Consortium mucus gel" model. (A) AFM surface morphology of the processed mucus gel model at a scale of (10x10 µm) showing a 5 micron pore at one site in the mucus (B) AFM surface morphology of the mucus at a scale of (25x25 µm) showing 8 micron pores at another site in the mucus.

These mucin aggregates were evident throughout the mucus gel model. For example, Figure 2.4 shows large mucin aggregates with sizes up to 5 µm (black arrows). Figure 2.4 also shows that the mucin aggregates are separated by channels and spaces (red arrow), the diameter of these channels are around 40-80 nm. Figure 2.5 shows also the

bundling of mucin fibres into thick cables separated by channels (red arrows) with an average width of 100 nm.

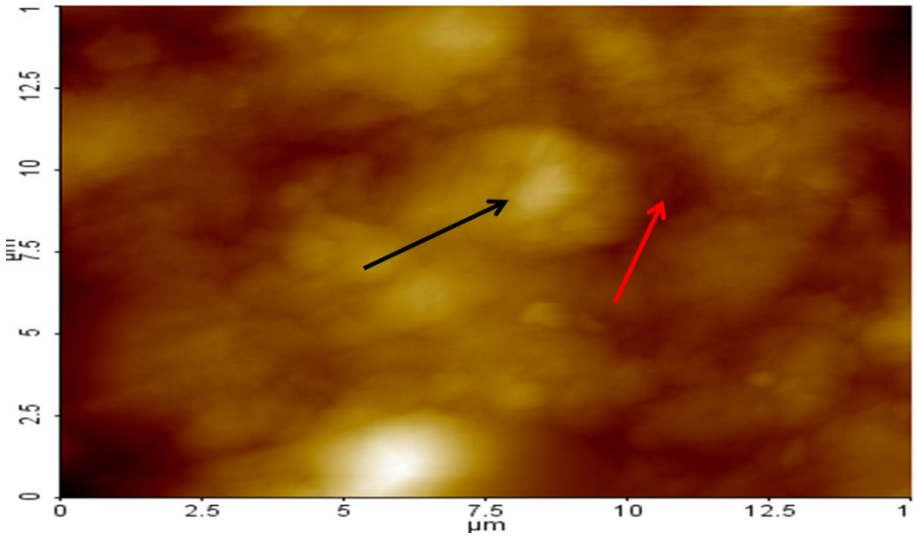

Figure 2.4: AFM imaging of the "Consortium mucus gel" model at a scale of (15x15 µm) showing a 5 micron aggregated mucin fibres at one site in the mucus (black arrow) and channels separated these mucin aggregates (red arrow).

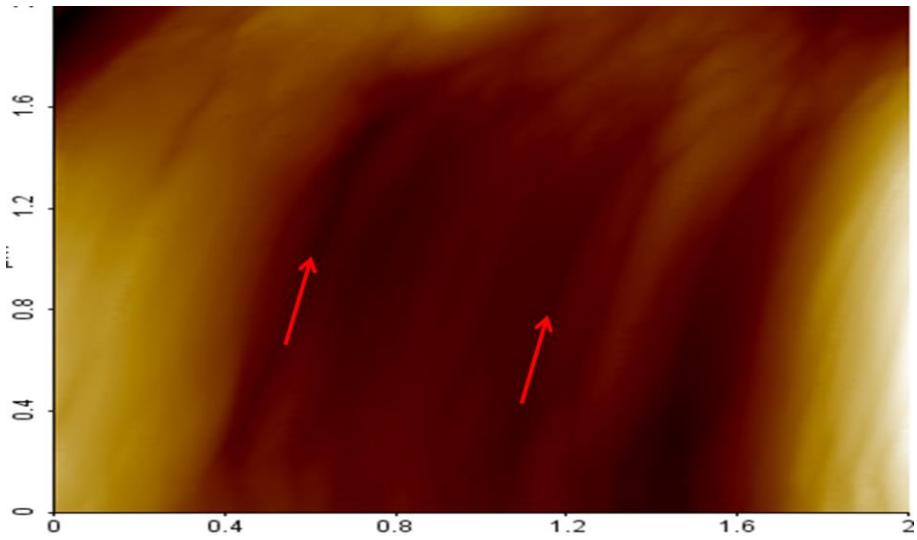

Figure 2.5: AFM imaging of the "Consortium mucus gel" model at a scale of (2x2 µm) showing the mucin fibres bundling into thick cables.

Although small pores were evident within the mucin aggregates of the "Consortium mucus gel" model, they were below the resolving power of the AFM. This inability to quantify pore sizes within the aggregated mucus-gel clusters will compromise the full

value of plotting a pore size distribution diagram similar to the one generated for the "Cardiff native mucus" model. Specifically, the pore size distribution produced will ignore the spaces that we are unable to measure.

The structural features of the "Consortium mucus gel" model were to a large extent dependent upon the mucus processing methodology, specifically the centrifugation of the harvested mucus material. Centrifugation at high speed will lead to collapse of the mucin network leading to the aforementioned sizeable aggregates of compacted mucin fibres, within which are very small pores, but as a consequence of collapse of the network, the gel contained numerous large inter-fibre pores.

Previous studies showed that these aggregates and bundles of mucin fibres are stable in the mucin network and not re-annealing to its original morphology due to the formation of hydrophobic interactions among the mucin fibres within these aggregates [62,63]. These interactions expected to increase in frequency as the mucin network undergoes external pressures such as those imposed by centrifugation to bring the mucin fibres close enough to form hydrophobic interactions. The above is also consistent with the lack of capacity to retain water content in the "Consortium mucus-gel" model. That is the collapse of polymeric network forms a macro-porous spacing allowing the water to be more easily extracted from the mucus and hence the greater water syneresis and loss from the system [64,65].

The structural changes described above for the mucin network in both the "Cardiff native mucus" model and the "Consortium mucus-gel" model will likely have differential effects upon the diffusion of particles, although it is difficult to predict how the mucin structures will affect diffusion. The studies below using MPT represent an excellent experimental system to reveal the effect of the large pores, clusters aggregations and mucin bundles on particle diffusion.

3.d Rheological Studies on Mucus

The two mucus models in this study were prepared using distinctly different methods. While both are gels, the Consortium model was produced mainly with the aim for use by the Consortium as high mechanical strength gel able to be used in Transwell permeation chambers studies, a requirement of this model is that the mucus is able to serve as a layer placed upon porous polycarbonate membranes. The Cardiff native mucus model is a gel system also but with obvious mechanical properties that differ from the Consortium model [66]. This difference in the gel structure between the two models can be explored through study of their viscoelastic properties using rheology methods, and in particular conduct strain sweep tests to measure the G′ versus the G″ in response to the applied oscillating strain.

Figure 2.6 shows that both mucus samples were tested within the % strain range of 12 to 95 across which the "Cardiff native mucus" develops a plateau response in the G′ and G″ parameters. The strain sweep test showed both models to possess a gel structure defined by G′ values that were higher than the G″ values within the plateau region [67]. Figure 2.6A shows that the "Cardiff native mucus" displayed a plateau curve with a range of G′ values between 100 and 150 Pascal and a range of G″ values between 25 and 30 Pascal at the % strain range of 12% to 95%. Moreover, the "Cardiff native mucus" model exhibited a phase angle (δ) range of 14.82 to 16.22° with an average of 15.36, which is another indication of the viscoelastic gel property of this model; an elastic gel is defined as a system having a δ of less than 45° [68].

In contrast the "Consortium mucus-gel" model was expected to have higher mechanical strength due to compacting of the mucin fibres. This model showed a linear viscoelastic region within the % strain range of 12 to 78%. Within this linear viscoelastic region, the set of G′ and G″ values of this mucus model were much higher than that of the "Cardiff

native mucus". Specifically, the G′ values of the "Consortium mucus-gel" model were higher by almost 300 Pascals compared to that of the native mucus. This high elasticity of the processed mucus gel is due to the fibre bundling, as observed by the AFM imaging. Fibre bundles are reported to lead to higher mechanical and elastic behaviour of the mucus [62].

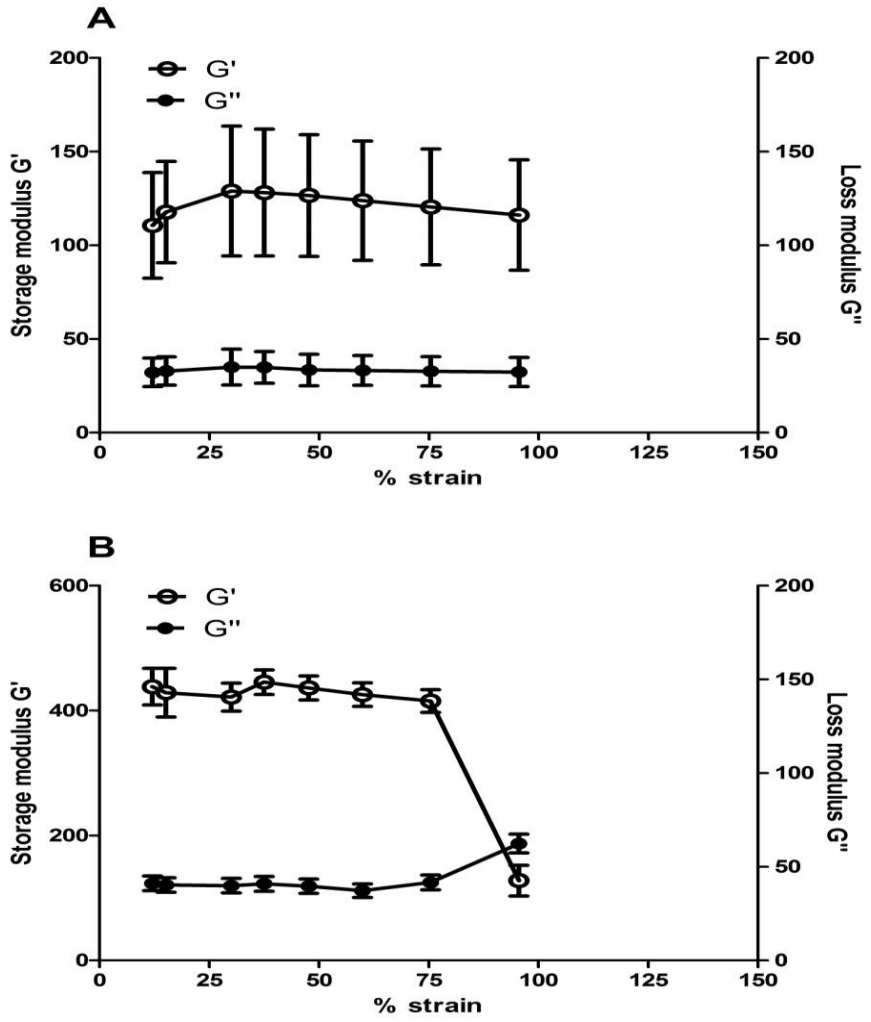

Figure 2.6: Strain sweep test within the % strain range of 12 to 95%. (A) "Cardiff native mucus" which shows a linear viscoelastic region at the % strain range of 12 to 95. (B) "Consortium gel mucus" model which shows a critical breaking point at a % strain of 78.

Moreover, the viscoelastic region of the "Consortium mucus-gel" model is followed by drop off of the G′ and an increasing of the G″ until these moduli cross at a 95% strain indicating the breaking down of the system (Figure 2.6B). This break down of the mucin structure at a strain value lower than "Cardiff native mucus" model is due to former having a reduced water content that makes the mucin fibres less flexible and more susceptible to breakage when the strain level increases [69].

3.e Assessment of Particles' Diffusivity through the Intestinal Mucus

This study was carried out to assess and validate the MPT technique for the measurement of particle diffusion through the mucus barrier, and to examine two distinctly different mucus models in terms of their suitability for this objective. In this validation work two types of particles were selected, i.e. NPs of PEG-PLGA and PLGA alone, which represent examples of fast and slow permeating NPs, respectively. Previous MPT studies have showed that PEGylation of PLGA core NPs improves the diffusion of the essentially non-diffusive PLGA NPs through the muco-inert nature of the PEG [70,71].

There are various elements which can affect the tracking of movement of NPs by MPT technique. These include, the fluorescent dye associated with the NP, the microscopy settings and the experimental procedures involved in the addition of the NPs into the biological sample (mucus).

Selecting the appropriate fluorescent dye is obviously critical for the specific visualisation of fluorescently labelled particles. Specific visualisation of the particles enables the specific tracking of particle movement through the mucus rather than any other endogenous mucus components. The fluorescent dye should thus have fluorescence characteristics that differ from the mucus auto-fluorescence. Mucus has a

high intensity excitation-emission spectrum of 280-340 nm [72]. For this reason, selected NPs (PLGA, PEG-PLGA) were loaded with a dye having higher emission-excitation spectrum. Lumogen red 305 was selected as the dye. It has a high stable excitation-emission spectrum of 573-613 nm [73]. It was encapsulated into the NPs to eliminate as much background signal from soluble dye leaching to the mucus matrix. Lumogen red 305 was encapsulated at a concentration of 0.1% into the selected particles. Specificity and efficiency of Lumogen red 305 was tested by examining for fluorescence in mucus before and after the addition of the fluorescently labelled NPs. Mucus was placed in the glass bottom imaging dish and examined using Epifluorescence microscopy at the excitation-emission range of Lumogen red (573-613nm).

In the absence of Lumogen red 305 NPs, there was no fluorescence observed from the mucus sample alone. However, following addition to the mucus of fluorescently labelled NPs encapsulating 0.1% Lumogen red 305, the signals obtained were very bright against the mucus's blank background and the signals showed high photo-stability. Indeed, photo-stability against fluorescence bleaching for particles loaded with Lumogen red 305 has been reported by other groups [73,74].

The microscopy settings including the objective of lens, the camera speed and the position of sample in the microscopy have a direct impact on the temporal, spatial and tracking resolution. In this study we used a lens with a 63X objective in conjunction with a digital magnification system of 20X as part of the high speed camera (30 frames per sec). With these settings, the temporal resolution was 0.033 ms and each pixel within the frame equal to 154 nm and each point spread function was 200 nm. This allows Image software to track very small particles and generate a high accurate spatial tracking due to the spreading of the light over more than one pixel. Spatial tracking is

controlled by the tracking software (Image) which can detect any change in the position of the fluorescently labelled particles with sensitivity of parts of pixels.

Moreover, the tracking resolution (σ) was measured to identify the minimum detectable displacement resulted by wiggling of trapped particles. The σ was measured for each NP type individually by gluing the particles into the glass bottom dish as described in the methods section and shown in Figure 2.7. The proper setting of microscopy produces an σ from 5 to 10 nm [75]. In this study, the σ for the PLGA and PEG-PLGA NPs was found to be 5 nm. Indeed, the geometric mean of the displacements of these tracked particles was around 5 nm but approximated to 5 nm (5.3 and 4.2 for the PEG-PLGA and PLGA NPs, respectively). This indicates that the microscopy setting was appropriate and measurement of particle diffusion could be carried out with high tracking resolution.

Figure 2.7: Measurement of σ by gluing the particles into the glass bottom dish.

Experimental procedures involving the preparation of the mucus sample and the manner by which the fluorescently labelled NPs are added to the mucus are also obviously very influential factors. Use of two different mucus models requires individualisation of the experimental procedures for each model. As described in the AFM study, the "Consortium mucus gel" model showed various structural regions which seemed anisotropic in nature. Also, the lower water content of the processed mucus gel model made the sample very rigid (Figure 2.1, page 16, mucus gel model

seemed to have solid appearance with high rigidity). In contrast the "Cardiff native mucus" model is a soft gel in which the water content is high. These structural characteristics will not only affect particle diffusion but also the initial addition of particles into the mucus sample prior to imaging.

The addition of a suspension of NPs onto the surface of the "Consortium mucus gel" model resulted in the formation of a precipitated layer of these particles on the surface of the processed mucus gel (Figure 2.8). It appeared that the particles were unable to penetrate the rigid mucus gel model which resulted in their precipitation rather than distribution into the mucus matrix itself. However, while this is totally unsatisfactory outcome for the performance of MPT, it appeared to satisfy the needs of the Consortium for conducting Transwell permeation studies across mucus. That is, the highly compact nature of this mucus-gel model affords its layering onto a Transwell membrane with reduced a tendency (but not totally devoid) of leakage of the material through the Transwell membrane pores into the receptor chamber [76]. The low water content of this mucus model (81%) is balanced by the water absorbed from the receptor media in the chamber system. This absorbed water could be responsible to increase the water content of this mucus up to the normal level (> 90%) which can improve particles diffusion through this mucus model. Thus, in the transwell chamber system, the mechanism of particles movement into the receptor compartment could be a mix of diffusion and convection within the moving mucus downstream.

On the other hand, for the setting of MPT method, NPs addition into the mucus sample was performed by 2 different methods due to the presence of 2 different mucus models. In the first method, NPs suspension was added onto the surface of mucus layer; hence, this method involves 2 processes which are: particles penetration and distribution into the mucus outer layer followed by particles diffusion through the mucus layer. Particle

penetration through the mucus outer layer is governed by the difference in the interfacial tension between the NPs suspension and the mucus which depends upon the particles' charge and solubility in each media [77]. Thus after the addition of particles, their initial distribution within the mucus is directly related to the interfacial tension and not related to the diffusion of particles through the mucus which depends essentially on the steric hindrance and electrostatic interaction of mucus components with the particles [78].

Specifically, the low water content of the "Consortium mucus gel" model negates penetration of the particles across the mucus layer. In contrast, the properties of the "Cardiff native mucus" model afforded the simple addition of a suspension of NPs onto the surface of the mucus (Method 1) with the subsequent diffusive dispersion of the particles throughout the mucus sample, as recognised by Wang et al. (2011) [63] and others [12]. Thus for the "Cardiff native mucus" model, the inoculation process of NPs (e.g. PLGA and PEG-PLGA NPs suspensions) involved the simple surface addition of the NPs to the mucus sample followed by a two hr period of equilibration after which the fluorescent particles appeared to be distributed thoroughly in the mucus sample.

However, as described above, the simple NPs inoculation was amenable to the "Cardiff native mucus" model, but was not appropriate for the "Consortium mucus-gel" model. Hence, for the Consortium mucus gel samples, another method (Method 2) was explored whereby the NPs were directly inoculated into the core of the mucus sample, i.e. the idea being to bypass the issues of the interfacial tension barrier in the Consortium model preventing access of the NPs to the core of the mucus matrix.

Prior to use in the "Consortium processed mucus-gel" model, Method 2 was initially tested using the "Cardiff native mucus" model. Specifically, the movement of PLGA and PEG-PLGA NPs within the Cardiff native mucus model was assessed using MPT

following NP inoculation by: (i) simple addition of a suspension of NPs onto the surface of the mucus sample "surface inoculation" (Method 1) (ii) inoculation of the NPs into the core of the mucus sample (Method 2). In both cases, small volumes of the NP suspension (25 µl) were added to 0.5 gm of the "Cardiff native mucus" sample followed by a 2 hr equilibration period prior to MPT. The MPT analysis revealed no significant difference in the diffusivity of test particles, PLGA and PEG-PLGA NPs, between the two inoculation methods (See below in Table 2.2).

However, the use of the inoculation Method 2 with the "Consortium processed mucus gel" model resulted in the appearance (Epifluorescence microscopy) of large channels in the mucus through which the NPs were freely moving in a directional manner. This was interpreted as a lack of homogenous mixing of the NPs within the mucus sample especially as these channels did not disappear even after the 2 hr equilibration period. The channels arose due to a hydrodynamic phenomenon whereby two fluids of highly different viscosity are mixed. This phenomenon is called "viscosity fingering" [79] (Figure 2.8) with the less viscous fluid (NPs suspension) penetrating the more highly viscous fluid (mucus gel) due to the convective forces of the inoculation procedure itself. This behaviour has been reported in previously in which the injection of HCL acid solution into a dispersion of gastric mucin formed channels of HCL solution throughout the mucus sample [80].

In an attempt to remove these 'viscosity fingering' channels and to ensure a more uniform distribution of NPs within the mucus sample, we incorporated one more step, i.e. after the inoculation of NPs into the core of the mucus, the samples were centrifuged (as described in methods) taking care not to alter the water content of the mucus model. Logically this centrifugation process would not have caused any more damage to the mucin network beyond that caused by the steps of centrifugation and removal of water

involved in the original processing of the mucus material. Examination of the mucus by Epifluorescence microscopy showed that the centrifugation step to disperse the particles more effectively resulted in a removal of the 'viscosity fingering' channels and with the particles appearing to be thoroughly distributed within the mucus sample.

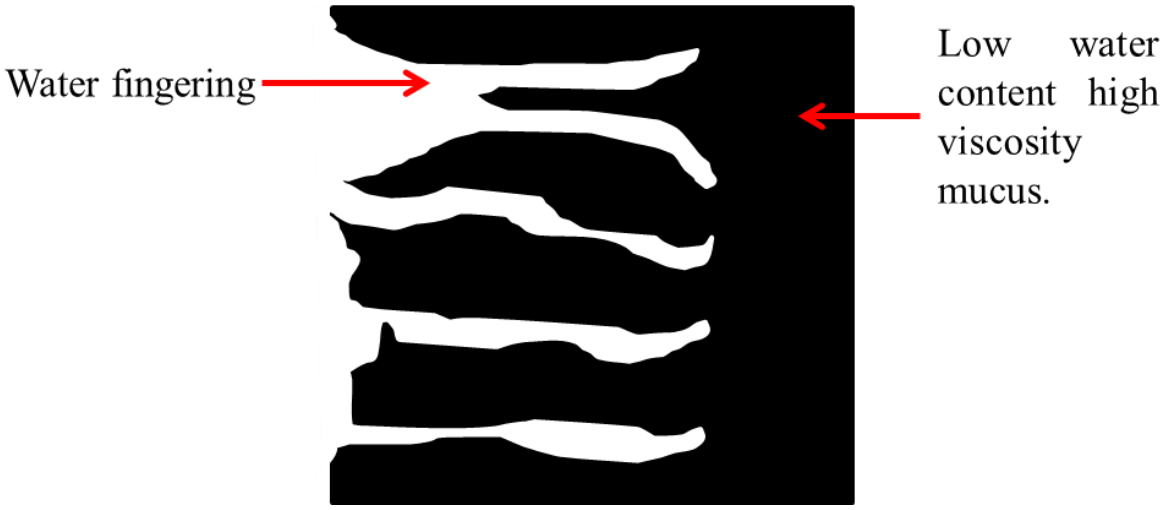

Figure 2.8: Formation of viscosity fingering from the low viscous NPs suspension that injected into the highly viscous, low water content "Consortium mucus gel" model.

Following the methods development described above, the NPs trajectories were tracked by MPT technique. Figure 2.9 shows the tracking of a number of fluorescently labelled PEG NPs in mucus. It exemplifies how the particles are being tracked in 1 video for 1 mucus sample (each NP type is examined in 3 different mucus samples, for each mucus sample, 20 videos are recorded in which each particle in this video is tracked individually). Most of the particles in figure 2.9 show high diffusion through mucus, this is represented by the area that these particles move through during the time of the video. Very few particles in figure 2.9 are shown to have low diffusivities through mucus represented by particles which moved within a limited area in the video. Thus, for the particles with pink trajectories, the total area (MSD) moved is much higher than that for particles with white trajectories. Measuring the diffusion of both particles leads to highly different diffusion coefficients for each of these particles. Since PEG NPs are

known to be highly diffusive through the mucus barrier, it can be seen that the number of particles with a high diffusion coefficient is greater than the number of particles trapped in the mucus.

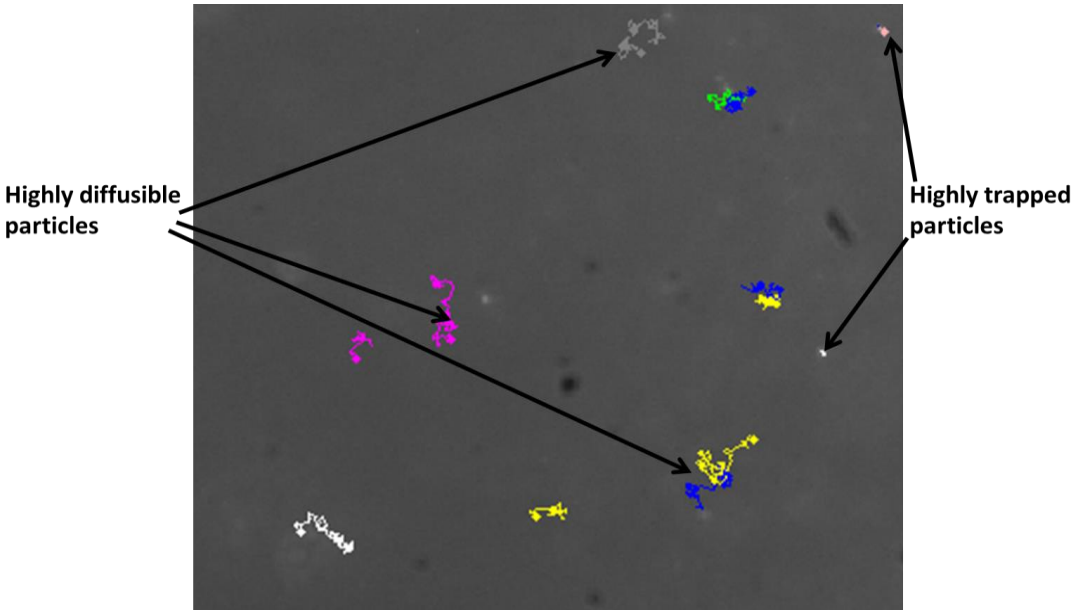

Figure 2.9: Tracking of particles by the MPT technique where the trajectories of each particle are transformed into MSD.

Table 2.2 shows physicochemical properties of the NPs, their <Deff> in mucus (cm^2 S^{-1} x 10^{-9}) and their respective D °in water (cm^2 S^{-1} x 10^{-9}). The first two rows show the diffusion data for the NPs in the "Cardiff native mucus" model using the simple surface addition of NPs suspension (Method 1) and the inoculation method into the core of NPs (method 2). The third and fourth rows of data show the diffusion for the same NPs in the "Consortium processed mucus gel" model with inoculation by direct administration into the core of the sample followed by centrifugation (Method 2).

Moreover, the table shows the ratio of the two diffusion parameters expressed as (% ratio <Deff> / D°). This ratio provides a measure of the relative efficiency of particle diffusion through mucus when the particles' intrinsic free Brownian motion in water is taken into account. As such it affords comparison of particle diffusion in mucus after

accounting for the impact of the particle's size upon its unrestricted diffusion in solution. It is essentially a measure that more directly addresses the relative impact between particles of differing surface physicochemical properties and the interactions with, and the steric hindrance of, the mucin network.

Table 2.2: Particles' composition, physical characteristics and diffusion behaviour of PLGA and PEG-PLGA NPs in the "Cardiff native mucus" model and "Consortium mucus gel" model. (PDI and S.D. are included where necessary).

Mucus model	NP Code	Zeta Potential (mV) Mean	Particle Size (nm) Mean	D° (water) $cm^2. S^{-1}$ $x10^{-9}$	<Deff> (mucus) **Method 2** $cm^2. S^{-1}$ $x10^{-9}$ Mean (± s.e.m)	<Deff> (mucus) **Method 1** $cm^2. S^{-1}$ $x10^{-9}$ Mean (± s.e.m)	**T Test** comparison of **<Deff>** from **method 1** and **2** **(P value)**	% Ratio <Deff>/D° **Method 2**	% Ratio <Deff>/D° **Method 1**
Cardiff Native mucus	PLGA	-30	161	27.91	0.00013 (±0.00002)	0.00011 (±0.00004)	Non-significant (0.4818)	0.0005	0.0004
	PLGA-15% PEG (6000)	-8.3	54	83.22	0.46889 (±0.12699)	0.48211 (±0.09876)	Non-significant (0.8937)	0.5634	0.5739
Consortium gel mucus	PLGA	-30	161	27.91	0.00010 (±0.00005)	-		0.0004	
	PLGA-15% PEG (6000)	-8.3	54	83.22	0.01396 (±0.00477)	-		0.0168	

Figure 2.10A shows the ensemble effective diffusion coefficient (<Deff>) versus particle size for each of the tested particles. Figure 2.10B shows the zeta potential of each particle versus the % ratio <Deff> / D°. In the figures, the PEG-PLGA NPs are shown in red while the PLGA NP is shown in green. Table 2.1 and Figure 2.10 illustrate in both mucus models the high diffusivity of the PEG-PLGA NP as compared to the PLGA NP. The <Deff> values in the "Cardiff native mucus" model were 0.46889 and 0.00013 for the PEG-PLGA NP and PLGA NP respectively, indicating a 3600 greater diffusion rate of the PEG-PLGA NPs. Similarly in the same mucus model when the diffusivities of the particles were compared based on % ratio <Deff>/D° values, the diffusivity of the PEG-PLGA NPs was greater by 1200 times as compared to the PLGA. This much higher diffusivity of PEG-PLGA as compared to the PLGA particles is in accordance with previous MPT studies [46,81]. This indicates that the MPT technique developed in the PhD is a sensitive one able to discriminate diffusion differences due to the chemical nature of a particles' surface; the PEGylated particles possessing a hydrophilic surface and showing a considerably greater diffusion as compared to the lipophilic surface of the PLGA NPs.

In the "Consortium processed mucus-gel" model, the PEG-PLGA NP was only x50-fold faster than the PLGA NP, substantiating that the two mucus models represented distinct properties. In the native mucus model, it is recognised that in the absence of particle interaction with the mucin fibres, then particle transport involves unhindered movement through the water filled spaces within the mucin network [82]. Accordingly, in the same native mucus model, The PLGA NP will interact with the mucin fibres through their hydrophobic properties which disabled their movement through the water-filled pores [71]. Obviously, these conditions are not the same in the "Consortium

mucus gel" model where the difference in the diffusivity between the PEG-PLGA and PLGA NPs are not that high.

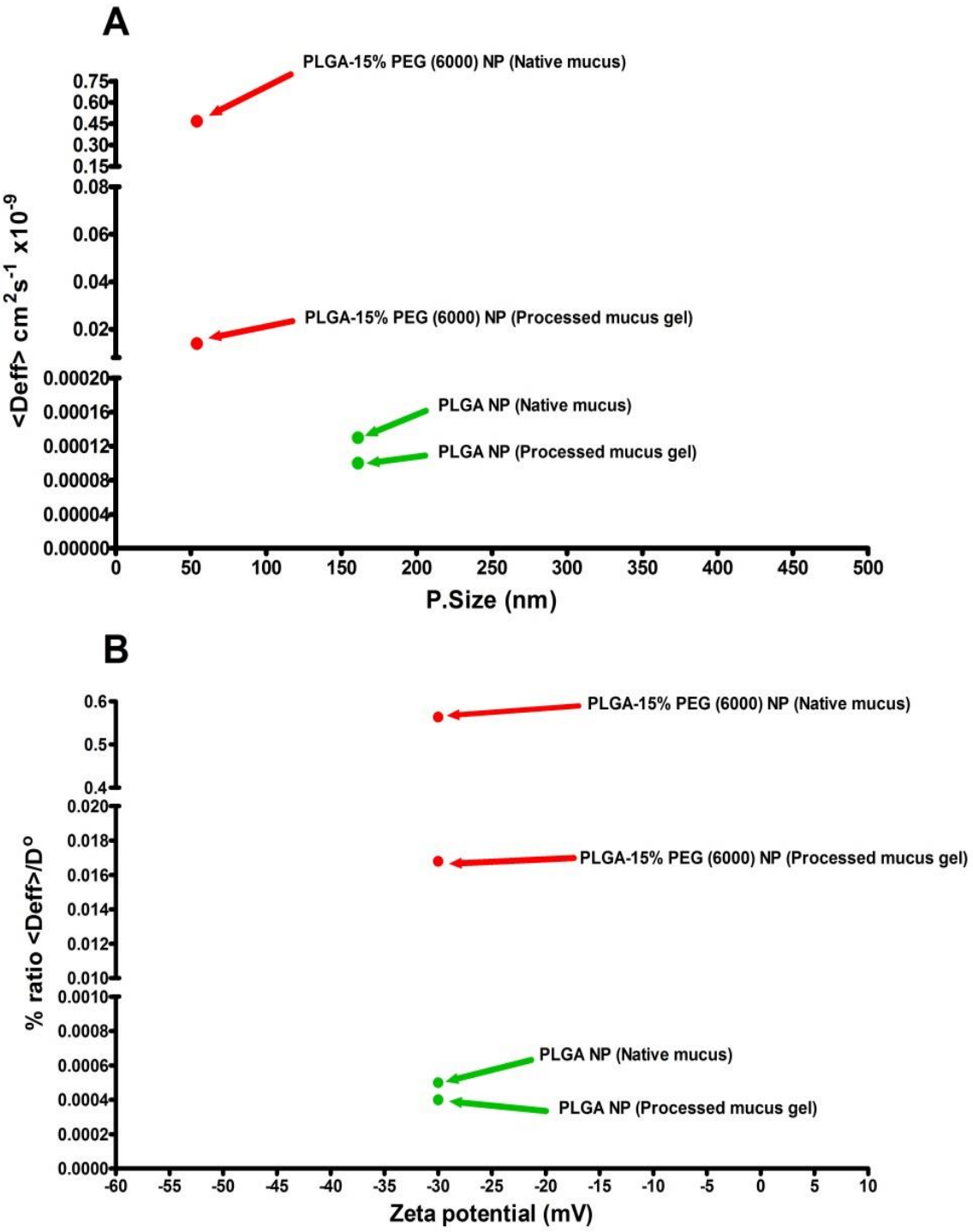

Figure 2.10: (A) Mucus diffusion <Deff> versus particle size of PLGA and PEG-PLGA NP in the both mucus models. (B) % ratio <Deff>/D° versus zeta potential of PLGA and PEG-PLGA NP in the both mucus models.

The diffusion of the PEGylated NP was 35 times faster in the “Cardiff native mucus” as compared to the “Consortium mucus gel” model. This is due almost entirely to the reduced permeation of the PEG-PLGA in the Consortium mucus. In other words, the reduced water content and ‘collapsed’ mucin structure of the “Consortium mucus gel” model limited significantly the movement of PEG-PLGA NPs through this mucus model. However, no previous MPT studies on this type of mucus gel have been conducted and further studies are required to study separately the impact of water content and the shrinkage of the mucin network on the diffusivity of particles.

On the other hand, it is important to note that the diffusion of the PLGA NPs was almost similar between the two mucus models, where the diffusivity of the PLGA NP in the “Cardiff native mucus model was higher by 1.3 times than that in the “Consortium mucus gel” model. This indicates that the diffusion of the muco-adhesive PLGA NPs was less influenced by the type of the mucus model. This could be due to the muco-adhesive nature of this NP type [83,84] such that, these particles move and adhere preferably to the mucin fibres where they stuck within the ‘normal‘ mesh network and when the water content of the mucus is high. In other words, these muco-adhesive NP behave similarly in both mucus models.

4 SUMMARY AND CONCLUSION

In this study, two different intestinal mucus models were tested to be used as a barrier for study of NPs diffusion by the MPT technique. One of the mucus models, namely, "Cardiff native mucus" model was scraped from the pig intestine without any further processing steps. The other mucus model was squeezed from intestine followed by further washing and centrifugation step to increase the mechanical strength of this model. To examine these mucus models, a group of biophysical techniques including rheological and AFM imaging were used to identify the physical, structural and mechanical properties for the both models. Moreover, MPT technique was validated for the in vitro measurement of particles diffusion through mucus models. Validation technique included the assessment of suitability of the fluorescent dye (Lumogen red), microscopy, NPs and mucus for efficient measurement of particles diffusion.

Biophysical studies revealed several differences between the tested mucus models including their water contents, structural and mechanical properties. The "Consortium mucus gel" model was found to have less water content, anisotropic and higher mechanical strength. Also, the native mucus model was more suitable for studying of particles diffusion by the MPT technique since no further steps were needed to distribute particles into the mucus samples. The MPT technique was found to be sensitive and representative for studying of diffusion of particles loaded with Lumogen.

It can be concluded that centrifugation of mucus can massively change the physical, structural and mechanical properties of the mucus system. This indicates that mucus should be used with minimum processing procedures so as to be used as a model to study particles diffusion through it. Also, for imaging of fluorescently labelled particles in mucus, a selected dye should have higher emission wave length than the auto-fluorescent emission of the mucus sample. The microscopy should be set carefully to

avoid any misleading outcomes. Finally, the MPT technique was found to be a good *in vitro* test to analyse particles diffusion through the mucus.

5. References

[1] K. Matsuo, H. Ota, T. Akamatsu, A. Sugiyama, T. Katsuyama, Histochemistry of the surface mucous gel layer of the human colon, Gut. 40 (1997) 782–789. doi:10.1136/gut.40.6.782.

[2] F.J. Fogg, A. Allen, S.E. Harding, J.P. Pearson, The structure of secreted mucins isolated from the adherent mucus gel: comparison with the gene products., Biochem. Soc. Trans. 22 (1994) 229S.

[3] D.J. Thornton, J.K. Sheehan, From mucins to mucus: toward a more coherent understanding of this essential barrier., Proc. Am. Thorac. Soc. 1 (2004) 54–61. doi:10.1513/pats.2306016.

[4] T. a. Waigh, a. Papagiannopoulos, a. Voice, R. Bansil, a. P. Unwin, C.D. Dewhurst, et al., Entanglement coupling in porcine stomach mucin, Langmuir. 18 (2002) 7188–7195. doi:10.1021/la025515d.

[5] E.Y.T. Chen, Y.C. Wang, C.S. Chen, W.C. Chin, Functionalized positive nanoparticles reduce mucin swelling and dispersion, PLoS One. 5 (2010) 1–9. doi:10.1371/journal.pone.0015434.

[6] P. Tian, M. Brandi, R. Mandrell, Porcine gastric mucin binds to recombinant norovirus particles and competitively inhibits their binding to histo-blood group antigens and Caco-2 cells, Lett. Appl. Microbiol. 41 (2005) 315–320. doi:10.1111/j.1472-765X.2005.01775.x.

[7] T.T. Kararli, Comparison of the gastrointestinal anatomy, physiology, and biochemistry of humans and commonly used laboratory animals, Biopharm. Drug Dispos. 16 (1995) 351–380. doi:10.1002/bdd.2510160502.

[8] J.R. Gum, J.W. Hicks, N.W. Toribara, E.M. Rothe, R.E. Lagace, Y.S. Kim, The human MUC2 intestinal mucin has cysteine-rich subdomains located both upstream and downstream of its central repetitive region, J. Biol. Chem. 267 (1992) 21375–21383.

[9] J. Kočevar-Nared, J. Kristl, J. Šmid-Korbar, Comparative theological investigation of crude gastric mucin and natural gastric mucus, Biomaterials. 18 (1997) 677–681. doi:10.1016/S0142-9612(96)00180-9.

[10] a W. Larhed, P. Artursson, J. Gråsjö, E. Björk, Diffusion of drugs in native and purified gastrointestinal mucus., J. Pharm. Sci. 86 (1997) 660–5. doi:10.1021 /js960503w.

[11] A.C. Groo, F. Lagarce, Mucus models to evaluate nanomedicines for diffusion, Drug Discov. Today. 19 (2014) 1097–1108. doi:10.1016/j.drudis.2014.01.011.

[12] R. Bansil, E. Stanley, J.T. LaMont, Mucin biophysics., Annu. Rev. Physiol. 57 (1995) 635–657. doi:10.1146/annurev.physiol.57.1.635.

[13] J.K. Sheehan, K. Oates, I. Carlstedt, Electron microscopy of cervical, gastric and bronchial mucus glycoproteins., Biochem. J. 239 (1986) 147–153.

[14] J.K. Sheehan, I. Carlstedt, Electron microscopy of cervical mucus glycoproteins and fragments therefrom, Biochem. J. 265 (1990) 169–178.

[15] I. Carlstedt, H. Lindgren, J.K. Sheehan, The macromolecular structure of human cervical-mucus glycoproteins. Studies on fragments obtained after reduction of disulphide bridges and after subsequent trypsin digestion., Biochem. J. 213 (1983) 427–435.

[16] I. Carlstedt, A. Herrmann, H. Karlsson, J. Sheehan, L.Å. Fransson, G.C. Hansson, Characterization of two different glycosylated domains from the insoluble mucin complex of rat small intestine, J. Biol. Chem. 268 (1993) 18771–18781.

[17] G. a Naganagowda, T.L. Gururaja, J. Satyanarayana, M.J. Levine, NMR analysis of human salivary mucin (MUC7) derived O-linked model glycopeptides: comparison of structural features and carbohydrate-peptide interactions., J. Pept. Res. 54 (1999) 290–310. doi:doi:10.1034/j.1399-3011.1999.00102.x.

[18] C. Her, W.M. Westler, T. Yang, Significance of Proline Residue on Short Mucin Peptide Interactions with Mouse MUC1 Monoclonal Antibody Studied by Saturation Transfer Difference NMR Spectroscopy, SciMedCentral. 1 (2013) 1–8.

[19] D.T.N. Chen, Q. Wen, P. a. Janmey, J.C. Crocker, A.G. Yodh, Rheology of Soft Materials, Annu. Rev. Condens. Matter Phys. 1 (2010) 301–322. doi:10.1146 / annurev-conmatphys-070909-104120.

[20] M. Gašperlin, L. Tušar, M. Tušar, J. Kristl, J. Šmid-Korbar, Lipophilic semisolid emulsion systems: Viscoelastic behaviour and prediction of physical stability by neural network modelling, Int. J. Pharm. 168 (1998) 243–254. doi:10. 1016 / S0378-5173(98)00099-4.

[21] J.R. Stokes, J.H. Telford, Measuring the yield behaviour of structured fluids, J. Nonnewton. Fluid Mech. 124 (2004) 137–146. doi:10.1016/j.jnnfm.2004.09.001.

[22] S.K. Lai, Y.-Y. Wang, D. Wirtz, J. Hanes, Micro- and macrorheology of mucus., Adv. Drug Deliv. Rev. 61 (2009) 86–100. doi:10.1016/j.addr.2008.09.012.

[23] C. Taylor, K.I. Draget, J.P. Pearson, O. Smidsrød, Mucous systems show a novel mechanical response to applied deformation, Biomacromolecules. 6 (2005) 1524–1530. doi:10.1021/bm049225i.

[24] C.T. Nordgård, K.I. Draget, Dynamic responses in small intestinal mucus: Relevance for the maintenance of an intact barrier, Eur. J. Pharm. Biopharm. 95 (2015) 144–150. doi:10.1016/j.ejpb.2015.01.024.

[25] F. Madsen, K. Eberth, J.D. Smart, A theological assessment of the nature of interactions between mucoadhesive polymers and a homogenised mucus gel, Biomaterials. 19 (1998) 1083–1092. doi:10.1016/S0142-9612(98)00037-4.

[26] R.G. Riley, J.D. Smart, J. Tsibouklis, P.W. Dettmar, F. Hampson, J.A. Davis, et al., An investigation of mucus/polymer rheological synergism using synthesised and characterised poly(acrylic acid)s, Int. J. Pharm. 217 (2001) 87–100.

[27] Y.-Y. Wang, S.K. Lai, C. So, C. Schneider, R. Cone, J. Hanes, Mucoadhesive nanoparticles may disrupt the protective human mucus barrier by altering its microstructure., PLoS One. 6 (2011) e21547. doi:10.1371/journal.pone.0021547.

[28] M.D. Wilcox, L.K. Van Rooij, P.I. Chater, I. Pereira de Sousa, J.P. Pearson, The effect of nanoparticle permeation on the bulk rheological properties of intestinal mucus from the small intestine, Eur. J. Pharm. Biopharm. 96 (2015) 484–7. doi:10.1016/j.ejpb.2015.02.029.

[29] T.J. McMaster, M.J. Miles, a E. Walsby, Direct observation of protein secondary structure in gas vesicles by atomic force microscopy., Biophys. J. 70 (1996) 2432–2436. doi:10.1016/S0006-3495(96)79813-2.

[30] a R. Kirby, a P. Gunning, V.J. Morris, Atomic force microscopy in food research: A new technique comes of age, Trends Food Sci. Technol. 6 (1995) 359–365. doi:10.1016/S0924-2244(00)89191-8.

[31] T.J. McMaster, M. Berry, a P. Corfield, M.J. Miles, Atomic force microscopy of the submolecular architecture of hydrated ocular mucins., Biophys. J. 77 (1999) 533–541. doi:10.1016/S0006-3495(99)76910-9.

[32] M.P. Deacon, S.M.C. Gurk, C.J. Roberts, P.M. Williams, S.J.B. Tendler, M.C. Davies, et al., Atomic force microscopy of gastric mucin and chitosan mucoadhesive systems., Biochem. J. 348 (2000) 557–563.

[33] P. Sriamornsak, N. Wattanakorn, H. Takeuchi, Study on the mucoadhesion mechanism of pectin by atomic force microscopy and mucin-particle method, Carbohydr. Polym. 79 (2010) 54–59. doi:10.1016/j.carbpol.2009.07.018.

[34] Z. Hong, B. Chasan, R. Bansil, B.S. Turner, K.R. Bhaskar, N.H. Afdhal, Atomic force microscopy reveals aggregation of gastric mucin at low pH., Biomacromolecules. 6 (2005) 3458–66. doi:10.1021/bm0505843.

[35] L.A. Sellers, A. Allen, E.R. Morris, S.B. Ross-Murphy, Mucus glycoprotein gels. Role of glycoprotein polymeric structure and carbohydrate side-chains in gel-formation., Carbohydr. Res. 178 (1988) 93–110. doi:10.1016/0008-6215(88) 80104-6.

[36] R. Bansil, B.S. Turner, Mucin structure, aggregation, physiological functions and biomedical applications, Curr. Opin. Colloid Interface Sci. 11 (2006) 164–170. doi:10.1016/j.cocis.2005.11.001.

[37] L.E. Bromberg, D.P. Barr, Self-association of mucin., Biomacromolecules. 1 (2000) 325–334. doi:10.1021/bm005532m.

[38] J. Perez-Vilar, Mucin granule intraluminal organization, Am. J. Respir. Cell Mol. Biol. 36 (2007) 183–190. doi:10.1165/rcmb.2006-0291TR.

[39] C. Taylor Nordgård, K.I. Draget, Oligosaccharides as modulators of rheology in complex mucous systems, Biomacromolecules. 12 (2011) 3084–3090. doi:10.102 1/bm200727c.

[40] A.I. Yudin, F.W. Hanson, D.F. Katz, Human cervical mucus and its interaction with sperm: a fine-structural view., Biol. Reprod. 40 (1989) 661–671. doi:10. 10 95/biolreprod40.3.661.

[41] R. a Cone, Barrier properties of mucus., Adv. Drug Deliv. Rev. 61 (2009) 75–85. doi:10.1016/j.addr.2008.09.008.

[42] A.W. Larhed, P. Artursson, E. Björk, The influence of intestinal mucus components on the diffusion of drugs, Pharm. Res. 15 (1998) 66–71. doi:10.1023 /A:1011948703571.

[43] E.C. Preedy, E. Brousseau, S.L. Evans, S. Perni, P. Prokopovich, Adhesive forces and surface properties of cold gas plasma treated UHMWPE, Colloids Surfaces A Physicochem. Eng. Asp. 460 (2014) 83–89. doi:10.1016 /j. colsurfa .2014.03 .052.

[44] C. Taylor, A. Allen, P.W. Dettmar, J.P. Pearson, Two rheologically different gastric mucus secretions with different putative functions., Biochim. Biophys. Acta. 1674 (2004) 131–8. doi:10.1016/j.bbagen.2004.06.007.

[45] J. Hanes, S. Lai, Compositions and methods for enhancing transport through mucus, US20100215580 A1, 2010.

[46] S.K. Lai, D.E. O'Hanlon, S. Harrold, S.T. Man, Y.-Y. Wang, R. Cone, et al., Rapid transport of large polymeric nanoparticles in fresh undiluted human mucus., Proc. Natl. Acad. Sci. U. S. A. 104 (2007) 1482–7. doi:10.1073/ pnas .0608611104.

[47] A. Macierzanka, A.R. Mackie, B.H. Bajka, N.M. Rigby, F. Nau, D. Dupont, Transport of particles in intestinal mucus under simulated infant and adult physiological conditions: impact of mucus structure and extracellular DNA., PLoS One. 9 (2014) e95274. doi:10.1371/journal.pone.0095274.

[48] J. Philibert, One and a half century of diffusion: Fick, Einstein, before and beyond, Diffus. Fundam. 4 (2006) 1–19.

[49] S.K. Lai, and J.H. , Ying-Ying Wang, Mucus-penetrating nanoparticles for drug and gene delivery to mucosal tissues, Drug Deliv. 61 (2010) 158–171. doi:10. 1016/j.addr.2008.11.002.Mucus-penetrating.

[50] J.J. Wine, The genesis of cystic fibrosis lung disease., J. Clin. Invest. 103 (1999) 309–312. doi:10.1172/JCI6222.

[51] D.P. Wolf, L. Blasco, M.A. Khan, M. Litt, Human cervical mucus. I. Rheologic characteristics., Fertil. Steril. 28 (1977) 41–46.

[52] J.S. Crater, R.L. Carrier, Barrier Properties of Gastrointestinal Mucus to Nanoparticle Transport, Macromol. Biosci. 10 (2010) 1473–1483. doi:10.1002/mabi.201000137.

[53] S.A. Galindo-Rodriguez, E. Allemann, H. Fessi, E. Doelker, Polymeric nanoparticles for oral delivery of drugs and vaccines: a critical evaluation of in vivo studies., Crit. Rev. Ther. Drug Carrier Syst. 22 (2005) 419–464.

[54] M. Juntunen, P. V Kirjavainen, a C. Ouwehand, S.J. Salminen, E. Isolauri, Adherence of probiotic bacteria to human intestinal mucus in healthy infants and during rotavirus infection., Clin. Diagn. Lab. Immunol. 8 (2001) 293–6. doi:10.1128/CDLI.8.2.293-296.2001.

[55] S. Macfarlane, E.J. Woodmansey, G.T. Macfarlane, Colonization of mucin by human intestinal bacteria and establishment of biofilm communities in a two-stage continuous culture system., Appl. Environ. Microbiol. 71 (2005) 7483–92. doi:10.1128/AEM.71.11.7483-7492.2005.

[56] E. Akat, H. Arıkan, B. Göçmen, Histochemical and Biometric Study of the Gastrointestinal System of Hyla Orientalis (Bedriaga, 1890) (Anura, Hylidae), Eur. J. Histochem. 58:2452 (2014) 291–295. doi:10.4081/ejh.2014.2452.

[57] D. Martinez-Martin, C. Carrasco, M. Hernando-Perez, P.J. de Pablo, J. Gomez-Herrero, R. Perez, et al., Resolving structure and mechanical properties at the nanoscale of viruses with frequency modulation atomic force microscopy, PLoS One. 7 (2012) 2–9. doi:10.1371/journal.pone.0030204.

[58] P. Verdugo, Supramolecular dynamics of mucus., Cold Spring Harb. Perspect. Med. 2 (2012) 1–14. doi:10.1101/cshperspect.a009597.

[59] B.S. Schuster, J.S. Suk, G.F. Woodworth, J. Hanes, Nanoparticle diffusion in respiratory mucus from humans without lung disease, Biomaterials. 34 (2013) 3439–3446. doi:10.1016/j.biomaterials.2013.01.064.

[60] S.S. Olmsted, J.L. Padgett, a I. Yudin, K.J. Whaley, T.R. Moench, R. a Cone, Diffusion of macromolecules and virus-like particles in human cervical mucus., Biophys. J. 81 (2001) 1930–7. doi:10.1016/S0006-3495(01)75844-4.

[61] R. Brunelli, M. Papi, G. Arcovito, A. Bompiani, M. Castagnola, T. Parasassi, et al., Globular structure of human ovulatory cervical mucus., FASEB J. 21 (2007) 3872–3876. doi:10.1096/fj.07-8189com.

[62] S.K. Lai, Y.Y. Wang, R. Cone, D. Wirtz, J. Hanes, Altering mucus rheology to "solidify" human mucus at the nanoscale, PLoS One. 4 (2009) 1–6. doi:10.1371/journal.pone.0004294.

[63] Y. Wang, K. Hida, R. Cone, M. Sanson, Y. Vengrenyuk, J. Liu, et al., Nanoparticles reveal that human cervicovaginal mucus is riddled with pores larger than viruses, Proc. Natl. Acad. Sci. 108 (2011) 14371–14371. doi:10.1073/pnas.1111693108.

[64] O. Okay, Macroporous copolymer networks, Prog. Polym. Sci. 25 (2000) 711–779. doi:10.1016/S0079-6700(00)00015-0.

[65] B.B. García, D. Liu, S. Sepehri, S. Candelaria, D.M. Beckham, L.W. Savage, et al., Hexamethylenetetramine multiple catalysis as a porosity and pore size modifier in carbon cryogels, J. Non. Cryst. Solids. 356 (2010) 1620–1625. doi:10.1016/j.jnoncrysol.2010.06.033.

[66] C. Atuma, V. Strugala, a Allen, L. Holm, The adherent gastrointestinal mucus gel layer: thickness and physical state in vivo., Am. J. Physiol. Gastrointest. Liver Physiol. 280 (2001) G922–G929.

[67] L. Weng, X. Chen, W. Chen, Rheological characterization of in situ crosslinkable hydrogels formulated from oxidized dextran and N-carboxyethyl chitosan, Biomacromolecules. 8 (2007) 1109–1115. doi:10.1021/bm0610065.

[68] C. Taylor, A. Allen, P.W. Dettmar, J.P. Pearson, The gel matrix of gastric mucus is maintained by a complex interplay of transient and nontransient associations, Biomacromolecules. 4 (2003) 922–927. doi:10.1021/bm025767t.

[69] C.T. Nordgård, K.I. Draget, Dynamic responses in small intestinal mucus: Relevance for the maintenance of an intact barrier, Eur. J. Pharm. Biopharm. 95 (2015) 144–150. doi:10.1016/j.ejpb.2015.01.024.

[70] M. Yang, S.K. Lai, Y.Y. Wang, W. Zhong, C. Happe, M. Zhang, et al., Biodegradable nanoparticles composed entirely of safe materials that rapidly penetrate human mucus, Angew. Chemie - Int. Ed. 50 (2011) 2597–2600. doi:10.1002/anie.201006849.

[71] T. Yu, Y.Y. Wang, M. Yang, C. Schneider, W. Zhong, S. Pulicare, et al., Biodegradable mucus-penetrating nanoparticles composed of diblock copolymers of polyethylene glycol and poly(lactic-co-glycolic acid), Drug Deliv. Transl. Res. 2 (2012) 124–128. doi:10.1007/s13346-011-0048-9.

[72] A. Agrawal, U. Utzinger, C. Brookner, C. Pitris, M.F. Mitchell, R. Richards-Kortum, Fluorescence spectroscopy of the cervix: Influence of acetic acid, cervical mucus, and vaginal medications, Lasers Surg. Med. 25 (1999) 237–249. doi:10.1002/(SICI)1096-9101(1999)25:3<237::AID-LSM8>3.0.CO;2-F.

[73] W. Zhang, J. Li, H. Chen, B. Li, Photobleaching induced time-dependent light emission from dye-doped polymer nanofibers, RSC Adv. 5 (2015) 55126–55130.

[74] K. Trofymchuk, A. Reisch, I. Shulov, Y. Mély, A.S. Klymchenko, Tuning the color and photostability of perylene diimides inside polymer nanoparticles: towards biodegradable substitutes of quantum dots, Nanoscale. 6 (2014) 12934–12942. doi:10.1039/C4NR03718A.

[75] S.K. Lai, J. Hanes, Real-time multiple particle tracking of gene nanocarriers in complex biological environments., Methods Mol. Biol. 434 (2008) 81–97. doi:10.1007/978-1-60327-248-3_6.

[76] N.N. Sanders, S.C. De Smedt, J. Demeester, The physical properties of biogels and their permeability for macromolecular drugs and colloidal drug carriers, J. Pharm. Sci. 89 (2000) 835–849. doi:10.1002/1520-6017(200007)89:7

[77] Y. Cu, W.M. Saltzman, Controlled surface modification with PEG enhances diffusion of PLGA nanoparticles in human cervical mucus., Mol. Pharm. 6 (2010) 173–81. doi:10.1021/mp8001254.

[78] M. Dawson, D. Wirtz, J. Hanes, Enhanced Viscoelasticity of Human Cystic Fibrotic Sputum Correlates with Increasing Microheterogeneity in Particle Transport, J. Biol. Chem. 278 (2003) 50393–50401. doi:10.1074/ jbc. M3090 26 200.

[79] Homsy, Viscous Fingering in POROUS MEDIA, Ann. Rev. Fluid Mech. 19 (1987) 271–311. doi:0066-4 1 89/87/01 1 5-027 1 $02.00.

[80] K.R. Bhaskar, P. Garik, B.S. Turner, J.D. Bradley, R. Bansil, H.E. Stanley, et al., Viscous fingering of HCl through gastric mucin., Nature. 360 (1992) 458–461. doi:10.1038/360458a0.

[81] Y. Wang, S.K. Lai, J.S. Suk, A. Pace, R. Cone, J. Hanes, Addressing the PEG mucoadhesivity paradox to engineer nanoparticles that “slip” through the human mucus barrier., Angew. Chem. Int. Ed. Engl. 47 (2008) 9726–9. doi:10.1002 /anie.200803526.

[82] L.M. Ensign, C. Schneider, J.S. Suk, R. Cone, J. Hanes, Mucus penetrating nanoparticles: Biophysical tool and method of drug and gene delivery, Adv. Mater. 24 (2012) 3887–3894. doi:10.1002/adma.201201800.

[83] D. Pawar, A.K. Goyal, S. Mangal, N. Mishra, B. Vaidya, S. Tiwari, et al., Evaluation of Mucoadhesive PLGA Microparticles for Nasal Immunization, AAPS J. 12 (2010) 130–137. doi:10.1208/s12248-009-9169-1.

[84] D. Pawar, S. Mangal, R. Goswami, K.S. Jaganathan, Development and characterization of surface modified PLGA nanoparticles for nasal vaccine delivery: Effect of mucoadhesive coating on antigen uptake and immune adjuvant activity, Eur. J. Pharm. Biopharm. 85 (2013) 550–559. doi:10.1016/ j.ejpb .2013 .06.017.

CHAPTER THREE

Nano-Strategies by the Alexander European Consortium to Develop Mucus Permeable NPs

1. INTRODUCTION

1.a Nanoparticle(s) as a Vehicle to Improve Mucus Permeability

As described in Chapter One, while small drug molecules can permeate relatively easily through intestinal mucus [1], orally administered therapeutic peptides and proteins are highly susceptible to degradation in the intestinal mucus layer by various protease enzymes such trypsin, chymotrypsin, and carboxypeptidase [2]. The incorporation of such therapeutic agents into a nano-delivery system can provide protection against enzymes and other environmental factors [3] [4]. However, the mucus barrier can adhere to these NPs through electrostatic or hydrophobic interactions, or simply by spatial entrapment in the mucin network [5,6]. Therefore, an appropriate NP for peptide or protein delivery should protect the cargo from mucosal enzymes [7] but not itself be trapped by the mucus [8].

Any selected NP formulation should display rapid permeation through the loose mucus layer of the intestine in order to avoid rapid clearance with the loose layer as it transits down the intestinal tract [9]. In contrast a long residence in the unstirred layer close to the epithelial surface will increase the chances of the NP to permeate the epithelial membrane or allow the release of the cargo in close proximity to the intestinal epithelial membrane [10]. As an example, when chitosan NPs were brought in contact with the epithelial barrier, these particles were found to permeate the epithelial membrane by an endocytosis process [11]; although the exact mechanism by which chitosan NPs permeate epithelial barriers is controversial. One delivery strategy that exploits some elements of the above involves the muco-adhesion of NPs that have been engineered to interact with the mucus either through electrostatic interactions (chitosan, polyethyleneimine, polylysine and polycarbophil), hydrogen bonding or simple van der Waal's forces (Eudragit) [12]. The muco-adhesion increases the residence time of the

particle close to the absorption barrier and as such the chances of increased absorption of released cargo that would have otherwise been transited down the intestinal tract.

The more specific adhesion and interaction into the intestinal mucosa has emerged through the targeting of M cells which cover the peyers patches (lymphatic follicles) in the ileum. This strategy is mainly to avoid the particles becoming trapped in the mucus since these cells are covered with only a 30 nm glycocalyx layer [13]. Various ligands such as lectin, tomato lectin, invasin and wheat germ agglutinin lectin have been used so as to target the NP to M cells through the interaction to the specific carbohydrate residues at the M cells [14].

The importance of targeting M cells vs. Enterocytes was significant when the absorption of 300 nm polystyrene NP was improved 500 folds when cultured Caco-2 cells were converted to follicle associated epithelium like cells so as to express the M cells predominantly [15]. Lectins Ulex europaeus was found to be very efficient ligand to bind the mouse Peyer's patch M-cells in the mouse gut loop model. The binding efficiency of 500 nm carboxylated microspheres to M-cells was higher by 100 times as compared to the BSA-coated microspheres [16]. Moreover, the coating of 500 nm polystyrene NP with invasin-C192 showed a high improvement of the uptake of particles through the rat intestinal epithelium [17].

Mucus not only serves as a physical barrier to trap particles by steric hindrance but a selectively permeable barrier interacting with particles depending on the surface chemistry of the particle [18]. Hence NPs designed for their mucus permeating properties are also classified depending on the nature of their surface chemistry and the mechanism of their permeation through mucus.

1.b Alexander Consortium strategies for Mucus Permeable NPs

The primary aim of the Alexander European Consortium is to produce mucus permeable NPs able to improve the intestinal bioavailability of therapeutic agents, such as polypeptides or DNA-based drugs, whose exposure to the intestinal milieu would otherwise lead to degradation. Such NPs should have the following characteristics: (i) prolonged residence time at the mucosal barrier, (ii) enhanced mucus permeation, (iii) ability to protect the cargo against enzymatic degradation, (iv) improved uptake of the NP or release of cargo at the epithelial surface.

The key requirement for particles is to be muco-diffusive, hence researchers have approached this problem using various strategies, some of which have been previously described [19]. The high diffusion of particles through mucus is afforded by escape of the particles from entrapment by either hydrophobic or hydrophilic bonding to the mucus components. This may be achieved through: (i) particles bearing an 'inert surface' that does not form any bonds with mucus, or (ii) through the reversible destruction of the mucus structure by the NP [20].

1.c Alexander Nano-Strategies to Overcome the Mucus Barrier

The following strategies were adopted by various partners within the consortium:

Slippery Surface Nano-Carriers

The concept of the slippery particles is based on previous findings demonstrating positively charged NPs form electrostatic interaction with the mucin fibres, while negatively charged NPs, while not undergoing electrostatic interaction with the mucin fibres, can form H-bonding interactions with mucus components. As a result a neutral surface presents an inert character that should afford enhanced mucus permeation [21]. An example from nature of a neutral particle surface is that of certain viruses such as the

poliovirus, the Norwalk virus and the human papilloma virus which appear to be freely permeable through mucus [22]. These viruses have no lipophilic membrane but only the capsid cover which comprises a densely-charged coat containing almost equivalent positively and negatively charged groups each separated by only a short 5 Å distance [23]. Laboratory synthesized viruses such as the cowpea mosaic virus have also shown a very high oral bioavailability [24]. However, the synthesis and stability of these viruses are associated with numerous difficulties [25,26] such that drug delivery strategies may be better developed around synthetic particles bearing similar surface characteristics to be above classified viruses.

To deliver the 'slippery surface' strategy, three techniques were utilised by Consortium partners; (1) Polyelectrolyte (PEC) NPs with densely charged surface based on the co-precipitation of oppositely charged polymers such as alginate (-ve) and chitosan (+ve); (2) PEGylation of various polymeric NPs such as PLGA, with the PEGylation carried out using different techniques and with the aim of achieving a complete coating of the selected particles by the hydrophilic PEG coat; (3) copolymerization or coating of a lipophilic polymer with a hydrophilic polymer to obtain particles in which the lipophilic core is covered with muco-inert hydrophilic electrically-neutral surfaces.

Self-Mico-Emulsifying Drug Delivery (SMEDD) Systems

Besides solid NPs, the Consortium partners investigated the appropriateness of the oil-in-water SMEDD systems. A SMEDD system forming droplets of less than 100 nm can form spontaneously when the oil phase, surfactant(s)/co-surfactant(s) and an aqueous phase are mixed together [27,28]. Friedl et al. (2013) [29] showed the influence the ingredients of the SMEDD system can have on their diffusion through mucus . The Alexander Consortium aimed to investigate the effect of different oils, surfactants and co-surfactants mixtures on the diffusion of SMEDD systems. Moreover, other mucus

permeable agents, like thiomers, were loaded into the SMEDD systems to study the potential synergistic effects with respect to mucus diffusion.

Nano-Carriers Loaded with Mucolytic Agents

Mucolytic agents released from NPs can have a significant benefit within pathological conditions adversely affecting mucus properties such as Cystic Fibrosis or Chronic Obstruction Pulmonary Disease (COPD), where the mucus may display abnormal viscoelasticity or water and DNA content [30]. There are three types of mucolytic agents that are used for the management of mucus abnormalities. These are disulfide breaking agents, proteolytic agents and DNA hydrolysing agents which work, respectively, through: the cleavage of the mucin disulfide bond, the hydrolysis of peptide bonds within the mucin fibre or the hydrolysis of the DNA responsible for mucin entanglements [31,32]. The resulting improvement of NP permeation through mucus is due to the disruption of the mucus network by the released mucolytic agents [33].

Mucolytic agents such as N-acetyl cysteine (NAC), dithiotreitol and glutathione (disulfide breaking strategy), bromelain, trypsin and papain (proteolytic enzyme), have previously been used to improve the permeation of NP through the mucus barrier [34], however, the Alexander Consortium sought to develop this strategy with by the loose release of mucolytic agents released from the 'diffusing' NPs themselves which contrasts with the established approach of exogenous parallel application of mucolytic agent which disrupt the entire mucosal tissue. The approach by the Alexander partners was exemplified through loading of NPs such as PLGA or PAA with disulfide breaking agents, in which NPs were designed to deliver a sustained release of mucolytic agents as the particles move through the mucus. Other approaches included the immobilization of proteolytic enzymes (papain and bromelain) on the surface of NPs by carbodiimide

chemistry to enable these surface attached mucolytic agents to cleave mucin fibres which come in contact with NPs.

Thiomer-Nanocarriers

This is an aligned strategy in which thiomer NPs are claimed to have mucolytic activity through the sulfhydryl molecules which interact with mucin disulfide bonds resulting in the destruction of the mucus network [9]. In the Consortium various thiol NPs and SMEDD systems were studied for their enhanced diffusion through the intestinal mucus barrier.

1.D Aim of the Study

The primary aim of this section of work was to provide quantitative and some mechanistic data on the mucus diffusion of the wide range of different NPs produced by the Alexander Consortium in order to make recommendations for in-vivo evaluation that could be done on these NPs. The MPT analysis validated in Cardiff and described in Chapter Two, became the most reliable approach within the Consortium to assess particles diffusion. Both of pig intestinal mucus models, the "Cardiff native mucus" model and the "Consortium mucus gel" model, were utilised. However, in this thesis chapter due to the enormity of NPs investigated, the focus on detailed reporting was restricted to studies using the "Cardiff native mucus" model. Appendix B, reports the diffusivities of NPs through the alternative "Consortium mucus gel" model.

A secondary aim was to see if across the wide range of particle types, some global particle parameters could still predict NP mucus permeating efficiency.

2. MATERIAL AND METHODS

2.a Materials

Glass bottom imaging dishes (35 mm diameter dish with a glass coverslip at 1.5 mm thick and 10mm diameter) were from MatTek Corporation (USA). All other reagents and solvents were purchased from Fisher Scientific (Loughborough, UK). In order to image NPs by MPT, all the NPs studied in this chapter were loaded with Lumogen red by encapsulation. The NPs were supplied by the partners in the Alexander consortium and are detailed in the respective tables in Results and Discussion section.

2.b Methods

The collection and preparation of the mucus models and the implementation of MPT were undertaken as described in Chapter 2.

Particle Preparation

Particles were received from the Consortium partners either as freeze-dried powder or as particles dispersed in an aqueous phase. Samples of freeze-dried powder were re-suspended in the aqueous phase as defined by the respective partner. Physicochemical properties of these NPs (particle sizes and zeta potential) were measured by the partners using the DLS technique and were confirmed by our group when necessary.

Diffusion Coefficient of Particles through the "Cardiff native mucus" *Barrier*

The diffusion of the NPs was studied in both the "Cardiff native mucus" and the "Consortium mucus gel" models. The detailed data for the latter is reported in Appendix B, while the data for the Cardiff model is presented here but, where approached, some general comparisons made between the two models. The NPs were classified into six

groups depending on the strategy adopted to enhance NP diffusion through the mucus barrier:

1. Slippery-PEGylated strategy: involving particles coated or copolymerized with PEG.

2. Slippery-Amphiphilic polymer strategy: involving particles comprising amphiphilic polymers with the hydrophilic polymer at the surface and the lipophilic polymer at the core.

3. Slippery-PEC strategy: involving particles comprising +ve and -ve charged polymers.

4 Self-microemulsifying drug delivery (SMEDD) systems: involving microemulsion systems in which the effects of the various ingredients were studied.

5. Mucolytic NPs strategy: involving particles loaded with mucolytic agents.

6. Thiolated NPs strategy: involving particles loaded with thiomers.

To identify and compare the diffusion of each particle and to highlight the effect of their varying surface chemistries independent of particle size, the particles were ranked from the fastest to the slowest depending on their calculated % <Deff>/D° data. Moreover, NPs within each nano-strategy were further sub-classified into sub-groups representing ostensibly the same particles made by the same partner in the Consortium but containing some formulation variables. Due to the confidential nature of the technologies made by the Consortium partners, only the variable ingredients or classes of the ingredients subject to the experiments have been mentioned.

The diffusion of NPs within each strategy was used to identify factors enhancing or reducing diffusion. Moreover, after comparison of diffusivities of NPs within each strategy, a general comparison was carried out for all NPs representing all strategies. This general comparison was done to identify the best strategy that can be used to

improve particle diffusion through the mucus. (The structures of all the polymers used by the partners in this chapter are presented in Appendix B).

3. RESULTS AND DISCUSSION

The data obtained for the diffusivity of each particle through intestinal mucus was presented in two ways. First, the <Deff> of each particle was referred against particle size to highlight the effect of size per *se*. Second, to normalise for particle size, the particle diffusion data in mucus was referenced to the particle respective data in water. In other words, by measuring the % <Deff>/D°, we normalise for the effect of particle size on the diffusion of particle through the mucus. The % <Deff>/D° of each particle was presented against the zeta potential of that particle to highlight the effect of particle surface charge (surface chemistry) on mucus diffusion.

3.a Slippery-PEGylated NP Strategy

The strategy of PEGylation of NPs has previously been found to be promising to improve the mucus permeability of NPs through normal cervicovaginal mucus [35], abnormal cystic fibrosis sputum [36,37] and pulmonary mucus [38]. The improved mucus permeability was attributed to the polyethylene units of the PEG polymer. This agrees with studies involving the coating of particles with polymers having structural similarity with PEG and which resulted in an enhancement of particle diffusion through mucus. For example, coating of PLGA NP with a low molecular weight pluronic surfactant bearing hydrophilic polypropylene oxide units generated highly mucus permeable NPs [39,40]. Hence, it is not surprising that a PEGylation strategy was adopted by a number of Consortium partners. The term (coated with PEG) is used throughout this chapter to describe all the surface modified PEGylated NPs.

Table 3.1 shows particles that were surface modified with PEG. The Table details the following: Consortium Partner; NP code (as defined by the partner); chemical composition of the particle (where known including the chemical core of the particle,

PLGA etc.); physico-chemical properties of the particle (Zeta potential and particle size); MPT diffusion data [cm^2 S^{-1} x 10^{-9}] in the Cardiff mucus model. The latter included D° water (calculated by Stocks Einstein equation), < Deff> and the % ratio <Deff>/D°; finally the rank order of the particle diffusion (i.e. 1= fastest) based on %<Deff>/D° amongst the entire screening exercise of 102 different NPs. Figure 3.1A shows the < Deff> versus the particle size data for the respective PEGylated NPs. Figure 3.1B shows the %<Deff>/D of each of the PEGylated NPs versus zeta potential. The PEGylated NPs prepared by the different partners are represented in the Table and Figures by different colours i.e. Nanomi is Red; LEK is Blue; Thessaloniki University is Green for the 50:50 PLGA: PEG formulation; Thessaloniki University is brown for the 25:75 PLGA: PEG formulation; Nevara University is Pink. For reasons related to absence of detailed formulation issues, the Evonik data is not reproduced in the Figures.

Table 3.1: Particles' composition, physical characteristics and diffusion behavior of various PEGylated NPs. (PDI and S.D. are included where necessary).

Partner	NP Code	Compositions	Zeta Potential (mV) Mean	Particle Size (nm) Mean	D° (water) $cm^2. S^{-1} x10^{-9}$	<Deff> (mucus) $cm^2. S^{-1} x10^{-9}$ Mean (± s.e.m)	% <Deff>/ D°	Ranking Fastest =1 and slowest 102
Nanomi	PLGA	Poly(D,L-lactide-co-glycolide) (50:50)	-30	161	27.91	0.00013 (±0.00002)	0.0005	99
	PLGA-15% PEG (5000)	PLGA coated with 15% methoxy PEG (MW: 5000).	-18	35	127.8	0.16823 (±0.09498)	0.1317	19
	PLGA-15% PEG (6000)	PLGA coated with 15% PEG (MW: 6000).	-8.3	54	83.22	0.46889 (±0.12699)	0.5634	4
	PLGA-10% PEG (5000)	PLGA coated with 10% methoxy PEG (MW: 5000).	-26	41	110.7	0.06458 (±0.01566)	0.0583	32
LEK	PEC- 22.5% PEG	(70:30) Negatively charged polymer+ Positively charged polymer conjugated to 75% PEG (Total ratio of PEG is 22.5%)	-28	250	17.98	0.03351 (±0.00557)	0.1864	15
	PEC- 52.5% PEG	(30:70) Negatively charged polymer+ Positively charged polymer conjugated to 75% PEG (Total ratio of PEG is 52.5%)	-12	250	17.98	0.05472 (±0.00620)	0.3045	8
	PEC- 15.0% PEG	(70:30) Negatively charged polymer+ Positively charged polymer conjugated to 50% PEG (Total ratio of PEG is 15%)	-27	250	17.98	0.01883 (±0.00230)	0.1048	20
	PEC- 35.0% PEG	(30:70) Negatively charged polymer+ Positively charged polymer conjugated to 50% PEG (Total ratio of PEG is 35%)	-15	250	17.98	0.04937 (±0.00719)	0.2747	10

Table 3.1 (Continuation): Particles' composition, physical characteristics and diffusion behavior of various PEGylated NPs.

Partner	NP Code	Compositions	Zeta Potential (mV) Mean	Particle Size (nm) Mean	D° (water) $cm^2. S^{-1} x10^{-9}$	<Deff> (mucus) $cm^2. S^{-1} x10^{-9}$ Mean (± s.e.m)	% <Deff>/ D°	Ranking Fastest =1 and slowest 108
AUTH	RG502H-PEG2000	Acidic PLGA (50:50) coated with 25% methoxy PEG (MW:2000)	-20	300	15.01	0.00368 (±0.00113)	0.0245	42
	RG502H-PEG5000	Acidic PLGA (50:50) coated with 25% methoxy PEG (MW:5000)	-14	287	15.64	0.00079 (±0.00019)	0.0050	74
	RG752H-PEG2000	Acidic PLGA (75:25) coated with 25% methoxy PEG (MW:2000)	-11	301	14.91	0.00142 (±0.00034)	0.0096	64
	RG752H-PEG5000	Acidic PLGA (75:25) coated with 25% methoxy PEG (MW:5000)	-9	261	17.21	0.00081 (±0.00011)	0.0047	75
Nevara	G-15% PEG (2000)	Lipophilic polymer coated with 15% PEG (MW: 2000)	-45	178	25.21	0.00166 (±0.00051)	0.0066	71
	G-15% PEG (6000)	Lipophilic polymer coated with 15% PEG (MW: 6000)	-47	230	19.54	0.00035 (±0.00001)	0.0018	93
Evonik	Mix 3	PLGA-PEG		120	37.45	0.03084 (±0.00771)	0.0824	26
	Mix 4	PLGA-PEG		342	13.13	0.00016 (±0.00003)	0.0013	96
	Mix 10	PLGA-PEG		424	10.58	0.06343 (±0.01313)	0.5997	3
	Mix 18	PLGA-PEG		183	24.56	0.02551 (±0.00527)	0.1039	22
	Mix 19	PLGA-PEG		171	26.28	0.11984 (±0.02907)	0.4560	6

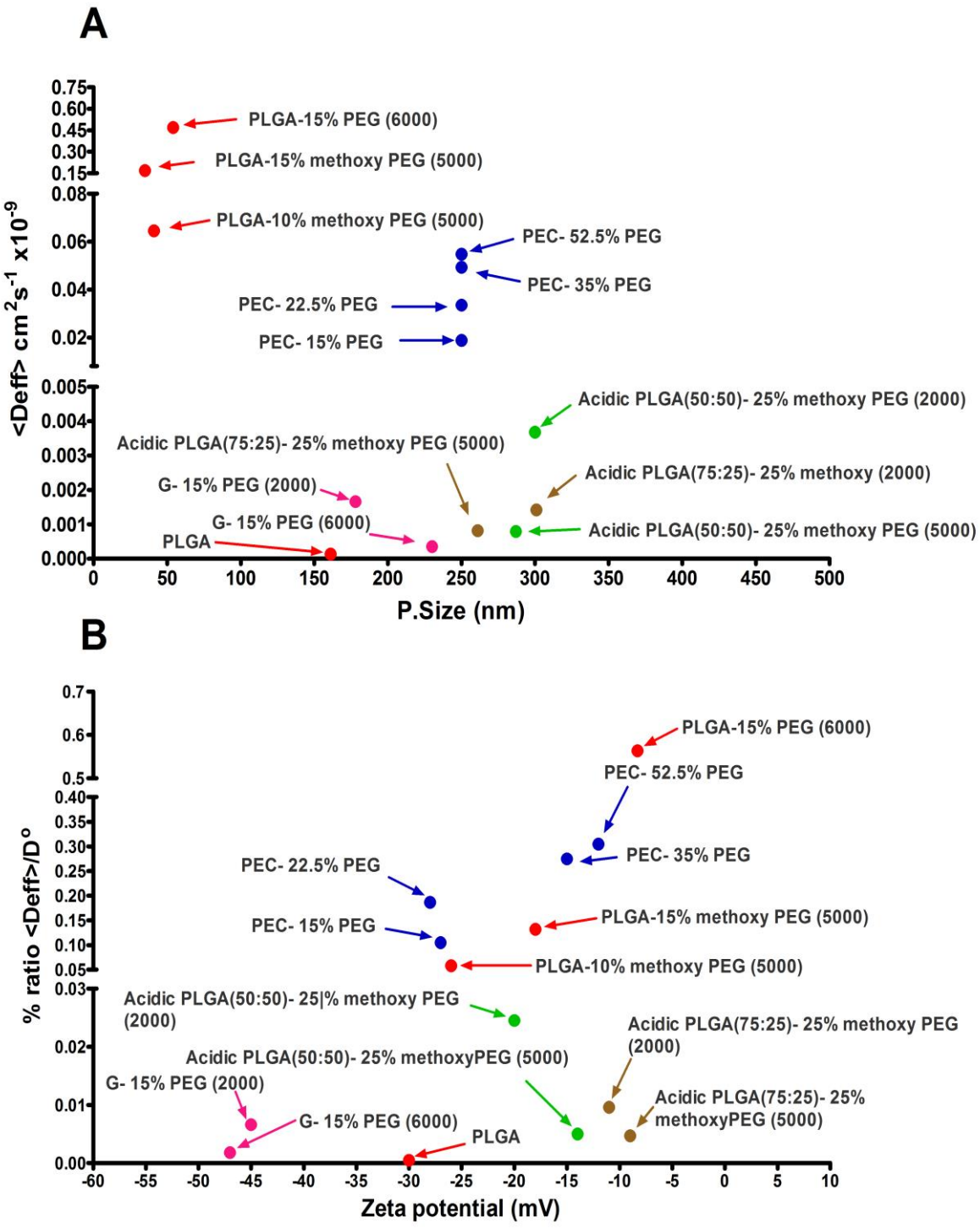

Figure 3.1: (A) Mucus diffusion <Deff> versus particle size of various PEGylated NPs in the "Cardiff native mucus" model. (B) % ratio <Deff>/D° versus zeta potential of various PEGylated NPs in the "Cardiff native mucus" model.

As can be seen from Table 3.1 and Figure 3.1, most of the PEGylated NPs in this study possessed a lipophilic PLGA core coated with PEG. PLGA is a hydrophobic biodegradable poly α-hydroxy acid polymer [41], consisting of either 50:50 or 75:25 (lactic: glycolic), respectively [42]. PLGA is widely used in the synthesis of NPs due to its capacity to load high molecular weight lipophilic drugs and for the safety of its hydrolytic components [43]. However, PLGA NPs have low diffusion through mucus due to lipophilic interactions with mucin. Hence, PLGA is often either copolymerized [44] or coated [45] with a hydrophilic polymer to improve its diffusion through the mucus barrier. Therefore, it was not surprising that the uncoated PLGA NP (red coloured symbols) showed a lower diffusivity through the mucus as compared with PLGA NPs coated with PEG (Figure 3.1).

Figure 3.1 A shows a very general trend only for increased <Deff> as the PEG particles get smaller. Indeed the impacts of the various PEG subtypes seem to have a greater effect on <Deff> however. Figure 3.1B also shows there is no global correlation between diffusion (when normalised to particle size; <Deff>/D°) and particle zeta potential. However, within each subgroup such distinctions may occur but the number of different formulations is not great enough to make any such conclusions.

A key point to make is that the variation in the diffusion of particles amongst the various sub-groups of PEG-coated NPs will also reflect differences between the pegylation chemistries between the different partners. As such for this particular mucus permeation strategy inter-laboratory comparisons should be made with caution and must be deliberately limited. For example, there is no real way for the Cardiff team to confirm the actual density of Pegylation. Previous studies have showed that the density of PEG at the surface of NPs is very influential on the diffusion of particles through mucus. Hanes et al. (2008) [46] studied the effect of the PEG density at the surface of

polystyrene NPs on their diffusion through the cervico-vaginal mucus They showed that a reduction in density of PEG polymer on the surface of polystyrene NPs from 65% to 40% resulted in a x700-fold reduction in the diffusion coefficient.

Further, it has been reported that the density of PEG coating at the surface of PLGA NPs varies depending on the conditions of coating [47]. A study by Xu et al. (2013) [48] showed that the type of the emulsifier used to coat the particles impacts upon the subsequent diffusion of the coated particles. Specifically, an increase in the molecular weight of the emulsifier resulted in a reduced diffusive capacity. Similarly, the type of particle core and the cargo itself has an effect on the efficiency of coating with PEG [49]. Nevertheless, of particular note Figure 3.1B highlights the impact of the type of PEG polymer on diffusion. Specifically, the Nanomi particles (Red symbols) show the negative influence of the methoxy functional group upon the diffusion of PLGA particles coated with PEG or methoxy-PEG. The reduced <Deff>/D° ratio for the methoxy PEG is likely due to the higher lipophilicity of methoxy –PEG polymer which can form hydrophobic interactions with mucin [50]. Indeed, Gref et al. (2012) [51] reported that conjugation of methoxy PEG polymer onto the surface of PLGA particles resulted in the positioning of the methoxy groups at the terminal position of the PEG chain which was considered to result in increased contact of the methoxy group with mucus components.

It was also noted that for the NP sub-groups represented by Brown, Green and Pink coloured symbols (Figure 3.1B) showed that the lower molecular weight PEG (2000) was at least x2-fold higher (% <Deff/D°) compared to its corresponding NP coated with higher molecular weight PEG (5000 or 6000). Previous studies on the effect of PEG molecular weight upon particle diffusion through mucus can appear contradictory. Hanes' group showed that NPs coated with low molecular weight PEG (PEG2000)

display the highest permeation compared with higher molecular weight PEG [52]. In contrast another study by the same research group showed that NPs coated with PEG 5000 possesses slightly greater diffusion than that of PEG2000 which in its own right was greater followed by PEG1000 [48,53]. On the other hand, a recent study showed no significant difference between the permeation of particles coated with either PEG 2000 or PEG 5000 [54].

The debate about the effect of the molecular weight of PEG on particle diffusion through the mucus was clarified by Cu and Saltzman (2010) [55]. Their study showed that PLGA when coated with at a low density of PEG (low ratio of PEG at the surface of particle) then the higher molecular weight PEG (PEG 10 KDa) showed the higher diffusivity through the mucus as compared to particles coated at the same density but with a lower molecular weight PEG polymer. Moreover, when PLGA particles were coated at a high density the particle with the lower molecular weight PEG (PEG 2KDa) exhibited the highest diffusivity through the mucus. It seems that higher molecular weight PEG is able to form a more complete layer on the surface of the particles at a lower PEG concentration, whereas at a higher PEG concentration, the high molecular weight PEG forms tethered chains at the surface of the NP which inter-penetrate with the mucin bio-polymer network leading to particle trapping by the mucus [56,57].

With respect to low molecular weight PEG (PEG2000) then at a high concentration of coating the PEG totally covers the particle surface by efficient positioning around the curvature of the particle [55]. Further, it appears that at very high concentrations PEG 2000 also forms tethered chains but these do not inter-penetrate with the mucin fibers and only form very weak H-bonding with the mucin [58]. Therefore at a high density of surface PEG, the PEG 2000 would show a higher diffusivity through the mucus as compared to PEG5000 or PEG 10kDa.

3.b Slippery-Amphiphilic Polymers Strategy

The slippery amphiphilic (co)polymer strategy involves the use of hydrophilic polymers rather than PEG to copolymerize or coat a hydrophobic core. Previous work by Beloqui et al. (2014) [59] has shown the impact of hydrophilic polymers such as dextran on the diffusion of lipophilic particles through a mucus barrier such as that represented by the combined Caco-2/HT29-MTX monolayers mucus model cells. Beloqui et al. (2014) showed a significant increase in the mucus permeability of solid lipid NP when it was coated with the near neutrally charged polymer mixture of dextran–protamine.

In this section of work, the polyanhydrides polymer (Gantrez) was served as the source of the hydrophobic nanoparticle core. Gantrez is a co-polymer of methyl-vinyl-ether and maleic anhydride, and it is classified as a lipophilic biodegradable poly α-hydroxy acids [41]. It was introduced as a muco-adhesive polymer due to the high capacity to form H-bonds to the mucin glycosidic chains [60]. There are many advantages for the usage of Gantrez as NP for oral delivery. These advantages are: (i) non-toxic degradation products; (ii) ease of preparation [61], and (iii) good nano-carrier capacity for various ligands and proteins [62,63]. Hence, this polymer was selected by the Alexander consortium partner (Nevara) to be used as the lipophilic core. Moreover, the hydrophilic polymers, D-mannosamine hydrochloride (D-M), low methoxylated pectin (LMPEC) and high methoxylated pectin (HMPEC) were selected to form the hydrophilic shell of the Gantrez lipophilic core by either coating to or copolymerization with the Gantrez polymer.

Table 3.2 shows particles that were surface modified with hydrophilic polymer, i.e. D-M, LMPEC or HMPEC. The Table details the following: Consortium Partner; NP code (as defined by the partner); chemical composition of the particle where known including the chemical core of the particle, Gantrez etc.; physico-chemical properties of the

particle (Zeta potential and particle size); MPT diffusion data [cm^2 S^{-1} x 10^{-9}] in the Cardiff mucus model including also D° water (calculated by Stokes Einstein equation), the <Deff> and the ratio of % <Deff>/D°; finally the rank order of the particle diffusion (i.e. 1= fastest) based on %<Deff>/D° across the entire screening exercise of 102 different particles). All the codes for particles are described in the Table and will be used throughout the section.

Figure 3.2A shows the <Deff> versus the particle size data for the respective amphiphilic polymer NPs coated or copolymerized with, i.e. D-M, LMPEC or HMPEC. Figure 3.2A shows no essentially effect of particle size on the diffusion coefficient of these particles through the "Cardiff native mucus" model. The optimum range appeared to be between 250 nm to 350 nm. The hydrophilic polymer associated with the highest <Deff> was G-5%LMPEC.

Table 3.2: Particles' composition, physical characteristics and diffusion behavior of slippery amphiphilic polymers NPs. **(Gantrez NPs Coated or Copolymerized with D-mannosamine hydrochloride)** (PDI and S.D. are included where necessary).

Partner	NP Code	Compositions	Zeta Potential (mV) Mean	Particle Size (nm) Mean	D° (water) $cm^2. S^{-1} x10^{-9}$	<Deff> (mucus) $cm^2. S^{-1} x10^{-9}$ Mean (± s.e.m)	% <Deff>/ D°	Ranking Fastest =1 and slowest 102
Nevara	NPA-L-L	Gantrez NP	-53	217	20.71	0.00167 (±0.00032)	0.0081	66
	G-1% D-M	Gantrez coated with 1% D-mannosamine hydrochloride	-40	242	18.56	0.00273 (±0.00060)	0.0147	56
	G-2.5% D-M	Gantrez coated with 2.5% D-mannosamine hydrochloride	-35	271	16.56	0.00092 (±0.00019)	0.0055	72
	G-5% D-M	Gantrez coated with 5% D-mannosamine hydrochloride	-45	263	17.09	0.01105 (±0.00276)	0.0647	30
	G-7.5% D-M	Gantrez coated with 7.5% D-mannosamine hydrochloride	-49	332	13.54	0.01247 (±0.00220)	0.0921	23
	G-10% D-M	Gantrez coated with 10% D-mannosamine hydrochloride	-39	367	12.25	0.00203 (±0.00040)	0.0166	53
	G-1% CO-DM	Gantrez copolymerized with 1% D-mannosamine hydrochloride	-37	265	16.96	0.00433 (±0.00069)	0.0255	41
	G-2.5% CO-D M	Gantrez copolymerized with 2.5% D-mannosamine hydrochloride	-31	249	18.05	0.00133 (±0.00027)	0.0074	69
	G-5% CO-DM	Gantrez copolymerized with 5% D-mannosamine hydrochloride	-37	242	18.57	0.00354 (±0.00064)	0.0190	50
	G-7.5% CO-DM	Gantrez copolymerized with 7.5% D-mannosamine hydrochloride	-45	254	17.69	0.00037 (±0.00006)	0.0021	91
	G-10% CO-DM	Gantrez copolymerized with 10% D-mannosamine hydrochloride	-39	243	18.49	0.00364 (±0.00069)	0.0197	47

Table 3.2 (Continuation): (Gantrez NPs Coated or Copolymerized with low methoxylated pectin (LMPEC).

Partner	NP Code	Compositions	Zeta Potential (mV) Mean	Particle Size (nm) Mean	D° (water) $cm^2. S^{-1} x10^{-9}$	<Deff> (mucus) $cm^2. S^{-1} x10^{-9}$ Mean (± s.e.m)	% <Deff>/ D°	Ranking Fastest =1 and slowest 102
Nevara	G-1% LMPEC	Gantrez coated with 1% low methoxylated pectin	-49	340	13.22	0.04625 (±0.00882)	0.3499	7
	G-5% LMPEC	Gantrez coated with 5% low methoxylated pectin	-59	237	18.96	0.10683 (±0.02458)	0.5634	5
	G-5% LMPEC - 0.5 BSA	Gantrez coated with 5% low methoxylated pectin and loaded with 0.5% BSA	-47	174	25.83	0.00063 (±0.00003)	0.0025	86
	G-5% LMPEC- 1 BSA	Gantrez coated with 5% low methoxylated pectin, loaded with 1% BSA	-43	161	28.00	0.00507 (±0.00030)	0.0181	52
	G-5% LMPEC- 1.5 BSA	Gantrez coated with 5% low methoxylated pectin and loaded with 1.5% BSA	-41	174	25.90	0.00790 (±0.00046)	0.0305	38
	G-5% LMPEC- 2 BSA	Gantrez coated with 5% low methoxylated pectin and loaded with 2% BSA	-42	163	27.62	0.00200 (±0.00012)	0.0072	70
	G-10% L MPEC	Gantrez coated with 10% low methoxylated pectin	-53	251	17.90	0.05246 (±0.00235)	0.2930	9
	G-1% Co-LMPEC	Gantrez copolymerized with 1% low methoxylated pectin	-49	221	20.34	0.00676 (±0.00133)	0.0332	36
	G-5% Co-LMPEC	Gantrez copolymerized with 5% low methoxylated pectin	-35	221	20.34	0.00305 (±0.00097)	0.0150	55
	G-10% Co-LM PEC	Gantrez copolymerized with 10% low methoxylated pectin	-39	175	25.68	0.00075 (±0.00032)	0.0029	83

Table 3.2 (Continuation): (Gantrez NPs Coated or Copolymerized with high methoxylated pectin (HMPEC) and other Amphiphilic polymer mixture NPs

Partner	NP Code	Compositions	Zeta Potential (mV) Mean	Particle Size (nm) Mean	D° (water) $cm^2. S^{-1} x10^{-9}$	<Deff> (mucus) $cm^2. S^{-1} x10^{-9}$ Mean (± s.e.m)	% <Deff>/ D°	Ranking Fastest =1 and slowest 102
Nevara	G-1% HMPEC	Gantrez coated with 1% high methoxylated pectin	-45	239	18.80	0.00142 (±0.00030)	0.0076	67
	G-5% HMPEC	Gantrez coated with 5% high methoxylated pectin	-52	261	17.22	0.02707 (±0.00720)	0.1572	17
	G-10% HMPEC	Gantrez coated with 10% high methoxylated pectin	-46	274	16.40	0.00034 (±0.00006)	0.0021	92
	G-1% Co-HMPEC	Gantrez copolymerized with 1% high methoxylated pectin	-43	178	25.25	0.00798 (±0.00190)	0.0316	37
	G-5% Co-HMPEC	Gantrez copolymerized with 5% high methoxylated pectin	-47	157	28.63	0.00075 (±0.00017)	0.0026	85
	G-10% Co-HM PEC	Gantrez copolymerized with 10% high methoxylated pectin	-36	168	26.75	0.00065 (±0.00012)	0.0024	88
Nevara	CG-O-TH	Gantrez copolymerized with thiamine (spray dried NP)	-29	231	19.46	0.00008 (±0.00001)	0.0004	101
	G-OA-NSD	Gantrez copolymerized with octadecyl-amine (spray dried NP)	-57	227	19.80	0.00033 (±0.00006)	0.0017	94
	G-NIC	Gantrez copolymerized with nicotin-amide (spray dried NP)	-40	297	15.13	0.00054 (±0.00012)	0.0036	81
	HPCD	Gantrez copolymerized with 2-hydroxypropyl-beta-cyclodextin (spray dried NP)	-57	245	18.34	0.00041 (±0.00008)	0.0022	90
	TH-SD	Gantrez coated with thiamine NP (lyophylised)	-41	240	18.75	0.00017 (±0.00004)	0.0009	97

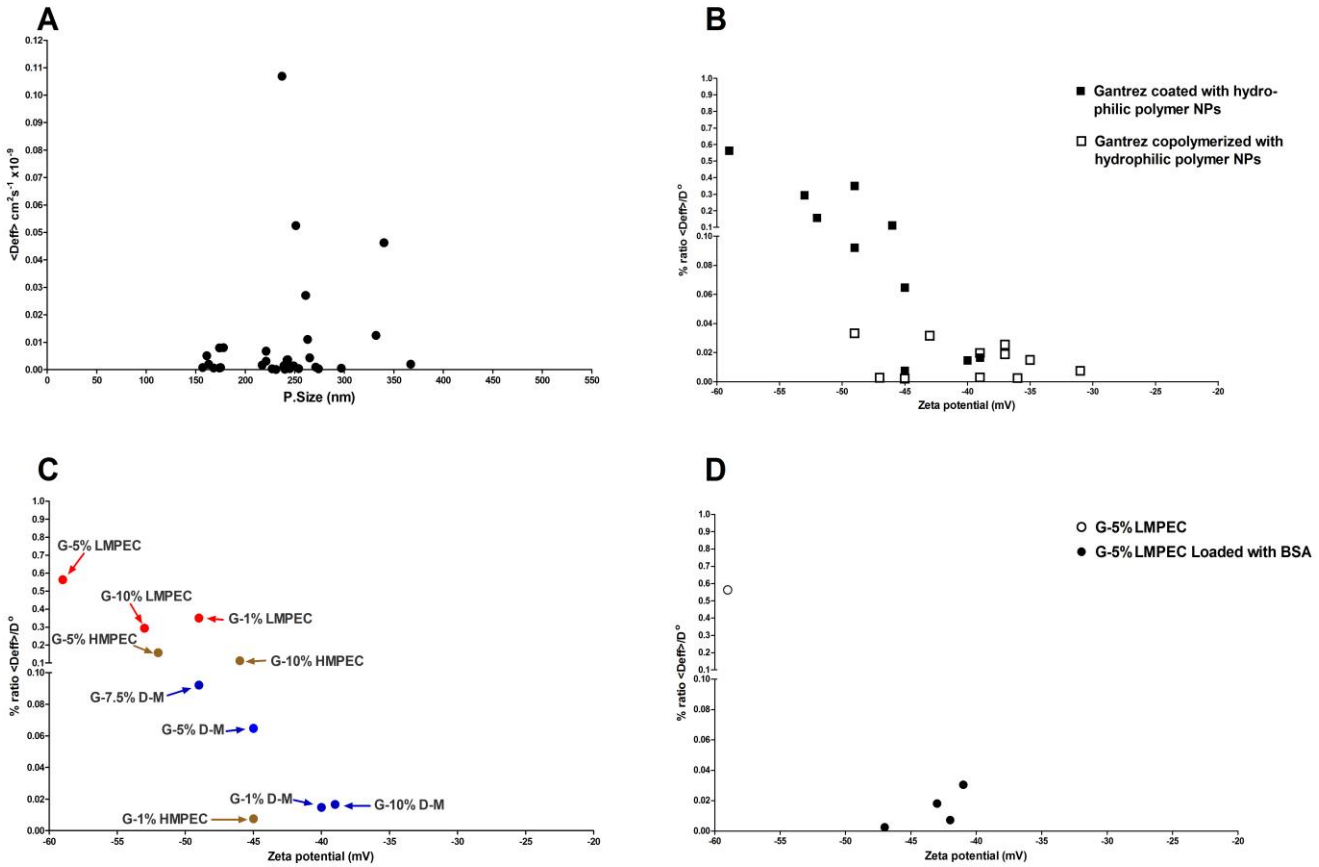

Figure 3.2: Diffusion behaviour of various slippery amphiphilic polymers NPs in the "Cardiff native mucus" model. (A) Diffusion <Deff> versus particle size of all amphiphilic polymers NPs (B) The % ratio <Deff>/D° versus zeta potential of coated amphiphilic polymers NPs (■) versus copolymerized amphiphilic polymers NPs (□) (C) The % ratio <Deff>/D° versus zeta potential of amphiphilic polymers NPs coated with D-M (blue particles), amphiphilic polymers NPs coated with LMPEC (Red particles) and amphiphilic polymers NPs coated with HMPEC (brown particles) (D) The % ratio <Deff>/D° versus zeta potential of Gantrez NPs coated with 5% LMPEC (○) versus the same particles loaded with different concentration BSA(●).

Each of the Figures 3.2B, 3.2C and 3.2D shows the %<Deff>/D° ratio versus zeta potential of amphiphilic polymer NPs. Specifically, Figure 3.2B shows the %<Deff>/D° ratio of the Gantrez particles coated with either hydrophilic polymers or copolymerized to hydrophilic polymers. The technique by which NPs were synthesized showed a crucial effect on the diffusion of the NPs through the mucus. NPs synthesized by coating of Gantrez with D-M, LMPEC or HMPEC polymers exhibited higher diffusivities than NPs synthesized by copolymerization of Gantrez with D-M, LMPEC or HMPEC polymers. This is true even for the relatively low diffusing NPs coated with 10% hydrophilic polymer. This finding has not been discussed in the literatures previously and it could be related to the conditions of the synthesis of these NPs species. However, this difference in the diffusion of NPs consisting of same polymers but synthesized by coating or copolymerization could be due to the resulting differences in surface chemistry of the NPs.

Figure 3.2C shows the effect of concentration and the type of the coated hydrophilic polymer on the diffusivity of the NPs through mucus barrier. These NPs are represented in Figure 3.2C by different colours depending on the type of the hydrophilic polymer coat, i.e. Gantrez NPs coated with D-M are Blue, Gantrez NPs coated with LMPEC are Red and Gantrez NPs coated with HMPEC are Brown. NPs coated with LMPEC (Red symbols) showed higher diffusivities than particles coated with HMPEC (Brown symbols) or D-M (Blue symbols). The high diffusivity of LMPEC particles as compared with HMPEC could be due to the lower methyl content of this polymer which resulted in lower lipophilicity at the surface of the NPs and lower interaction to the mucus [64].

Moreover, the ratio of the hydrophilic polymer exhibited an impact on the diffusivities of the particles, the influence is however complex. Specifically, for each of the coating type, there appeared to be an optimum coating concentration that confers the greatest

diffusion through mucus. Between coating concentration of 1% and 10%, the optimum concentration for LMPEC and HMPEC was 5% while for D-M, it was 7.5%. These optimum concentration happened to coincide with the NPs coating concentration associated with the most -ve zeta potential, i.e. 5%LMPEC had the most –ve zeta potential among all the of the coated LMPEC particles. This zeta potential association with the diffusion of NPs is same for NPs coated with HMPEC and D-M.

This kind of relationship is not dissimilar to that observed for PEG coating. For example, the optimum coating concentration of the Gantrez particles may be due to the formation of an efficient inert hydrophilic shell at the surface of the particles [45]. Concentration either lower or higher than the optimum may simply represent respectively an inefficient coating or the production of a thick layer at the particle surface that can interpenetrate with the mucin fibres [56].

Lastly, Figure 3.2D shows the effect of loading of BSA on the diffusivity of G-5%LMPEC. The Figure shows the unloaded NP to display higher diffusion than particles loaded with 0.5%, 1%, 1.5% and 2% BSA. Although G- 5% LMPEC showed the highest % ratio <Deff>/D° through the pig intestinal mucus among all the Gantrez-hydrophilic NP, the loading of G-5% LMPEC NP with BSA resulted in sharp drop in the % ratio <Deff>/D°. It was also noticeable that BSA loading resulted in a less negative zeta potential than the unloaded particles.

Other hydrophilic polymers were used to coat Gantrez particle, however, the effects of these polymers were not studied thoroughly by the partner in the Consortium .As consequence, only one particular formulation of a given particle type was synthesized by the partner. Hence, such particles are presented in Table 3.2 but without any further discussion.

3.c Slippery-PEC NP Strategy

This strategy was selected by the consortium to mimic the capsid shell of freely permeable viruses through the mucus. Such viruses are characterized by a high density of positive and negative charges at their surface yielding a net neutral charge [65]. This surface property enables these viruses to permeate freely through the mucus barrier [66]. Capsid shell viruses inspired researchers to synthesize particles having the same surface properties [52]. Self-assembled PEC NPs are synthesized by mixing positively and negatively charged polymers to form electrostatically complex particles with the aim of achieving a high charge density at the surface. The charge at the surface can be modified to be neutral to mimic the muco-inert surface of capsid virus. Laffleur et al. (2014) [67] studied the permeation of PEC NP composed of poly(acrylic acid) (PAA) and poly(allylamine) (PAM) through pig intestinal mucus layer using the Ussing chamber technique. The study showed that the neutral PEC NP had a 2.5-fold and 1.8-fold higher permeation than that of the positively and negatively charged NP respectively, and indicating the promising nature of this strategy to overcome a mucus barrier.

Table 3.3 shows the diffusion of various PEC NPs. The Table details the following: Consortium Partner; NP code (as defined by the partner); chemical composition of the particle, where known, including the chemical core of the particle, chitosan etc.; physico-chemical properties of the particle (Zeta potential and particle size); MPT diffusion data [cm^2 S^{-1} x 10^{-9}] in the Cardiff mucus model including D° water (calculated by Stokes Einstein equation), the <Deff> and the % ratio of <Deff>/D°; finally the rank order of the particle diffusion (i.e. 1= fastest) based on %<Deff>/D° amongst the entire screening exercise of 102 different particles. All codes for particles are described in the Table and will be used throughout the section.

Figure 3.3A shows the <Deff> versus particle size data for the respective PEC NPs. It shows that particle size had no real effect on the <Deff> of all the tested PEC NPs described in Table 3.3. Figure 3.3 B shows that the diffusion behavior of the PEC NP made by LEK (Table 3.3) using either alginate or chondroitin as the negatively charged polymer complexed at varying ratios with the unknown +ve charged polymer. From the limited study design, it is hard to conclude why L1011 should be close to 3-fold greater diffusion compared to L1010. Although the poor diffusion associated with the +ve charge NP is clear. The zeta potential of the LEK particles is also shown in figure 3.3A and demonstrated the positive charged particles to be much slower compared to the negative species.

Moreover, Figure 3.3B shows the Sagetis PEC-NPs, all of which used an unknown PBAE polymer as the source of –ve charges, and either chitosan (CS) or again unknown polymer (CR, CH) as the source of positive charge. What is clear is that despite a positive zeta potential, the new sagetis polymer (CR, CH) provided a high % <Deff>/D° then particles made from chitosan. More interestingly, whatever the particle type, these particles conjugated with peptide resulted in superior diffusion characteristics compared to the respective particles conjugated with DNA. It can be seen that this case was irrespective of zeta potential and clearly was not determined by this particular physico-chemical property, i.e. CR and CH PEC NPs all displayed the same zeta potential of + 10 mV. Without knowledge of actual components of the NPs, it is difficult to consider why the peptide formulations were consistently better than that of DNA formulation.

Table 3.3: Particles' composition, physical characteristics and diffusion behavior of various PEC NPs. (PDI and S.D. are included where necessary).

Partner	NP Code	Compositions	Zeta Potential (mV) Mean	Particle Size (nm) Mean	D° (water) $cm^2. S^{-1} x10^{-9}$	<Deff> (mucus) $cm^2. S^{-1} x10^{-9}$ Mean (± s.e.m)	% <Deff>/ D°	Ranking Fastest =1 and slowest 102
Lek	L1009	[90:10] (+ve) polymer unknown / (-ve) polymer alginate	16	250	17.98	0.00004 (±0.00001)	0.0002	102
	L1010	[30:70] (+ve) polymer unknown / (-ve) polymer chondroitin 4-sulfate	-22	250	17.98	0.00022 (±0.00003)	0.0012	96
	L1011	[40:60] (+ve) polymer unknown / (-ve) polymer chondroitin 4-sulfate	-18	250	17.98	0.00063 (±0.00012)	0.0035	82
Sagetis	CS/CEF3.5	[ratio unknown] (+ve) polymer chitosan / (-ve) polymer poly(β-amino esters) (PBAEs) conjugated to peptide.	5	194	23.17	0.00327 (±0.00021)	0.0141	57
	CS/CDF3.5	[ratio unknown] (+ve) polymer chitosan / (-ve) polymer poly(β-amino esters) (PBAEs) conjugated to DNA.	5	194	23.17	0.00098 (±0.00006)	0.0042	77
	CR3/CDf3.5	[ratio unknown] (+ve) polymer unknown / (-ve) polymer poly(β-amino esters) (PBAEs) conjugated to DNA.	10	499	9.01	0.00617 (±0.00035)	0.0685	28
	CR3/CEf3.5	[ratio unknown] (+ve) polymer unknown / (-ve) polymer poly(β-amino esters) (PBAEs) conjugated to peptide.	10	499	9.01	0.00747 (±0.00040)	0.0829	24
	CH3/CDf3.5	[ratio unknown] (+ve) polymer unknown / (-ve) polymer poly(β-amino esters) (PBAEs) conjugated to DNA.	10	499	9.01	0.00112 (±0.00006)	0.0124	59
	CH3/CEf3.5	[ratio unknown] (+ve) polymer unknown / (-ve) polymer poly(β-amino esters) (PBAEs) conjugated to peptide.	10	499	9.01	0.00179 (±0.00013)	0.0198	46

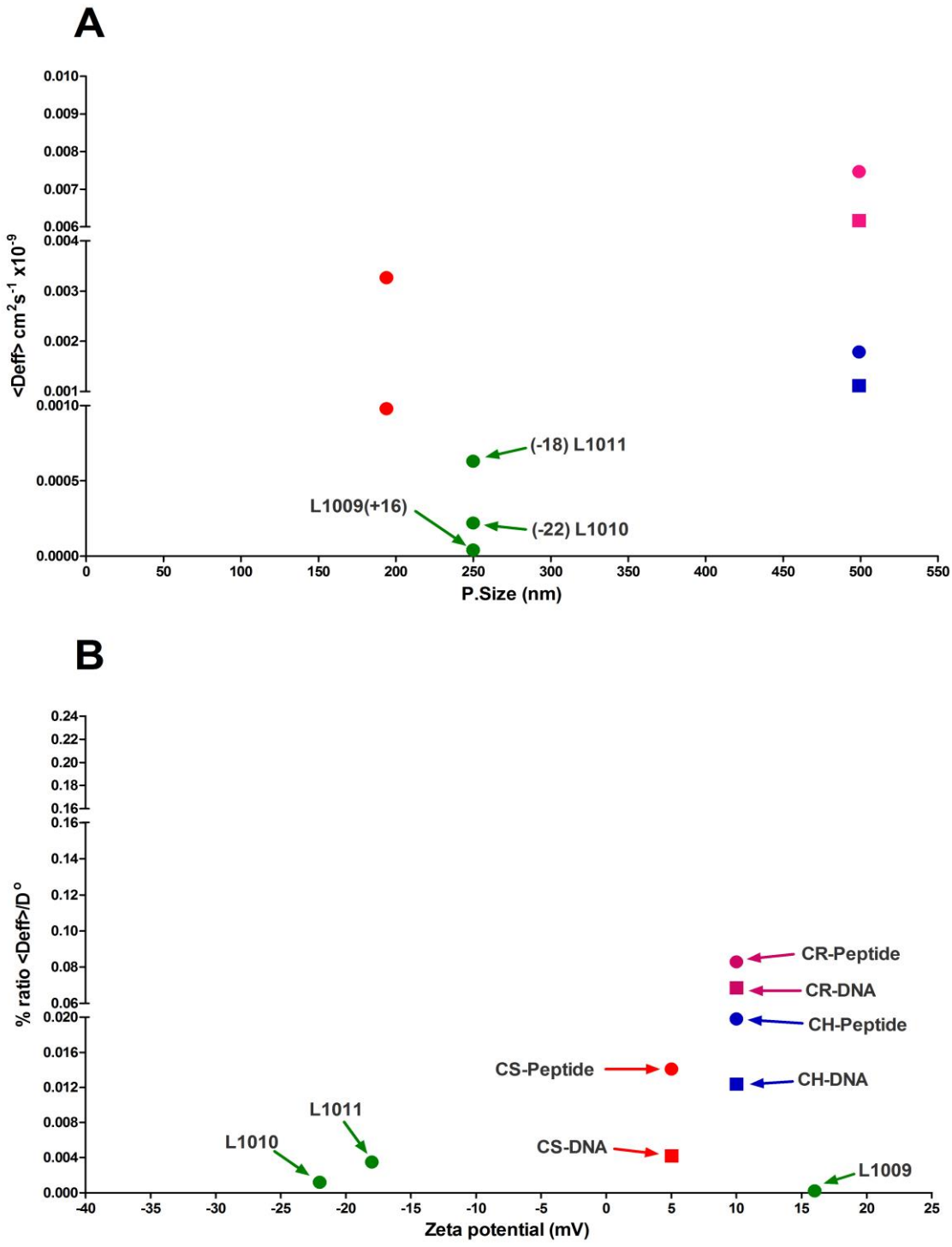

Figure 3.3: (A) Mucus diffusion <Deff> versus particle size of PEC NPs in the "Cardiff native mucus" model. (B) % ratio <Deff>/D° versus zeta potential of PEC NPs in the "Cardiff native mucus" model.

3.d SMEDD System Strategy

Previous *in vivo* studies of orally administered SMEDD systems have shown promise in term of enhancing the bioavailability of loaded drugs [68,69]. SMEDD systems were selected by the Alexander Consortium as one of the muco-diffusive nano-strategies. A SMEDD system is aimed at having a muco-inert droplet surface due to the hydrophilic nature of the surfactant/co-surfactant shell at the surface of the oil droplet [70].

Table 3.4 shows the SMEDD systems that were made by three different partners in the Consortium. The Table details the following: Consortium Partner; SMEDD system code; chemical composition of the SMEDD system where known including the oil phase, surfactant and co-surfactant etc.; physico-chemical properties of the system (Zeta potential and particle size); MPT diffusion data [$cm^2\ S^{-1} \times 10^{-9}$] in the Cardiff mucus model including D° water (calculated by Stokes Einstein equation), <Deff> and the % ratio of < Deff>/D°; finally the rank order of the particle diffusion (i.e. 1= fastest) based on %<Deff>/D° ratio amongst the entire screening exercise of 102 different particles. Figure 3.4A shows the < Deff> versus the particle size data for the respective SMEDD systems.

Figure 3.4B shows the %<Deff>/D of each of the SMEDD system versus zeta potential. The SMEDD systems prepared by the different partners are represented in Table 3.4 and Figure 3.4 by different colours i.e. Thessaloniki University (AUT) is Black; Nevara University (NEV) is Blue; Insbruck University (INS) is red.

Table 3.4: Particles' composition, physical characteristics and diffusion behavior of various SMEDDS systems. (PDI and S.D. are included where necessary).

Partner	SMEDDS code	Compositions (O/W) (Oil/Surf) Mixture / Co-surfactant	Zeta Potential (mV) Mean	Particle Size (nm) Mean (PDI)	D° (water) $cm^2. S^{-1} x10^{-9}$	<Deff> (mucus) $cm^2. S^{-1} x10^{-9}$ Mean (± s.e.m)	% <Deff>/ D°	Ranking Fastest =1 and slowest 102
AUTH	AUT-A	Mix1 / Labrafil-M1944CS (Co-surfactant)	-0.06	35	128.4	0.00085 (±0.00020)	0.0007	100
	AUT-B	Mix1 / Transcut-ol P (Co-surfactant)	-0.09	45	99.87	0.22873 (±0.06054)	0.2290	14
	AUT-C	Mix2 / LabrafilM19444CS (Co-surfactant)	0.20	25	179.8	0.10990 (±0.00326)	0.0611	33
Nevarra	NEV-A	Mix3 / Plurol Oleique (Co-surfactant)	-22	167	26.88	0.00528 (±0.00114)	0.0196	49
	NEV-B	Mix4 / Span 20 (Co-surfactant)	-16	240	18.72	0.13846 (±0.00601)	0.7397	2
Innsbruck	INS-A	Mix5 / PEG (Co-surfactant)/ TBA–Dodecylamine (Thiol agent)	-2.1	44	101.18	0.87123 (±0.1223)	0.8611	1
	INS-B	Mix5 / PEG (Co-surfactant)/ TGA-Octylamine (Thiol agent)	-2.2	53	82.28	0.05135 (±0.0089)	0.0624	32
	INS-C	Mix5 / PEG (Co-surfactant)/	-0.8	36	122.12	0.01318 (±0.0003)	0.0108	61
	INS-D	Mix5 / PEG (Co-surfactant)/ /NAC (mucolytic agent)	-7.1	43	102.41	0.24624 (±0.0376)	0.2405	12

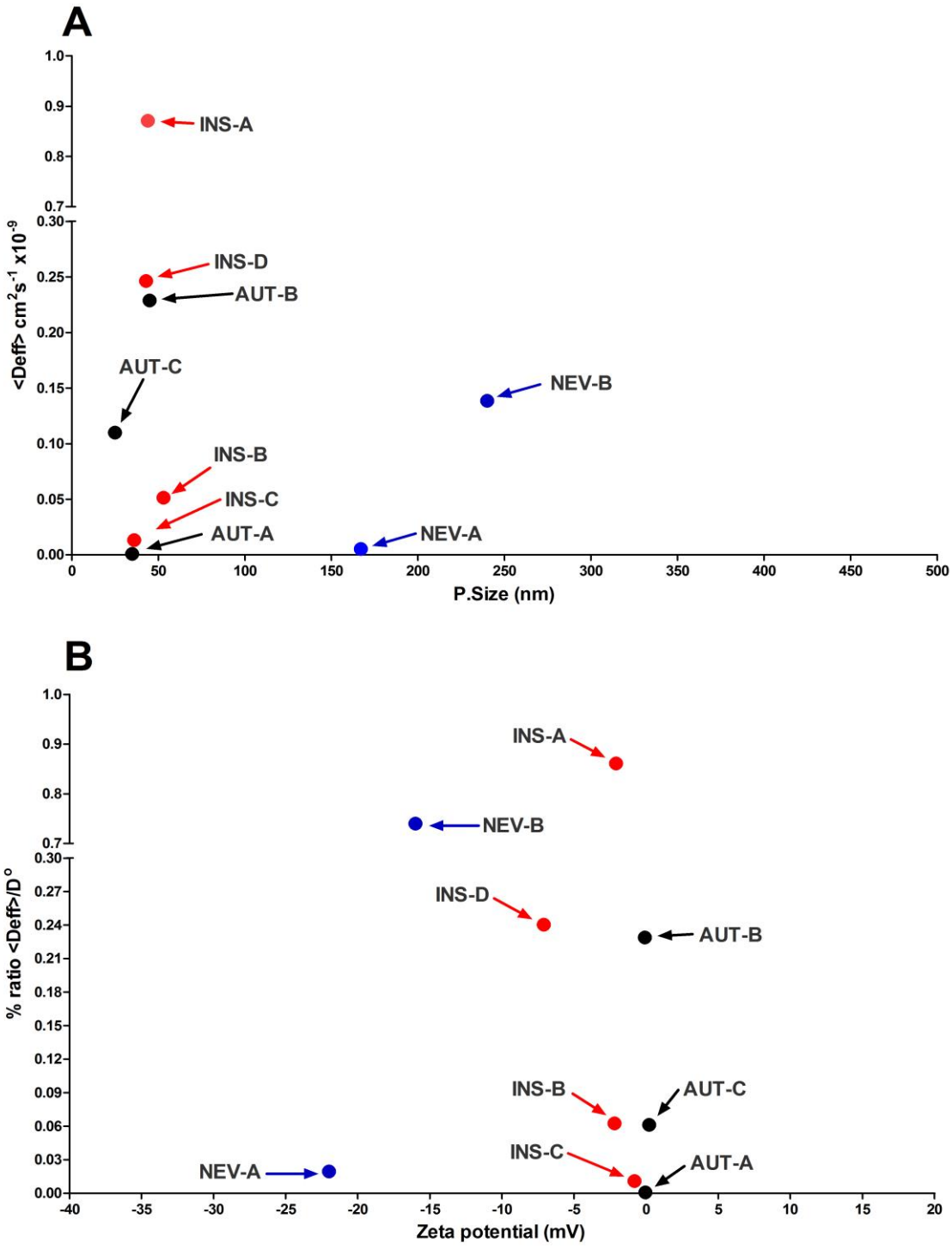

Figure 3.4: (A) Mucus diffusion <Deff> versus particle size of various SMEDDS in the "Cardiff native mucus" model. (B) % ratio <Deff>/D° versus zeta potential of various SMEDDS in the "Cardiff native mucus" model. (See Table 3.4 for compositions and codes).

The systems have two main inter-independent variables that can affect the diffusion of these systems through the mucus. These are: the physicochemical properties of the SMEDD systems and the ingredients in each system. Table 3.4 shows that SMEDD systems from AUTH and INS have particle sizes less than 50 nm, while the SMEDD systems from NEV have particle size range between 167 and 240 nm. Figure 3.4A shows no real correlation of particle size to <Deff>, with particles as small as 50 nm showing a wide range of diffusion.

Similarly, Figure 3.4B fails to reveal any correlation of zeta potentials to % ratio <Deff>/D°, although almost all particles are within the range of 0 to -15 mV. Figure 3.4 does show however that the SMEDD systems are affected by their formulation ingredients. This effect was observed for the all three partners contributed to this nano-strategy.

It is exemplified by the Innsbruck SMEDD systems where the incorporation of a thiol agent, either NAC, TBA Dodecylamine or TGA Octylamine (INS A,B,D) outperforms the SMEDD bearing just the co-surfactant (INS C). Thiol groups can interact with the mucin network to break inter-molecular bonds in the fibres (see sections 3.e and 3.f). This section of work revealed the SMEDD bearing TBA-dodecylamine to have the highest diffusivity among all the Innsbruck SMEDD systems, indeed across all 102 NP studied from the Consortium. This is possibly the result of the high release of this thiol agent into the mucus and the resultant local destruction of the mucus structure to increase in diffusion of the SMEDD system [71]. High release of ingredients from SMEDD system was reported for some (active) ingredients when they are located in the surfactant/co-surfactant layer rather than incorporated in the oil phase [72]. The TBA Dodecylamine could be subject to greater release than the other thiol or mucolytic agents incorporated into the SMEDD systems.

Another example of the formulation differences can be seen with the SMEDD systems AU-A and AU-B which have the same oil phase (Mix 1) but showed distinct diffusion differences depending on the co-surfactant. The SMEDD AU-B system used Transcutol as a co-surfactant and showed x327 fold greater % ratio <Deff>/D° than that of SMEDD AU-A system which used Labrafil M 1944 CS as the co-surfactant. This finding agrees with previous study which showed that the type of the oil has a high impact on the SMEDD system interaction with mucin [73]. This was explained on the basis that different oil with same surfactant shell has different capability to form a hydrophobic interaction with the hydrophobic domains of the mucin.

3.e Mucolytic NPs Strategy

Previous studies showed the impact of mucolytic agents on the diffusion of NPs through mucus. As example, pre-treating of cystic fibrosis mucus with NAC improved the diffusion of muco-inert PEGylated NP [74], oppositely, the same PEG NP that administered without NAC pre-treatment showed low diffusivity through the mucus barrier. Based on these previous studies, partners in the Alexander Consortium used mucolytic strategy represented by either disulfide breaking agents (NAC, thioglycolic acid and glutathione) or proteolytic agents (bromelain and papain agents) to improve NPs permeation through mucus. Consequently, the synthesized NPs by the consortium were designed for the purpose of careful disintegration of the mucus layer that come in contact with mucolytic NPs. This contrasts with studies by other groups which showed massive destruction of the entire intestinal mucosal tissue in Sprague Dawley rat model [75] and in Ussing chamber model [76].

Table 3.5 shows the diffusivities of NPs loaded with either proteolytic or disulfide breaking agents and synthesized by different partners in the Consortium. The Table details the following: Consortium Partner; NP code (as defined by the partner);

chemical composition of the particle where known including the chemical core of the particle, polyacrylic acid (PAA) etc.; physico-chemical properties of the particle (Zeta potential and particle size); MPT diffusion data [cm^2 S^{-1} x 10^{-9}] in the Cardiff mucus model including also D° water (calculated by Stokes Einstein equation), the <Deff> and the ratio of % <Deff>/D°; finally the rank order of the particle diffusion (i.e. 1= fastest) based on %<Deff>/D° across the entire screening exercise of 102 different particles). All the codes for particles are described in the Table and will be used throughout the section.

Figure 3.5A shows no correlation between the particle size and the <Deff> of respective mucolytic particles. This absence of correlation is obvious and exemplified by observing that PAA-BRO NP with particle size of 304 nm showed 7 times higher <Deff> than CSGSH188/CD3 NP with particle size 299 nm (table 3.5). Similarly, Table 3.5 shows no correlation between the zeta potential and the % ratio <Deff>/D° of mucolytic NPs, for example, NPs with same zeta potential (3 mV) represented by CSGSH188/CD3 and CSTGA360/-CD3 showed 7-folds difference in their % ratio <Deff>/D°. Each of the Figures 3.5B, 3.5C and 3.5D shows the %<Deff>/D° versus zeta potential of mucolytic NPs in which one variable affecting the diffusion of particles is illustrated.

Table 3.5: Particles' composition, physical characteristics and diffusion of various NP loaded with mucolytics. (PDI and S.D. are included where necessary).

Partner	NP Code	Compositions	Zeta Potential (mV) Mean	Particle Size (nm) Mean (PDI)	D° (water) $cm^2. S^{-1} x10^{-9}$	<Deff> (mucus) $cm^2. S^{-1} x10^{-9}$ Mean (± s.e.m)	% <Deff>/ D°	Ranking Fastest =1 and slowest
Innsbruck	PAA-PAP	PAA NP loaded with 25% Papaine (proteolytic agent)	-27	352	12.77	0.00389 (±0.00077)	0.0305	39
	PAA-BRO	PAA NP loaded with 25% Bromelain (proteolytic agent)	-20	304	14.78	0.04029 (±0.01280)	0.2725	11
Sagetis	CSTGA360/-CD3	Chitosan-thioglycolic acid+ unknown (-) charged Poly(β-amino ester)s (PBAEs) (disulfide breaking agent).	3	137	32.80	0.00079 (±0.00006)	0.0024	89
	CSNAC177/ CD3	Chitosan-NAC+ unknown (-) charged Poly(β-amino ester)s (PBAEs) (disulfide breaking agent).	6	156	28.81	0.00384 (±0.00015)	0.0133	58
	CSGSH188/ CD3	Chitosan-Glutathione + unknown (-) charged Poly(β-amino ester)s (PBAEs) (disulfide breaking agent).	3	299	15.03	0.00671 (±0.00043)	0.0447	33
Nevarra	0.3P-NPA-L-L	Muco-adhesive NP loaded with papain (0.3 %) (lyophilized NP)	-45	315	14.27	0.03326 (±0.00600)	0.2331	12
	0.3P-NPB-L-L	Muco-adhesive NP loaded with papain (0.3 %) (spray dried NP)	-46	216	20.80	0.00057 (±0.00018)	0.0028	84
	20NAC-NPA-L-L	Muco-adhesive NP loaded with NAC (5 %) (lyophilized NP)	-53	189	23.77	0.03513 (±0.00216)	0.1478	18
	20NAC-NPB-L-L	Muco-adhesive NP loaded with NAC (5 %) (spray dried NP)	-28	231	19.49	0.00753 (±0.00072)	0.0386	34
	200NAC-NPA-L-L	Muco-adhesive NP loaded with NAC (50 %) (lyophilized NP)	-51	145	30.95	0.00465 (±0.00022)	0.0150	54
	200NAC-NPB-L-L	Muco-adhesive NP loaded with NAC (50 %) (spray dried NP)	-23	440	10.21	0.00098 (±0.00006)	0.0096	63

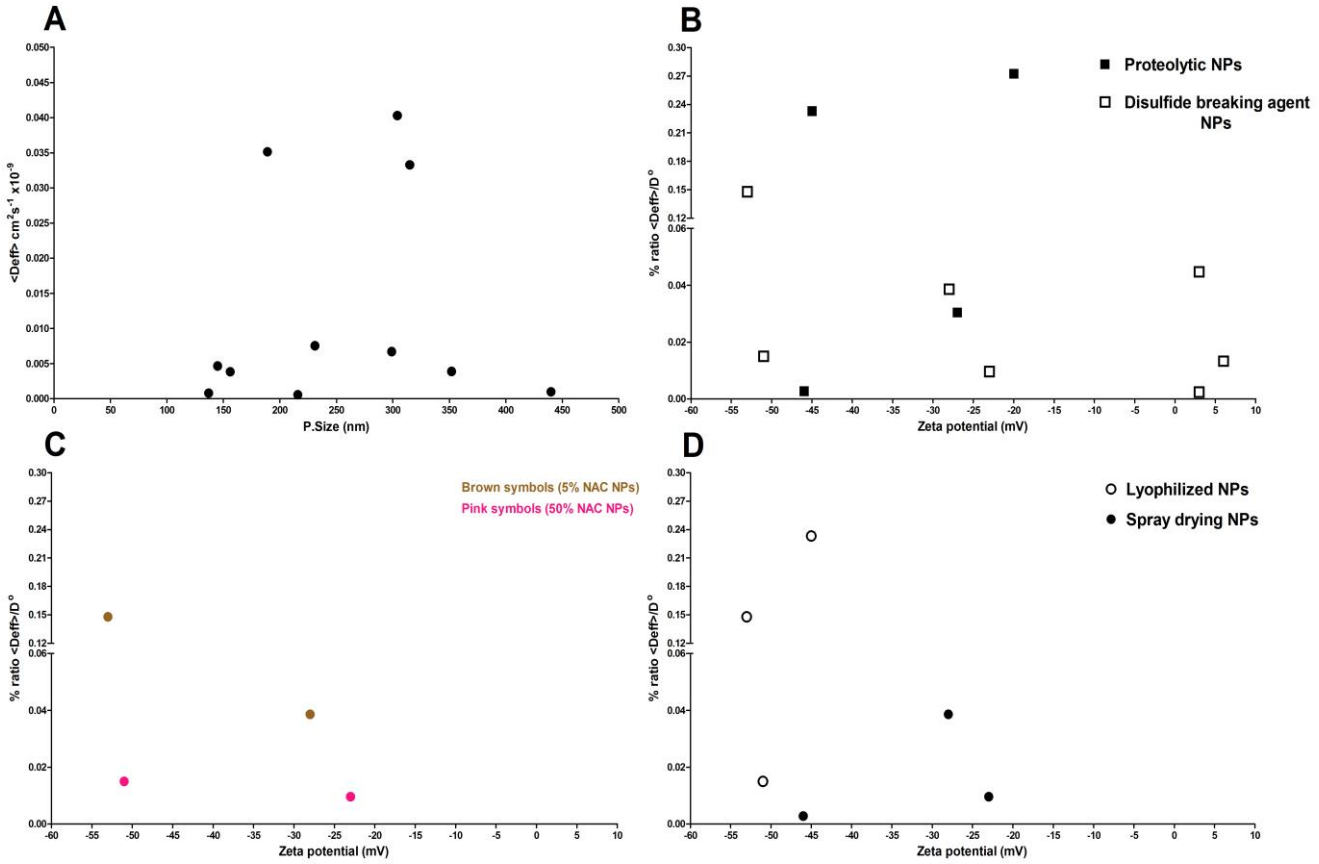

Figure 3.5: Diffusion behaviour of various NPs loaded with mucolytic agent in the "Cardiff native mucus" model. (A) Diffusion <Deff> versus particle size of all mucolytic NPs (B) The % ratio <Deff>/D° versus zeta potential of NPs loaded with proteolytic agent (■) versus NPs loaded with disulfide breaking agent (□) (C) The % ratio <Deff>/D° versus zeta potential of NPs loaded with 5% NAC (brown particles) versus NPs loaded with 50% NAC (pink particles) (D) The % ratio <Deff>/D° versus zeta potential of lyophilized mucolytic NPs (○) versus spray dried mucolytic NPs (●).

Figure 3.5B shows % ratio <Deff>/D° of NPs loaded with proteolytic agent versus NPs loaded with disulfide breaking agent. It can seen that NPs loaded with proteolytic agents represented by PAA-BRO NP synthesized by Innsbruck and 0.3P-NPA-L-L synthesized by Nevarra showed much higher % ratio <Deff>/D° compared with other NP loaded with disulfide breaking agent indicating general higher diffusion of proteolytic agents. However, the presence of some NPs loaded with proteolytic agent with similar diffusivities to NPs loaded with disulfide breaking agents limits any finding in this comparison.

The "general" higher diffusion of NPs loaded with proteolytic agents is related to the activity of each mucolytic type at the pH (5.5-6.9) of intestinal mucus. Comparatively, proteolytic agent is efficient within wide range of pH including the intestinal pH [77–79]. This makes these agents to be efficient in Cardiff mucus model with pH mimicking the *in vivo* pH of 6.7. This is in agreement with Müller et al study (2014), which showed extended residence time of PAA-papaine NP in the duodenum and jejunum of Sprague Dawley rats indicating the activity of proteolytic agents at the *in vivo* pH conditions [80].

On the other hand, Disulfide breaking agents require high pH (7-9) to cleave disulfide bridges between mucin fibres leading to more leaky mucus [31]. In literature, experiments on NAC mucolytic activity is accompanied by modifying the pH of the mucus to more than 7 [81] while the pH of Cardiff mucus model is 6.7 (Chapter Two) which could be a limiting factor for the maximum activity of the NAC agent. Thus, several studies showed that NAC was ineffective to improve NPs diffusion through the mucus. For example, studying of NAC mucolytic activity on CF sputum by the MPT technique revealed that NAC was inactive when mucin concentration increased from less than 1% to 2.2% [82]. Accordingly, *in vivo* study by Ferrari et al. (2001) [83]

showed a non-significant efficiency of NPs loaded with NAC to deliver gene therapeutic agent into the pulmonary tissues of mouse.

Figure 3.5C shows the %<Deff>/D° of NPs loaded with 5% NAC (Brown symbols) versus NPs loaded with 50% NAC (Pink symbols). Surprisingly, NPs loaded with 5% NAC showed 5-10 times higher % ratio <Deff>/D° than the same particles loaded with 50% NAC. This inverse relation could be due to the excessive destruction of mucin network when high concentration of NAC (50%) was used. This results in release of the mucin component into the mesh spaces leading to increase of the micro-viscosity of the water in these spaces [84]. In normal condition, these spaces should be filled with water through which, small enough particles can freely move through [85]. Hence, the increase in the micro-viscosity limits particles diffusion through these spaces. This effect was also observed in previous study where NPs loaded with high concentration bromelain resulted in an increase of the viscosity of the water in these spaces [86].

Lastly, figure 3.5D shows %<Deff>/D° of lyophilized mucolytic NPs versus spray dried mucolytic NPs. This Figure shows that NPs dried by the spray drying technique showed much lower diffusivities than the same NPs but dried by the freeze drying technique. This indicates that spray drying method altered the surface chemistry of these NPs which affected the release or the stability of proteolytic agent conjugated into NPs surface. This finding is consistent with a study [87] which showed that changing the properties of the NP surface reduced the release of the mucolytic agents and in turn affected its mucolytic activity and permeation though the mucus.

3.f Thiolated NP Strategy

Thiomers are formed by the conjugation of a sulfhydryl group into another polymer [88]. These polymers can form disulfide linkages with cysteine subdomains in the mucin at pH range of (7.2-7.4). All the NPs in this strategy were synthesized by the

partners in the consortium using the same thiolated polymer source (thiolated chitosan). Chitosan-thiol NPs were reported widely by other groups, for example: chitosan-thioglycolic acid [89], chitosan –cysteine [90], chitosan-4-thio-butylamidine [91] and chitosan glutathione [92]. It was found that adding of thiol agent into a muco-adhesive polymer resulted in 130 times increase of the muco-adhesivity of that polymer by [93].

Table 3.6 shows two thiolated NPs sub-groups that were synthesized by Sagetis. The Table details the following: Consortium Partner; NP code (as defined by the partner); chemical composition of the particle, where known, including the chemical core of the particle, chitosan etc.; physico-chemical properties of the particle (Zeta potential and particle size); MPT diffusion data [$cm^2 S^{-1} \times 10^{-9}$] in the Cardiff mucus model including D° water (calculated by Stokes Einstein equation), the <Deff> and the % ratio of <Deff>/D°; finally the rank order of the particle diffusion (i.e. 1= fastest) based on %<Deff>/D° amongst the entire screening exercise of 102 different particles. All codes for particles are described in the Table and will be used throughout the section.

Figure 3.6A shows the <Deff> versus particle size data for the respective thiolated NPs. The particles for both sub-groups (Blue and Red symbols) have almost similar particle sizes but different <Deff> indicating no effect of particle size on the <Deff> of all thiolated NPs described in Table 3.3. Similarly, Figure 3.6B which illustrates the %<Deff>/D° versus zeta potential of the thiolated NPs shows no impact of zeta potential on %<Deff>/D° of these NPs indicated by different %<Deff>/D° obtained for NPs having same zeta potential values.

It can be seen also that the diffusivity of the same thiolated NPs (Red symbols) was varied depending on the type of the attached molecule (either DNA or peptide), i.e. the NP attached to peptide showed 5 times higher diffusivity than that attached to DNA. This is in agreement with the data obtained in the previous section for PEC NPs where

the PEC NPs attached to peptide had higher diffusion than the same PEC NP attached to DNA. However the lack of information about the peptide or the DNA used in this study limited the finding in this section.

The most important factor which was found to affect the diffusion of NPs was the ratio of the thiol agent attached to the NPs. It can be seen from figure 3.6 (Blue symbols) that the increase in the ratio of the thiol agent from 150 to 168 µmole/gm then to 300 µmole/gm resulted in almost 2-folds increase in the <Deff> and the % ratio <Deff>/D° of these particles. This increase in the diffusion is attributed to the destructive effect of these agents on the mucus structure by forming disulfide bonds with mucin. This destructive effect was proven by Leitner et al. (2003) [93] who found the competitive destructive effect of thiomer and NAC on the porcine mucus. Moreover, Gradauer et al. (2013) [94] showed that thiolated agents can destroy mucus structure even if it is not released from NPs into the mucus. In Gradauer study, the increase in the permeation of thiolated liposomes was attributed to the destruction effect exerted by the population of the thiolated particles firstly come in contact with mucus which allows the permeation of the remaining particles through the already destructed mucin network. For the above reasons, Thiomers were used as permeation enhancers for the oral delivery of hydrophilic [95] and polypeptide drugs [96]. Similarly, *in vivo* studies showed that thiomers can improve the bioavailability of peptide drugs [97].

Table 3.6: Particles' composition, physical characteristics and diffusion behavior of various thiolated NP. (PDI and S.D. are included where necessary).

Partner	NP Code	Compositions	Zeta Potential (mV) Mean	Particle Size (nm) Mean (PDI)	D° (water) $cm^2. S^{-1} x10^{-9}$	<Deff> (mucus) $cm^2. S^{-1} x10^{-9}$ Mean (± s.e.m)	% <Deff>/ D°	Ranking Fastest =1 and slowest 102
Sagetis	CSMPAA300/ CD3	Thiolated chitosan (300 thiol µmole/gm of polymer) + unknown (-) charged Poly(β-amino ester)s (PBAEs).	4	140	32.10	0.00725 (±0.00045)	0.0226	44
	CSMBA168/ CD3	Thiolated chitosan (168 thiol µmole/gm of polymer) + unknown (-) charged Poly(β-amino ester)s (PBAEs).	4	143	31.43	0.00569 (±0.00033)	0.0181	51
	CSMPAA150/CD3	Thiolated chitosan (150 thiol µmole/gm of polymer) + unknown (-) charged Poly(β-amino ester)s (PBAEs).	2	109	41.23	0.00399 (±0.00032)	0.0097	62
	CSSH/CDf3.5	Thiolated chitosan + unknown (-) charged Poly(β-amino ester)s (PBAEs) attached to DNA.	1	147	30.57	0.00230 (±0.00013)	0.0075	68
	CSSH/CEf3.5	Thiolated chitosan + unknown (-) Poly(β-amino ester)s (PBAEs) attached to peptide.	1	147	30.57	0.01050 (±0.00060)	0.0343	35

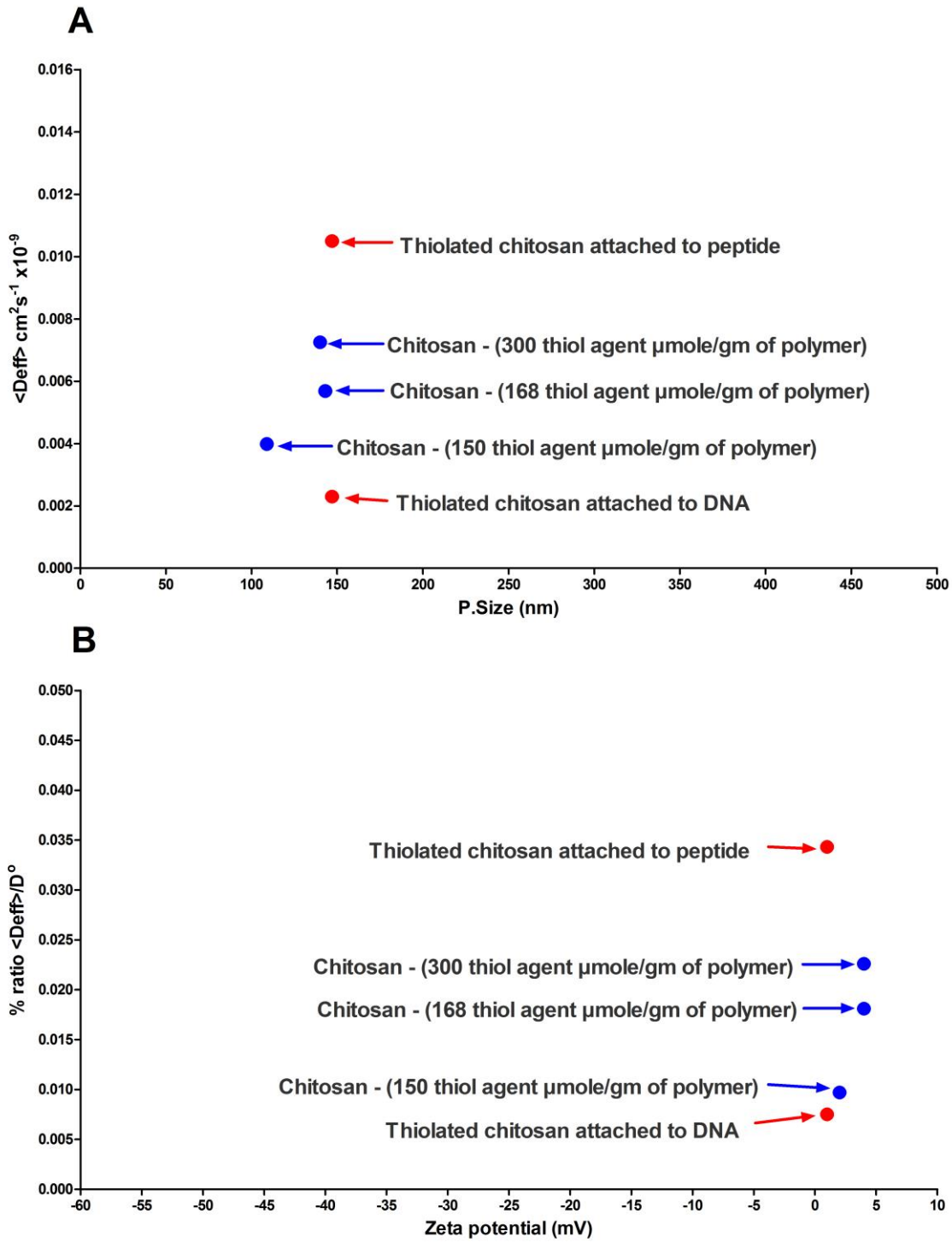

Figure 3.6: (A) Mucus diffusion <Deff> versus particle size of various thiolated NPs in the "Cardiff native mucus" model. (B) % ratio <Deff>/D° versus zeta potential of various thiolated NPs in the "Cardiff native mucus" model.

3.g Comparison of Mucus Diffusivity of all Nano-Strategies in the "Cardiff Native Mucus" Model and "Consortium Mucus-Gel" Model

This chapter has provided comparison of six different nano-strategies for NPs diffusion through mucus. Each NP was ranked to allow comparison with other NPs. Tables (3.1-3.6) show the ranking of the particles from the fastest (1) to the slowest (102) particle. This ranking enables identification of the nano-strategy which showed the highest permeation through the "Cardiff native mucus model". This data was used by the consortium to select NPs for *in vivo* experimentation.

Figure 3.7A shows the PEG NPs (Red symbols) and SMEDD systems (Blue symbols) to be generally superior in performance to most of the other nano-strategies, although, such particles were mostly of a small size (ca 50 nm). Hydrophilic particles such as those coated with PEG generally display diffusion that is inversely correlated to their particle size. For example some of the PEG NPs of greater than 200 nm showed significantly diminished diffusion. Accordingly when expressing the diffusion data in terms of %ratio $<D_{eff}>/D^o$ (Figure 3.7B) it is evident that the best performing particles with respect to surface chemistries remained the SMEDDs, the PEG NPs and some NPs from the slippery-polymer and mucolytic strategies.

The generally high diffusivity of the SMEDD systems depends very much on the high hydrophilic nature of the oil droplet surface. SMEDDs require a mixture of surfactant and co-surfactants with a very high hydrophilic-lipophilic balance (HLB) [70]. As mentioned above this high hydrophilic surface character is one determinant for the high diffusivity through the mucus [98] and the high bioavailability of the drugs administered in SMEDDs [99,100]. It is noticeable however that the highest diffusivity among all 102 particles was the Innsbruck SMEDD incorporating the thiomer TBA-dodecylamine. Clearly the collective effect of the loaded thiol agent and the hydrophilic

surface of the SMEDDs contributed to this high diffusivity, where the thiol agent could serve a mucolytic role [71].

NPs representing the slippery-PEG strategy (RED symbols; Figure 3.7) and the slippery-polymer strategy (BLACK symbols; Figure 3.7) also showed higher diffusivities. This finding is not surprising as improved diffusion of NPs by coating them with a muco-inert hydrophilic shell is recognised [44,101]. For example, the coating of PLGA- dimethyldioctadecylammonium bromide (DDAB) NP with -DNA showing a 10-fold increase in the diffusion coefficient of uncoated PLGA NP of the same size [102].

NP loaded with mucolytic agents (GREEN symbols; Figure 3.7) were generally less diffusive than slippery surface (PEGylated and polymer mixture). The diffusive capacity of PEGylated particles is consistent with the findings of Hanes' group who showed that the diffusion of PEGylated NPs through CF mucus pre-treated with NAC was 40 times higher than that of PLGA NPs through the same pre-treated CF mucus [74]. This indicates that the slippery surface of the PEG NP still exerts a predominant impact even in NAC pre-treated CF mucus. As for NPs loaded with mucolytic agents then the diffusive capacity will depend to a large extent on the release profile of the mucolytic agent into the mucus to allow the particle diffusion through the disturbed mucin structure [87]. Insufficient release could result in inadequate mucolytic activity. Moreover, with excessive destruction of mucus then the release of mucin or other mucus components into the spaces of mucin network will increase the micro-viscosity of these water-filled channels resulting in restriction of particle diffusion [103].

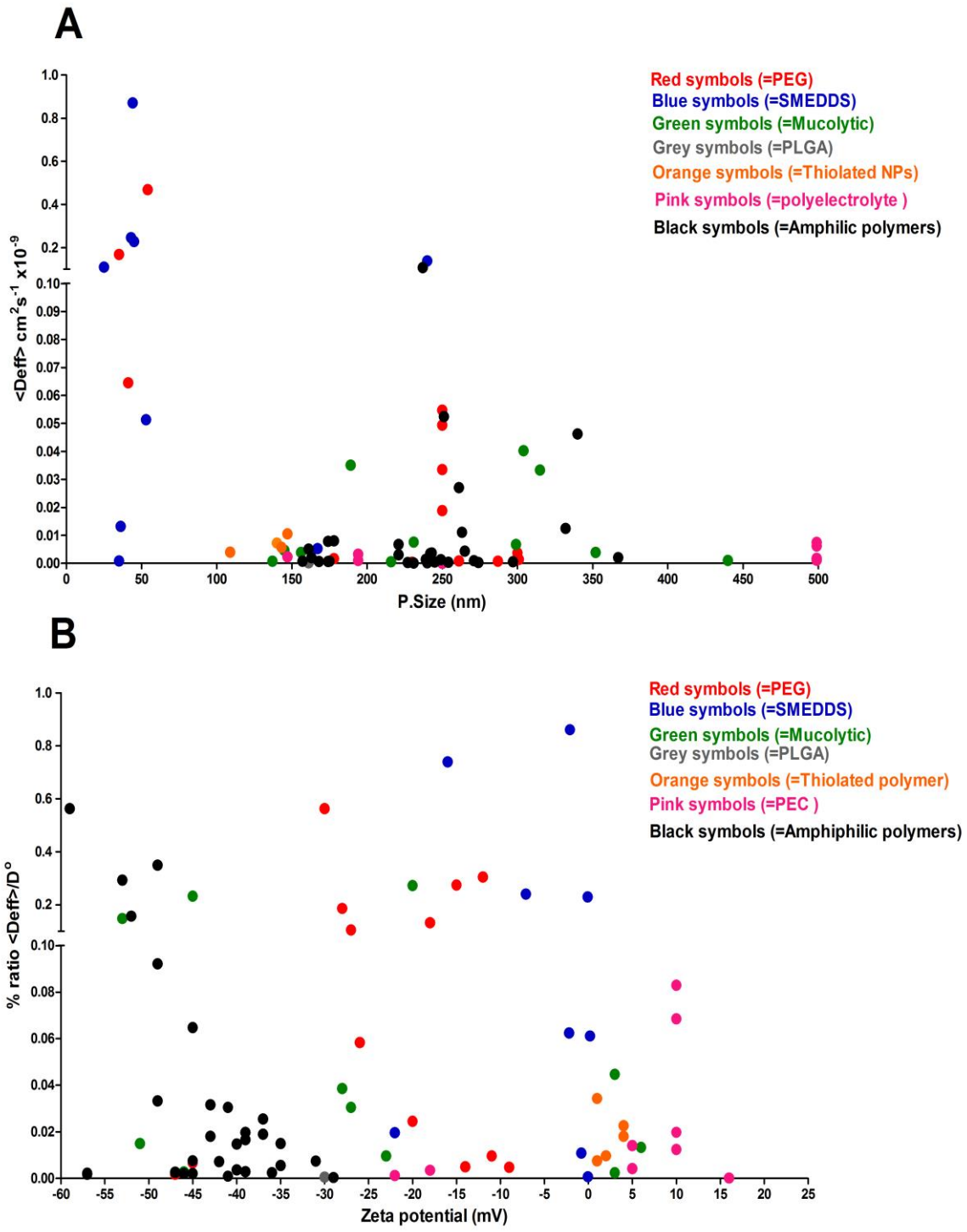

Figure 3.7: (A) Mucus diffusion <Deff> versus particle size of NPs made of various nano-strategies in the "Cardiff native mucus" model. (B) % ratio <Deff>/D° versus zeta potential of NPs made of various nano-strategies in the "Cardiff native mucus" model.

The PEC NP (PINK symbols) underpinning yet another slippery surface strategy generally showed lower diffusion capacity through mucus. The strategy represented an alternative easily fabricated NP approach toward mimicking the capsid virus with a highly charged surface with net neutral charge [21]. The low diffusion of PEC NPs reflects to some extent the heterogenous nature of the positive and negative polymer complexes resulting inevitably in polarised regions of surface charge unlike the very closely aligned positive and negative charges on viral capsids.

Thiomer technology (Orange symbols; Figure 3.7) showed very low diffusion capacity. As was mentioned earlier, the proposed mechanism of thiomer technology to improve diffusion through the mucus involves mucin cleavage, however, thiolated NPs showed less permeation through the mucus than that of the mucolytic NPs. This is consistent with the finding of Leitner et al. (2003) [93] who showed a more powerful mucolytic activity associated with NAC able to cleave the disulfide linkage between thiolated PAA NPs and porcine mucin. Another factor which can limit the activity of thiolated polymers is their stability as these polymers are readily oxidized in the solution [104]. The Bernkop-Schnürch group addressed this stability issue by protecting the thiomer polymer with mercaptonicotinic acid [105,106]. In their work the thiol groups were also conjugated to chitosan in the NPs such that the thiol agents were not be released into the mucus but remained conjugated with the chitosan NPs which assisted their muco-adhesive capabilities.

Lastly, PLGA NP was used by the partners as the lipophilic core for many of the strategies. The NPs formed only using polymer are muco-adhesive and were used in this section of work as a reference particle (Grey symbol; Figure 3.7). Not surprisingly the PLGA NPs showed almost the lowest permeation through mucus (ranked 99, Table 3.1). Although the low mucus permeation of PLGA is recognised [55,107], its muco-

adhesive properties can improve the in-vivo bioavailability of some drugs. For example, PLGA- fumaric anhydride- iron oxide NP improved the bioavailability of zinc insulin up to 11.4% of the intraperitoneally administered insulin [108].

Besides studies in the "Cardiff native mucus", the diffusion of all of the nano-strategies was also studied in the "Consortium mucus gel" In this latter mucus model the diffusivities of slippery-PEGylated particles, the slippery-polymer particles, the slippery-PEC particles and the mucolytic particles were studied. The diffusivities of the SMEDDS and the thiol particles were not studied as these particles were not stable under the circumstances required to undertake MPT with this "Consortium mucus gel" model. Specifically, this model required a centrifugation step to install particles into the mucus sample.

To obtain an improved perspective of the behaviour of the particles between the mucus models the data is compared in Figures 3.8 and 3.9. Figure 3.8 immediately shows that the diffusion of all particles was considerably more restricted in the Consortium mucus - gel model. Figure 3.9 shows the correlation in the ranking of diffusivities of NPs in both the Cardiff mucus model and the Consortium mucus-gel model. A good correlation was found with NPs ranked fast in the "Consortium mucus gel" model also ranked fast in the "Cardiff native mucus" model. Note the use of zero in the ranking co-ordinates, e.g. (0, 1) indicates the diffusion of the respective particle in the Consortium mucus-gel model could not be studied. The correlation indicates that particles have the same mechanism of diffusion and trapping in both mucus models but are slower in the "consortium mucus-gel" model due to the differences of the mechanical and physical proprties of each mucus model.

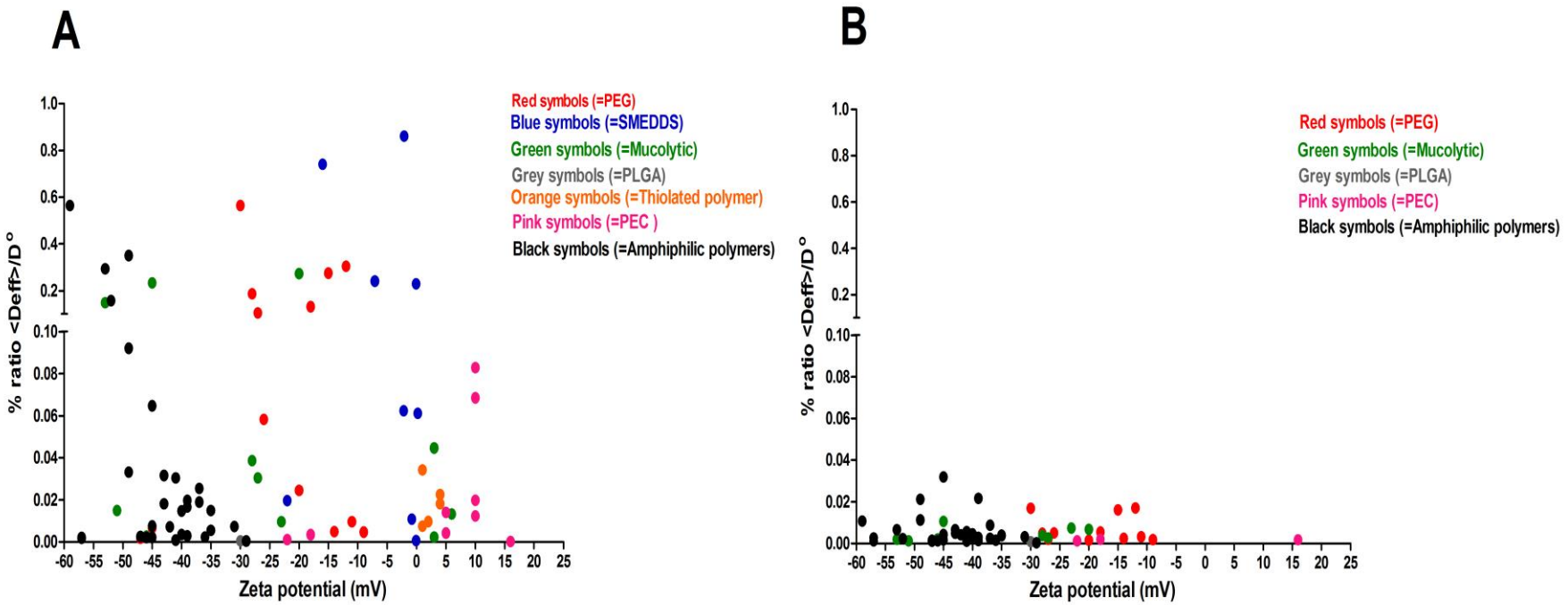

Figure 3.8: (A) % ratio <Deff>/D° versus zeta potential of NPs made of various nano-strategies in the "Cardiff mucus gel" (B) % ratio <Deff>/D° versus zeta potential of NPs made of various nano-strategies in the "Consortium mucus gel". (% ratio <Deff>/D° were expressed in the same scale for both figures (A and B) to highlight the differences in the values of diffusion between the two mucus models.

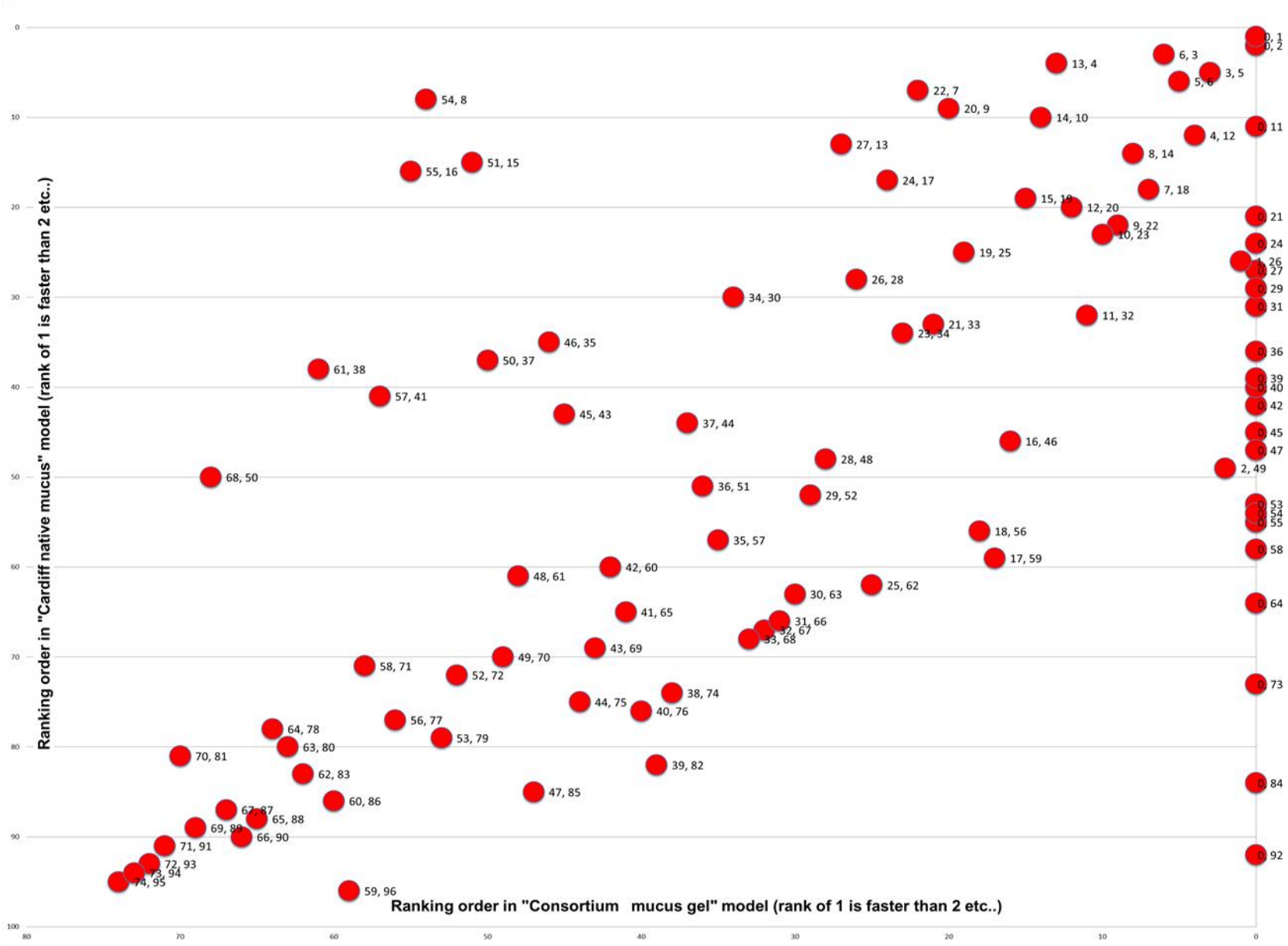

Figure 3.9: Correlation in ranking order of diffusivities of NPs in "Cardiff native mucus" model versus diffusivities of NPs in "Consortium mucus-gel" model.

4. SUMMARY AND CONCLUSION

In this chapter, NPs representing various nano-strategies to improve the diffusion through the mucus was studied. Within each nano-strategy, several findings were revealed. These conclusions can be classified for each nano-strategy as follows:

- **Slippery-PEG Strategy:**

1. NPs coated with PEG polymer have higher <Deff> and % <Deff>/D° than that of NPs coated with methoxy PEG.
2. NPs coated with low molecular weight PEG (2000 Da) have higher diffusion through the mucus as compared with NPs coated with high molecular weight PEG (5000 Da).
3. The diffusion of PLGA-PEG NPs through the mucus is highly affected by the method and condition of PEGylation of these NPs.

- **Slippery-Amphiphilic Polymers Strategy**

1. The diffusion of NPs in which the lipophilic core is coated with a hydrophilic shell increased as the ratio of the hydrophilic polymer increased to certain degree, this is followed by a reduction in the diffusion when the ratio of hydrophilic polymer further increased.
2. NPs coated with hydrophilic polymer showed higher diffusivities than NPs copolymerized with the same hydrophilic polymer.

- **Slippery-PEC NP Strategy**

1. There was not enough data to relate the diffusion of PEC NPs to their zeta potentials.
2. The diffusion of PEC NPs is highly influenced by the type of polymers forming these PEC NPs or the molecules conjugated within these PEC NPs.

- **SMEED Strategy**

1. There is no correlation between the particle size or zeta potential of SMEDD systems and their diffusivities through the mucus barrier.
2. The diffusion of SMEDD systems through the mucus is influenced by the ingredients in the system (oil, surfactant and co-surfactant).

- **Mucolytic NPs Strategy**

1. NPs loaded with proteolytic enzymes have generally higher diffusion through the mucus barrier than NPs loaded with disulfide breaking agents.
2. There is inverse relation between the concentration of NAC in the NPs and the diffusion of these NPs.
3. For all NPs loaded with mucolytic agents, NP dried by freeze drying method showed higher diffusion through the mucus than the same NP dried by the spray drying method.

- **Thiomer Strategy**

1. The diffusion of the thiolated NPs increases as the ratio of the thiomer in the NPs increases.

- **General Conclusion**

1. Slippery surface nano-strategy represented by the PEG NPs and amphiphilic polymer NPs and SMEDD systems were found to have the highest diffusion through the “Cardiff native mucus”.
2. PEC NPs were not covered properly in this chapter by the partners in the Consortium, hence, this strategy needs further studies to identify the impact of zeta potential on the diffusion of these NPs through mucus barrier.

5. References

[1] S.C. Bischoff, G. Barbara, W. Buurman, T. Ockhuizen, J.-D. Schulzke, M. Serino, et al., Intestinal permeability ¿ a new target for disease prevention and therapy., BMC Gastroenterol. 14 (2014) 189–214. doi:10.1186/s12876-014-0189-7.

[2] B.J. Bruno, G.D. Miller, C.S. Lim, Basics and recent advances in peptide and protein drug delivery., Ther. Deliv. 4 (2013) 1443–67. doi:10.4155/tde.13.104.

[3] A.F. Soares, R. de A. Carvalho, F. Veiga, Oral administration of peptides and proteins: nanoparticles and cyclodextrins as biocompatible delivery systems., Nanomedicine (Lond). 2 (2007) 183–202. doi:10.2217/17435889.2.2.183.

[4] A.J. Almeida, E. Souto, Solid lipid nanoparticles as a drug delivery system for peptides and proteins, Adv. Drug Deliv. Rev. 59 (2007) 478–490. doi:10.1016 /j.addr.2007.04.007.

[5] G.C. Hansson, Role of mucus layers in gut infection and inflammation, Curr. Opin. Microbiol. 15 (2012) 57–62. doi:10.1016/j.mib.2011.11.002.

[6] M. Ruponen, A. Urtti, Undefined role of mucus as a barrier in ocular drug delivery, Eur. J. Pharm. Biopharm. 96 (2015) 442–446. doi:10.1016/j.ejpb. 2015.02.032.

[7] M.L. Tan, P.F.M. Choong, C.R. Dass, Recent developments in liposomes, microparticles and nanoparticles for protein and peptide drug delivery, Peptides. 31 (2010) 184–193. doi:10.1016/j.peptides.2009.10.002.

[8] W. Shan, X. Zhu, M. Liu, L. Li, J. Zhong, W. Sun, et al., Overcoming the Diffusion Barrier of Mucus and Absorption Barrier of Epithelium by Self-Assembled Nanoparticles for Oral Delivery of Insulin, ACS Nano. 9 (2015) 2345–2356. doi:10.1021/acsnano.5b00028.

[9] S. Köllner, S. Dünnhaupt, C. Waldner, S. Hauptstein, I. Pereira de Sousa, A. Bernkop-Schnürch, Mucus permeating thiomer nanoparticles, Eur. J. Pharm. Biopharm. 97 (2015) 265–272. doi:10.1016/j.ejpb.2015.01.004.

[10] J. Woodley, Bioadhesion New Possibilities for Drug Administration? John, Clin. Pharmacokinet. 40 (2001) 77–84.

[11] K. Bowman, K.W. Leong, Chitosan nanoparticles for oral drug and gene delivery, Int. J. Nanomedicine. 1 (2006) 117–128. doi:10.2147/nano. 2006.1.2 .117.

[12] G. Ponchel, J.M. Irache, Specific and non-specific bioadhesive particulate systems for oral delivery to the gastrointestinal tract, Adv. Drug Deliv. Rev. 34 (1998) 191–219. doi:10.1016/S0169-409X(98)00040-4.

[13] D.J. Brayden, M. a. Jepson, A.W. Baird, Keynote review: Intestinal Peyer's patch M cells and oral vaccine targeting, Drug Discov. Today. 10 (2005) 1145–1157. doi:10.1016/S1359-6446(05)03536-1.

[14] M. a. Jepson, M.A. Clark, B.H. Hirst, M cell targeting by lectins: A strategy for mucosal vaccination and drug delivery, Adv. Drug Deliv. Rev. 56 (2004) 511–525. doi:10.1016/j.addr.2003.10.018.

[15] A. Des Rieux, E.G.E. Ragnarsson, E. Gullberg, V. Préat, Y.J. Schneider, P. Artursson, Transport of nanoparticles across an in vitro model of the human intestinal follicle associated epithelium, Eur. J. Pharm. Sci. 25 (2005) 455–465. doi:10.1016/j.ejps.2005.04.015.

[16] N. Foster, M.A. Clark, M. a. Jepson, B.H. Hirst, Ulex europaeus 1 lectin targets microspheres to mouse Peyer's patch M-cells in vivo, Vaccine. 16 (1998) 536–541. doi:10.1016/S0264-410X(97)00222-3.

[17] N. Hussain, A.T. Florence, Utilizing bacterial mechanisms of epithelial cell entry: Invasin-induced oral uptake of latex nanoparticles, Pharm. Res. 15 (1998) 153–156. doi:10.1023/A:1011981610840.

[18] O. Lieleg, K. Ribbeck, Biological hydrogels as selective diffusion barriers, Trends Cell Biol. 21 (2011) 543–551. doi:10.1016/j.tcb.2011.06.002.

[19] A. des Rieux, V. Fievez, M. Garinot, Y.J. Schneider, V. Préat, Nanoparticles as potential oral delivery systems of proteins and vaccines: A mechanistic approach, J. Control. Release. 116 (2006) 1–27. doi:10.1016/j.jconrel.2006.08.013.

[20] M. Liu, J. Zhang, W. Shan, Y. Huang, Developments of mucus penetrating nanoparticles, Asian J. Pharm. Sci. (2015) 8–15. doi:10.1016/j.ajps.2014.12.007.

[21] M. Abdulkarim, N. Agulló, B. Cattoz, P. Griffiths, A. Bernkop-Schnürch, S.G. Borros, et al., Nanoparticle diffusion within intestinal mucus: Three-dimensional response analysis dissecting the impact of particle surface charge, size and heterogeneity across polyelectrolyte, pegylated and viral particles, Eur. J. Pharm. Biopharm. 97 (2015) 230–238. doi:10.1016/j.ejpb.2015.01.023.

[22] R. a Cone, Barrier properties of mucus., Adv. Drug Deliv. Rev. 61 (2009) 75–85. doi:10.1016/j.addr.2008.09.008.

[23] a Wada, H. Nakamura, Nature of the charge distribution in proteins., Nature. 293 (1981) 757–758. doi:10.1038/293757a0.

[24] C.S. Rae, I. Wei Khor, Q. Wang, G. Destito, M.J. Gonzalez, P. Singh, et al., Systemic trafficking of plant virus nanoparticles in mice via the oral route, Virology. 343 (2005) 224–235. doi:10.1016/j.virol.2005.08.017.

[25] J. Sun, C. Dufort, M. Daniel, A. Murali, C. Chen, K. Gopinath, et al., Core-controlled polymorphism in virus-like particles, PNAS. 104 (2007) 1354–1359.

[26] C. Chen, E.-S. Kwak, B. Stein, C.C. Kao, B. Dragnea, Packaging of gold particles in viral capsids., J. Nanosci. Nanotechnol. 5 (2005) 2029–2033. doi:10.1166/jnn.2005.506.

[27] P.P. Constantinides, Lipid microemulsions for improving drug dissolution and oral absorption: physical and biopharmaceutical aspects., Pharm. Res. 12 (1995) 1561–72. doi:10.1023/A:1016268311867.

[28] C.W. Pouton, Formulation of self-emulsifying drug delivery systems, Adv. Drug Deliv. Rev. 25 (1997) 47–58. doi:10.1016/S0169-409X(96)00490-5.

[29] H. Friedl, S. Dünnhaupt, F. Hintzen, C. Waldner, S. Parikh, J.P. Pearson, et al., Development and Evaluation of a Novel Mucus Diffusion Test System Approved by Self-Nanoemulsifying Drug Delivery Systems, J. Pharm. Sci. 102 (2013) 4406–4413. doi:10.1002/jps.23757.

[30] B.K. Rubin, Mucus structure and properties in cystic fibrosis, Paediatr. Respir. Rev. 8 (2007) 4–7. doi:10.1016/j.prrv.2007.02.004.

[31] M.O. Henke, F. Ratjen, Mucolytics in cystic fibrosis, Paediatr. Respir. Rev. 8 (2007) 24–29. doi:10.1016/j.prrv.2007.02.009.

[32] N.N. Sanders, S.C. De Smedt, E. Van Rompaey, P. Simoens, F. De Baets, J. Demeester, Cystic fibrosis sputum: A barrier to the transport of nanospheres, Am. J. Respir. Crit. Care Med. 162 (2000) 1905–1911. doi:10.1164/ ajrccm. 162.5.9909009.

[33] A.E. Bell, L.A. Sellers, A. Allen, W.J. Cunliffe, E.R. Morris, S.B. Ross-Murphy, Properties of gastric and duodenal mucus: effect of proteolysis, disulfide reduction, bile, acid, ethanol, and hypertonicity on mucus gel structure., Gastroenterology. 88 (1985) 269–280. doi:10.1016/S0016-5085(85)80180-3.

[34] S. Dünnhaupt, O. Kammona, C. Waldner, C. Kiparissides, A. Bernkop-Schnürch, Nano-carrier systems: Strategies to overcome the mucus gel barrier, Eur. J. Pharm. Biopharm. 96 (2015) 447–453. doi:10.1016/j.ejpb.2015.01.022.

[35] Y. Wang, K. Hida, R. Cone, M. Sanson, Y. Vengrenyuk, J. Liu, et al., Nanoparticles reveal that human cervicovaginal mucus is riddled with pores larger than viruses, Proc. Natl. Acad. Sci. 108 (2011) 14371–14371. doi:10.1073 /pnas.1111693108.

[36] J.S. Suk, S.K. Lai, Y.-Y. Wang, L.M. Ensign, P.L. Zeitlin, M.P. Boyle, et al., The penetration of fresh undiluted sputum expectorated by cystic fibrosis patients by non-adhesive polymer nanoparticles., Biomaterials. 30 (2009) 2591–7. doi:10. 1016/j.biomaterials.2008.12.076.

[37] A.J. Kim, N.J. Boylan, J.S. Suk, M. Hwangbo, T. Yu, B.S. Schuster, et al., Use of single-site-functionalized PEG dendrons to prepare gene vectors that penetrate human mucus barriers, Angew. Chemie - Int. Ed. 52 (2013) 3985–3988. doi:10. 1002/anie.201208556.

[38] B.S. Schuster, J.S. Suk, G.F. Woodworth, J. Hanes, Nanoparticle diffusion in respiratory mucus from humans without lung disease, Biomaterials. 34 (2013) 3439–3446. doi:10.1016/j.biomaterials.2013.01.064.

[39] M. Yang, S.K. Lai, Y.Y. Wang, W. Zhong, C. Happe, M. Zhang, et al., Biodegradable nanoparticles composed entirely of safe materials that rapidly penetrate human mucus, Angew. Chemie - Int. Ed. 50 (2011) 2597–2600. doi:10.1002/anie.201006849.

[40] S.K. Lai, J.S. Suk, A. Pace, Y.Y. Wang, M. Yang, O. Mert, et al., Drug carrier nanoparticles that penetrate human chronic rhinosinusitis mucus, Biomaterials. 32 (2011) 6285–6290. doi:10.1016/j.biomaterials.2011.05.008.

[41] K.E. Uhrich, K.E. Uhrich, S.M. Cannizzaro, S.M. Cannizzaro, R.S. Langer, R.S. Langer, et al., Polymeric systems for controlled drug release, Chem. Rev. 99 (1999) 3181–3198. doi:10.1021/cr940351u.

[42] D.K. Sahana, G. Mittal, V. Bhardwaj, M.N.V.R. Kumar, PLGA nanoparticles for oral delivery of hydrophobic drugs: Influence of organic solvent on nanoparticle formation and release behavior in vitro and in vivo using estradiol as a model drug, J. Pharm. Sci. 97 (2008) 1530–1542. doi:10.1002/jps.21158.

[43] C. Wischke, S.P. Schwendeman, Principles of encapsulating hydrophobic drugs in PLA/PLGA microparticles, Int. J. Pharm. 364 (2008) 298–327. doi:10.1016/j.ijpharm.2008.04.042.

[44] T. Yu, Y.Y. Wang, M. Yang, C. Schneider, W. Zhong, S. Pulicare, et al., Biodegradable mucus-penetrating nanoparticles composed of diblock copolymers of polyethylene glycol and poly(lactic-co-glycolic acid), Drug Deliv. Transl. Res. 2 (2012) 124–128. doi:10.1007/s13346-011-0048-9.

[45] M. Yang, S.K. Lai, Y.Y. Wang, W. Zhong, C. Happe, M. Zhang, et al., Biodegradable nanoparticles composed entirely of safe materials that rapidly penetrate human mucus, Angew. Chemie - Int. Ed. 50 (2011) 2597–2600. doi:10.1002/anie.201006849.

[46] Y. Wang, S.K. Lai, J.S. Suk, A. Pace, R. Cone, J. Hanes, Addressing the PEG mucoadhesivity paradox to engineer nanoparticles that “slip” through the human mucus barrier., Angew. Chem. Int. Ed. Engl. 47 (2008) 9726–9. doi:10.1002/anie.200803526.

[47] J. V Jokerst, T. Lobovkina, R.N. Zare, S.S. Gambhir, Nanoparticle PEGylation for imaging and therapy., Nanomedicine (Lond). 6 (2011) 715–728. doi: 10.2217/nnm.11.19.

[48] Q. Xu, N.J. Boylan, S. Cai, B. Miao, H. Patel, J. Hanes, Scalable method to produce biodegradable nanoparticles that rapidly penetrate human mucus, J. Control. Release. 170 (2013) 279–286. doi:10.1016/j.jconrel.2013.05.035.

[49] N.J. Boylan, J.S. Suk, S.K. Lai, R. Jelinek, M.P. Boyle, M.J. Cooper, et al., Highly compacted DNA nanoparticles with low MW PEG coatings: In vitro, ex vivo and in vivo evaluation, J. Control. Release. 157 (2012) 72–79. doi:10.1016/j.jconrel.2011.08.031.

[50] N. a. Fefelova, Z.S. Nurkeeva, G. a. Mun, V. V. Khutoryanskiy, Mucoadhesive interactions of amphiphilic cationic copolymers based on [2-(methacryloyloxy)ethyl]trimethylammonium chloride, Int. J. Pharm. 339 (2007) 25–32. doi:10.1016/j.ijpharm.2007.02.019.

[51] R. Gref, a. Domb, P. Quellec, T. Blunk, R.H. Müller, J.M. Verbavatz, et al., The controlled intravenous delivery of drugs using PEG-coated sterically stabilized nanospheres, Adv. Drug Deliv. Rev. 64 (2012) 316–326. doi:10.1016/ j.addr .2012.09.008.

[52] S.K. Lai, D.E. O'Hanlon, S. Harrold, S.T. Man, Y.-Y. Wang, R. Cone, et al., Rapid transport of large polymeric nanoparticles in fresh undiluted human mucus., Proc. Natl. Acad. Sci. U. S. A. 104 (2007) 1482–7. doi:10.1073/pnas. 0608611104.

[53] O. Mert, S.K. Lai, L. Ensign, M. Yang, Y.Y. Wang, J. Wood, et al., A poly(ethylene glycol)-based surfactant for formulation of drug-loaded mucus penetrating particles, J. Control. Release. 157 (2012) 455–460. doi:10. 1016 /j.jconrel.2011.08.032.

[54] A.-C. Groo, K. Mircheva, J. Bejaud, C. Ailhas, I. Panaiotov, P. Saulnier, et al., Development of 2D and 3D mucus models and their interactions with mucus-penetrating paclitaxel-loaded lipid nanocapsules., Pharm. Res. 31 (2014) 1753–65. doi:10.1007/s11095-013-1280-4.

[55] Y. Cu, W.M. Saltzman, Controlled surface modification with poly(ethylene)glycol enhances diffusion of PLGA nanoparticles in human cervical mucus., Mol. Pharm. 6 (2010) 173–81. doi:10.1021/mp8001254.

[56] P. Bures, Y. Huang, E. Oral, N. a. Peppas, Surface modifications and molecular imprinting of polymers in medical and pharmaceutical applications, J. Control. Release. 72 (2001) 25–33. doi:10.1016/S0168-3659(01)00259-0.

[57] Y. Huang, W. Leobandung, A. Foss, N. a Peppas, Molecular aspects of muco- and bioadhesion: Tethered structures and site-specific surfaces, J. Control. Release. 65 (2000) 63–71. doi:10.1016/S0168-3659(99)00233-3.

[58] N. V. Efremova, Y. Huang, N. a. Peppas, D.E. Leckband, Direct measurement of interactions between tethered poly(ethylene glycol) chains and adsorbed mucin layers, Langmuir. 18 (2002) 836–845. doi:10.1021/la011303p.

[59] A. Beloqui, M.Á. Solinís, A. Des Rieux, V. Préat, A. Rodríguez-Gascón, Dextran-protamine coated nanostructured lipid carriers as mucus-penetrating nanoparticles for lipophilic drugs, Int. J. Pharm. 468 (2014) 105–111. doi:10.1016/j.ijpharm.2014.04.027.

[60] M. a Campanero, M. a Arangoa, M.J. Renedo, J.M. Irache, I nfluence of the surface characteristics of PVM / MA nanoparticles on their bioadhesive properties, J. Control. Release. 89 (2003) 19–30.

[61] J. De Souza Rebouças, I. Esparza, M. Ferrer, M.L. Sanz, J.M. Irache, C. Gamazo, Nanoparticulate adjuvants and delivery systems for allergen immunotherapy, J. Biomed. Biotechnol. 2012 (2012). doi:10.1155/2012/474605.

[62] P. Arbós, M. Wirth, M. a Arangoa, F. Gabor, J.M. Irache, Gantrez®AN as a new polymer for the preparation of lignad-nanoparticle conjugates, J. Control. Rel. 83 (2002) 321–330.

[63] P. Arbós, M. a. Arangoa, M. a. Campanero, J.M. Irache, Quantification of the bioadhesive properties of protein-coated PVM/MA nanoparticles, Int. J. Pharm. 242 (2002) 129–136. doi:10.1016/S0378-5173(02)00182-5.

[64] A.C. Groo, F. Lagarce, Mucus models to evaluate nanomedicines for diffusion, Drug Discov. Today. 19 (2014) 1097–1108. doi:10.1016/j.drudis.2014.01.011.

[65] L.J. Saif, E.H. Bohl, K.W. Theil, R.F. Cross, J.A. House, Particles Associated with Diarrhea in Young Pigst, J. Clin. Microbiol. 12 (1980) 105–111.

[66] S.S. Olmsted, J.L. Padgett, a I. Yudin, K.J. Whaley, T.R. Moench, R. a Cone, Diffusion of macromolecules and virus-like particles in human cervical mucus., Biophys. J. 81 (2001) 1930–7. doi:10.1016/S0006-3495(01)75844-4.

[67] F. Laffleur, F. Hintzen, G. Shahnaz, D. Rahmat, K. Leithner, A. Bernkop-Schnürch, Development and in vitro evaluation of slippery nanoparticles for enhanced diffusion through native mucus., Nanomedicine (Lond). 9 (2014) 387–96. doi:10.2217/nnm.13.26.

[68] X. Sha, J. Wu, Y. Chen, X. Fang, Self-microemulsifying drug-delivery system for improved oral bioavailability of probucol: Preparation and evaluation, Int. J. Nanomedicine. 7 (2012) 705–712. doi:10.2147/IJN.S28052.

[69] Z.Q. Chen, Y. Liu, J.H. Zhao, L. Wang, N.P. Feng, Improved oral bioavailability of poorly water-soluble indirubin by a supersaturatable self-microemulsifying drug delivery system, Int. J. Nanomedicine. 7 (2012) 1115–1125. doi:10.2147/IJN.S28761.

[70] T. Do Thi, M. Van Speybroeck, V. Barillaro, J. Martens, P. Annaert, P. Augustijns, et al., Formulate-ability of ten compounds with different physicochemical profiles in SMEDDS, Eur. J. Pharm. Sci. 38 (2009) 479–488. doi:10.1016/j.ejps.2009.09.012.

[71] J. Rohrer, Mucus permeating SMEDDS containing thiolated compounds, in: Pharm. Nov. Drug Deliv. Syst., omics, 2015: p. 75. doi:org/10.4172/2153-2435.S1.024.

[72] M.F. Abdulkarim, G.Z. Abdullah, M. Chitneni, I.M. Salman, O.Z. Ameer, M.F. Yam, et al., Topical piroxicam in vitro release and in vivo anti-inflammatory and analgesic effects from palm oil esters-based nanocream., Int. J. Nanomedicine. 5 (2010) 915–924. doi:10.2147/IJN.S13305.

[73] J. Zhang, Y. Lv, B. Wang, S. Zhao, M. Tan, G. Lv, et al., Influence of Microemulsion–Mucin Interaction on the Fate of Microemulsions Diffusing through Pig Gastric Mucin Solutions, Mol. Pharm. 12 (2015) 695–705. doi:10.1021/mp500475y.

[74] J.S. Suk, S.K. Lai, N.J. Boylan, M.R. Dawson, M.P. Boyle, J. Hanes, Rapid transport of muco-inert nanoparticles in cystic fibrosis sputum treated with N-acetyl cysteine., Nanomedicine (Lond). 6 (2011) 365–75. doi:10.1016/j.

[75] J. Khan, Y. Iiboshi, L. Cui, M. Wasa, A. Okada, Role of intestinal mucus on the uptake of latex beads by Peyer's patches and on their transport to mesenteric lymph nodes in rats., JPEN. J. Parenter. Enteral Nutr. 23 (1999) 19–23. doi:10.1177/014860719902300119.

[76] C.T. Albanese, S.D. Smith, S. Watkins, A. Kurkchubasche, R.L. Simmons, M.I. Rowe, Role of intestinal mucus in transepithelial passage of bacteria across the intact ileum in vitro., J. Am. Coll. Surg. 116 (1994) 76–82.

[77] S.R. Hoover, Elsie L. C. Kokes, Effect ofF pH upon proteolysis by papaine, J. Biol. Chem. 167 (1946) 199–207.

[78] M.L. Scott, C.A. Johnson, P.K. Phillips, The pH optima for papain and bromelain treatment of red cells., Vox Sang. 52 (1987) 223–227.

[79] C. Müller, K. Leithner, S. Hauptstein, F. Hintzen, W. Salvenmoser, A. Bernkop-Schnürch, Preparation and characterization of mucus-penetrating papain/poly(acrylic acid) nanoparticles for oral drug delivery applications, J. Nanoparticle Res. 15 (2012) 1353–1366. doi:10.1007/s11051-012-1353-z.

[80] C. Müller, G. Perera, V. König, A. Bernkop-schnürch, Development and in vivo evaluation of papain-functionalized nanoparticles, Eur. J. Pharm. Biopharm. 87 (2014) 125–131. doi:10.1016/j.ejpb.2013.12.012.

[81] J. Akhter, K. Pillai, T.C. Chua, N. Alzarin, D.L. Morris, Efficacy of a novel mucolytic agent on pseudomyxoma peritonei mucin, with potential for treatment through peritoneal catheters., Am. J. Cancer Res. 4 (2014) 495–507.

[82] J.S. Suk, N.J. Boylan, K. Trehan, B.C. Tang, C.S. Schneider, J.-M.G. Lin, et al., N-acetylcysteine Enhances Cystic Fibrosis Sputum Penetration and Airway Gene Transfer by Highly Compacted DNA Nanoparticles, Mol. Ther. 19 (2011) 1981–1989. doi:10.1038/mt.2011.160.

[83] S. Ferrari, C. Kitson, R. Farley, R. Steel, C. Marriott, D. a Parkins, et al., Mucus altering agents as adjuncts for nonviral gene transfer to airway epithelium., Gene Ther. 8 (2001) 1380–1386. doi:10.1038/sj.gt.3301525.

[84] V.J. Broughton-Head, J.R. Smith, J. Shur, J.K. Shute, Actin limits enhancement of nanoparticle diffusion through cystic fibrosis sputum by mucolytics, Pulm. Pharmacol. Ther. 20 (2007) 708–717. doi:10.1016/j.pupt.2006.08.008.

[85] L.M. Ensign, C. Schneider, J.S. Suk, R. Cone, J. Hanes, Mucus penetrating nanoparticles: Biophysical tool and method of drug and gene delivery, Adv. Mater. 24 (2012) 3887–3894. doi:10.1002/adma.201201800.

[86] M.D. Wilcox, L.K. Van Rooij, P.I. Chater, I. Pereira de Sousa, J.P. Pearson, The effect of nanoparticle permeation on the bulk rheological properties of intestinal mucus from the small intestine, Eur. J. Pharm. Biopharm. 96 (2015) 484–7. doi:10.1016/j.ejpb.2015.02.029.

[87] V. Bourganis, T. Karamanidou, E. Samaridou, K. Karidi, O. Kammona, C. Kiparissides, On the synthesis of mucus permeating nanocarriers, Eur. J. Pharm. Biopharm. 97 (2015) 239–49. doi:10.1016/j.ejpb.2015.01.021.

[88] A. Bernkop-Schnürch, V. Schwarz, S. Steininger, Polymers with thiol groups: A new generation of mucoadhesive polymers?, Pharm. Res. 16 (1999) 876–881. doi:10.1023/A:1018830204170.

[89] C.E. Kast, A. Bernkop-Schnürch, Thiolated polymers - thiomers: Development and in vitro evaluation of chitosan-thioglycolic acid conjugates, Biomaterials. 22 (2001) 2345–2352. doi:10.1016/S0142-9612(00)00421-X.

[90] F. Talaei, E. Azizi, R. Dinarvand, F. Atyabi, Thiolated chitosan nanoparticles as a delivery system for antisense therapy: evaluation against EGFR in T47D breast cancer cells., Int. J. Nanomedicine. 6 (2011) 1963–1975. doi:10.2147/ IJN. S22731.

[91] A. Bernkop-Schnürch, D. Guggi, Y. Pinter, Thiolated chitosans: Development and in vitro evaluation of a mucoadhesive, permeation enhancing oral drug delivery system, J. Control. Release. 94 (2004) 177–186. doi:10.1016/j.jconrel. 2003.10.005.

[92] P. Yousefpour, F. Atyabi, R. Dinarvand, E. Vasheghani-Farahani, Preparation and comparison of chitosan nanoparticles with different degrees of glutathione thiolation., Daru. 19 (2011) 367–75.

[93] V.M. Leitner, G.F. Walker, A. Bernkop-Schnürch, Thiolated polymers: Evidence for the formation of disulphide bonds with mucus glycoproteins, Eur. J. Pharm. Biopharm. 56 (2003) 207–214. doi:10.1016/S0939-6411(03)00061-4.

[94] K. Gradauer, J. Barthelmes, C. Vonach, G. Almer, H. Mangge, B. Teubl, et al., Liposomes coated with thiolated chitosan enhance oral peptide delivery to rats, J. Control. Release. 172 (2013) 872–878. doi:10.1016/j.jconrel.2013.10.011.

[95] A. Bernkop-Schnürch, C.E. Kast, D. Guggi, Permeation enhancing polymers in oral delivery of hydrophilic macromolecules: Thiomer/GSH systems, J. Control. Release. 93 (2003) 95–103. doi:10.1016/j.jconrel.2003.05.001.

[96] A. Bernkop-Schnürch, S.C. Thaler, Polycarbophil-cysteine conjugates as platforms for oral polypeptide delivery systems, J. Pharm. Sci. 89 (2000) 901–909. doi:10.1002/1520-6017(200007)89:7<901::AID-JPS7>3.0.CO;2-0.

[97] S. Hauptstein, A. Bernkop-Schnürch, Thiomers and thiomer-based nanoparticles in protein and DNA drug delivery, Expert Opin. Drug Deliv. 9 (2012) 1069–1081. doi:10.1517/17425247.2012.697893.

[98] F. Laffleur, A. Bernkop-Schnürch, Strategies for improving mucosal drug delivery., Nanomedicine (Lond). 8 (2013) 2061–75. doi:10.2217/nnm.13.178.

[99] B.K. Kang, J.S. Lee, S.K. Chon, S.Y. Jeong, S.H. Yuk, G. Khang, et al., Development of self-microemulsifying drug delivery systems (SMEDDS) for oral bioavailability enhancement of simvastatin in beagle dogs, Int. J. Pharm. 274 (2004) 65–73. doi:10.1016/j.ijpharm.2003.12.028.

[100] F. Hintzen, G. Perera, S. Hauptstein, C. Müller, F. Laffleur, A. Bernkop-Schnürch, In vivo evaluation of an oral self-microemulsifying drug delivery system (SMEDDS) for leuprorelin, Int. J. Pharm. 472 (2014) 20–26. doi:10.1016 /j.ijpharm.2014.05.047.

[101] L.M. Ensign, B.C. Tang, Y.-Y. Wang, T.A. Tse, T. Hoen, R. Cone, et al., Mucus-Penetrating Nanoparticles for Vaginal Drug Delivery Protect Against Herpes Simplex Virus, Sci. Transl. Med. 4 (2012) 138ra79–138ra79. doi:10.1126/ scitr anslmed.3003453.

[102] M. Dawson, E. Krauland, D. Wirtz, J. Hanes, Transport of polymeric nanoparticle gene carriers in gastric mucus, Biotechnol. Prog. 20 (2004) 851–857. doi:10.1021/bp0342553.

[103] M. Dawson, D. Wirtz, J. Hanes, Enhanced Viscoelasticity of Human Cystic Fibrotic Sputum Correlates with Increasing Microheterogeneity in Particle Transport, J. Biol. Chem. 278 (2003) 50393–50401. doi:10.1074/jbc. M30902 6200.

[104] E. Lallana, N. Tirelli, Oxidation-responsive polymers: Which groups to use, how to make them, what to expect from them (biomedical applications), Macromol. Chem. Phys. 214 (2013) 143–158. doi:10.1002/macp.201200502.

[105] S. Dünnhaupt, J. Barthelmes, C.C. Thurner, C. Waldner, D. Sakloetsakun, A. Bernkop-Schnürch, S-protected thiolated chitosan: Synthesis and in vitro characterization, Carbohydr. Polym. 90 (2012) 765–772. doi:10.1016/j. carbpol. 2012.05.028.

[106] J. Iqbal, G. Shahnaz, S. Dünnhaupt, C. Müller, F. Hintzen, A. Bernkop-Schnürch, Preactivated thiomers as mucoadhesive polymers for drug delivery, Biomaterials. 33 (2012) 1528–1535. doi:10.1016/j.biomaterials.2011.10.021.

[107] E. Samaridou, K. Karidi, I.P. de Sousa, B. Cattoz, P. Griffiths, O. Kammona, et al., Enzyme-Functionalized PLGA Nanoparticles with Enhanced Mucus

Permeation Rate, Nano Life. 04 (2014) 1441013. doi:10.1142/S179398 441441 013X.

[108] G.P. Carino, J.S. Jacob, E. Mathiowitz, Nanosphere based oral insulin delivery, J. Control. Release. 65 (2000) 261–269. doi:10.1016/S0168-3659(99)00247-3.

CHAPTER FOUR

KINETIC STUDIES ON THE DIFFUSION THROUGH THE "CARDIFF NATIVE MUCUS" MODEL OF POLYELECTROLYTE NPs

1 INTRODUCTION

1.a Slippery Surface NPs: PEC NPs versus PEG Surface NPs and Adenovirus

In Chapter three, diffusion coefficient of 102 NPs representing six different nano-strategies were screened to identify a nano-strategy that can be adopted by our group. Slippery NPs strategies (especially PEG) were found to be promising nano-strategies where the MPT analysis showed them to have high diffusions through both "Cardiff Native Mucus" model and "Consortium Mucus gel" model. This strategy was utilised to mimic the capsid virus shell which was reported to be freely diffusible through the mucus. The concept of modifying surfaces of NPs by PEGylation to generate a polar particle surface was first described by Lai et al. (2007) [1]. The term "slippery surface NPs" was used to describe the polar, electrically neutral surface synthetic particle by Cu & Saltzman (2009) [2]. This concept identifies the surface chemistry of NPs as the most influential factor on the diffusion of NPs through the mucus barrier. For example, Hanes' group [3] has shown that PEGylation of a 500 nm polystyrene particle increased its diffusion through mucus by >1000-fold, where particle's surface had a more profound impact than NPs particle size. PEGylation is preferable to mimic the surface characteristics of viruses since PEG NPs do not aggregate when their surface charges approaches neutrality [4].

On the other hand, PEC NP which is one of the techniques to synthesize slippery surface nano-strategy was not widely studied in the previous chapter and PEC NPs synthesized by partners in the consortium were limited in term of their range of zeta potential. Moreover, in the literatures, there is no enough data available about the impact of PEC NPs on the diffusion through the mucus. Nevertheless, there is some evidence that a synthetic particle of near-neutral surface charge (+0.9 mV), and

comprising PAA (-ve) and PAM (+ve) polymers (Figure 4.1B), does show improved mucus permeation, at least in an in-vitro side-by-side diffusion chamber model [5]. Hence, PEC NPs could be another synthetic strategy that can mimic capsid viruses to slip through mucus.

The process by which PEC NPs formed is called self-assembly in which, negatively charge (polyanions) polymer and positively charged (polycations) polymers are assembled spontaneously to form NPs with net charge proportional to the ratio of each polymer [6]. These PEC NPs are characterized by very high charge density on their surface, other characteristics of these NPs are determined by the polymers' molecular weights and concentration, pH, ionic strength of the solvent and mixing time [7]. Chitosan (Figure 4.1) is an amino-polysaccharide polymer that is formed by the de-acetylation of the naturally amino-polysaccharide Chitin which is found in the fungal cell walls [8]. Presence of amino group as well as the low toxicity of chitosan makes this polymer a good candidate as a source of the polycation polymer for the formation of PEC NPs [9]. On the other hand, PAA (Figure 4.2) is biocompatible non cytotoxic polymer possessing carboxylate group in each acrylate unit which makes it a good source of the negatively charged polymer [10]. For these reasons, these polymers were selected to be used as the source of the oppositely charged polymers to form PEC NPs in this chapter.

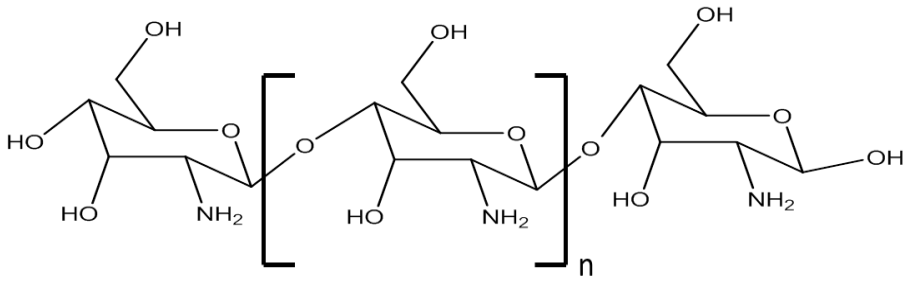

Figure 4.1: Chitosan polymer structure consisting of repetitive D-glucosamine unit.

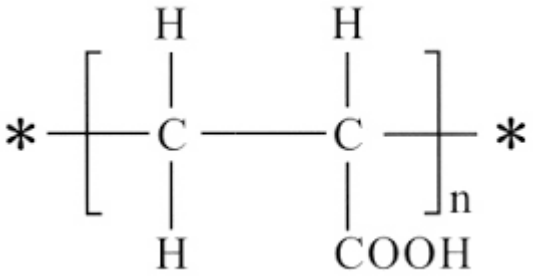

Figure 4.2: PAA polymer consisting of repetitive acrylic acid units.

Both of the abovementioned synthetic NPs were used to mimic the capsid viruses which are known to freely diffuse through the mucus. For example, some viral particles are well adapted for efficient mucus permeation, for example, the Norwalk virus (38 nm) and human Papilloma virus (55nm) appeared to penetrate intestinal mucus in an unrestricted manner [11]. The general features enabling the permeation of such viruses appear to be their small size, the lack of a hydrophobic envelope, and the possession of an exposed hydrophilic protein capsid shell characterised by a high surface density of +/- charges giving a net membrane potential close to neutrality [11,12].

Generally, growing of the aforementioned slippery viruses in the laboratory is complicated [12]. However, some other capsid viruses such as adenoviruses (AD), specifically AD5, can be grown and amplified safely in the laboratory. These viruses are characterized by a hydrophilic protein shell consisting of hexon and penton peptides

domains [13]. Some types of AD were found to permeate through and infect intestinal mucosal membrane in children resulting in gastroenteritis [14]. Hence, these viruses are a good slippery surface model to be studied for mucus permeation by the MPT technique.

1.b Aim of the Study

The purpose of the current work is to explore the impact upon NP diffusional kinetics through "Cardiff Native Mucus" Model of the variables of particle surface charge and size. To do so, PEC NPs were assembled at various ratios of (PAA:chitosan) to synthesize PEC NPs with wide range of surfaces' charge extending from highly negative to neutral up to highly positive charge and with various particles sizes. In particular we sought to examine the impact of zeta potential and particle sizes on the diffusion of synthetic PEC NPs. Beyond diffusion coefficients per se, we will report on the proportion of diffusive particles in each formulation, and the heterogeneity of diffusion within sub-populations of a given particle type.

The aim of this chapter is to compare the diffusion behaviour of different slippery (synthetic and natural) surface NPs. To do so, the diffusion kinetics of PEC NPs will be compared with the diffusion kinetics of PEG-PLGA NP (non-charged hydrophilic particle), and with the naturally near neutral surface charge capsid virus. PLGA NPs was used as a reference representing a muco-adhesive lipophilic particle.

2. MATERIALS AND METHODS

2.a Materials

The chitosan polymer (low MW), PAA polymer (MW 1800) and MES buffer were obtained from Sigma-Aldrich (UK). PLGA NPs, PEGylated-PLGA NPs and Lumogen Red-305 (excitation 573 nm emission 612 nm) were supplied by Nanomi (Netherlands). The amplified AD5 virus was kindly provided by the Institute of Cancer Genetics (Cardiff University). Alexa Fluor® 488 Protein labelling kit was from Life Technologies (UK). Glass bottom imaging dishes (35 mm diameter dish with a glass coverslip at 1.5 mm thick and 10mm diameter) were from MatTek Corporation (USA). All other reagents and solvents were from Fisher Scientific (Loughborough, UK).

2.b NPs Preparation

The polyelectrolyte NPs were synthesized by the self-assembly technique [15] in which 0.02% $^{w}/_{v}$ chitosan solution was added drop wise (1 drop/min) into 0.02% $^{w}/_{v}$ PAA solution under continuous magnetic stirring (100 rpm) for overnight. To prepare the stock solution of each polymer, chitosan stock solution of 1% $^{w}/_{v}$ was prepared by dissolving chitosan in 1% glacial acetic acid, oppositely, 1% $^{w}/_{v}$ PAA stock solution was prepared by dissolving the polymer in distilled deionised water (DDW). The dilute solutions of both polymers were prepared by diluting the stock solutions of them to 0.02% $^{w}/_{v}$ with MES buffer pH 6.5. The use of MES buffer in the NP self-assembly process avoided precipitation issues evident when phosphate or citrate buffers were used. To synthesise NPs with a wide range of zeta potentials, chitosan and PAA were mixed at different ratios of each polymer, these ratios are described in Table 4.1.

Lumogen Red-305 was loaded into the NPs by the co-acervation technique [16], whereby Lumogen Red-305 was dissolved in acetone at a concentration of 0.2 % $^{w}/_{v}$

then added to the dilute solution of PAA prior to the drop-wise addition of chitosan solution. The mass of Lumogen Red-305 added equated to 75 μg Lumogen Red-305 per 30 mg of combined PAA:chitosan polymer. The acetone was evaporated during the overnight mixing allowing the loading of Lumogen Red-305 to the core of the PEC NPs.

2.c NPs Sonication

Polyelectrolyte NPs displaying a neutral surface charge (i.e. PAA:chitosan mass ratios of 1:2.2) gave rise to large particles. Given a key aim of the study to investigate the relative significance of charge and size as independent variables, these large neutral particles were temporarily reduced in size by probe sonication. Accordingly, suspensions of the neutral NPs (ca 1200 nm) were sonicated (Fisher scientific probe sonicator, UK) for 2 min at 20 KHz and 70% amplitude with the suspension then syringe-filtered through 0.45μm membrane (Millipore, UK). Particle size and zeta potential were measured immediately after filtration and over a subsequent test period (2 hr) to ensure a sufficient duration of size stability to enable the conduct of the mucus diffusion studies. To serve as controls for the sonication process, both positively-charged (i.e. PAA:chitosan mass ratio of 1:8) and negatively-charged (i.e. PAA:chitosan mass ratio of 1:1) polyelectrolyte NPs were also subject to the sonication process and their diffusion characteristics (before and after) were determined.

2.d Characterisation of PEC NPs

Zeta Potential Measurement

A Malvern NANO ZS (Malvern, UK) was used to measure the zeta potential of the NP samples. The instrument was standardised prior to each experiment by use of calibration standards.

Particle Size Measurement

Particle size was measured by photon correlation spectroscopy (Malvern NANO ZS) with data collected in uni-modal setting. The instrument was standardised prior to each experiment by use of calibration standards.

2.e Multiple Particle Tracking (MPT) in "Cardiff Native Mucus" Model

Diffusion coefficients in mucus and water were measured following the same procedures and method described in chapter 2. Other kinetic analysis data were measured as follows:

Proportion of Diffusive Particles

Measuring particle diffusion across various time intervals allows for a description of the proportion of particles that are diffusive through the mucus matrix [1].

Equation 4.1 was used to determine a Diffusivity Factor (DF) which expresses the effective diffusion coefficient for each individual particle (Deff) across the time intervals (Δt) of 1 sec. and 0.2 sec.

$$DF = Deff_{\Delta t=1\ sec} / Deff_{\Delta t=0.2\ sec} \qquad \text{Equation 4.1}$$

Where the individual particle Deff = MSD/ (4 * Δt). Particles with a DF value of 0.9 and greater were defined as diffusive. The proportion of the diffusive particles within a given NP type under study was then calculated and expressed as % Diffusive particles.

Heterogeneity in Particle Diffusion

Profiling the diffusive properties of each particle within an entire population provides information on the heterogeneity of particle movement and the presence of outlier sub-populations that may follow distinct pathways of diffusion through the matrix. Here the effective diffusion coefficient for each individual particle (Deff) was calculated at the time interval (Δt) of 1 sec, and for any NP type all 360 Deff $_{\Delta t=1\ sec}$ were then ranked to allow comparison of the highest (90^{th}) and lowest (10^{th}) percentiles, where for example the 90^{th} percentile is the Deff value below which 90% of the Deff observations may be found.

Statistical Analysis

One-way analysis of variance test was used to compare the percent of ratio of Deff vs D° for all the particles with significant value of $p < 0.05$.

3. RESULTS AND DISCUSSION

In Chapter three, various strategies were examined including PEC NPs. However, all the PEC NPs that have been designed by the partners in the Alexander consortium did not express the critical points about using of PEC NPs as slippery surface nano-strategy. I.e, studies did not mimic the surface properties of the muco-inert capsid shell viruses in term of having neutrally charged surfaces (minimum zeta potential was +5 for the NPs synthesized by consortium partners). Moreover, studies did not show the effect of the charge variation on the diffusivity of these particles through the mucus (PEC NPs in chapter three were not synthesized with a wide range of zeta potentials). To overcome these issues, the study in this chapter was designed to examine the slippery surface properties of PEC NPs that mimicking the capsid shell viruses and having a wide range of highly negative and positive charged surface NPs.

Specifically, MPT methodology was used to explore the PEC NPs diffusivity and how the diffusivity through the "Cardiff Native Mucus" Model is influenced by the variation of particle surface charge, where a series of PEC NPs composed of different ratios of the charged polymers PAA (-ve) and chitosan (+ve) were synthesized. In particular, to mimic the neutrally highly charged capsid shell viruses, reasonably small sized PEC NPs with near neutral charged was formulated and its diffusivity through the mucus barrier was studied. To overcome the aggregation of neutrally surface charged particles, sonication technique was used to produce near neutral charged PEC NPs that is stable enough to be examined for its diffusivity.

This aim was driven by the fact of the effectiveness of some viral particles to permeate through mucus not only as a result of their small particle dimensions, but also through possession of a highly charged near-neutral exterior facing surface. Hence, the kinetic

diffusivities of the PEC NPs were compared to the diffusion kinetics of a capsid virus represented by AD5 with a near neutral surface charge. Also, the comparisons of the kinetics of diffusion include the use of the non-charged hydrophilic particle represented by PEGylated PLGA. Lastly, muco-adhesive lipophilic NP represented by PLGA NP was used as a negative control since it is expected to have the lowest permeability through the mucus barrier.

3.a PEC NPs Synthesis and Characterisation

PEC NP based on chitosan and PAA has been widely studied in term of particle size and stability [17]. Fourier transforms infrared spectroscopy (FT-IR) analysis has shown an electrostatic interaction between the Chitosan NH3+ group and the PAA COO- group, this electrostatic interaction was found to be responsible for the self-assembly process associated with the formation of these PEC NPs [18]. In our study, low molecular weight chitosan was used which was reported to induce smaller particle size NPs as compared to the higher molecular weight [19]. Mixing of chitosan and PAA at various ratios enables the formation of NPs with a wide variety of surface charges extending form highly positive to near neutral charge up to highly negative charges. However, the mechanism of the PEC NPs formation requires that both polymers to be ionized to complete the self-assembly process. Hence, these polymers were mixed at pH 6.5. This pH value was selected to be close to the pH in the intestine and to induce the ionization of chitosan and PAA depending on their pK_a values [20].

Among all the types of buffers tried, MES buffer showed the best reproducibility and consistency of particle sizes and zeta potentials. Carboxylate containing buffers like citrate and phosphate precipitated chitosan when they were used as the buffer system. This was due to the ionic interaction of chitosan amino group and carboxylate group of

these buffers [21]. Accordingly, use of HEPES buffer generated unstable dissociated PEC NP which was attributed to the high salt content in HEPES buffer. It seems this high salt content initiated a screening effect on the functional groups of the oppositely charged polymers which eliminate the electrostatic interaction between the polymers [22]. Dissociation effect was similar when the highly ionic strength buffer, formic acid was used.

Table 4.1 shows the zeta potential and particle size measurements of PEC NPs comprising formulations of various PAA to chitosan polymer mass ratios. In the table, PEC NPs were classified into the negatively charged, neutral and the positively charged particles. A range of ratios of PAA:Chitosan extending from (5:1) to (1:8) was examined in this study to achieve the highest possible positively and negatively charged PEC NPs. It can be seen that a broad range of surface charges was obtained ranging from -30 mV (PAA: chitosan mass ratio of 5:1) to +20 mV (PAA: chitosan mass ratio of 1:8). Also, PEC NPs were given symbol of F that is increasing from F1 to F14 in accordance with the change of the PAA:Chitosan ratios from (5:1) to (1:8).

A zeta potential value close to neutral (i.e. -0.5 mV) was attained at a PAA: chitosan mass ratio of 1:2.2 indicating higher charge density of PAA than that of the chitosan. This could be attributed to the higher number of the small acrylic acid units (72.06 gm/mole) per the chain of the PAA polymer as compared with the chitosan polymer chain which has less number of the large glucosamine units (179.17 gm/mole) [22].

Accordingly, Table 4.1 shows that at the maximum level of zeta potentials (30 to +20), any decrease or increase in the ratio of PAA-chitosan did not affect the final zeta potentials. That is, increase the ratio of PAA:Chitosan from (1:5) (F11, +19.2) to (1:8) (F14, +19.2) did not change the zeta potential value, similarly, when the ratio increased

in the other direction from (4:1) (F2, -30.6) to (5:1, -29.1) (F1), no change was observed for the zeta potential of these NPs. This is in contrast for NPs with lower zeta potential where any change in the ratio of PAA:Chitosan is accompanied by a change in the zeta potential value. For example, changing the ratio of PAA:Chitosan from (1:2.2) (F7) to (1:1) (F6) resulted in the change of zeta potential from -0.5 (F7) to -15.2. This was interpreted in previous study based on the mechanism of the formation of PEC NPs where the further increase in one polymer resulted in mutual presence of PEC NPs and that free polymer, i.e, extra polymer content will not be self-assembled with the oppositely charged polymer but remain free in the solution which keeps the final zeta potential of PEC NPs unchanged [17].

Table 4.1: Particle sizes and zeta potentials of various PEC NPs including the 3 different sonicated particles (*).

Nature of NPs	PAA:Chitosan Mass ratio	Code	Zeta Potential (mV) Mean (± s.d.)	Particle Size (nm) Mean (PDI)
Negatively charged Polyelectrolyte	5:1	F1	-29.1 (±3.6)	104 (0.14)
	4:1	F2	-30.6 (±4.4)	149 (0.10)
	3:1	F3	-25.0 (±4.0)	204 (0.21)
	2:1	F4	-18.9 (±1.3)	225 (0.13)
	1:1	F5	-15.4 (±0.8)	357 (0.21)
	1:1*	F6	-15.2 (±1.2)	365 (0.21)
Neutral Polyelectrolyte	1:2.2	F7	-0.5 (±1.9)	1244 (0.32)
	1:2.2*	F8	+1.1 (±2.4)	334 (0.19)
Positively charged Polyelectrolyte	1:3	F9	+6.0 (±1.1)	144 (0.18)
	1:4	F10	+14.3 (±0.3)	104 (0.09)
	1:5	F11	+19.2 (±0.5)	180 (0.17)
	1:6	F12	+19.5 (±0.9)	293 (0.17)
	1:8	F13	+19.2 (±0.6)	359 (0.11)
	1:8*	F14	+19.5 (±2.3)	373 (0.23)

For particles formulated at a PAA: chitosan mass ratio either greater or equal to 1 (i.e. negatively charged particles) or less or equal to 0.33 (i.e. positively charged particles), the particle size varied in a pattern between 104 to 359 nm. Specifically, for negatively charged particles, the particle size increased from 104 to 357 nm in line with the approach of zeta potential toward neutrality and the relative reduction in PAA and increase in chitosan content. Accordingly, for the positively charged particles, the relative increase in chitosan content led to increasing of particle size from 144 to 359 nm. This increase of particle sizes in response to increase of chitosan content could be due to the alignment of the spatially large chitosan polymer at the surface of NP, swelling of these chitosan units at the surface of particles will enlarge the hydrodynamic sizes of NPs [23].

At near neutral charge (mass ratio 1:2.2) (F7), the particle size increased dramatically to greater than 1µ due to a predictable aggregation arising from the lack of electrostatic repulsion or steric hindrance [24]. The 3-dimensional study design, however, required a comparatively small particle size that possessed a neutral charge. Besides that, small neutral charged particle is required to mimic the surface properties of capsid shell viruses. To achieve this, large neutral particle F7 (1244 nm, +1.1 mV) was subjected to probe sonication and filtration to achieve a particle size of 334 nm.

The stability of the smaller sonicated particle was confirmed over a period (up to 2 hr) that would allow for setup of MPT diffusion experiment for the NP. The absence of re-aggregation of these particles in the mucus was confirmed visually during the MPT experiment by the Epifluorescence microscopy. Stability of neutral particles for long time was not the subject in this chapter since these PEC NPs were used as proof of concept for being slippery surface particles. As controls, the largest sized negative

particle F5 (1:1 ratio, -15.2 mV, 357 nm) and the largest sized positive particle F13 (1:8 ratio, +19.2 mV, 359 nm) were also subjected to probe sonication and filtration to ensure that the sonication process did not artificially increase mucus diffusion of the particular particle formulation.

3.b Multiple Particle Tracking (MPT) in "Cardiff Native Mucus" Model

Table 4.2 shows, besides the physicochemical properties, the Effective Diffusion Coefficient (<Deff>) in mucus and the respective Diffusion Coefficient in water (D °) for each NP type. Moreover, the ratio of these two parameters expressed as (% ratio <Deff> / D°), provides a measure of the relative efficiency of particle diffusion through "Cardiff Native Mucus" Model when the particles' intrinsic free Brownian motion in water is taken into account. As such it affords comparison of particle diffusion in mucus after accounting for the impact of the particle's size upon its unrestricted diffusion in solution. It is essentially a measure that more directly addresses the relative impact between particles of differing surface physicochemical properties and the interactions with, and the steric hindrance of, the mucin network.

While more generally there was no obvious pattern between PEC particle diameter and <Deff> (Figure 4.3A), it is clear that size had a significant role in restricting the movement of F7 compared to its smaller derivative particle F8 (+1.1 mV, 334 nm), the latter displaying an approximate 12-fold greater <Deff> (Figure 4.3B). The F8 particle was derived by sonication and filtration of F7 specifically with the aim to provide a neutral particle whose size was consistent with the other polyelectrolyte NP formulations. The size stability of F8 in water was confirmed over a time period of 2 hr, sufficient to allow its physical characterisation and the conduct of the MPT

experiments; the absence of re-aggregation of these particles in mucus during the MPT experiment itself was confirmed by fluorescence microscopy.

To address if the sonication process may have led to an increase in particle diffusion by mechanisms beyond a reduction in particle size *per se*, the largest +ve particle, F5, and largest -ve particle, F13, were also subjected to the sonication process; neither of the respective derived particles, F6 and F14, showed enhanced diffusion.

Table 4.2: physical characteristics and diffusion kinetics in "Cardiff Native Mucus" Model of various PEC NPs including sonicated particles (*), PLGA, PEG-PLGA and AD5.

Nature of NPs	PAA:Chitosan Mass ratio	Code	Zeta Potential (mV) Mean (± s.d.)	Particle Size (nm) Mean (PDI)	D° (water) $cm^2. S^{-1} x10^{-9}$	<Deff> (mucus) $cm^2. S^{-1} x10^{-9}$ Mean (± s.e.m)	% Ratio <Deff> / D°	% Diffusive particles
Negatively charged Polyelectrolyte	5:1	F1	-29.1 (±3.6)	104 (0.14)	43.21	0.00163 (±0.00031)	0.0038	1
	4:1	F2	-30.6 (±4.4)	149 (0.10)	30.16	0.00366 (±0.00067)	0.0121	2
	3:1	F3	-25.0 (±4.0)	204 (0.21)	22.03	0.01781 (±0.00378)	0.0809	6
	2:1	F4	-18.9 (±1.3)	225 (0.13)	19.97	0.01574 (±0.00329)	0.0788	4
	1:1	F5	-15.4 (±0.8)	357 (0.21)	12.59	0.02286 (±0.00534)	0.1816	5
	1:1*	F6	-15.2 (±1.2)	365 (0.21)	12.31	0.01749 (±0.00365)	0.1421	-
Neutral Polyelectrolyte	1:2.2	F7	-0.5 (±1.9)	1244 (0.32)	3.61	0.00239 (±0.00064)	0.0661	1
	1:2.2*	F8	+1.1 (±2.4)	334 (0.19)	13.46	0.02887 (±0.00501)	0.2146	13
Positively charged Polyelectrolyte	1:3	F9	+6.0 (±1.1)	144 (0.18)	31.21	0.03182 (±0.00650)	0.1019	9
	1:4	F10	+14.3 (±0.3)	104 (0.09)	43.21	0.00849 (±0.00213)	0.0196	2
	1:5	F11	+19.2 (±0.5)	180 (0.17)	24.97	0.00104 (±0.00018)	0.0042	1
	1:6	F12	+19.5 (±0.9)	293 (0.17)	15.34	0.00084 (±0.00014)	0.0055	1
	1:8	F13	+19.2 (±0.6)	359 (0.11)	12.52	0.00031 (±0.00009)	0.0024	1
	1:8*	F14	+19.5 (±2.3)	373 (0.23)	11.92	0.00032 (±0.00006)	0.0030	-
Lipophilic	PLGA	-	-29.2 (±2.1)	161 (0.03)	27.91	0.00013 (±0.00002)	0.0005	1
Hydrophillic	PEG-PLGA	-	-8.3 (±1.2)	54 (0.03)	83.22	0.46889 (±0.09343)	0.5634	32
Capsid Virus	AD5	-	-0.5 (±2.3)	146 (0.18)	30.78	0.04391 (±0.00891)	0.1426	19

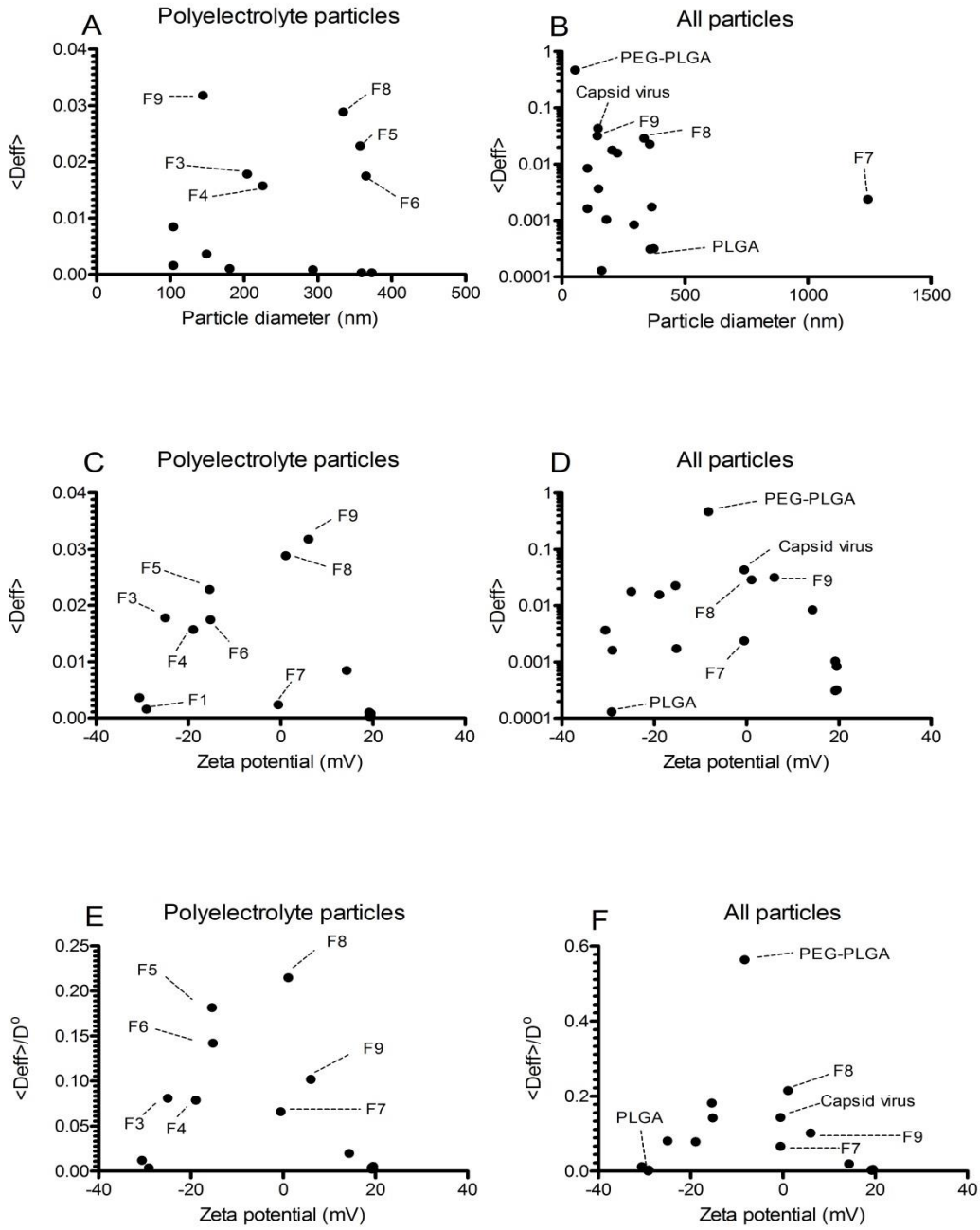

Figure 4.3: Relationships between particle size/zeta potential with particle diffusion kinetics in mucus. (A) Plot of particle size of the PEC NPs *versus* <Deff>; (B) Plot of particle size of the PEC NPs, the PEG-PLGA and the capsid virus AD5 *versus* <Deff>; (C) Plot of zeta potential of the PEC NPs *versus* <Deff>; (D) Plot of zeta potential of the PEC NPs, the PEG-PLGA and the capsid virus AD5 *versus* <Deff>; (E) Plot of zeta potential of the PEC NPs *versus* %ratio <Deff>/D°, (F) Plot of zeta potential of the polyelectrolyte NPs, the PEG-PLGA and the capsid virus AD5 *versus* %ratio <Deff>/D°.

The more general issue of size-dependency in particle diffusion through mucus appears to be more discernible for particles of a consistent surface chemistry. For example, Dawson et al. (2003) [25] using either amine or carboxylate terminated polystyrene NPs showed size-dependency (range 100 nm to 500 nm) in particle diffusion within cystic fibrosis sputum. Similarly, the movement of DNA through cervical mucus has been shown to be dependent upon DNA particle diameter in the range 115 to 310 nm [26]. Nevertheless, the effect of particle size upon diffusion within mucus is just one variable and, depending upon context; the surface properties can potentially be more significant.

The polyelectrolyte particles in the current work displayed zeta-potentials ranging between -30 mV [F1] to +20 mV [F14] (Table 4.2). An essentially neutral zeta potential was obtained at a PAA:chitosan mass ratio of 1:2.2 (F7, F8), a mass ratio consistent with the PAA polymer possessing a relatively higher density of negatively charged groups compared to the density of positive charges on each chitosan molecule [22]. Particles less than 365 nm and which displayed the greater <Deff> (Figure 4.3C, Table 4.2) were those which bore negative (-25 mV and greater) (i.e. particles F3-F6) or near neutral surface charge (i.e. F8 and F9). For example, the F5 particle (-15.4 mV) showed an approximate 14-fold greater <Deff> than the F1 particle (-29.1 mV) despite the former being of a larger size (357 nm vs 104 nm). Positively charged particles of greater than +14 mV displayed a <Deff> that was at least x10-fold lower than the neutral F8 formulation.

Generally the positively charged particles displayed a much reduced diffusion compared to the negatively charged species. For the positive particles the increasing content of chitosan provides greater opportunity for mucin to interact through both electrostatic

and hydrophobic forces with the chitosan polymer [27]. While the carboxylate groups of the PAA polymer provide opportunity for H-bonding interactions [28].

Figure 4.4 uses the data from Table 4.2 to show a 3-dimensional response surface of polyelectrolyte NP diffusion <Deff> through mucus as a function of both particle size and zeta potential. The crucial impact of zeta-potential is clear with a 'backbone of greatest diffusion' corresponding with particles of neutral surface charge. Figure 4.3E shows the relative permeation of the polyelectrolyte particles in mucus expressed as %ratio <Deff>/ D° and plotted against zeta-potential. Here, after accounting for the impact of a particle's size upon its unrestricted diffusion in solution, the superior performance of the neutral (F8, +1 mV) is more profound, with this particle displaying a significantly greater ($P<0.05$) diffusion ratio than any other polyelectrolyte formulation.

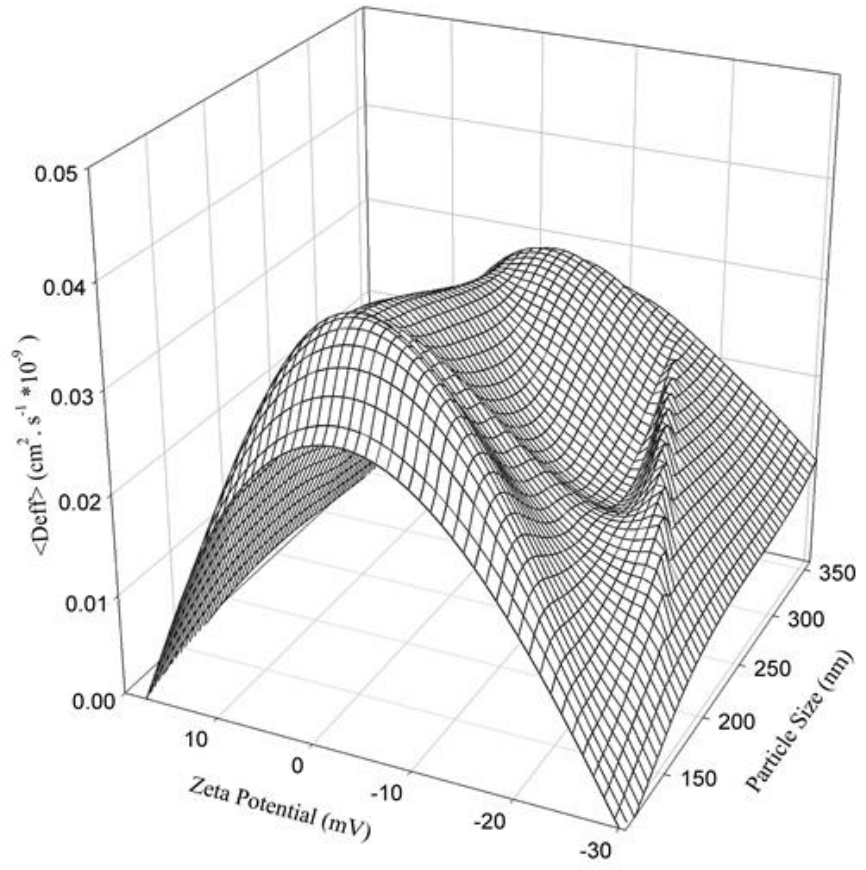

Figure 4.4: 3D plot showing the multi-variate relationship between particle size and zeta potential to polyelectrolyte particle diffusion kinetics in mucus.

Moreover, tracking of particle transport at sequential time intervals enables us to determine the change in the diffusion of these particles as they come in contact with more restricted mucus environments over time. Thus, by determining the Effective Diffusion Coefficient (Deff) for each individual particle among the 360 tested particles across the time intervals of 1 sec and 0.2 sec, we were able to calculate the proportion of the entire population of particles that can be defined as diffusive through the "Cardiff Native Mucus" Model [1]. Figure 4.5 illustrates individual Deff measurements for 20 randomly selected particles from the neutrally charged sonicated F8 PEC NP across the time intervals of 0.2 sec and 1 sec. The vast majority of these measurements show a decline in Deff as the monitoring interval is extended to 1 sec compared to the 0.2 sec

interval. This is interpreted as the occurrence with time of increased interactions of a particle with the micro-domains of the mucin network. Some particles, however, display a rise in Deff across the 1 sec interval indicative of free diffusive transport, and it is those particles that display such an increase that are taken to represent the proportion of diffusive particles for any particle type, i.e. for F8 the proportion of diffusive particles was 13% (Table 4.2) and was significantly greater ($P<0.05$) than for all other polyelectrolyte particles despite its greater size of 334 nm.

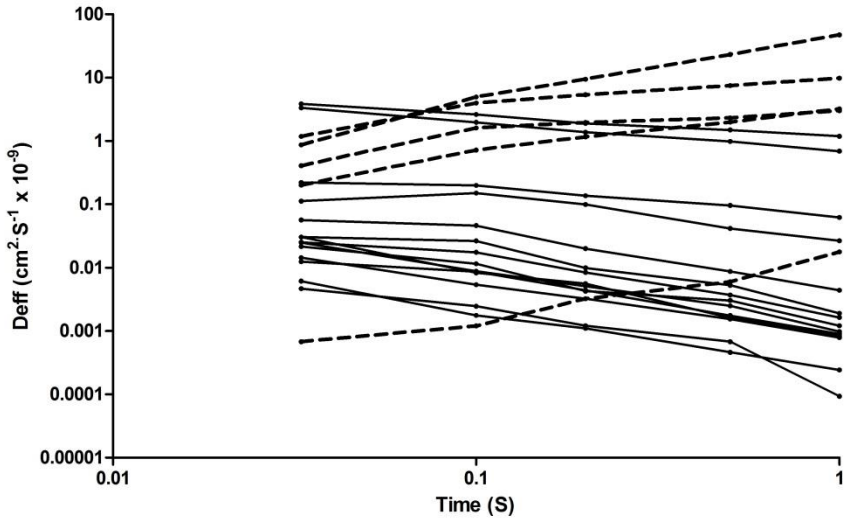

Figure 4.5: Effective Diffusion Coefficients (Deff) for 20 randomly individual particles. The profile shows 20 particles from formulation F8 across the time intervals of 1 sec and 0.2 sec. Some particles display a rise in Deff across the 1 sec interval indicative of diffusive transport; those particles that display such an increase represent the proportion of diffusive particles. The online source random.org was used to randomly select the particles.

Examining particle diffusion over these short time scales substantially eliminates the effect that the contractile and stretching behaviour of the mucin fibres themselves may have on particle movement [29]. It is noteworthy that the difference in <Deff> between the neutrally charged F7 and F8 particles (i.e. an approximate x12-fold difference) was

directly proportional to their respective proportion of Diffusive particles, i.e. 1% to 13%, respectively.

The PEGylation of particles is aimed at providing a uniform uncharged hydrophilic external layer that minimises hydrophobic and electrostatic interactions of the particle's surface with, for example, the hydrophobic domains or glycosidic linkages of the mucin fibres [30]. Indeed PEGylated NPs have been shown to display high permeation through cervical-vaginal mucus [31] and within sputum from cystic fibrosis patients [32]. Not surprisingly on most measures of particle diffusion through mucus we found the PEG-PLGA particle was superior to any other particle examined. For example, the <Deff> of the PEG-PLGA particle was approximately x15-fold greater than that of the neutral F8 particle (Table 4.2, Figures 4.3B and D).

Similarly, the proportion of diffusive particles in the PEG-PLGA formulation was substantially greater ($P<0.05$) at 32% than for any other particle type examined (Table 4.2). Nevertheless, when accounting for the impact of particle size and unrestricted particle diffusion in solution, then the advantage of PEG-PLGA particle over the neutral F8 PEC particle is less pronounced, i.e. the %ratio <Deff>/D° was only x2.6-fold greater (Figure 4.3F, Table 4.2), despite the size of the PEG-PLGA particle (54 nm) accommodating a reduced steric hindrance with the mucin network (Figure 4.3F, Table 4.2).

Some capsid virus particles can display rapid permeation through a mucus gel, e.g. Norwalk virus and human papilloma virus [11]. Of importance in this context is the lack of significant steric effects facilitated by the virus' relatively small geometry (typically <100 nm). However, as for synthetic particles, the electrostatic stability of the virus particle in extracellular conditions is critical [33] and capsid viruses that permeate

mucus effectively tend to possess an external facing surface that comprises a high density of positive and negative charges while presenting an essentially electrically neutral or near-neutral character, i.e. properties that minimising hydrophobic and electrostatic interactions. For example, Siber et al [34] analysed the spatial distribution of positive and negative charges across the capsid wall of 130 viral capsids and reported the majority to possess an external charge close to zero, or slightly negative. Consistent with this, Michen and Graule (2010) [35] evaluated the isoelectric points (IEP) of a number of viruses species, some of which are known to infect through intestinal or pulmonary mucus. They reported, for example, the IEP for the Norwalk virus to be 5.5 - 6.0, for the Polio virus to be 6.6 -7.4, for the Rotavirus A to approximate 8.0, and the Influenza A virus to be 6.5 -7.0.

In this study we tracked the diffusion of the neutrally charged (-0.5 mV) AD5 particle (size 145 nm) through "Cardiff Native Mucus" Model. The determined <Deff> of the AD5 particle indeed ranked highly, second only to the much smaller PEG-PLGA particle (54 nm) but only some 1.5-fold greater than the much larger sized neutral PEC F8 formulation (334 nm) (Figures 4.3B and D, Table 4.2). However, when accounting for the impact of unrestricted particle diffusion in solution, then the neutral PEC F8 particle now showed a slightly improved (x1.5 fold greater) mucus permeation over the AD5 particle despite the greater size and likelihood of steric hindrance in the mucus (Figure 4.3F, Table 4.2). Clearly, while the AD5 particle displayed a neutral surface charge other determinants such as interaction of the capsid proteins will have likely impacted, at least in this study, on mucus permeation. Indeed glycocalyx and tethered mucin within the respiratory tract have been shown to inhibit adsorption of certain adenovirus serotypes to lung tissue [36,37].

The heterogeneity in the movement of individual particles through mucus can provide an insight into how different subpopulations within a given formulation (particle) type may exploit divergent permeation pathways. Here we assessed such heterogeneity by measuring over a time interval of 1 sec. the effective diffusion coefficient Deff for each of 360 individual particles from any given particle type, and ranking this Deff data into percentiles. Figure 4.6 shows the percentile data for four different particle types. Generally, the more positively or negatively charged the particle type then the less heterogeneous was the diffusion data. For example, for the highly negative (104 nm sized) F1 NP, some 90% of the particles displayed a Deff (cm^2. S^{-1} $x10^{-9}$) below 0.024, while 10% of the particles had a Deff below 0.00015 (Figure 4.7A). The resulting ratio $90^{th}/10^{th}$ percentile was 150. For the highly positive (373 nm sized) F14 particle, the corresponding ratio was 180 (Figure 4.6B). It is not unreasonable that the more highly charged polyelectrolyte particles will display a more homogenous physical character (size, charge), and as such the variability in forces influencing particle diffusion through the mucus will be determined predominantly by the structure of the mucus mesh itself rather than any distinct particle subpopulations [25].

Similarly, the PEG-PLGA particle (54 nm sized) exhibited a $90^{th}/10^{th}$ percentile ratio of 200 (Figure 4.6D), consistent with previously published PEGylated particle diffusion through mucus [1]. In contrast, the sonicated (334 nm sized) neutrally charged F8 particle displayed a marked heterogeneity with a $90^{th}/10^{th}$ percentile ratio of 11,000 (Figure 4.6C). This is not readily attributable solely to the heterogeneous structure of the mucus mesh but must reflect additional diversity involving particle subpopulations and differential forces hindering their movement. Creating a charged but neutral synthetic particle through the simple process of self-assembly of polyelectrolyte polymers will inevitably lead to opposing surface charges that are not uniformly

distributed with the result of forming surface 'hotspots' or surface domains of a particular electrical sign that will have differential interactions with the mucin network. Indeed, the spatial arrangement of charge on a particle's surface, even for particles of the same overall net surface charge, has been shown to be influential in particle transport through a mucin gel [38]. Such heterogeneity reflects one of the limitations of creating a charged but neutral synthetic particle through the simple process of self-assembly of polyelectrolyte polymers. Nevertheless, the fastest particles (90^{th} percentile) seen for the neutral polyelectrolyte F8 NP (i.e. Deff of 5.81; Figure 4.6C) were at least as fast as the 90^{th} percentile particles recorded for the much smaller PEG-PLGA (i.e. Deff of 4.06; Figure 4.6D).

The abovementioned results revealed a broad and meaningful relationship between particle diffusion in mucus (x1000 difference between slowest and fastest particle types), particle size (104 nm to 373 nm) and particle surface charge (-29 mV to + 19.5 mV). In particular the crucial impact of zeta-potential was clear, with highest diffusion in mucus (from amongst the series of polyelectrolyte particles) observed for those of a neutral surface charge (e.g. particle [F8] at +1.1 mV, 334 nm). The diffusion of the neutral polyelectrolyte particle compared favourably with that of a highly diffusive PEGylated-PLGA particle (54 nm) despite the size of the latter accommodating a reduced steric hindrance with the mucin network. Assessment of the heterogeneity of diffusion within a given particle type revealed the most diffusive neutral PEC NPs formulation F8 to display a x11,000-fold difference in particle diffusion between the fastest 10% sub-population and the slowest 10% sub-population; a finding likely reflecting a non-uniform distribution of surface charge expected for a neutral particle of this type. Of significance, the most diffusive 10% sub-population for this neutral PEC

NP was faster than that of the most diffusive 10% sub-populations obtained for both the PEGylated-PLGA particle as well as for a capsid adenovirus particle.

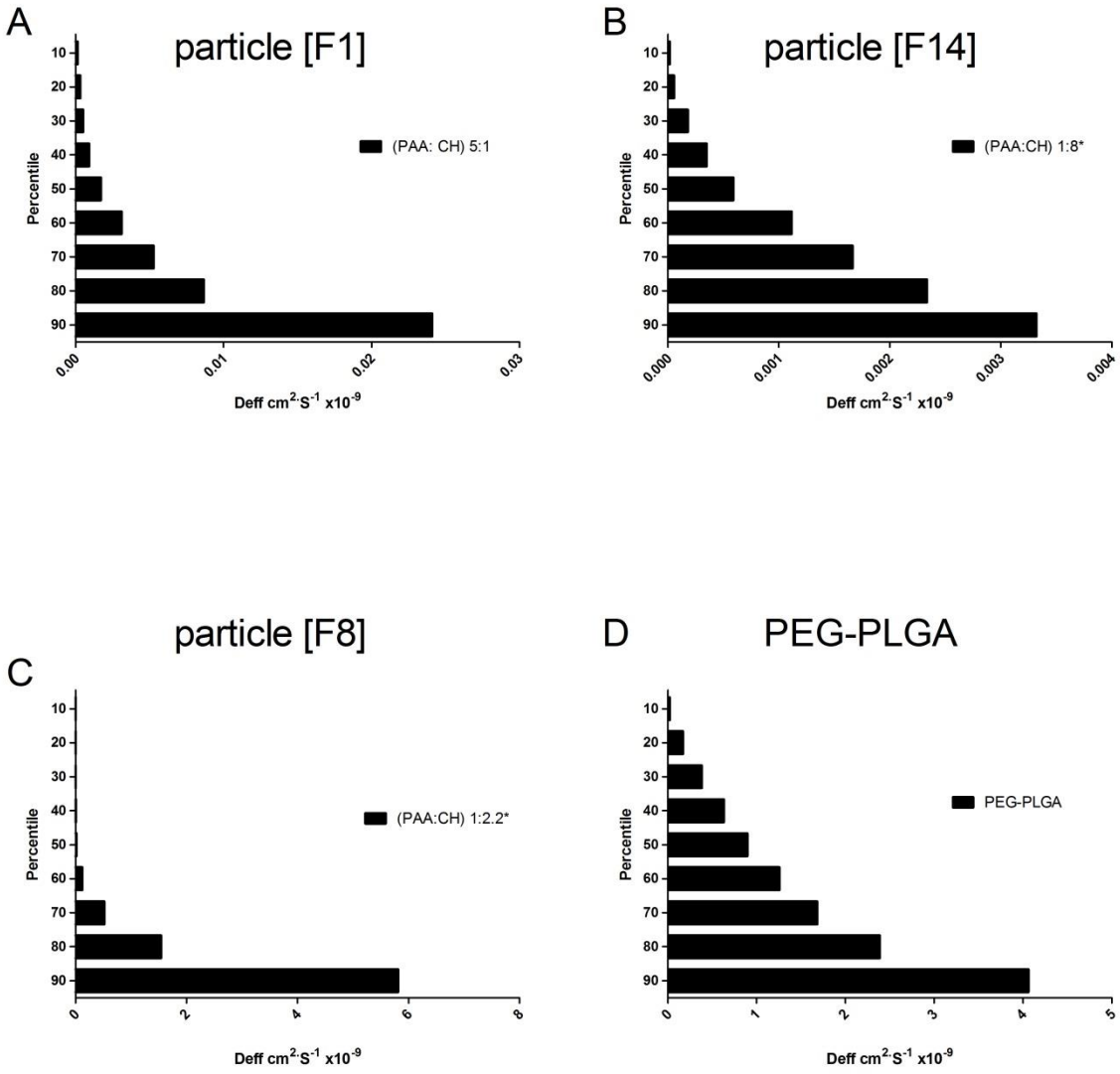

Figure 4.6: Heterogeneity of (PAA:Chitosan) PEC NPs movement through mucus. For each particle type a Deff was calculated for each of 360 individual particles over a time interval of 1 sec. The data was ranked into percentiles from the 90^{th} through to 10^{th} percentile, where the 90^{th} percentile is the Deff value below which 90% of the Deff observations may be found. (A) data for the negatively charged [F1] polyelectrolyte formulation; (B) data for the positively charged [F14] polyelectrolyte formulation; (C) data for the neutrally charged [F8] polyelectrolyte formulation; (D) data for the PEG-PLGA particle. Figure presents data of from three separate experiments, i.e. ≥ 360 individual particles examined for each particle type.

4. SUMMARY AND CONCLUSION

While this study has used a simple self-assembly PEC system to explore the impact of particle size and charge upon "Cardiff Native Mucus" Model permeation, it has revealed in a robust manner the clear benefits for a particle possessing a neutral or near neutral surface. Beyond polyelectrolyte systems exploitation of polymer synthesis approaches such as living free radical chemistry should deliver stable, size-controlled nanoparticles possessing a uniform and balanced high density distribution of positive and negative surface charges, ultimately yielding particles with a net neutral surface potential that will provide an additional strategy to that of PEGylated systems when seeking to avoid interactions with the mucus barrier.

5. References

[1] S.K. Lai, D.E. O'Hanlon, S. Harrold, S.T. Man, Y.-Y. Wang, R. Cone, et al., Rapid transport of large polymeric nanoparticles in fresh undiluted human mucus., Proc. Natl. Acad. Sci. U. S. A. 104 (2007) 1482–7. doi:10.1073/pnas.0608611104.

[2] Y. Cu, W.M. Saltzman, Drug delivery: Stealth particles give mucus the slip., Nat. Mater. 8 (2009) 11–3. doi:10.1038/nmat2347.

[3] J.S. Suk, S.K. Lai, N.J. Boylan, M.R. Dawson, M.P. Boyle, J. Hanes, Rapid transport of muco-inert nanoparticles in cystic fibrosis sputum treated with N-acetyl cysteine., Nanomedicine (Lond). 6 (2011) 365–75. doi:10.1016/j.

[4] A. Verma, F. Stellacci, Effect of Surface Properties on Nanoparticle-Cell Interactions, Small. 6 (2010) 12–21. doi:10.1002/smll.200901158.

[5] F. Laffleur, F. Hintzen, G. Shahnaz, D. Rahmat, K. Leithner, A. Bernkop-Schnürch, Development and in vitro evaluation of slippery nanoparticles for enhanced diffusion through native mucus., Nanomedicine (Lond). 9 (2014) 387–96. doi:10.2217/nnm.13.26.

[6] J.P. Chapel, J.F. Berret, Versatile electrostatic assembly of nanoparticles and polyelectrolytes: Coating, clustering and layer-by-layer processes, Curr. Opin. Colloid Interface Sci. 17 (2012) 97–105. doi:10.1016/j.cocis.2011.08.009.

[7] N.P. Birch, J.D. Schiffman, Characterization of self-Assembled polyelectrolyte complex nanoparticles formed from chitosan and pectin, Langmuir. 30 (2014) 3441–3447. doi:10.1021/la500491c.

[8] Y. Yuan, B.M. Chesnutt, W.O. Haggard, J.D. Bumgardner, Deacetylation of Chitosan: Material Characterization and in vitro Evaluation via Albumin Adsorption and Pre-Osteoblastic Cell Cultures, Materials (Basel). 4 (2011) 1399–1416. doi:10.3390/ ma 408 1399.

[9] R. Yoksan, S. Chirachanchai, Amphiphilic chitosan nanosphere: Studies on formation, toxicity, and guest molecule incorporation, Bioorganic Med. Chem. 16 (2008) 2687–2696. doi:10.1016/j.bmc.2007.11.037.

[10] L. Yin, X. Zhao, L. Cui, J. Ding, M. He, C. Tang, et al., Cytotoxicity and genotoxicity of superporous hydrogel containing interpenetrating polymer networks, Food Chem. Toxicol. 47 (2009) 1139–1145. doi:10.1016/j.fct.2009.01.043.

[11] S.S. Olmsted, J.L. Padgett, a I. Yudin, K.J. Whaley, T.R. Moench, R. a Cone, Diffusion of macromolecules and virus-like particles in human cervical mucus., Biophys. J. 81 (2001) 1930–7. doi:10.1016/S0006-3495(01)75844-4.

[12] L.J. Saif, E.H. Bohl, K.W. Theil, R.F. Cross, J.A. House, Particles Associated with Diarrhea in Young Pigst, J. Clin. Microbiol. 12 (1980) 105–111.

[13] L. Coughlan, R. Alba, A.L. Parker, A.C. Bradshaw, I. a McNeish, S. a Nicklin, et al., Tropism-modification strategies for targeted gene delivery using adenoviral vectors., Viruses. 2 (2010) 2290–355. doi:10.3390/v2102290.

[14] G. Gonçalves, E. Gouveia, J.R. Mesquita, a Almeida, a Ribeiro, J. Rocha-Pereira, et al., Outbreak of acute gastroenteritis caused by adenovirus type 41 in a kindergarten., Epidemiol. Infect. 139 (2011) 1672–5. doi:10.1017/S0950268810002803.

[15] Y. Hu, X. Jiang, Y. Ding, H. Ge, Y. Yuan, C. Yang, Synthesis and characterization of chitosan–poly (acrylic acid) nanoparticles, Biomaterials. 23 (2002) 3193–3201. doi:10. 1016/S0142-9612(02)00071-6.

[16] C. Bamford, H. Tompa, The theory of coacervation, Trans. Faraday Soc. 46 (1950) 310–316.

[17] J. Rolland, P. Guillet, J.-M. Schumers, N. Duhem, V. Préat, J.-F. Gohy, Polyelectrolyte complex nanoparticles from chitosan and poly(acrylic acid) and Polystyrene- block - poly(acrylic acid), J. Polym. Sci. Part A Polym. Chem. 50 (2012) 4484–4493. doi:10. 10 02/pola.26255.

[18] J.H. Hamman, Chitosan based polyelectrolyte complexes as potential carrier materials in drug delivery systems., Mar. Drugs. 8 (2010) 1305–22. doi:10.3390/md8041305.

[19] L. Becherán-Marón, C. Peniche, W. Argüelles-Monal, Study of the interpolyelectrolyte reaction between chitosan and alginate: influence of alginate composition and chitosan molecular weight., Int. J. Biol. Macromol. 34 (2004) 127–33. doi:10.1016/ j.ijbiomac .2004.03.010.

[20] L.F. Gudeman, N. a. Peppas, pH-sensitive membranes from poly(vinyl alcohol)/poly(acrylic acid) interpenetrating networks, J. Memb. Sci. 107 (1995) 239–248. doi:10.1016/0376-7388(95)00120-7.

[21] T. López-León, E.L.S. Carvalho, B. Seijo, J.L. Ortega-Vinuesa, D. Bastos-González, Physicochemical characterization of chitosan nanoparticles: electrokinetic and stability behavior., J. Colloid Interface Sci. 283 (2005) 344–51. doi:10.1016/j.jcis.2004.08.186.

[22] T. Etrych, L. Leclercq, M. Boustta, M. Vert, Polyelectrolyte complex formation and stability when mixing polyanions and polycations in salted media: a model study related to the case of body fluids., Eur. J. Pharm. Sci. 25 (2005) 281–8. doi:10.1016/ j.ejps.2005.03.005.

[23] Q. Gan, T. Wang, C. Cochrane, P. McCarron, Modulation of surface charge, particle size and morphological properties of chitosan-TPP nanoparticles intended for gene delivery., Colloids Surf. B. Biointerfaces. 44 (2005) 65–73. doi:10.1016/j.colsurfb.2005.06.001.

[24] R. a Sperling, W.J. Parak, Surface modification, functionalization and bioconjugation of colloidal inorganic nanoparticles., Philos. Trans. A. Math. Phys. Eng. Sci. 368 (2010) 1333–1383. doi:10.1098/rsta.2009.0273.

[25] M. Dawson, D. Wirtz, J. Hanes, Enhanced viscoelasticity of human cystic fibrotic sputum correlates with increasing microheterogeneity in particle transport., J. Biol. Chem. 278 (2003) 50393–401. doi:10.1074/jbc.M309026200.

[26] H. Shen, Y. Hu, W.M. Saltzman, DNA diffusion in mucus: effect of size, topology of DNAs, and transfection reagents., Biophys. J. 91 (2006) 639–44. doi:10.1529/ biophysj .105.077404.

[27] M.P. Deacon, S.S. Davis, R.J. White, H. Nordman, I. Carlstedt, N. Errington, et al., Are chitosan–mucin interactions specific to different regions of the stomach? Velocity ultracentrifugation offers a clue, Carbohydr. Polym. 38 (1999) 235–238. doi:10.1016/ S0144-8617(98)00097-6.

[28] S.A. Mortazavi, An in vitro assessment of mucus/mucoadhesive interactions, Int. J. Pharm. 124 (1995) 173–182. doi:10.1016/0378-5173(95)00073-R.

[29] S.K. Lai, Y.-Y. Wang, D. Wirtz, J. Hanes, Micro- and macrorheology of mucus., Adv. Drug Deliv. Rev. 61 (2009) 86–100. doi:10.1016/j.addr.2008.09.012.

[30] Y. Wang, S.K. Lai, J.S. Suk, A. Pace, R. Cone, J. Hanes, Addressing the PEG mucoadhesivity paradox to engineer nanoparticles that "slip" through the human mucus barrier., Angew. Chem. Int. Ed. Engl. 47 (2008) 9726–9. doi:10.1002/anie.200803526.

[31] B.C. Tang, M. Dawson, S.K. Lai, Y.-Y. Wang, J.S. Suk, M. Yang, et al., Biodegradable polymer nanoparticles that rapidly penetrate the human mucus barrier., Proc. Natl. Acad. Sci. U. S. A. 106 (2009) 19268–73. doi:10.1073/pnas.0905998106.

[32] J.S. Suk, S.K. Lai, Y.-Y. Wang, L.M. Ensign, P.L. Zeitlin, M.P. Boyle, et al., The penetration of fresh undiluted sputum expectorated by cystic fibrosis patients by non-adhesive polymer nanoparticles., Biomaterials. 30 (2009) 2591–7. doi:10.1016/j.biom aterials.2008.12.076.

[33] X. Yang, K. Forier, L. Steukers, S. Van Vlierberghe, P. Dubruel, K. Braeckmans, et al., Immobilization of pseudorabies virus in porcine tracheal respiratory mucus revealed by single particle tracking., PLoS One. 7 (2012) e51054. doi:10.1371/ journal. pone.0051054.

[34] A. Siber, A.L. Božič, R. Podgornik, Energies and pressures in viruses: contribution of nonspecific electrostatic interactions., Phys. Chem. Chem. Phys. 14 (2012) 3746–65. doi:10.1039/c1cp22756d.

[35] B. Michen, T. Graule, Isoelectric points of viruses, J. Appl. Microbiol. 109 (2010) 388–397. doi:10.1111/j.1365-2672.2010.04663.x.

[36] C. Kitson, B. Angel, D. Judd, S. Rothery, N.J. Severs, a Dewar, et al., The extra- and intracellular barriers to lipid and adenovirus-mediated pulmonary gene transfer in native sheep airway epithelium., Gene Ther. 6 (1999) 534–46. doi:10.1038/sj.gt.3300840.

[37] J.R. Stonebraker, D. Wagner, R.W. Lefensty, K. Burns, S.J. Gendler, J.M. Bergelson, et al., Glycocalyx restricts adenoviral vector access to apical receptors expressed on respiratory epithelium in vitro and in vivo: role for tethered mucins as barriers to lumenal infection., J. Virol. 78 (2004) 13755–68. doi:10.1128/JVI.78.24.13755-13768.2004.

[38] L.D. Li, T. Crouzier, A. Sarkar, L. Dunphy, J. Han, K. Ribbeck, Spatial configuration and composition of charge modulates transport into a mucin hydrogel barrier., Biophys. J. 105 (2013) 1357–65. doi:10.1016/j.bpj.2013.07.050.

CHAPTER FIVE

SYNTHESIS OF NOVEL ZWITTERIONIC SULFOBETAINE POLYMERIC NPs USING RAFT POLYMERIZATION TECHNIQUE: STUDIES ON THE DIFFUSIONAL BEHAVIOUR OF THE ZWITTERIONIC SULFOBETAINE NPS THROUGH THE MUCUS BARRIER

1. INTRODUCTION

1.a Polymer and Polymerization

The term polymer is originally a Greek word in which *poly* means many and *meros* means parts [1]. The polymer definition is not far from the source of the word. Polymers are chains of repetitive units, namely, monomers linked together by covalent bonds to form macromolecules with a molecular weights reaching to millions Da [2]. The process of polymer synthesis is called polymerization, wherein, the monomers are driven to react with themselves under certain circumstances and in the presence of reactivating agents. A few monomers are linked together in the early stage of the polymerization process to produce small chains of monomers which are called oligomers. As the process is continued, longer chains are produced.

Polymers can be classified depending on their skeletal structure into linear, branched or cross-linked polymers (Figure 5.1) [3]. Polymers can also be classified into semi-crystalline or amorphous depending on their microstructure, where the chains look semi-arranged within the semi-crystalline type or randomly ordered in the amorphous type [4]. Chemically, polymers can be classified depending on the chemical nature of the monomers into either homopolymers which consist of one type monomer or copolymers which consist of different types of monomers (Figure 5.2). Accordingly, these copolymers can be sub-classified depending on the arrangement of the monomers into: block, random and alternating (Figure 5.2). Moreover, polymers can be classified depending on their (i) origin into natural or synthetic, (ii) nature into biodegradable or non-biodegradable [5], (iii) thermal properties into thermoplastic or thermosetting, (iv) tacticity into atactic or isotactic or (v) mechanism of the polymerization [6].

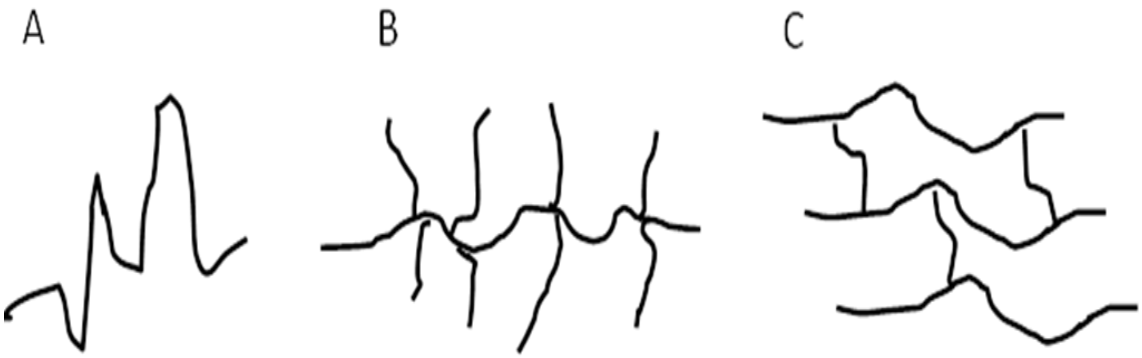

Figure 5.1: Skeletal structure of polymer: (A) Linear polymer (B) Branched polymer and (C) Cross-linked polymer.

- Homo-polymer A-A-A-A-A-A-A-A-A-A-A-A-A-A-A-
- Block B- B- B- A- A- A- B- B- B- A- A- A-
- Alternating A- B- A- B- A- B- A- B- A- B- A- B-
- Random A- A- A- B- A- B- B- B- A- B- A- B-A-

Figure 5.2: Polymer classification depending on the type and the structural arrangements of monomers within the polymer chain.

1.b Methods and Mechanisms of Polymerization

Polymers can be classified based on the method of polymerization into condensation or addition polymerization [7]. Polymers synthesized by condensation process are formed of repetitive units which lack, or have more, chemical entities than that of the monomers synthesized from. That is to say, condensation of (XAAX, YBBY) molecules to form the repetitive unit (AABB) with the release of a by-product (X,Y) is a condensation polymerization process [8], this can be exemplified by the condensation of alcohol and acid to produce a simple polymer with the release of water. Condensation polymerization has been the pathway to synthesize different types of polymers, such as linear and cyclic aromatic peptides [9] and ketonic resin [10].

On the other hand, Polymers synthesized by addition polymerization hold exactly the same structural unit of the monomer. In other words, synthesized polymers are just repetition of the monomer units synthesized from. Addition polymerization is characterized by the quick consecutive addition of hundreds or thousands of pre-activated monomers into the growing chain polymer [3]. Hence, the terms addition polymerization and chain growth polymerization are used interchangeably. Addition polymerization is preferable over condensed polymerization, due to the high yield and quick formation of polymers with no need to the gradual step-growth process [11]. Addition polymerization starts with activating the monomers into an active unsaturated centre, to which the other unsaturated monomers are added successively to from a chain polymer. The activation of monomer is called the initiating step in which unsaturated molecules, namely, initiator is added into the monomers to form new unsaturated species. Addition polymerization can be sub-classified depending on the type of desaturation of the reactive centre into radical, cationic or anionic addition polymerization [11]. Among the three types of addition polymerization, radical polymerization (RP) has been shown to be suitable for most types of monomers and is therefore mostly used.

1.c Radical Polymerization

RP was first described by Flory in 1937 who described vinyl polymerization as a chain growing process characterized by consecutive addition of monomers [12]. RP is three steps process starts with initiation step followed by propagation and ended with termination step [13]. The initiator is most likely an organic compound with an unstable group such as Azo (-N=N-) or Peroxide (-O-O-), which at certain temperature and/or pressure conditions is hydrolyzed into two radicals; each of them can attack monomer

and activate it [14]. Radicals should have an adequate half-life in order to remain active during the polymerization process [15].

Monomers that are suitable for initiation and propagation are molecules having a pi-bond susceptible to consequent activation. After the initiation step (opening of the pi-bond), the monomer is activated and propagation step starts in which monomers are added consequently into the activated monomer to grow into a polymer chain [16]. RP is terminated through the binding of two radical species in the reaction media, these radical species could be two propagating polymers or an initiator and propagating polymer [3]. Nowadays, RP has become of high industrial importance with 50% of the rubber and plastic are produced nowadays through this process [17].

1.d Controlled Polymerization

One of the main concerns with addition polymerization (RP) is the short half-life of the growing chain. This issue has been the main obstacle in controlling the molecular weight and block copolymerization of propagating polymers [16]. Controlled polymerization was first achieved by Szwarc in 1956 through the use of an anionic polymerization technique to eliminate the un-controlled termination step and to produce a living polymer [18]. Decades after, control of the RP was achieved based on the formation of dormant species and the concurrent initiation and propagation [15].

The main differences between conventional RP and controlled radical polymerization (CRP) is the turning of the unsaturated active propagating polymer into a dormant species which can not be propagating or reacting to any other radical till it turned back to its unsaturated active species. This difference affects the steps of polymerization as follows. Firstly, the half-life of the propagating process is prolonged from a few seconds in RP to several hr in CRP due to the formation of dormant species. Secondly, in the

RP, most chains are dead due to radical-radical termination while only 10% of chains are dead in CRP due to the coexistence of dormant species which are very inert to be terminated by another radical interaction. Lastly, in RP, a steady state is achieved by the equilibration between the initiation and the termination steps, while, in CRP, this equilibration is achieved through the exchange of the active and dormant species [15].

Generally, there are two main pathways for CRP. These are, firstly, reversible termination of the propagating radical (Pm•, Pn• or Rm•) (Figure 5.3A) through reversible coupling/uncoupling with a stable agent such as a stable radical (nitroxide radical) [19] or transition metal complex (copper complex) [20]. Secondly, radical polymerization can be controlled through the 'reversible addition fragmentation chain transfer' (RAFT) of the propagating radical (Figure 5.3B). Both techniques depend on the equilibrium between the active propagating radical and the inactive centre, in which the radical addition and propagation is immobile [21]. In this work, RAFT technique will be used to synthesize controlled molecular weight polymers.

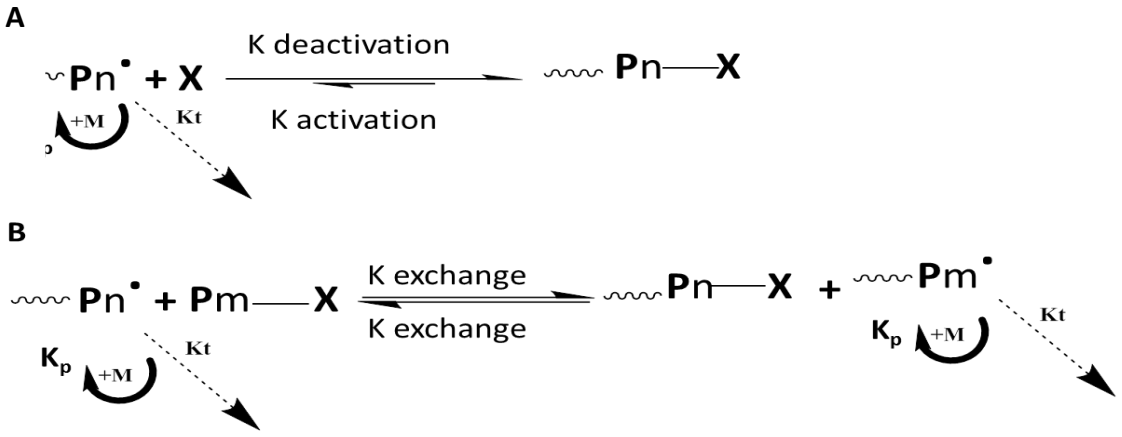

Figure 5.3: Mechanism of CRP (A) reversible activation/ deactivation of the propagating radical, (B) reversible addition fragmentation chain transfer of the propagating radical.

1.e Reversible Addition Fragmentation Chain Transfer (RAFT)

This technique depends on the use of an active unsaturated agent, namely, a chain transfer agent (CTA) which can reversibly hold the propagating radical to retard its growing [22]. The RAFT technique was firstly introduced by Gaynor et al. (1995) in the mid-nineties who used alkyl iodide as a CTA for the control polymerization of styrene polymer [23]. However, this technique did not show acceptable polydispersity (acceptable polydispersity should be <1.4). Subsequently, the patent of the Phuong et al. which was published in 1998 paved the way for a controlled radical polymerization process through the use of thiocabonylthio compounds as a CTA agent (Figure 5.4) [24]. These Thiocabonylthio agents are characterized by suitability to be used with various types of monomers to yield polymers with predictable molecular weights and low polydispersity (usually <1.2) [25].

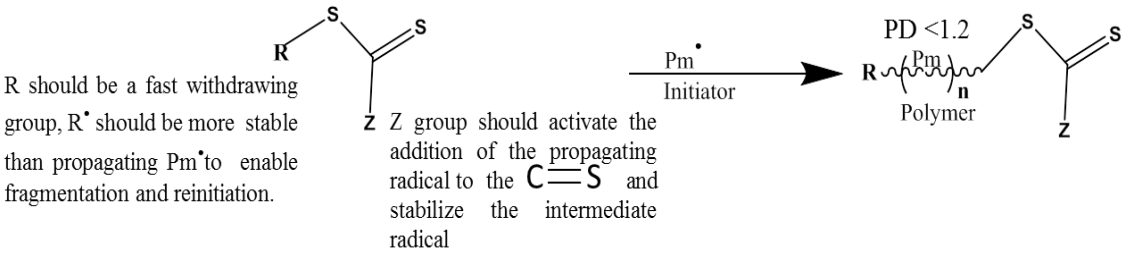

Figure 5.4: Functional groups responsible for the activity of the Thiocabonylthio CTA agent.

The chain transfer process is controlled by the three main functional groups in the CTA agent, these are: the carbon-thiol double bond, Z and R groups (Figure 5.4). Each of these functional groups has its own role in the RAFT technique. The carbon-thiol double bond is the site to which the propagating radical is added to form an intermediate radical. Z groups should activate and stabilize the addition of propagating radical and formation of the radical intermediate. As will be seen in Figure 5.6, stability of the intermediate is essential to hold the growing polymer and control the overall

polymerization. Depending on the types of Z groups, thiocabonylthio agents can be classified into four types. These types and their order of activity are as follows: Dithiobenzoates > trithiocarbonates > xanthates > dithiocarbamates (figure 5.5) [26].

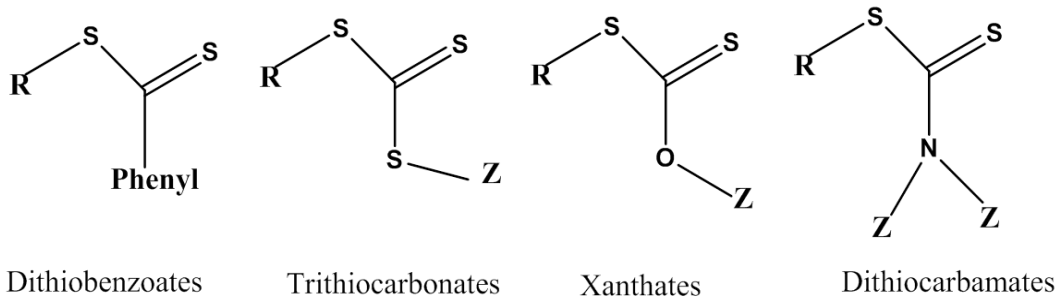

Figure 5.5: Types of thiocarbonylthio transfer agents.

Accordingly, R group in the CTA agent should be a fast leaving group to form a new radical (R˙), so the Thiol-R bond should be weak so as to allow fast homo breaking of the bond to release the R˙ (Figure 5.4). This formed R˙ should be stable enough to reinitiate and propagate again. Similar to the variety of Z groups, CTAs exist with a variable withdrawing efficiency R˙ group [27].

The mechanism of RAFT polymerization is described in Figure 5.6 [28]. RAFT polymerization shares the same initiation (K_i) and termination (K_t) steps (step 1 and 5, Figure 5.6) with conventional RP. The reversible addition/fragmentation step (step 2) involves the addition (k_a) of the propagating radical (Pm˙) to the CTA agent to reversibly form an intermediate agent holding the propagating radical (Pm˙-CTA) (compound X). The (Pm˙-CTA) could either degrade back (K_{-a}) into the original propagating radical (Pm˙) and the CTA or it could fragment (k_f) into the dormant species (Pm-CTA) with the breaking of the (S-R) bond and releasing of the radical (R˙). Then, (R˙) undergoes reinitiation and propagation (K_p) to form new propagating radical (RPm˙) (step 3).

With the appropriate type and concentration of the CTA agent, the pre-equilibrium addition should dominate over the conventional propagation. The equilibration step (step 4) involves the reversible re-addition of the propagating radical (RPm˙) to the dormant Pm-CTA (compound Y) to form a new intermediate radical (Pm-CTA˙-RPm) (compound K). This radical intermediate undergoes a reversible fragmentation to form propagating radical Pm˙ and dormant species (RPm-CTA) [28,29]. Each of the propagating radicals at either side of the equilibration step (step 4) has the chance to propagate for few milliseconds before it is held by the intermediate radical (compound K) for a few seconds. Hence, each polymer grows by a few monomers before it becomes dormant again. The equilibration step allows all the chains to grow equally with a min chance to produce dead polymers [15]. CTAs with a very high addition constant can produce polymers with very low polydispersity since the addition will be totally dominant over the propagation step. Termination (step 5) is responsible for the formation of dead polymers, although it counts for less than 10% of the total polymerization.

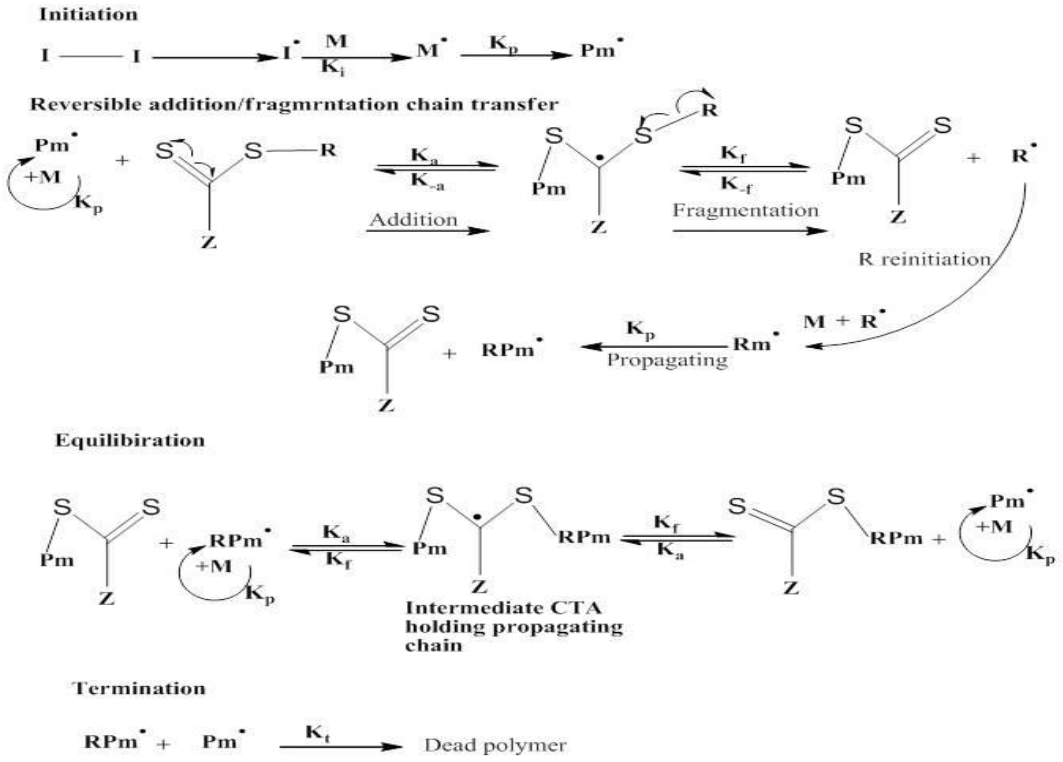

Figure 5.6: Mechanism of RAFT polymerization by the CTA agent. This Figure was modified from the original figure in [28].

1.f Zwitterionic Sulfobetaine Polymer

The Zwitterioinc (co)polymer is defined as the polymer possessing both anionic and cationic groups. At certain pH value, namely, the isoelectric point, the net charge is approximately zero. There are two types of Zwitterionic polymer: (i) polyampholyte, in which the opposite groups exist in different monomer units and (ii) polybetaine which is characterized by the presence of the opposite groups in the same monomer unit [30]. Each betaine monomer unit possesses a terminal anionic group next to the cationic group (Figure 5.7 While the cationic ion is usually amino group, the terminal anionic group could be either sulphate group (Figure 5.7A) or carboxylate groups (Figure 5.7B) [31]. Betaine monomer is called sulfobetaine when the anionic species is sulphate group (Figure 5.7A), and called carboxybetaine when the the anionic species is carboxylate groups (Figure 5.7B). The first synthesised carboxybetaine polymer was reported in 1957, while the first synthesis of sulfobetaine polymer was in 1958 [32].

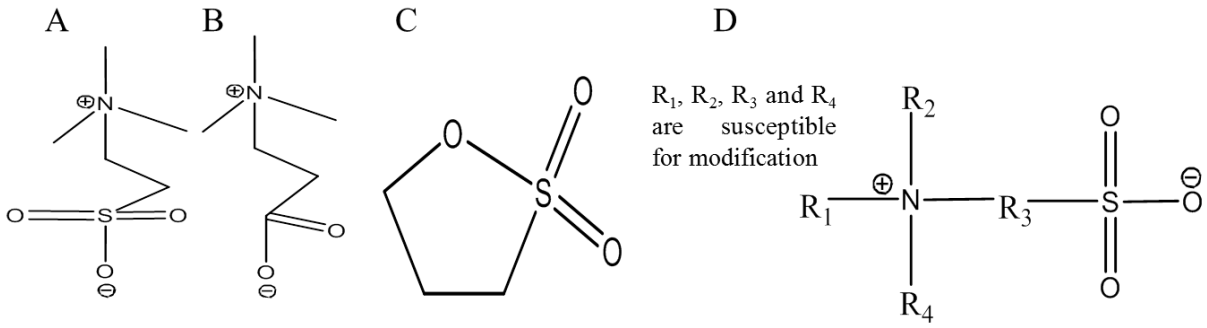

Figure 5.7: (A) Structure of sulfobetaine unit, (B) Structure of carboxybetaine unit, (C) 1,3-propane sultone structure, (D) Substituting groups in the sulfobetaine structure.

The betainisation of DMAEMA to form sulfobetaine polymer was firstly reported in the mid-eighties where the reaction of DMAEMA with 1,3-propane sultone (Figure 5.7 C) was carried out under an extremely high temperature (120 °C) and propylene carbonate as the solvent [33]. However, the betainisation of the DMAEMA polymer under a mild condition of 25 °C and tetrahydrofuran (THF) solvent was introduced in the late nineties which enabled the synthesis of the (DMAEMA)sulfobetaine by a one step akylsulfonation process of the tertiary amine group with a 100% yield [34].

Physicochemical properties of sulfobetaine polymer are affected by the molecular weight of this polymer. For example, the water solubility of this polymer was found to increase when the molecular weight of sulfobetaine polymer decrease [35]. Microscopically, examination of sulfobetiane polymer revealed a collapsed coil conformation in aqueous phase due to the intra-groups interaction, however, the low molecular weight sulfobetaine polymer exhibited a random coil configuration in better solubilizing solvents such as 2,2,2-trifluoroethanol (TFE) where the conformational dimensions was dependent on the polymer molecular weight [36].

1.g Biological Activity of Zwitterionic Polymer: Sulfobetaine Polymers

Polymers can be immobilised onto biological or chemical surfaces to form coating films. A coating film comprised of zwitterionic polymer is characterised by a densely

charged outer layer which serves as an anti-adherent layer minimising electrostatic or lipophilic interactions [37]. For example, immobilisation of Poly(3-trimethoxysilyl-propyl-methacrylate)-co-poly(2-methacryloyloxyethyl phosphoryl choline onto the surface of contact lenses is one of the techniques to enhance anti-adherent properties against micro-organisms and protein adsorption while retaining high wettability [38].

Accordingly, the anti-adherent properties of sulfobetaine polymers have been widely reported. For example, sulfobetaine polymer cross-linked onto a hollow membrane of poly(vinylidene-fluoride) showed considerably higher protein anti-fouling and hydrophilicity as compared to the non-modified hollow membrane [39]. Similarly, covering of vinylidene-fluoride membrane with grafted sulfobetaine highly improved the anti-adherent properties of the membrane such as reduced surface protein adsorption, platelet activation, plasma clotting and blood cell haemolysis [40].

Chemically, the sulfobetaine structure has various functional groups available for substitution. Specifically groups R1, R2, R3 and R4 (Figure 5.7D) can be substituted with either more lipophilic or more hydrophilic groups so as to have new compounds with modified properties. Developing new sulfobetaine compounds by modifying the sulfobetaine structure has been the subject for several patents. For example, Ballschuh et al. (1992) synthesized a patented sulfobetaine compound in which either R1, R2 or R4 was substituted with α-sulfonylcarboxylic acids and R3 was replaced with a highly lipophilic 20 alkyl unit chain [41]. Patented sulfobetaine compounds have been used for various applications such as drug delivery and chemical industries.

Substituting of R1 (Figure 5.7D) with up to a 30 alkyl unit chain and modifying of R2, R3 and R4 with small alkyl chains was the basis of a patented antibacterial layer applied onto contact lenses [42]. Coating contact lenses with modified sulfobetaine layers to improve wettability and biocompatibility was the subject of another patent

published in 2013 (Broad et al. 2013). Additionally, sulfobetaine was blended with a range of polymers to form a patented filter for blood purification, haemodialysis, hemofiltration and for water purification [44]. Sulfobetaine-co-acrylic acid copolymer has been used to cover blood contacting devices to prevent platelet adhesion and fibrinogen adsorption [31]. Similarly, sulfobetaine polymer has also showed impact as an anti-adherent layer in non-medical applications e.g. as in an electroplating suspension to improve the mechanical strength and appearance of nickel surfaces [45].

The Ben-Sasson group has modified R1, R2, R3 and R4 groups in the sulfobetaine polymer with a range of substituents from highly lipophilic to highly hydrophilic functional groups (Ben-Sasson & Dagan 2009). This patent showed that sulfobetaine is an excellent template to load various range of hydrophilic and lipophilic drugs such as cyclophosphamide, NSAIDs, betamethasone, cimetidine and rapamycin. Accordingly, Xiu et al (2013) studied the impact of sulfobetaine polymer on a gene delivery [47]. The target DNA was loaded into a comb-shaped vector consisting of dextran backbone with a comb-like surface consisting of either DMAEMA or sulfobetaine. The DNA stability and cellular uptake was much higher for the gene loaded into the sulfobetaine comb vector as compared with the DMAEMA comb vector.

The sulfobetaine polymer has also shown to be a promising nano-carrier for DNA delivery in the study by Dai et al (2008) [48]. Here the DNA was loaded into a NP fabricated from an (ABA) tri-block copolymer in which the A-block is sulfobetaine polymer and the B-block is 2-(2-methoxyethoxy)ethyl methacrylate. Ethidium bromide displacement assay showed that the sulfobetaine block in the NPs was responsible for the binding of the DNA with a very high efficiency, and an increase of sulfobetiane ratio resulted in an increase of DNA condensation by the NP [48].

As described above, the biological activity of the sulfobetaine polymer or NPs is due to the sulfobetaine moiety rather than any other copolymer included in the structures of these copolymers. This means that sulfobetaine NPs should have the sulfobetaine moiety at the surface of NPs (as a shell) to exert the desired effect. In this NP type, the zwitterionic sulfobetaine moiety is a very hydrophilic block polymer, this causes it to be localised at the shell of NPs when it is assembled in the presence of a lipophilic core [49] (Figure 5.8). This is in agreement with the principle of self-assembly of amphiphilic di-block copolymers, where the hydrophilic block will form the shell of the NP and the lipophilic block will accumulate in the core of the NP [50,51]. Thus, sulfobetaine NP with a lipophilic core should have the same anti-adherent effect as the sulfobetaine polymer since the zwitterionic block should be in contact with the biological media.

1.h Aim of the Study

The aim of this study is to produce novel zwitterionic sulfobetaine NPs having a densely charged surface but with a net neutral zeta potential at the physiological pH (Figure 5.8). These NPs will have a BMA lipophilic core and sulfobetaine as the highly charged zwitterionic shell. Moreover, these novel NPs should exhibit small particle size and be stable for at least the time required for the particles to deliver the therapeutic active agent to the required site of the body. Lastly, these sulfobetaine NPs should have a high diffusivity through the intestinal mucus barrier. The hypothesis is that the densely charged but net neutral shell with opposing charges on the same polymer chain will result in high mucus-diffusion of the respective NPs.

The purposes of this study are as follows:

- To synthesize a low molecular weight butyl methacrylate (BMA) lipophilic block polymer by the RAFT technique to serve as the lipophilic core for the shell-core sulfobetaine NP.
- To copolymerize the BMA block with various ratios of N,N-Dimethylaminoethyl Methacrylate (DMAEMA) copolymer to from a di-block copolymer of BMA-DMAEMA with the following ratios: 70:30, 60:40, 50:50, 40:60 and 30:70.
- To form BMA- sulfobetaine at the same above ratios of 70:30, 60:40, 50:50, 40:60 and 30:70 by reacting of each BMA-DMAEMA copolymers synthesized in step 2 with 1, 3 propane sultone. As a result, the synthesized block BMA-sulfobetaine will have BMA as the lipophilic block and the sulfobetiane as the zwitterionic hydrophilic block.

- To synthesize zwitterionic sulfobetiane NPs from the BMA-Sulfobetaine polymer by the nano-precipitation technique in which the BMA will form the lipophilic core and the sulfobetaine will form the hydrophilic shell (Figure 5.8). These sulfobetaine NPs will be fluorescently labelled with the lipophilic dye Lumogen red.
- To characterize all the synthesized polymers and NPs where the structures of polymer will be identified by IR, NMR and GPC while the particle size and zeta potential of NPs will be measured by DLS.
- Sixth is to investigate the mucus permeability of the novel synthesized zwitterionic sulfobetaine NPs. Specifically, studies here are to address the ability of sulfobetaine to form a muco-inert layer on the NP surface to reduce the interaction of NP particles with mucus components. On this basis, the kinetics of sulfobetaine particles transport through the "Cardiff native mucus" model will be studied to reveal the potential of the characteristic of sulfobetaine NPs.

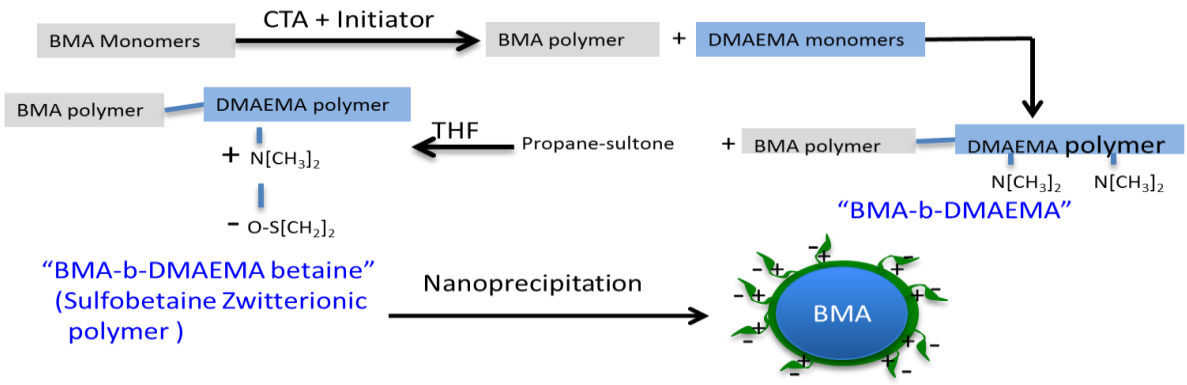

Figure 5.8: Diagram showing the aim of this study to synthesize sulfobetaine Zwitterionic NPs by successive steps starting with the synthesis of BMA, followed by the copolymerization of BMA-DMAEMA, then the synthesis of BMA-Sulfobetaine and finally the nano-precipitation to form the Zwitterionic NPs.

2. MATERIALS AND METHODS

2.a Materials

All the chemicals used in control polymerization were purchased from Sigma-Aldrich. These chemicals are: Butyl methacrylate (BMA), 2-Dimethylaminoethyl methacrylate (DMAEMA), 1,3-Propanesultone, 2-Cyano-2-propyl dodecyl trithiocarbonate (CTA), 2,2′-Azobis(2-methylpropionitrile) (AIBN) and tetrahalose. Methanol, Dioxane, dimethyl sulfoxide (DMSO), Hexane, THF and other solvents used to measure the solubility were purchased from Fisher scientific. Lumogen red was a gift from Nanomi, Netherland. Other chemicals like NaCl, KCl, Na2HPO4, KH2PO4, NaOH and HCL were also purchased from Fisher scientific. Similarly, dialysis tubing of molecular weight cut off (MWCO) 20 KDa and 12 KDa were bought from Sigma-aldrich. Lumogen Red-305 (LR) was supplied by Nanomi (Netherlands). Glass bottom imaging dishes (35 mm diameter dish with a glass coverslip at 1.5 mm thick and 10mm diameter) were from MatTek Corporation (USA).

2.b Synthesis of the Novel Zwitterionic Polymer

Synthesis of the Lipophilic BMA Block Polymer

RAFT control polymerization technique was used to polymerize the BMA block polymer. This polymerization was carried out using AIBN initiator, 2-Cyano-2-propyl dodecyl trithiocarbonate as the CTA and dioxane as the solvent of reaction (Figure 5.9). Prior to the synthesis, the initiator was purified by recrystallizing AIBN powder in cold methanol. BMA monomer was also purified prior to the polymerization by passing the monomer solution through aluminum oxide Pasteur tube to remove the anti-polymerizing agent (hydroquinone). The ratios of each of the reactants (BMA:CTA:AIBN) was calculated following the RAFT equation (Equation 5.1). Since

a final desired number of BMA monomers in each polymer chain was 25 units, BMA:CTA:AIBN were reacted at the ratio of (25:1:0.1) respectively [52].

$$Mn = \left(\frac{Mole\ monomer}{Mole\ CTA}\right) * MWmonomer + MW\ (CTA) \quad \ldots\ldots\ldots\ldots\ldots\ldots Eq\ 5.1$$

Mn = aimed molecular weight of the polymer,
(mol monomer/ mol CTA) = molar ratio of monomer to the CTA agent,
MWmonomer = molecular weight of the monomer and
MW (CTA) = molecular weight of the CTA agent.

Thus, following equation 5.1, 3.52 x 10^{-3} mole BMA monomer, 1.40 x 10^{-4} mole CTA and 1.40 x 10^{-5} mole AIBN were added in a dry borosilicate glass tube and dissolved in 2 ml dioxane (solvent of reaction). The solution in the glass tube (BMA, AIBN and CTA) was flushed with nitrogen gas for 30 min before the reaction; the container was kept under the nitrogen flushing during the polymerization process. The reason to evacuate the glass tube with an inert gas was to deoxygenate the container to allow the continuation of radical polymerization. Polymerization was started by moving the borosilicate glass tube containing the reactants into a preheated silicon oil bath at 70 °C, the polymerization was continued under heating (70 °C) and stirring (100 rpm) until the end of the synthesis.

The polymerization was carried out at three different polymerization times (6, 12 and 24 hr) to assess the effect of time on the degree of polymerization of BMA polymer. At the indicated time, the sealed rubber was removed and the mixture of polymer, unreacted monomer and other ingredients was exposed to the air to stop the polymerization process. BMA polymer was separated from other ingredients by precipitating in excess cold methanol and centrifugation at 3500 rpm for 20 min. The precipitate was washed twice with cold methanol. The supernatant was removed and the precipitated polymer

was dried under vacuum at room temperature. The dried polymer was used for further analysis and copolymerization with DMAEMA monomer in the next step [53].

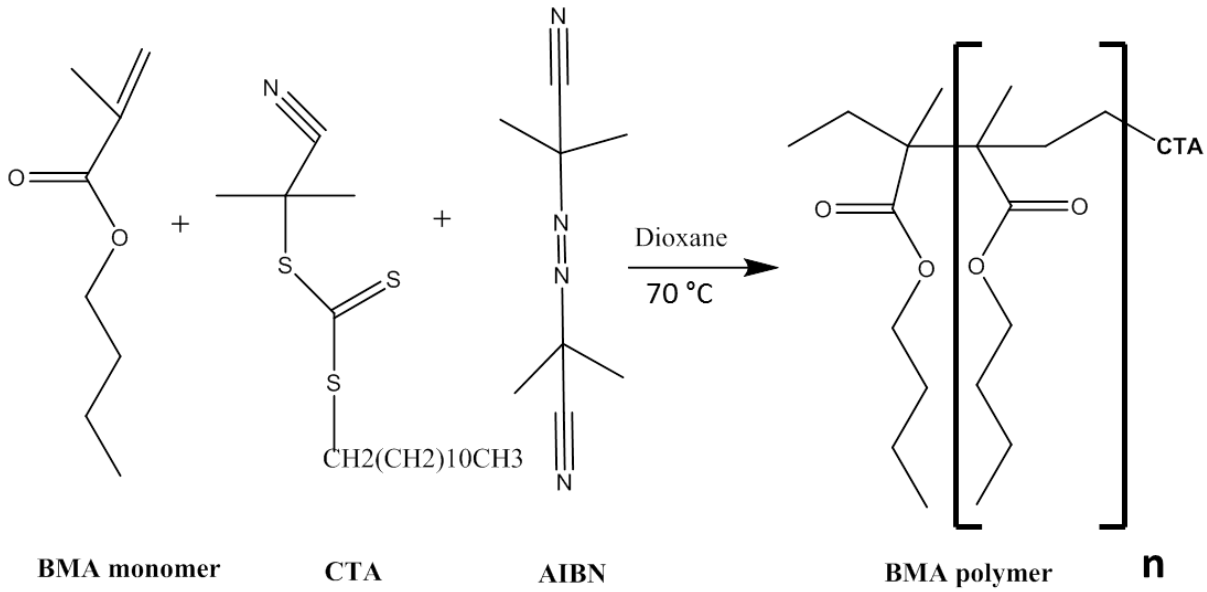

Figure 5.9: RAFT polymerization of BMA polymer by using CTA agent.

Copolymerization of BMA-DMAEMA Di-Block Copolymer

Following the synthesis of BMA block co-polymer in the previous section, in this section, the lipophilic block BMA polymer was copolymerized with DMAEMA monomers by the RAFT control polymerization technique (equation 5.1). Herein, BMA polymer holding CTA agent was served as the macro-CTA agent for controlling the RAFT polymerization of DMAEMA monomers. In other word, the block BMA-CTA was counted as the CTA agent in the calculations (equation 5.1) for the control polymerization of the DMAEMA monomers [54]. BMA was copolymerized with DMAEMA at different ratios so as to obtain BMA-DMAEMA copolymers with versatile hydrophilic-lipophilic properties. For this purpose, BMA:DMAEMA was copolymerized with the following aimed ratios (70:30, 60:40, 50:50, 40:60, and 30:70). Table 5.1 shows all the calculations including the molar ratios of DMAEMA monomer to CTA and AIBN ratios. As illustrated in Table 5.1, the (BMA: DMAEMA) ratios of

(70:30, 60:40, 50:50, 40:60, and 30:70) were symbolized as P1, P2, P3, P4 and P5 respectively.

Table 5.1: Calculations (DMAEMA monomer/CTA), BMA monomer and AIBN ratios to synthesize BMA-DMAEMA polymer at various block copolymers ratios.

Formula	PBMA: DMAEMA Calculated ratio	Ratio (DMAEMA /CTA)	PBMA-CTA Moles	DMAEMA Moles	AIBN Moles
P1	(70:30)	16.35	7.5×10^{-5}	1.23×10^{-3}	7.5×10^{-6}
P2	(60:40)	25.50	6.6×10^{-5}	1.70×10^{-3}	6.6×10^{-6}
P3	(50:50)	38.17	5.8×10^{-5}	2.22×10^{-3}	5.8×10^{-6}
P4	(40:60)	57.25	5.0×10^{-5}	2.86×10^{-3}	5.0×10^{-6}
P5	(30:70)	89.05	4.2×10^{-5}	3.71×10^{-3}	4.2×10^{-6}

Polymerization was carried out under the same conditions of polymerization of BMA except that the polymerizations of BMA:DMAEMA di-block copolymers was carried out for one polymerization time (24 hr), i.e. the effect of polymerization time was not studied for this copolymerization step. BMA-DMAEMA di-block copolymers were precipitated in cold hexane and the precipitates were washed twice in cold hexane prior to drying under vacuum pressure at room temperature. Figure 5.10 shows the structural copolymerization of BMA-DMAEMA copolymer where the BMA-CTA was served as the macro-CTA agent.

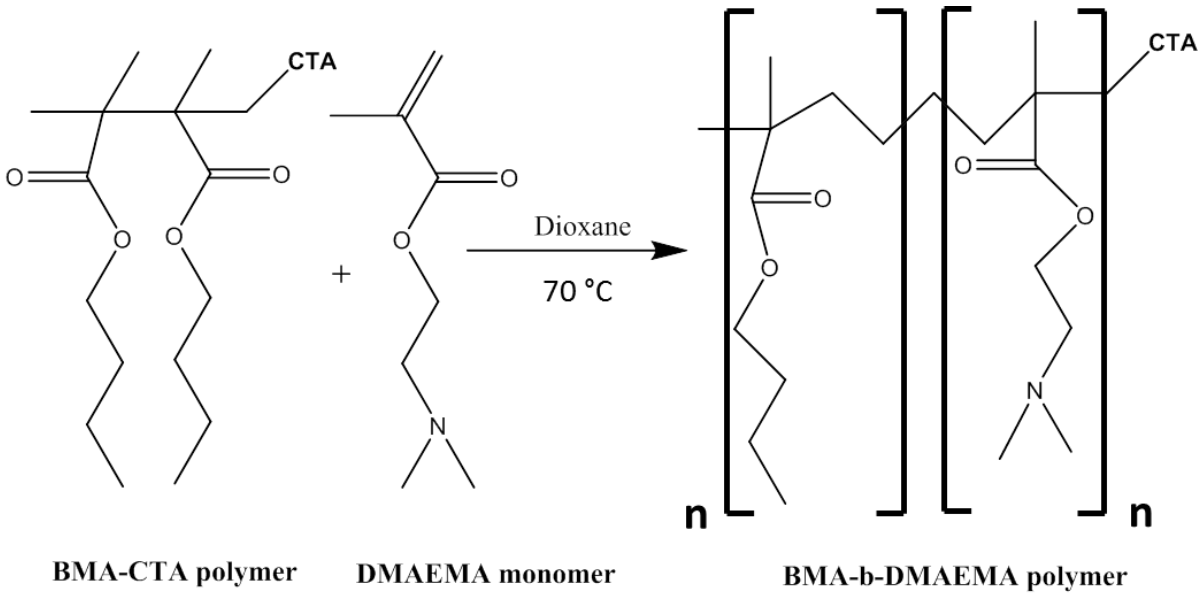

Figure 5.10: Copolymerization of BMA-DMAEMA in which BMA-CTA served as the macro-initiator to control the polymerization of DMAEMA monomers.

Synthesis of BMA-Sulfobetaine Di-Block Copolymer

In this step, BMA-DMAEMA di-block copolymers were betainised to form zwitterionic di-block BMA-Sulfobetaine. To do so, each of the BMA-DMAEMA di-block copolymers (P1, P2, P3, P4 and P5) were reacted with 1,3 propane sultone at a molar ratio of 1:2 receptively. The reactions were carried out in THF for 3 days under mild stirring and nitrogen supply [55]. Same reactions were also performed in DMSO under the same conditions. After 72 hr, BMA-Sulfobetaine polymers were precipitated in excess acetone then centrifuged at 3500 rpm. The precipitate was washed twice with acetone before left to dry under vacuum at room temperature. Figure 5.11 shows the reaction of the DMAEMA tertiary amine group with the propane sultone leading to the opening of the sultone ring and formation of the negatively charged sulfonate group next to the quaternary amino group on the same unit. The synthesized BMA-sulfobetaine di-block copolymers were symbolized following the same order used to symbolize BMA:DMAEMA di-block copolymers. Thus P1S, P2S, P3S, P4S and P5S were the synthesized copolymers from P1, P2, P3, P4 and P5 respectively, and

consisting of BMA:sulfobetaine ratios of (70:30, 60:40, 50:50, 40:60 and 30:70) respectively (table 5.2).

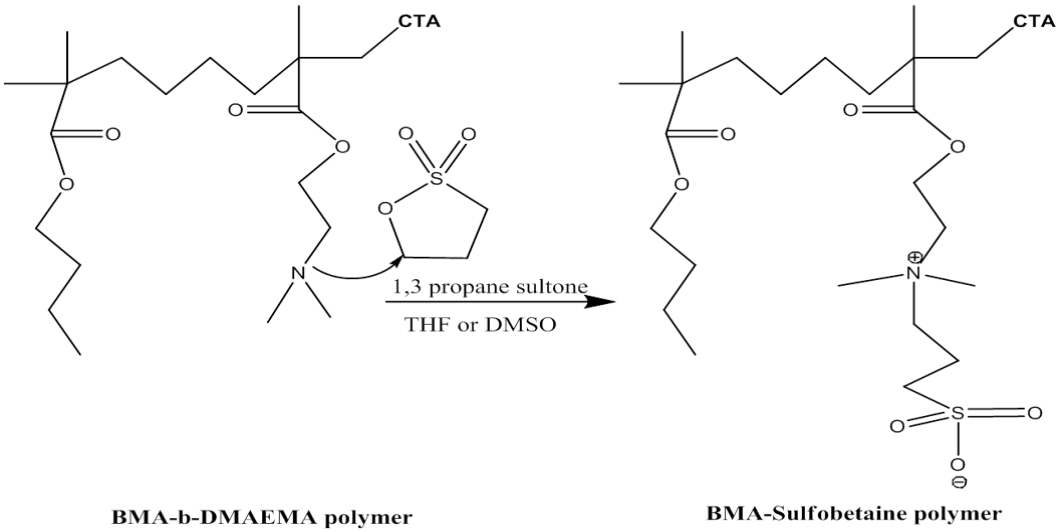

Figure 5.11: Synthesis of BMA-sulfobetaine where the tertiary amino group of the DMAEMA unit was reacted with the γ carbon of the 1,3 propane sultone.

NMR Analysis of the Synthesized Polymers

NMR proton (^{1}H-NMR) analysis was used to identify structures, degree of polymerization and purity of the synthesized polymers. NMR spectra were recorded in a 400 MHz (Varian NMR Instruments, Claredon Hills, IL) and auto-calibrated to the deuterated solvent reference peak. For BMA polymer, degree of polymerization was detected by measuring the NMR spectrum peak representing the number of BMA monomers in each chain polymer versus the reference peak representing the one CTA agent molecule within each chain polymer. Accordingly, the diminishing of any unreacted BMA monomers within the separated BMA polymer was confirmed by the disappearance of peaks of unreacted BMA monomers (BMA with double bonds) in the NMR spectrum of BMA polymer. In other words, these peaks of unreacted BMA monomers (double bonds) were shown in the NMR spectrum of BMA monomer but disappeared for the BMA polymer. Deuterated Chloroform (CDCL3) was used as the NMR solvent for the NMR analysis of both BMA polymer and monomer.

Similarly, CDCL3 was used to run the NMR analysis of BMA-DMAEMA polymer and DMAEMA monomer. Reference peak from BMA block polymer versus reference peak from DMAEMA block polymer were compared to identify the degree of polymerization of DMAEMA and the BMA:DMAEMA ratios within each di-block BMA-DMAEMA copolymer. Also, NMR spectrum was used to confirm the inexistence of any unreacted DMAEMA monomers in the final BMA-DMAEMA di-block copolymer by comparing the NMR spectrum of DMAEMA monomer and the BMA-DMAEMA polymer. Moreover, the degree of betainisation of BMA-DMAEMA and structures of BMA-sulfobetaine polymers were detected by the NMR analysis using Deuterated DMSO (DMSO-d6) as the NMR solvent [56].

Infrared (IR) Structural Analysis

IR structural spectra were performed to identify the structures of BMA, BMA-DMAEMA and BMA-Sulfobetaine using a Nicolet Magna 560 (Thermo Fisher Scientific, Waltham, MA) with a KBr beam splitter in evaporated film.

Gel Permeation Chromatography (GPC) Analysis of the Molecular Weight

Molecular weight was determined on an HPLC Elite LaChrom system (VWR-Hitachi) equipped with a GPC Shodex KF-603 column, 6,0 mm ID, 150 mm, and THF as the mobile phase. The average molecular weight (Mwa) was calculated by comparing the retention time of each assessed polymer with the retention times of polystyrene standards. The polymer polydispersity index (PDI) was calculated following equation 5.2:

$$PDI = \left(\frac{Mwa}{Mna}\right) \ldots\ldots\ldots\ldots\ldots\ldots Eq\ 5.2$$

Mwa = average weight molecular weight, Mna = number average molecular weight.

2.c Synthesis of the Novel Zwitterionic NPs

Polymer Solubilisation

In previous sections, di-block copolymers of BMA-sulfobetaine were synthesized at ratios of 60:40 (P2S), 50:50 (P3S), 40:60 (P4S) and 30:70 (P5S) (Table 5.2). These copolymers were insoluble in water. To solubilize these copolymers, various organic solvents, mixture of organic solvents and mixture of aqueous and organic solvents were used. Among all the mixtures of aqueous and organic solvents tested, the mixture of 2 M NaCL + methanol was used to solubilize BMA-sulfobetaine di-block copolymers. Each of the BMA-sulfobetaine copolymers (P2S, P3S, P4S and P5S) was dissolved in a solvent with different ratios of methanol to 2M NaCL. In other words, the ratios of the aqueous to the organic phase (methanol to 2 M NaCL) were varied depending on the ratios of BMA to the Sulfobetaine in each copolymer. Table 5.2 shows the solubilisation ratios (2M NaCL:methanol) for each sulfobetaine di-block copolymer. For example, for P2S, a 250 µl of 2 M NaCL and 250 µl of methanol were added into a tube containing 5 mg of P2S then the sample was sonicated for 10 min.

Fabrication of NPs by Nano-Precipitation Method

Sulfobetaine NPs were formulated by a modified nano-precipitation method in which the solubilisation media involved the usage of a co-solvent (2 M NaCL) rather than the usage of one organic solvent [57]. Simply, 5 µg of the Lumogen red and 5 mg of BMA-sulfobetaine di-block co-polymer (P2S, P3S, P4S or P5S) were dissolved in 500 µl of the specified solubilisation media (2M NaCL: methanol) (Table 5.2). Afterward, each solubilised polymers was added drop wise at a rate of 20 µl/min into a 10 ml external aqueous phase (PBS pH 6.8 or PBS pH 7.4) (table 5.2) using a programmable syringe pump (Razel, USA). Each of the formed NP suspension was further stirred for 45 min to

ensure the evaporation of the methanol before the physiochemical characterisation of these NPs.

Then, sulfobetaine NPs were freeze dried and stored for further studies. To do so, NPs suspensions were dialysed (dialysis tubing, MWCO: 20000) against 500 ml PBS 6.8 for 24 hr followed by collecting of NP suspension in the dialysis tube. Cryo-protectant (Tetrahalose) was added at a weight ratio of 5:1 to the total NPs weight [58]. The sample was freeze dried for 24 hr and particle size was measured to confirm the retaining of the original physicochemical properties of sulfobetaine NPs after freeze drying.

Table 5.2: The conditions of nano-precipitation of Zwitterionic polymer: the ratios of solvents solubilisation, weight of solubilised polymer, rate of polymer precipitation and volume of buffer media used for nano-precipitation of the Zwitterionic polymer.

Code	BMA:Sulfobetaine Ratios	Solubilisation media µl		Polymer weight (mg)	Rate of nano-precipitation µl/min	Volume of the buffer aqueous phase (ml)
		2 M NaCL	Methanol			
P1S	(70:30)	The yield of sample was low				
P2S	(60:40)	250	250	5	20	10
P3S	(50:50)	275	225	5	20	10
P4S	(40:60)	350	150	5	20	10
P5S	(30:70)	400	100	5	20	10

Table 5.3 shows the concentrations of chemicals dissolved in DDW to prepare PBS buffers of pH 6.8 and pH 7.4.

Table 5.3: Concentrations of the ingredients used to prepare the PBS buffers of pH 6.8 and pH 7.4.

Ingredients	pH 7.4	pH 6.8
NaCl (mM)	137	137
KCl (mM)	2.7	2.7
Na2HPO4 (mM)	10	4.3
KH2PO4 (mM)	1.8	1.4

2.d Characterization of NPs: Stability of NPs against Aggregation

Particle size and zeta potential were measured for the freshly prepared sulfobetaine NPs and at time intervals of 0.5, 1, 2, 3, 4 and 6 hr at 25 and 37 °C to assess the stability of these particles against aggregation at the physiological and the room temperatures. Also, particle sizes and zeta potentials were measured before and after freeze drying and loading of the Lumogen red to assess the effect of freeze drying and loading of hydrophobic cargo on the physicochemical properties of particles.

2.e Loading Capacity and in Vitro Release of Lumogen Red (Lipophilic Cargo)

Lumogen red has been used throughout this thesis as the fluorescent dye which is needed to be loaded at concentration of 0.1% w/w. In this study, the loading capacity of sulfobetaine NPs for lipophilic cargo was studied by using Lumogen red as the lipophilic model with the aimed loading capacity of 50%. As was described above, Lumogen red and sulfobetiane copolymers were dissolved in the solubilisation media of 2 M NaCL:methanol then NPs were prepared by the nano-precipitation method. However, to load Lumogen red at a concentration of 50%, 2.5 mg Lumogen red and 5 mg sulfobetaine copolymers were dissolved in the solubilisation media.

After the formation of NPs, 5 ml of the each of the NPs suspensions was added into the dialysis tube (MWCO: 20000) and the suspension was dialysed against an external media consisting of 500 ml PBS pH 6.8 for 24 hr. At the specified time, NPs suspension was collected and the concentration of Lumogen red in the NPs suspension before and after the dialysis was measured in triplicate using the fluorescence micro-plate reader (Fluostar Optima, BMG, Germany) [59]. Here, the quantity of Lumogen red was measured in the NPs suspension and not in the external media (500 ml PBS pH 6.8) due to the instability of Lumogen red in the buffer external media. This is based on the HPLC quantification analysis of Lumogen red which showed a self-quenching of Lumogen red in the PBS pH 6.8 and a high stability and concentration-absorbance correlation in the NPs. The entrapment efficiency (EE%) [60] and the loading capacity (LD%) [61] of sulfobetaine NPs were detected by the following equations:

$$EE(\%) = \frac{Amount\ of\ Lumogen\ loaded\ intoNP}{Total\ amount\ of\ Lumogen} * 100 \dots\dots\dots\dots\dots\dots\dots\dots\dots Eq\ 5.3$$

$$LD(\%) = \frac{Amount\ of\ Lumogen\ loaded\ intoNP}{Weight\ of\ NP} * 100 \dots\dots\dots\dots\dots\dots\dots\dots\dots Eq\ 5.4$$

Accordingly the in vitro release of the Lumogen red was studied as follows. Freeze dried NPs loaded with Lumogen red were re-suspended in phosphate buffer pH 6.8. Suspension was divided into 1 ml aliquots, each aliquot was added into dialysis tube (MWCO: 20000) then dialysed against 500 ml PBS 6.8. NP suspension from each dialysis tube was collected at the specified time interval and concentration of Lumogen red was measured in triplicate in each suspension before and after the dialysis. Suspension samples were collected at time intervals of 30 min, 1, 2, 3, 4, 6, 8, 16 and 24 hr.

2.f Study of Sulfobetiane Kinetics Diffusion through the "Cardiff Native Mucus" Model

All the experimental work to study the kinetics of particles' diffusion through the mucus was carried out following the same MPT methodology in chapter four.

Statistical Analysis

One-way analysis of variance test was used to compare the % ratio of <Deff> vs D° for all the sulfobetaine NPs with significant value of $p < 0.05$.

3. RESULTS AND DISCUSSION

3.a Synthesis of the Novel Zwitterion Polymer

RAFT technique was used to synthesize BMA lipophilic block polymer and BMA-DMAEMA di-block copolymers prior to the synthesis of the zwitterionic sulfobetaine polymer. This technique allows tailoring the molecular weight of the lipophilic and the hydrophilic block polymers. Thus, for sulfobetaine NPs, controlling the molecular weight of BMA block polymer will allow controlling the size of the lipophilic BMA core in the NPs and the same for the sulfobetaine hydrophilic shell [62,63]. This enables to design the NPs in response to the purpose it is synthesized for. This will be illustrated in the next section.

The other reason to use the RAFT technique is the presence of the CTA agent within the polymer synthesized by RAFT technique which introduces another opportunity to covalently bind targeting agents into the NPs [64]. In other words, targeting agent could be attached to the NPs through a replacement reaction in which the CTA is removed and replaced with the targeting agent. This replacement technique could be used in this work later to introduce any targeting agent.

Synthesis of the Lipophilic BMA Block Polymer

In this section, BMA block polymer was synthesized by RAFT technique with the purpose of producing low molecular weight lipophilic block. This lipophilic block polymer will be copolymerized in the next sections with a zwitterionic hydrophilic polymer where this block will be the lipophilic core in the NPs. The low molecular weight lipophilic polymer is supposed to form a small lipophilic core in the NP [65] which in turn leads to form a small NP size [66]. In this work, producing NPs with small lipophilic core was essential so as to reduce the lipophilic interaction with the mucus lipophilic component and to reduce the NP size which in turn will eliminate

trapping of NPs by mucus steric effect (explained in chapter 3). Hence, a ratio of 25:1 of the monomer to the CTA agent was selected to synthesize polymers with only 25 BMA units in each chain.

Figure 5.12 shows the ^{1}H-NMR spectra of the BMA polymer in which A, B and C show the spectra of BMA polymers after 6, 12 and 24 hr polymerization time. These NMR spectra were used to detect the number of BMA units in each polymer chain by comparing the area under the curve of the peak signal at 3.95 ppm representing two protons from the BMA monomer to the area under the curve of the peak signal at 3.2 ppm representing two protons in the CTA agent (Figure 5.12). To be more specific, Figure 5.12 shows that the peak signal at 3.95 ppm is related to the two protons of the methyl groups next to the ester group in the BMA monomer. Since in the RAFT polymerization, each polymer chain possesses a one CTA unit, so comparing of these 2 peaks reveals the number of the BMA units in each polymer as compared to the one CTA unit. (Note: ^{1}H-NMR spectra of the CTA agent and BMA monomer is presented in Appendix F).

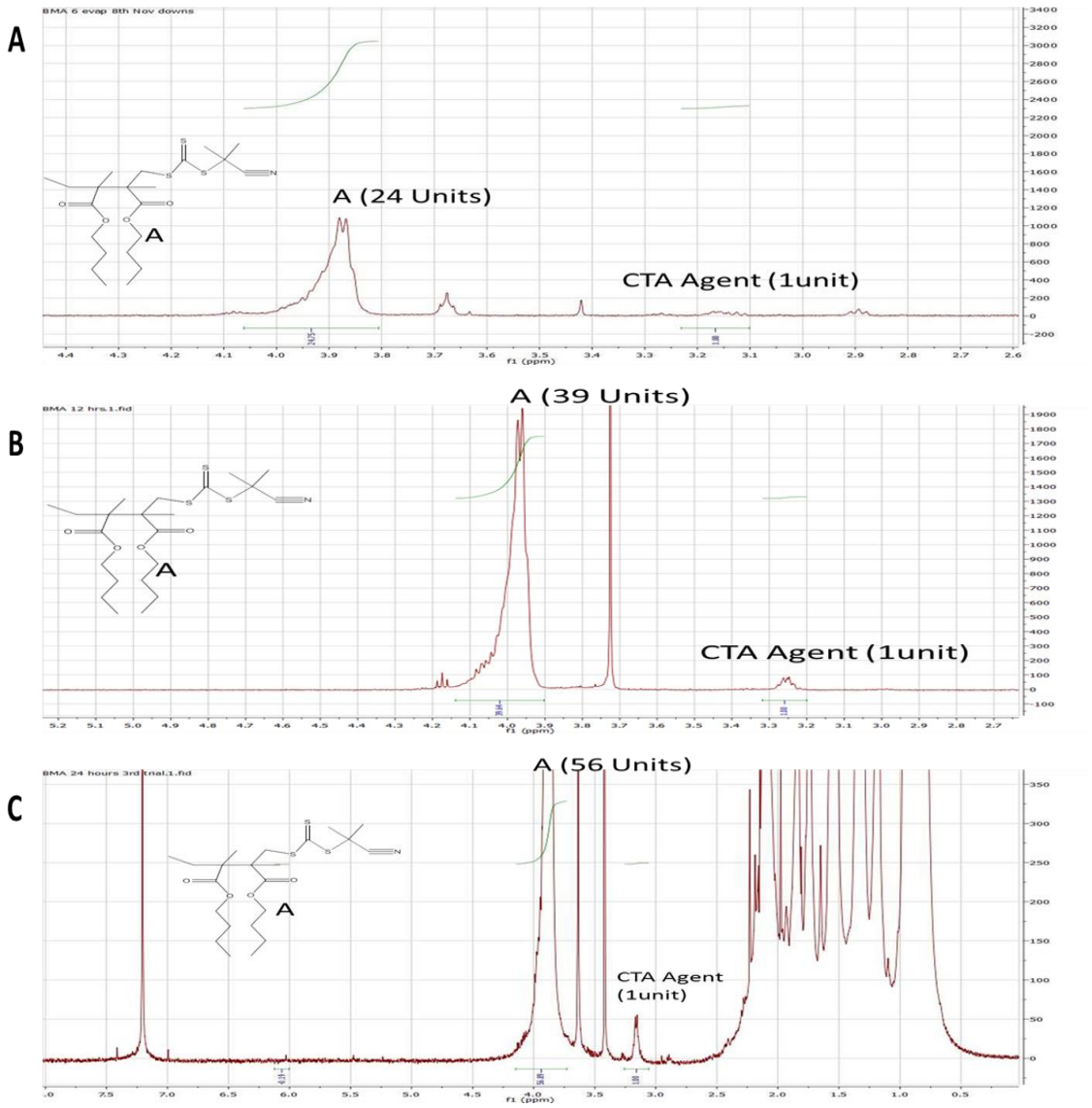

Figure 5.12: ^{1}H-NMR spectrum of the BMA polymer in which the peaks showing the number of BMA units in polymer chain was highlighted. (A) BMA polymerized for 6 hr. (B) BMA polymerized for 12 hr. (C) BMA polymerized for 24 hr. (Solvent: CDCL3).

It can be seen that BMA polymerized for 6, 12 and 24 hr were grown up to 24, 39 and 56 units respectively (Figure 5.12 A, B and C). Polymerization of BMA for 6 hr achieved the aimed number of units (25 monomers per polymer chain). However, stopping the polymerization of BMA after 6 hr could affect the PDI of this polymer since some chains could be still growing at this time interval (6 hr). This expectation could be true since the number of BMA monomers in each BMA chain was doubled after 24 hr. Hence, the PDI of BMA polymer should be assessed to assess the suitability

of the trithiocarbonate CTA agent for BMA polymerization. For this reason, GPC technique was used to detect the PDI of the BMA polymer that was polymerized for 6 hr, also, the PDI of the BMA polymer that was polymerized for 12 hr was also measured as a reference for a well grown polymer. Figure 5.13A shows that the PDI of the 6 hr polymerized BMA was 1.28 while Figure 5.13B shows that the PDI value for the 12 hr polymerized BMA was 1.19.

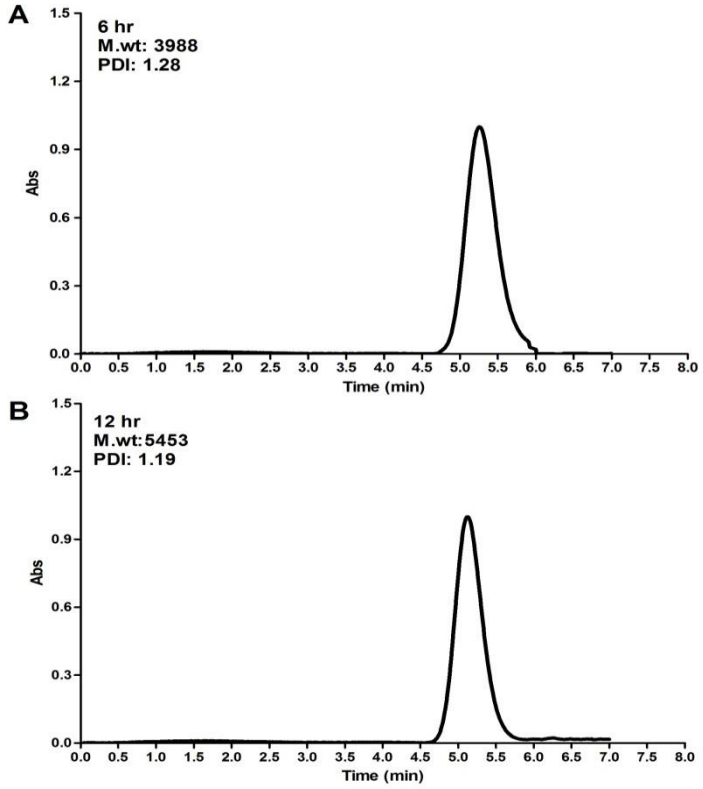

Figure 5.13: GPC profile of BMA showing the molecular weight and the PDI. (A) BMA polymerized for 6 hr. (B) BMA polymerized for 12 hr.

The pattern of polymer growing (Figure 5.12) indicates that time of polymerization had important impact on the degree of polymerization of the BMA, where only 6 hr polymerization achieved the aimed 24 units BMA polymer with a molecular weight of 3750 gm per mole, while, polymerization of BMA for 24 hr doubled the number of BMA monomers up to 56 per polymer chain. Previous studies showed that time can

play important role in the degree of polymerization of active monomers [28]. Hence, time effect here is predictive since BMA is an active monomer that can grow quickly up to tens of thousands of grams per mole with very high polydispersity when it is subjected to uncontrolled polymerization [67]. Like any active monomers, high activity is gained from the presence of high donating functional groups which stabilize the propagating radicals to grow up to thousands or millions Da [68,69]. In BMA monomer, butyl group is the donating species which stabilize the propagation of BMA. For this reason, obtaining low molecular weight BMA polymer have required various control polymerization techniques such as atomic transfer radical polymerization (ATRP) [70] and the use of chelating agent [71].

Moreover, obtaining the aimed 24 units BMA polymer at short time interval (6 hr) elucidates the suitability of trithiocarbonate CTA agent for RAFT polymerization of BMA polymer. This could also be confirmed by having PDI value of 1.28 for 6 hr polymerized BMA polymer which is within the acceptable limit (≤1.3) (Figure 5.13) [72,73]. In literature, 2-Cyano-2-propyl dodecyl trithiocarbonate has been defined as the CTA of choice for the control polymerization of highly active methacrylate monomers like BMA [28,74]. The cyano propyl trithiocarbonate CTA agent was modified by Moad and co-workers to control the polymerization of very active monomers like styrene and methacrylate [75]. Accordingly, CTA agent with cyano R group was widely reported for the RAFT polymerization of BMA polymer [76–78].

For all the above mentioned reasons, trithiocarbonate was selected as the CTA agent to polymerize BMA polymer for which it showed an acceptable suitability. With this achievement, BMA polymer that polymerized for 6 hr was selected to be the macro-CTA agent for copolymerization with DMAEMA.

Copolymerization of BMA-DMAEMA Di-Block Copolymer

As was described in previous section, BMA-CTA was used as the macro-CTA agent to copolymerize DMAEMA at various ratios. The codes P1, P2, P3, P4 and P5 were used to describe the di-block BMA:DMAEMA copolymer at ratios of (70:30, 60:40, 50:50, 40:60 and 30:70) respectively. At this stage, these various ratios cannot be considered as ratios of hydrophilic to lipophilic polymers since DMAEMA block polymer is not a hydrophilic polymer. However, DMAEMA itself will be the source of the hydrophilic block in the next step after the betainisation of DMAEMA.

Figure 5.14 A, B, C, D and E show the ^{1}H-NMR spectra of the 5 BMA-DMAEMA polymers (P1, P2, P3, P4 and P5) respectively. These spectra were used to detect the ratios of BMA to DMAEMA block polymers in each BMA-DMAEMA di-block copolymer by comparing the area under the curve of the signal peaks from BMA to that of DMAEMA. In Figure 5.14, symbols A and B were donated for the methyl groups next to the ester groups in BMA and DMAEMA units respectively (Note: structures of BMA-DMAEMA di-block copolymers with symbols A and B are presented to the left in Figure 5.14). Each of these methyl groups possesses two protons which makes the ratio between their signal peaks representative to the ratio of the number of units of BMA and DMAEMA in each block polymers. The signal peak for the BMA methyl group was at 3.95 ppm and for DMAEMA methyl group was at 4.1 ppm (^{1}H-NMR spectrum of the DMAEMA monomer is presented in Appendix F).

To assess the suitability of the CTA agent in this study, the ratios of each block polymer detected by NMR was compared to the calculated ratio by the RAFT equation 5.1. Thus, if the detected ratios by NMR are equal to the calculated ratios then this indicates the suitability of the macro BMA-CTA agent on the polymerization of DMAEMA. To clarify the ratios obtained by NMR versus the calculated ones, Table 5.4 shows the

ratios of BMA and DMAEMA blocks in the copolymers that were detected by comparing the peaks in the NMR spectra.

It can be seen that the detected ratios of BMA:DMAEMA are very close to the calculated ratios indicating the successful control polymerization of DMAEMA by the RAFT technique (Figure 5.14, Table 5.4). For example, P1 was aimed to be copolymerized at a ratio of 70:30 (BMA:DMAEMA) which is very close to the detected ratio by NMR (69:31) which indicates that trithiocarbonate is the proper CTA agent for the copolymerization of DMAEMA with BMA. This finding is consistent with previous study showed the successful use of trithiocarbonate for the di-block copolymerization of DMAEAM with styrene [79]. Additionally, trithiocarbonate as a macro-CTA agent was widely reported as a good source for di-block and tri-block control copolymerization [80,81].

Moreover, Table 5.4 shows the molecular weight of each di-block copolymer measured by calculating the sum of the molecular weight of monomers in each copolymer. In this study, only NMR analysis was used to detect the molecular weight due to the technical issue associated with the use of GPC to measure the molecular weight of DMAEMA, where the DMAEMA amino group was found to interact with the GPC column. However, NMR analysis showed that the number of DMAEMA monomers that copolymerized to BMA was precisely correlated to the calculated one which indicates the well control on the degree of polymerization of DMAEMA polymer.

Table 5.4: Calculated and detected ratios of BMA block polymer to DMAEMA block polymer and the molecular weights of each BMA-DMAEMA di-block copolymer.

Symbol	BMA-DMAEMA Calculated ratio	BMA-DMAEMA Detected ratio by NMR	BMA-DMAEMA Monomer ratio detected by NMR	Molecular weight of detected by the NMR gm/mole
P1	70:30	69:31	24:10	5370
P2	60:40	58:42	24:16	6265
P3	50:50	49:51	24:24	7517
P4	40:60	39:61	24:36	9396
P5	30:70	28:72	24:56	12528

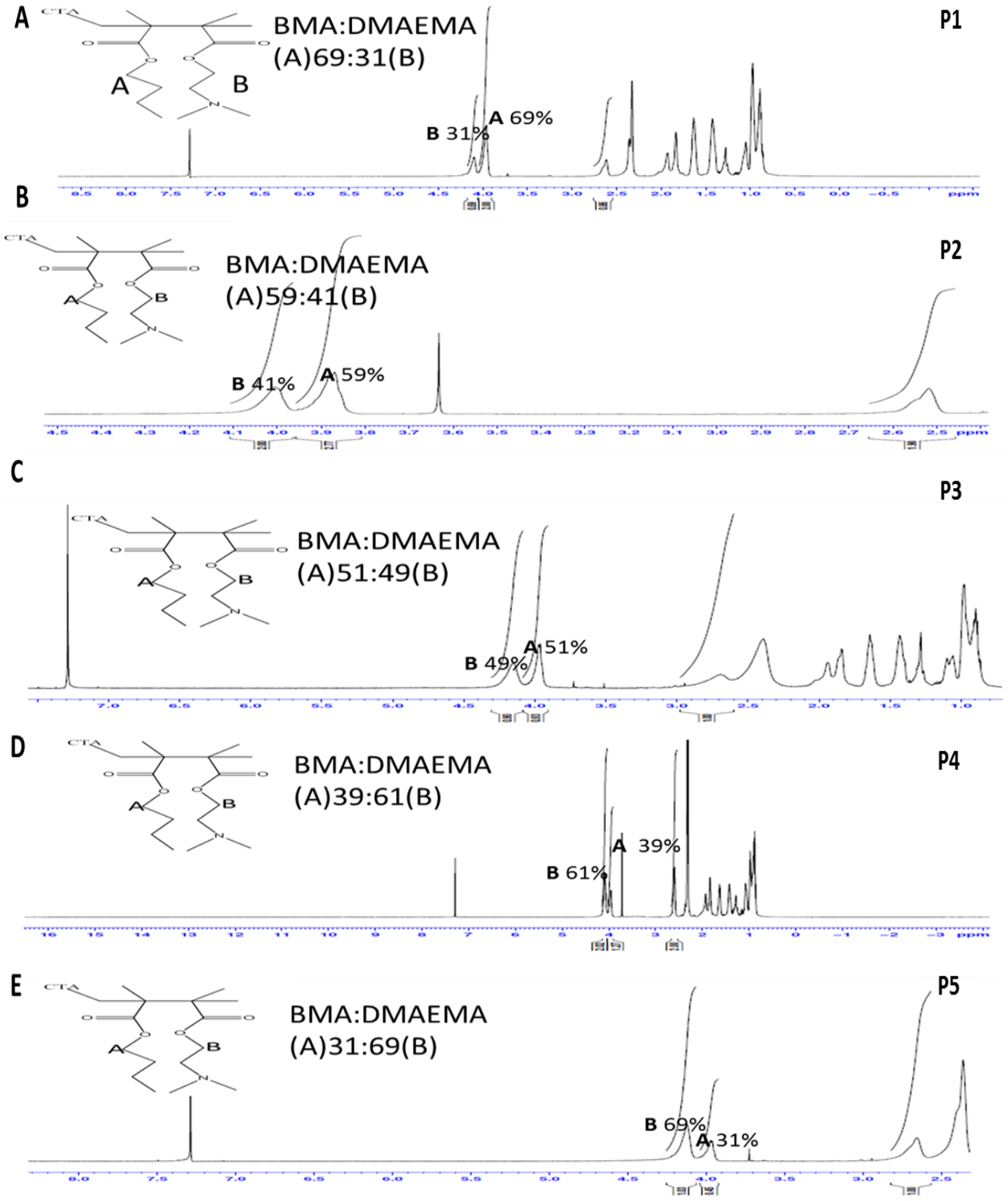

Figure 5.14: ^{1}H-NMR spectrum of the BMA:DMAEMA di-block copolymer in which the peaks showing the ratios of number of units of BMA to DMAEMA was highlighted. (A) (P1) BMA:DMAEMA (70:30). (B) (P2) BMA:DMAEMA (60:40). (C) (P3) BMA:DMAEMA (50:50). (D) (P4) BMA:DMAEMA (40:60). (E) (P5) BMA:DMAEMA (30:70). (Solvent: CDCL3).

Synthesis of BMA-Sulfobetaine Block Copolymer

The main aim in this section is to synthesize an amphiphilic polymer in which the hydrophilic block is zwitterionic highly charged polymer. This aim was approached by the betainisation of the DMAEMA block polymer in the BMA-DMAEMA di-block copolymer. Structurally, each DMAEMA tertiary amino group was aimed to be attached to the γ methyl group of the propane sultone. This leads to the formation of a positively charged quaternary amino group and negatively charged sulfonate group on the same polymer chain. That is, on the same chain, there will be two oppositely charged functional groups that are separated by three methyl groups. This zwitterionic sulfobetaine polymer, could form a NP mimicking the muco-inert capsid shell virus in term of the densely charged surface with a net neutral charge [82].

The reaction as described in the method section was carried out in THF for 72 hr followed by precipitation process. As a trial to facilitate the reaction between the propane sultone and BMA-DMAEMA, reaction was also carried out in DMSO which exhibited fast precipitation (24 hr) with no need for precipitating step. Visually, the precipitate formed from the reaction of the propane sultone and BMA-DMAEMA in DMSO seemed bulky and oily and soluble in most organic and aqueous solvent (visual appearance is described below in Figure 5.19). NMR analysis of the compound resulted from the reaction of BMA-DMAEMA with propane sultone in DMSO showed no structural indication of the presence of di-block copolymers, instead, NMR analysis showed the formation of dimethyl(sulfopropoxy) sulfonium salt (Figure 5.15A and 5.15B). These findings made doubts about the reaction of BMA-DMAEMA with propane sultone.

Hence, another reaction was carried out in which only DMSO and propane sultone were reacted so as to investigate the probability of the reaction of propane sultone with the

DMSO rather than BMA-DMAEMA. A bulky oily powder is formed which is visually similar to the one formed in the presence of BMA-DMAEMA. NMR analysis showed that the product of the reaction of propane sultone and DMSO alone was structurally similar to the product formed in the presence of BMA-DMAEMA (Figure 5.16A).The formation of dimethyl(sulfopropoxy) sulfonium salt by reacting DMSO with propane sultone was described early by Natus and Goethals (1965) [83]. However, our study, showed that DMSO and propane sultone could react preferably even with the prersence of other ingredients like BMA-DMAEMA di-block copolymer to form the same sulfonium salts (Figure 5.15B and Figure 5.16B).

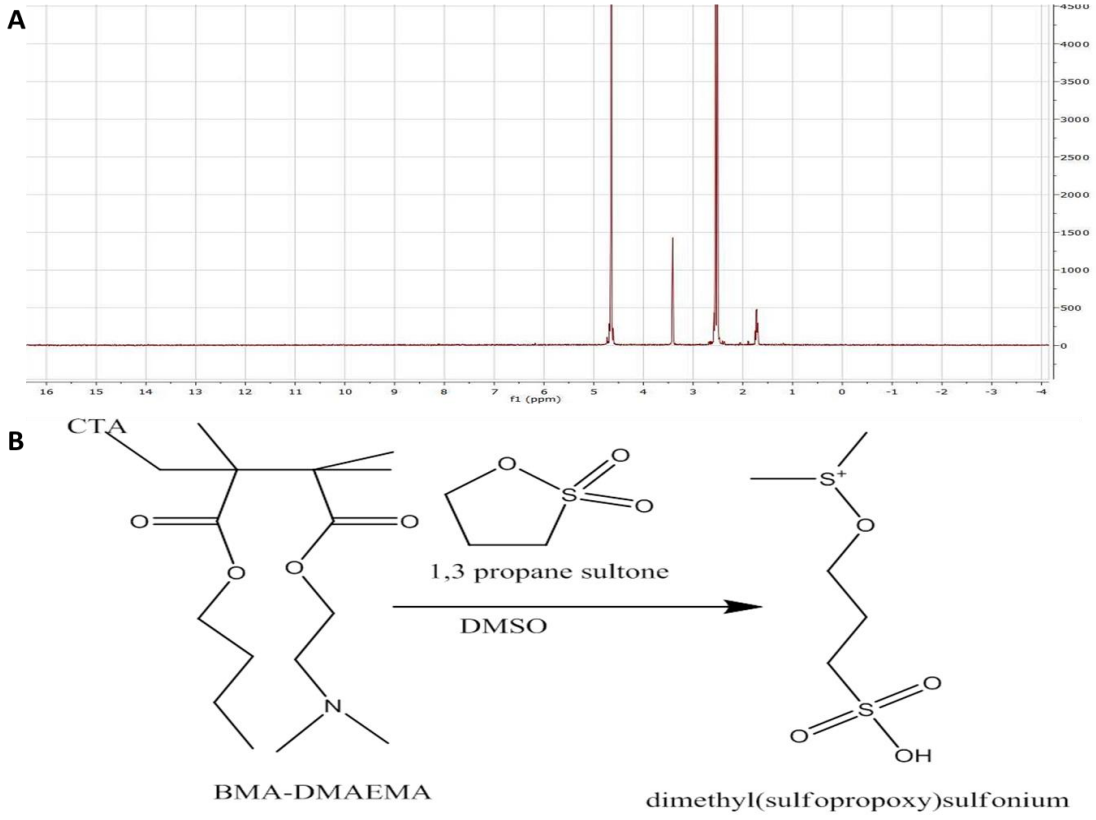

Figure 5.15: (A) ^{1}H-NMR spectrum of the sulfonium salt resulted from the reaction of DMSO with propane sultone in the presence of BMA-DMAEMA. (B) Formation of dimethyl(sulfopropoxy)sulfonium salt when propane sultone was reacted with DMSO in the presence of BMA-DMAEMA (Solvent: CD3OD).

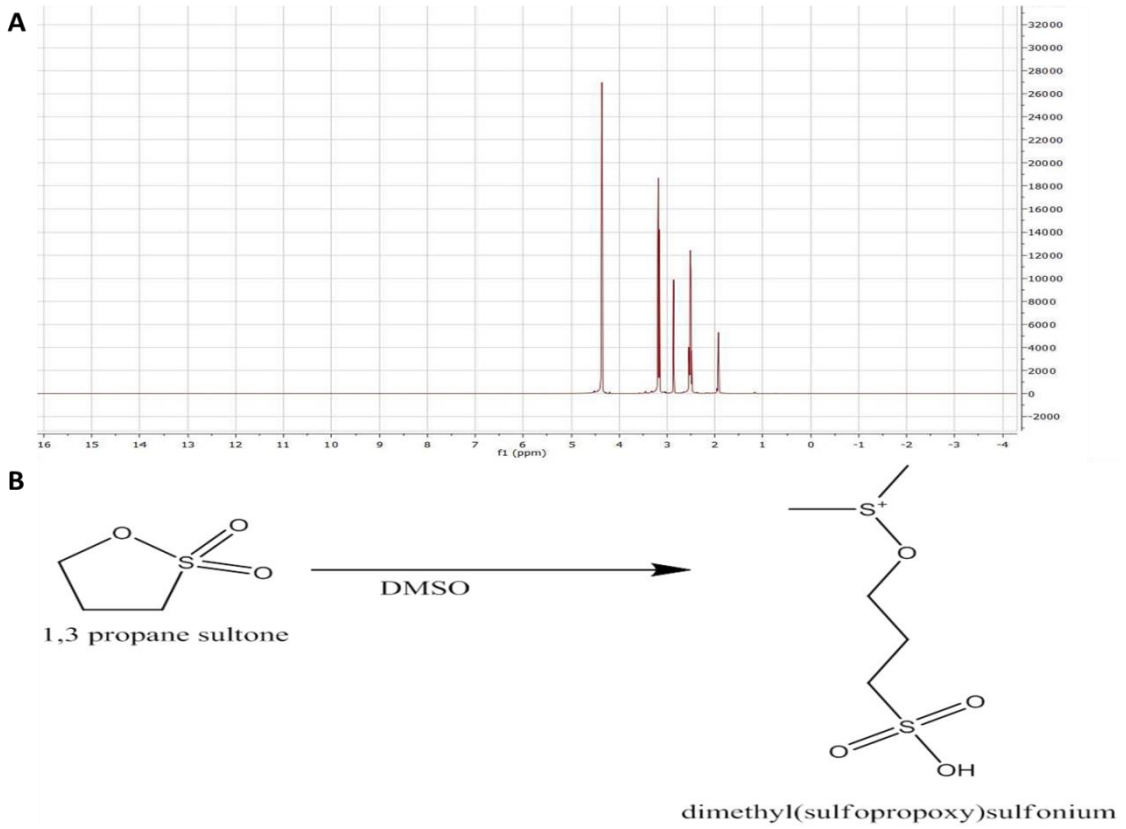

Figure 5.16: (A) ^{1}H-NMR spectrum of the sulfonium salt resulted from the reaction of DMSO with propane sultone in the absence of BMA-DMAEMA. (B) Formation of dimethyl(sulfopropoxy)sulfonium salt when propane sultone was reacted with DMSO in the absence of BMA-DMAEMA (Solvent: CD3OD).

On the other hand, the 5 BMA-DMAEMA di-block copolymers (P1, P2, P3, P4 and P5) were reacted with propane sultone in THF for 72 hr [55]. It was observed that the rate of the formation of BMA-sulfobetaine was directly correlated to the ratio of DMAEMA in the BMA-DMAEMA copolymer. Thus, for the polymers with higher DMAEMA ratios (P5 and P4), the products were started to precipitate after 24 hr. This fast precipitation was not observed for P3 with 50% DMAEMA, where the BMA-sulfobetaine polymer was started to precipitate within the last 24 hr of the reaction. Oppositely, for polymer with lesser DMAEMA ratios than BMA represented by P2 and P1, there was no precipitation even after 72 hr and products precipitated in excess acetone. The synthesized zwitterionic BMA-sulfobetaine copolymers were given symbols related to

the polymer they formed from. So, P2S, P3S, P4S and P5S were the BMA-sulfobetaine polymers that are formed from P2, P3, P4 and P5 respectively.

Precipitation by acetone increased the yield (precipitation) of all polymers with the highest yield obtained for P5S followed by P4S then P3S and the lowest P2S. Alternatively, P1S showed very low yield made the use of this polymer in the formulation of NPs is unreasonable. To explain the reason for the correlation between the DMAEMA ratio and degree of betainisation, yield results could be described the opposite way, where the yield of BMA-sulfobetaine was inversely correlated with the ratio of BMA. In other words, increase in the ratio of the copolymer (BMA) induced a reduction or retardation of the reaction between DMAEMA and propane sultone.

This is consistent with Bütün et al. (1997) study who showed that the increase in the ratio of the block polymer (2-diisopropylamino ethyl methacrylate) copolymerized to DMAEMA from 20% to 40% resulted in high reduction in the betainisation of DMAEMA [84]. Bütün explained the correlation between the ratio of the copolymer and the degree of betainisation of DMAEMA based on the steric effect of the 2-diisopropylamino ethyl methacrylate that minimize the ability of tertiary amine of DMAEMA to react with propane sultone. This also explains our data and the reason for the massive reduction in the yield of the BMA-sulfobetaine when the BMA ratio increased reaching to 70%.

Moreover, to confirm the synthesis of BMA-sulfobetaine, IR analysis was used to study the synthesis of BMA-sulfobetaine copolymers by investigating step by step structural transformation of the BMA to BMA-DMAEMA reaching to the synthesis of BMA-sulfobetaine. Figure 5.17 shows consequently the IR spectra of BMA block polymer (Figure 5.17A), BMA-DMAEMA di-block copolymer (Figure 5.17B) and BMA-sulfobetaine copolymer (Figure 5.17C) in which groups representing the structures of

BMA, BMA-DMAEMA and BMA-sulfobetaine polymer were highlighted (functional groups associated with CTA and AIBN initiator were not highlighted).

Figure 5.17A shows the main functional groups of the BMA block polymer including the methyl, ether and the ester groups at 2850-3000, 1210-1320 and 1750-1820 cm^{-1} respectively. Accordingly, Figure 5.17B shows the functional groups of DMAEMA polymer that is copolymerized to the BMA including the methyl, ether, ester and amino group at 2850-3000, 1210-1320, 1750-1820 and 1080 cm^{-1} respectively. Consequently, Figure 5.17C shows the formation of the sulfonyl group at 1030-1060 cm^{-1} and the sulfanol at 3200-3550 cm^{-1} besides the main functional groups of BMA. Thus, IR proved the formation of BMA-Sulfobetaine di-block copolymer; however, IR analysis could not confirm the total betainisation of the DMAEMA group and further NMR studies were required to show the ratio of BMA to sulfobetaine in the polymer.

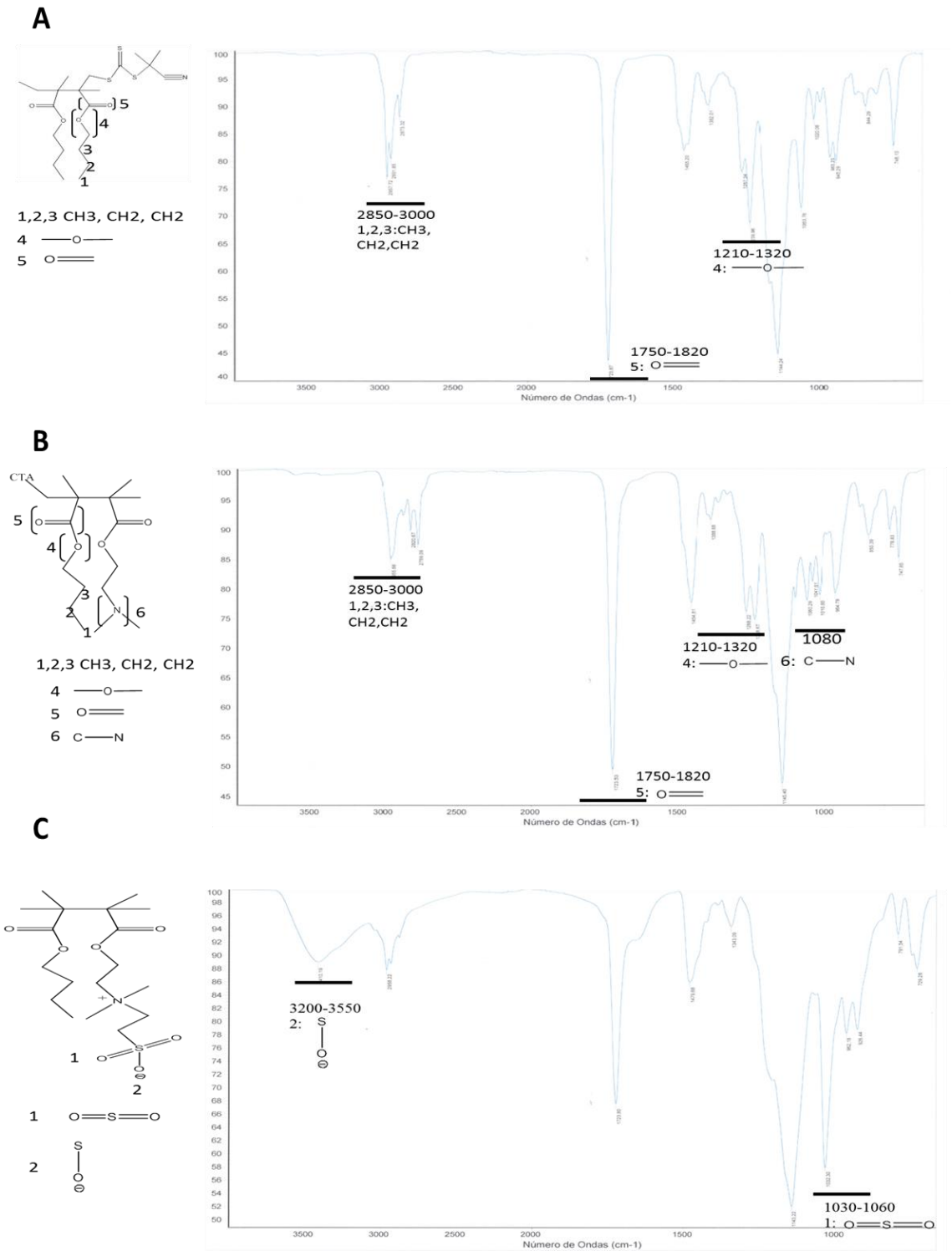

Figure 5.17: IR spectrum showing the structural formation of BMA-sulfobetaine step by step where step (A) shows the functional groups of the BMA, step (B) shows the functional groups of BMA-DMAEMA while step (C) shows the functional groups of BMA-sulfobetaine.

On the other hand, NMR structural analysis of BMA-sulfobetaine faced technical difficulties associated with the solubility of the BMA-sulfobetaine in NMR solvents. That is, all the BMA-sulfobetaine copolymers were insoluble in most of the organic or aqueous solvents due to the very high water solubility of the sulfobetaine block polymer which makes the copolymers insoluble in most organic solvent used for NMR analysis. Only the copolymers P1S and P2S which contains 70% and 60% BMA showed some solubility in DMSO-d6 (not totally dissolved), this low solubility in DMSO made NMR spectra of P1S and P2S very noisy. Nevertheless, noisy NMR spectra enabled to run a structural comparison of the BMA-sulfobetaine polymers (P1S and P2S) with BMA-DMAEMA polymers which was partly soluble in DMSO-d6 (comparison before and after the step of betainisation).

NMR spectrum of BMA-DMAEMA copolymer (before the betainisation step) shows no signal peak at 4.5 ppm but 2 signal peaks at 3.9 and 4.1 ppm representing the BMA and DMAEMA signal peaks respectively (Figure 5.18A). On the other hand, Figure 5.18 B and C for P1S and P2S show the BMA signal peak at 3.9 ppm with disappearance of the DMAEMA signal peak at 4.1 and appearance of a signal peak at 4.5 ppm indicating structural change in the DMAEMA block copolymer. This structural change (peak at 4.5 ppm) is associated with the formation of methyl group next to the quaternary amino group of DMAEMA indicating the betainisation of DMAEMA.

Moreover Figure 5.18 B and C show correlations between the ratios of the signal peaks at 3.9 ppm (BMA methyl group) and the signal peak at 4.5 ppm (methyl group next to the quaternary amino group) in P2S and P1S. Thus, for P2S, the ratio of the BMA signal peak to the sulfobetaine signal peak was 60% to 40% (Figure 5.18B) which is the same ratio for the original P2 BMA:DMAEMA copolymer. Similarly, for P1S, the ratio of the BMA signal peak to the sulfobetaine signal peak was 70% to 30% (Figures 5.18C)

which is the same ratio for the original P2 BMA:DMAEMA copolymer. These NMR spectra indicate the complete betainisation of DMAEMA block and formation of BMA-Sulfobetaine at the same original ratio of BMA-DMAEMA for both P1S and P2S.

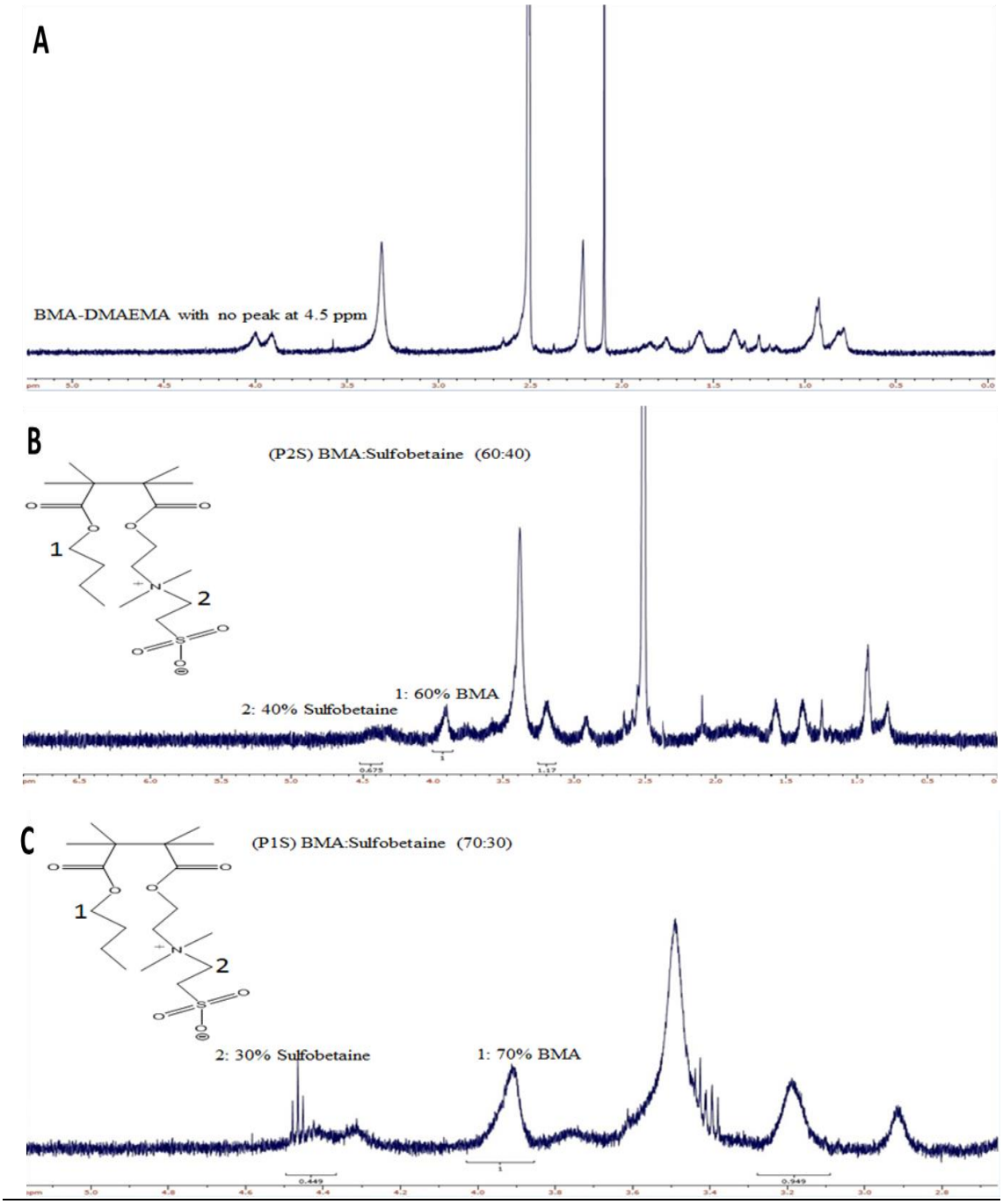

Figure 5.18: ^{1}H-NMR spectrum. (A) BMA-DMAEMA polymer. (B) BMA-sulfobetaine (60:40) P2S. (C) BMA-sulfobetaine (70:30) P1S.

Accordingly, the physical appearance of BMA-sulfobetaine copolymers formed in THF was entirely different from that of the sufonyl salt formed from reaction of propane sultone with DMSO. As was described earlier, sufonyl salt was oily white powder. Oppositely, pure crystals were formed for all BMA-sulfobetaine polymers resulted from the reaction in THF. The colour of these crystals varied from yellowish white for the

polymers with high BMA ratio (P1S and P2S) to white for the polymers with low BMA ratios (P4S and P5S). This yellowish appearance for P1S and P2S reflects the high content of the BMA polymer which has physical appearance of yellow brown oil.

3.b Synthesis and characterization of the Novel Zwitterionic NPs

Polymer Solubilisation

All the methods for the synthesis of polymeric NPs require polymers to be dissolved in a suitable organic or aqueous solvents [85]. BMA-sulfobetaine is characterized by a very lipophilic block polymer (BMA) that is soluble in highly lipophilic organic solvent and a very hydrophilic block sulfobetaine that is insoluble in any organic solvent but water. Any attempt to solubilize this zwitterionic hydrophilic-lipophilic copolymer in either organic solvent or aqueous phase alone did not work and polymer underwent micellization. Based on previous solubility studies on zwitterionic hydrophilic-lipophilic di-block copolymers, mixtures of organic and hydrophilic solvents were used to dissolve these types of polymers [86].

Thus, various mixtures of organic solvents and DDW were used to solubilize this zwitterionic polymer (Figure 5.19). These BMA-sulfobetaine polymers were insoluble in all tested mixture except the mixture of methanol and 1 N HCL which solubilized the polymer at a desired concentration (1 mg per 100 µl). However, the use of 1 N HCL was not suitable due to the high acidity of the medium which can affect the NPs themselves and it was necessary to replace HCL with another highly ionised hydrophilic solvent. This highly ionized media should be a highly concentrated electrolyte solvent that can be mixed with methanol to replace HCL acid. Thus, highly concentrated NaCL (2 M NaCL) solution was used due to its high ions content.

This mixture of 2 M NaCL and methanol showed a high solubilisation tendency towards all BMA-sulfobetaine copolymers. As was described in Table 5.2, the ratio of the organic phase to the hydrophilic phase (mtheanol to 2M NaCL) was varied depending on the ratio of the BMA to sulfobetaine with an average solubility of 10 mg/ml. As example, the ratio of the methanol:NaCL increased from 50:50 for P2S (BMA: sulfobetaine (60:40)) to 20:80 for the P5S (BMA:sulfobetaine) (30:70).

The solubilizing effect of 2 M NaCL was explained depending on the theory of the anti-polyelectrolyte effect [30]. This theory describes the conformation of the zwitterionic polymer in the aqueous phase as a collapsed globular structure due to dipolar interactions between the opposite charges. Addition of low molecular weight electrolytes such as NaCL will screen these dipolar interactions making the polymer having more extending conformation. This extended conformation enables the organic solvent like methanol to solubilize the lipophilic block that was originally hidden in the collapsed globular structure.

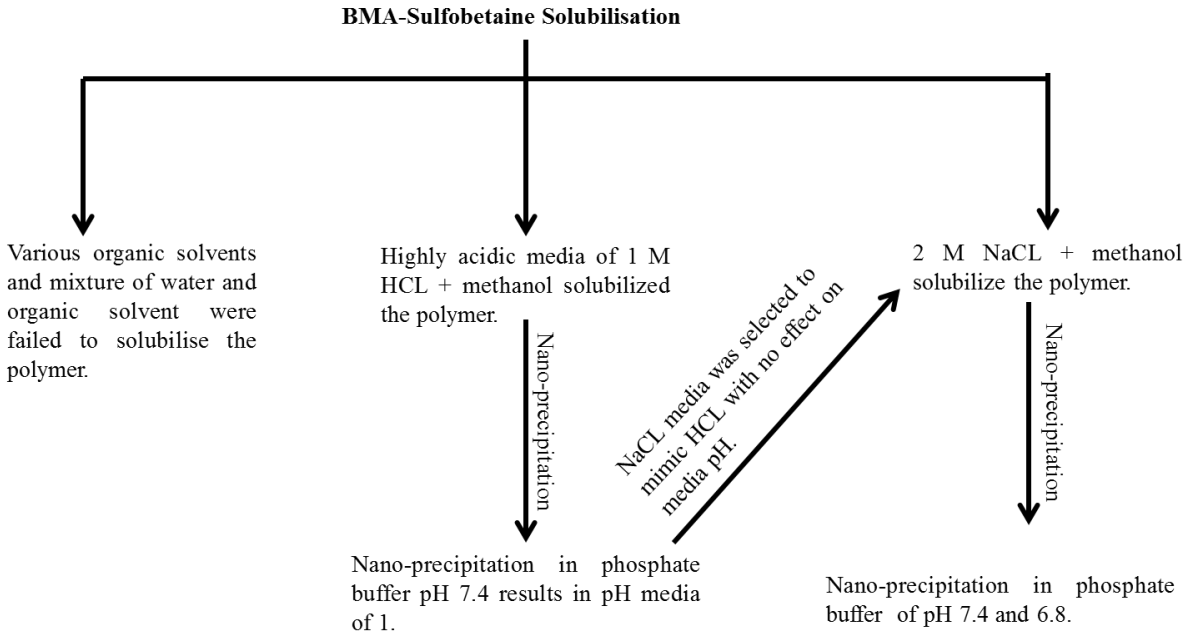

Figure 5.19: Solubilisation process of the BMA-sulfobetaine polymers including the use of various organic and hydrophilic mixtures.

Fabrication of NPs by Nano-Precipitation Method

Nano-precipitation technique is a one-step simple and reproducible method for formulation of NPs; therefore, it was selected for the fabrication of Sulfobetaine NPs [87]. Before analysing the data of sulfobetaine NPs, it is important to clarify the conditions at which sulfobetaine NPs were nano-precipitated. As was seen in Table 5.2, all BMA-sulfobetaine copolymers were nano-precipitated following the same parameters of polymer concentration in the solubilisation medium (5 mg/0.5 ml) and the rate of nano-precipitation (20µl/min). It is known that the solubilisation conditions of polymers prior to the nano-precipitation process affect the sizes of the particles. For example, changing the solubilisation solvent can reduce the solubility of polymer which in turn can increase the particle sizes of NPs [88]. However, in this section, studying the impact of solubilizing condition on the particle sizes was restricted by the limited solubility of the BMA-sulfobetaine copolymers (5 mg/0.5 ml) and the inability to

change the solvents in the medium since the polymer was soluble only in the mixture of methanol: 2 M NaCL.

Accordingly, the volume of the external phase (10 ml) and the rate of precipitation (20µl/min) were selected depending on the reproducibility and consistency of the results. Also, NPs were fabricated using 2 buffers (PBS pH 6.8 and pH 7.4) as the external phases to mimic the intestinal and physiological pH. The formulated NPs were characterised for their particle sizes and zeta potentials to ensure the formation of Zwitterionic NPs with small particle sizes at the intestinal and physiological pH. Also, particle sizes and zeta potentials were measured at a consequent time intervals of 0.5, 1, 2, 4 and 6 hr at temperatures of 25 and 37 °C to ensure the stability of these particles against aggregation during the time required for particles administered orally to reach the site of action [89,90].

Table 5.5 shows the effect of loading of Lumogen, freeze drying process, type of external media and storage time on particles sizes and zeta potentials of sulfobetaine NPs. All studies on the physicochemical properties were carried out on NPs suspensions with external phase PBS pH 6.8 which is the intestinal mucus pH, while, the effect of the external phase (PBS pH 7.4) was also summarized in the table by the term (no change). Accordingly, the effect of storage time on the particle sizes and zeta potential of sulfobetaine NPs at various time intervals (0.5, 1, 2, 3, 4, 6) hr and at (25 and 37) °C was summarized in Table 5.5 by the term (no aggregation) since these values were measured at consequent time intervals.

Table 5.5 shows that all the sulfobetaine NPs expressed a particle size below 50 nm. The smallest particles size was 28 nm for P2S with 60% BMA and the largest particle size was 48 nm for P5S with 30% BMA. Accordingly, polydispersity of these particles were within the range of (0.42-0.48) which is within the high acceptable limit (<0.5).

This high polydispersity was observed for all the NPs formulated by the nano-precipitation method, for example, Figure 5.20 shows the polydispersity obtained for P2S NP where the particle size was small and the polydispersity was 0.42. Moreover, zeta potentials of these NPs were near neutrality with slightly negative charges ranging from -0.57 to -2.26. As example, Table 5.6 shows the three zeta potential readings of P3S in the Malvern Nano ZS, it can be seen that this NP has slightly negative charge. Moreover, all the zeta potential and particle size values did not change for these NPs when the external phase was changed from PBS pH 6.8 to 7.4.

Also, Table 5.5 shows the effect of Lumogen loading on the particle sizes and zeta potential of these sulfobetaine NPs. It can be seen that Lumogen loading did not have any impact on the particle size and zeta potential of all sulfobetaine particles. Figure 5.20 shows the particle size of P2S loaded with 0.1% Lumogen which was the same size of the P2S without Lumogen. Accordingly, Table 5.5 shows the particle sizes of sulfobetaine NPs after freeze drying process. It can be seen that there were no changes in the particle sizes of sulfobetaine NPs before and after the freeze drying process indicating that sulfobetaine NPs were re-suspendable after freeze drying and retained the original particle size. Lastly, Table 5.5 shows that there was no aggregation of particles after 6 hr at 25 °C and 37 °C. The stability of these particles against aggregation is also presented in Table 5.7 which shows no changes in the particle size of one of the sulfobetaine NPs at consequent time intervals of 0.5, 1, 2, 3, 4 and 6 hr.

Table 5.5: Particle sizes and zeta potentials of sulfobetaine NPs at external phase PBS pH6.8 and after Lumogen loading, freeze drying, at PBS pH 7.4, and after 6 hr aggregation studies at 37 °C and 25 °C.

Code (BMA:Sulfobetaine)	**pH 6.8**		**Lumogen loading**		**Freeze drying**		**Change of particle size and zeta potential when external phase changed to PBS pH 7.4**	**Change of particle size and zeta potential after 6 hr storage at 25 °C and 37 °C**
	Zeta Potential (mV) Mean (± s.d)	Particle Size (nm) Mean (PDI)	Zeta Potential (mV) Mean (± s.d)	Zeta Potential (mV) Mean (± s.d)	Zeta Potential (mV) Mean (± s.d)	Zeta Potential (mV) Mean (± s.d)		
P2S (60:40)	-2.13 (±1.59)	28 (0.42)	-0.73 (±2.33)	28 (0.34)	-4.99 (±4.12)	26 (0.31)	No change	No aggregation
P3S (50:50)	-1.82 (±1.12)	47 (0.48)	-2.12 (±3.19)	45 (0.46)	-2.78 (±2.52)	46 (0.36)	No change	No aggregation
P4S (40:60)	-2.26 (±0.36)	45 (0.43)	-1.31 (±1.20)	43 (0.33)	-3.45 (±2.31)	39 (0.44)	No change	No aggregation
P5S (30:70)	-0.57 (±0.06)	49 (0.47)	-2.44 (±1.59)	48 (0.47)	-1.08 (±2.01)	51 (0.48)	No change	No aggregation

Sample Name:	2B lumogen 37C 6hr average		
SOP Name:	mansettings.nano		
File Name:	2A.dts	**Dispersant Name:**	phosphate buffer
Record Number:	65	**Dispersant RI:**	1.300
Material RI:	1.42	**Viscosity (cP):**	0.8900
Material Absorbtion:	0.010	**Measurement Date and Time:**	11 February 2015 20:04:22
Temperature (°C):	37.0	**Duration Used (s):**	20
Count Rate (kcps):	376.7	**Measurement Position (mm):**	4.65
Cell Description:	Disposable sizing cuvette	**Attenuator:**	11

			Size (d.nm):	**% Volume:**	**St Dev (d.nm):**
Z-Average (d.nm):	25.42	**Peak 1:**	14.35	99.6	7.686
PdI:	0.357	**Peak 2:**	4793	0.4	973.7
Intercept:	0.790	**Peak 3:**	0.000	0.0	0.000
Result quality :	Good				

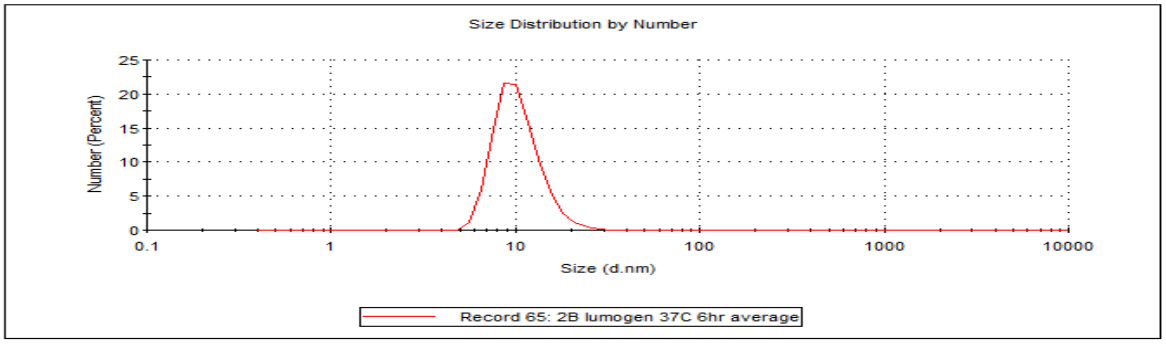

Figure 5.20: Particle size and polydispersity of P2S NPs indicating the high polydispersity of these particles.

Table 5.6: Zeta potential values of P3S NP showing the near neutral negatively charge nature of these NPs.

Sample Name	Measurement Date and Time	T	Z-Ave	PdI	Aggregation Index	ZP	Mob
		°C	d.nm			mV	µmcm/Vs
3B 1 hr 1	12 February 2015 18:48:58	25.0	44.40	0.517	0.00		
3B 1 hr 2	12 February 2015 18:50:00	25.0	50.31	0.443	0.00		
3B 1 hr 3	12 February 2015 18:51:01	25.0	45.15	0.542	0.00		
3B 1 hr 4	12 February 2015 18:52:04	25.0	50.60	0.450	0.00		
3B 1 hr average	12 February 2015 18:55:01	25.0	47.62	0.488	0.00		
3B 1	12 February 2015 18:56:09	25.0	0.000	0.000	0.00	-1.66	-0.1147
3B 2	12 February 2015 18:58:55	25.0	0.000	0.000	0.00	-2.34	-0.1616
3B 3	12 February 2015 19:00:21	25.0	0.000	0.000	0.00	-1.47	-0.1016

Table 5.7: Particle size of a sulfobetaine NP showing the particle sizes at consequent time intervals up to 6 hr and at 25 and 37 °C.

Type	Sample Name	Measurement Date and Time	T	Z-Ave	PdI
			°C	d.nm	
Size	2B (Lumogen) zero time average	11 February 2015 14:19:44	25.0	28.76	0.427
Size	2b (Lumogen) 30 minj average	11 February 2015 14:48:32	25.0	26.22	0.349
Size	2b (Lumogen) 1 hr average	11 February 2015 15:28:34	25.0	26.89	0.340
Size	2b (Lumogen) 2 hr average	11 February 2015 16:03:02	25.0	24.67	0.307
Size	2b (Lumogen) 37C 2 hr average	11 February 2015 16:17:53	37.0	36.20	0.400
Size	2B (Lumogen) 37C 4 hr average	11 February 2015 18:04:21	37.0	39.82	0.210
Size	2B (Lumogen) 4 hr average	11 February 2015 18:12:16	25.0	28.87	0.429
Size	2B lumogen 6hr average	11 February 2015 19:56:23	25.0	28.64	0.410
Size	2B lumogen 37C 6hr average	11 February 2015 20:04:22	37.0	25.42	0.357

It can be observed that these NPs have very small particle sizes. These small particles sizes are consistent with previous studies which showed that zwitterionic sulfobetaine NPs had particle sizes smaller than 50 nm [56,91] . This finding can be interpreted depending on the chemical nature of the synthesized di-block copolymer. That is, the size and type of NPs formed from pre-synthesized di-block copolymers is highly affected by the molecular weight of the lipophilic and the hydrophilic block polymers [92]. If the lipophilic block polymer is smaller than 9000 Da, micelles-like NPs are formed which are characterised by particle sizes as small as micelles [93,94]. This is in agreement with the synthesized BMA-sulfobetaine in this study in which the molecular weight of the BMA lipophilic block polymer is 3500 Da (much less than 9000 Da). Hence, these sulfobetaine NPs should have small particle sizes (less than 50 nm). Accordingly, the high polydispersity of these NPs is mainly due to the mechanism of formation of these particles by the nano-precipitation technique where the solubilised polymer is added drop-wise into the external phase [95]. After dropping into the

external phase, the solubilisation media (methanol and 2 M NaCL) diffuses quickly into the external phase leaving the polymer to undergo fast precipitation. This precipitation is very quick and not homogeneous leads to the formation of nano-sized particles with high polydispersity.

Accordingly, zeta potentials of these particles were shown to be slightly negative near neutral charge. These near neutral zeta potential values indicate the complete betainisation of the DMAEMA polymer where each positively charged amino group was neutralized by a negatively charged sulfonate group that existed on the same polymer chain [96]. The slightly negative charge of these particles is the result of the adsorption of anions from the external media onto the surface of the sulfobetaine polymer [97]. The phenomenon of anions adsorption onto the zwitterionic sulfobetaine NPs is called chameleon effect [98]. Also, this probably could be due to the position of the charged groups where the negatively charged sulfonate is located at the terminal position on the polymer chain making these groups in direct contact with the interface inducing slightly negative charge at the surface of the NPs.

Table 5.5 also showed that the change of the external phase did not affect the physicochemical properties of these particles. This is not surprising since both of the functional groups of sulfobetaine polymer (positively charged quaternary amine and negatively charged sulfonate) do not undergo protonation at any pH value [99]. In other words, the magnitude of the negative value of sulfonate and the positive value of quaternary amine will not change when pH of the media slightly changed from 6.8 to 7.4. As a result, no change on the nature of the surfaces of sulfobetiane NPs can be obtained at PBS pH 7.4 which leads to no change in the zeta potential and particle sizes of these sulfobetaine NPs.

The other factor which was studied in this section was the effect of Lumogen loading on the particle sizes and zeta potential of NPs. Previous studies showed the same lack of influence of lipophilic cargo on the sizes of NPs when it is incorporated into the lipophilic core of these

particles [100,101]. As example, the very lipophilic and highly molecular weight agent (docetaxel) did not increase the particle size of PLGA when it was loaded at a concentration of 20% [102]. Accordingly, the Lumogen red was incorporated into the lipophilic core of the sulfobetaine NPs at much lower concentration (0.1%) which eliminates any chance to increase particle sizes of these NPs.

Moreover, these sulfobetaine NPs were shown to be re-suspendable after the freeze drying process when trehalose was used the cryo-protectant at 5:1 weight ratio. This is in accordance with previous studies which showed the efficiency of trehalose at this weight ratio to re-suspend NPs to its original particle sizes after freeze drying [103,104]. The results from freeze drying make these particles practically suitable for *in vivo* and other pharmacological studies since these particles can be easily re-suspended in the buffer phase.

Lastly, it was shown in Table 5.5 and Table 5.7 that these particles were stable for the time and temperatures that they studied for. This stability was due to the highly charged nature of these particles where both of the quaternary amine and sulfobetaine are totally ionized at all pH values [105]. That is, these groups do not form H-bonding so when particles approached each other, the highly negatively charged sulfonate and the highly positively charged amino group will prevent any aggregation of particles due to the high repulsion forces they exert against approaching particles [106,107] .

3.c Loading Capacity and in Vitro Release of Lumogen Red (Lipophilic Cargo)

As was described in previous chapters, all the tested NPs were loaded with 0.1% Lumogen red and they were successfully tracked by the MPT technique to measure their diffusion coefficient through mucus barrier. This is in accordance with a previously reported work which showed no aggregation or self-quenching of Lumogen red when it is loaded in NPs at a concentration less than 1% [108]. This means that sulfobetaine NPs should be successfully

loaded with 0.1% Lumogen red to be tracked by the MPT technique. Hence, to meet this requirement, loading capacity and the in vitro release of Lumogen red was studied for sulfobetaine NPs loaded with 0.1% Lumogen red.

On the other hand, as novel NPs, the maximum loading capacity of sulfobetaine NPs to lipophilic cargo could reveal the nature of these NPs. Lumogen red is very large lipophilic molecules (Figure 5.21) with a molecular weight of 1079 gm which makes the loading of it to be very challenging [109]. Among the four sulfobetaine NPs, NP with the biggest lipophilic core (60%, P2S) and NP with the smallest lipophilic core (30%, P5S) were selected to be studied for their maximum loading capacity of Lumogen red. To study the maximum loading capacity for P5S and P2S, Lumogen was aimed to be loaded at very high concentration (50%).

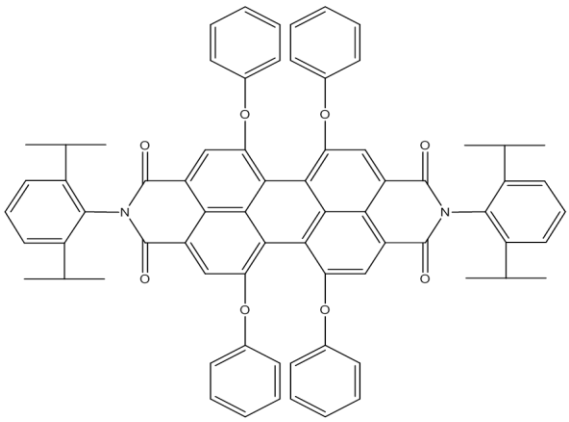

Figure 5.21: Chemical structure of Lumogen red 305.

Table 5.8 shows the EE% and LD% of the sulfobetiane NPs for the Lumogen red. The data in Table 5.8 was divided into 2 sections, second and third columns show the loading data of 0.1% Lumogen red, while, columns four and five show the loading data for 50% Lumogen red. Firstly, for the trial to load 0.1% Lumogen red, it can be seen that all the sulfobetiane NPs showed 100% EE% and 0.1% LD%. In other words, Lumogen red was loaded

completely into the sulfobetaine NPs at the concentration of 0.1% which was not surprising at this low concentration to be incorporated into the BMA core.

Table 5.8: Entrapment efficiency and loading capacity of sulfobetaine NPs to Lumogen red lipophilic dye at concentrations of 0.1% and 50%.

Sulfobetaine NPs	(0.1%) Lumogen		(50 %) Lumogen	
	Entrapment Efficiency %	Loading Capacity %	Entrapment Efficiency % (± s.d.)	Loading Capacity % (± s.d.)
P2S	100	0.1	82.26 (7.40)	40.33 (3.15)
P3S	100	0.1	-	-
P4S	100	0.1	-	-
P5S	100	0.1	4.53 (0.92)	2.26 (0.46)

On the other hand, for loading of 50% Lumogen red, Table 5.8 shows a big variation between the EE% and the LD% of P2S and P5S. While, P2S showed very high EE% (82.26%) and LD% (40.33%), P5S showed much lower EE% and LD% for Lumogen red (4.53 % and 2.26 % respectively). This reveals the very high capacity of sulfobetaine NP to load lipophilic cargo, where the very small (25 nm) P2S NPs showed very high loading capacity to the very large lipophilic molecule. Moreover, reasonably, this loading capacity for sulfobetaine NPs was associated with the ratio of the lipophilic BMA core, i.e, the loading capacity increased from 2.26% to 40.33% when the BMA ratio increased from 30% to 60%. This is in accordance with previous studies which showed positive correlations between the loading capacity for lipophilic cargos and the ratio of the lipophilic core in the NPs [110,111].

Moreover, *in vitro* release was studied for Lumogen red from sulfobetaine NP formulae loaded with 0.1% and 50%. Firstly, for sulfobetaine particles loaded with 0.1%, this study revealed no release of Lumogen red for all sulfobetaine particles (P2S, P3S, P4S and P5S) at all the time intervals, i.e, no release was detected even after 24 hr meaning that Lumogen red

was located in the NPs for 24 hours. These characteristics indicate the photo-stability of sulfobetaine NPs loaded with 0.1% during the release conditions which make the Lumogen red sufficiently stable to be tracked by the MPT technique. In other words, high and fast release of Lumogen red from the particles results in inadequate dye content in the particles and inability to track them. Also, high release of the dye is associated with high noise which affects the accuracy of tracking of these particles.

On the other hand, *in vitro* release of Lumogen red from particles loaded with 50% was carried out to ensure the release of the lipophilic cargo from sulfobetaine NPs. These sulfobetaine NPs loaded with 50% Lumogen red exhibited a release profile dependent on the ratio of the BMA core. Figure 5.22 shows the *in vitro* release profile of Lumogen red from formulae P2S and P5S loaded with 40.33% and 2.26% Lumogen red respectively. It can be seen that both particles exhibited incomplete release profile of Lumogen red after 24 hr, where P5S and P2S showed 80% and 48% release after 24 hr. P5S NP exhibited fast release (33%) within the first 2 hr followed by a gradual release within the time intervals between 2 and 8 hr. Oppositely, P2S showed a gradual release reaching to 30% after 8 hr. Both formulae showed almost a plateau release profile after 8 hr up to 24 hr. That is, P2S showed only 7% release within the time interval between 8 and 24 hr, while P5S showed 13% release for the same time interval. This indicates that for both formulae, 83% of the total release was occurred within the first 8 hr and 16% within the time interval between 8 and 24 hr.

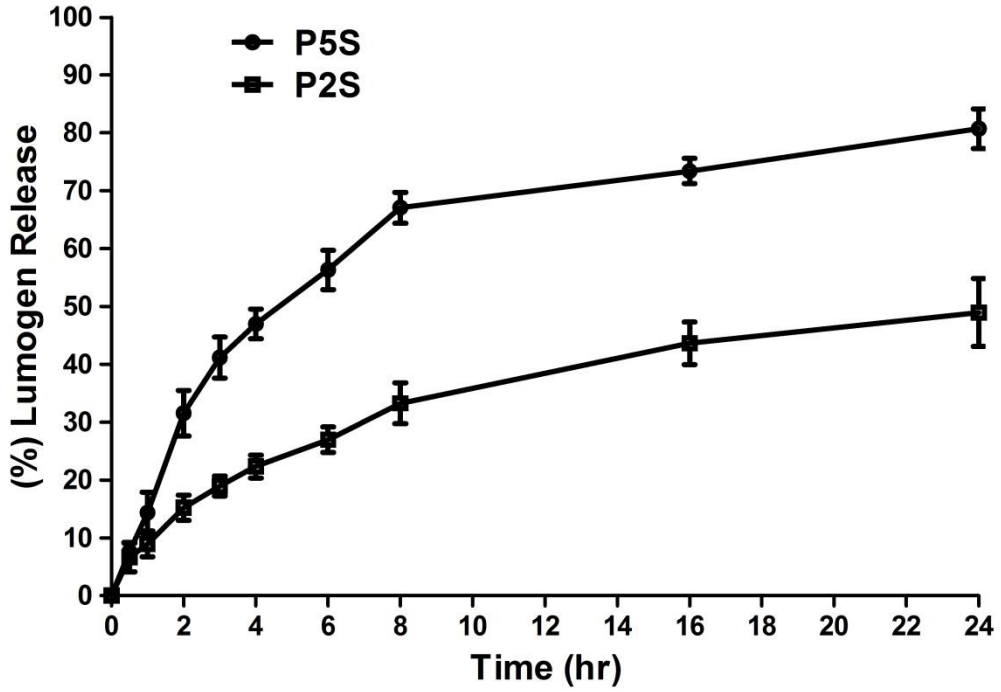

Figure 5.22: In vitro release profile of Lumogen red from sulfobetaine NPs (P2S and P5S).

The release profile of sulfobetaine particles loaded with 0.1% Lumogen red shows that that Lumogen red was preferably retained in the BMA lipophilic core and have not been released into the hydrophilic medium (PBS pH 6.8). This was also observed in the Epifluorescence microscopy (next section), where no released dye was viewed during the measurement of diffusion coefficient of sulfobetaine particles. This is in agreement with previous study on the release of a lipophilic drug (amiodarone) encapsulated at low concentration in a lipophilic core (solid lipid NP), where no release was detected into the phosphate buffer media even after 4 days of the *in vitro* dialysis study [112]. This indicates the suitability of loading of Lumogen at 0.1% concentration since the dye release is not preferred in the study of diffusion of particles through the mucus where the tracking of particles depends on the stability of the dye within the labelled particles.

Accordingly, the release profile of P2S loaded with 40% Lumogen and P5S loaded with 2.26% Lumogen was low for both formulae. Specifically, P2S showed only 48% Lumogen release after 24 hr. This low release is consistent with previous study which showed very low release of a lipophilic dye (Coumarine 6) from NPs with lipophilic core (polystyrene or PLGA NPs) in a buffer medium pH 6.8 (intestinal pH) [113]. The low release of Coumarine 6 was attributed to the high solubility of the lipophilic dye in the lipophilic NP and low solubility in the hydrophilic external medium. Similarly, in this study, the release is affected by the very hydrophilic nature of the external medium (PBS pH 6.8) which limits the release of the very lipophilic molecules like Lumogen. Use of co-solvents during the *in vitro* release should improve the release of the lipophilic molecule, however, this technique can damage the NPs [114].

3.d Study of diffusion of sulfobetaine NPs through the Cardiff Native Mucus" Model

As described in previous chapters, the capsid shell virus represents with an electrically neutral high charge density surface represents a model in nature inspirational for the construction of synthetic particles able to permeate mucus with high efficiency. However, the synthesis of particles replicating such properties is compromised by issues of particle aggregation. Sulfobetaine NPs exhibited relatively small particle sizes (ca 50 nm). While sulfobetaine is well-known for anti-bioadherant properties, the literature (both basic and patent) has to date not revealed evidence of any studies addressing the permeability through mucus of sulfobetaine NPs or NPs formed from the BMA-sulfobetaine copolymer.

Table 5.9 shows for the various sulfobetaine NPs synthesised the: physicochemical properties of the particle (Zeta potential and particle size); MPT diffusion data [$cm^2 S^{-1} \times 10^{-9}$] in the Cardiff mucus model < Deff> and in water D° (calculated by Stocks Einstein equation); the ratio of < Deff> to D° expressed as a %; and in the last column the % of diffusive particles. The <Deff> is a measure of the absolute diffusion of the NPs through

mucus reflecting both surface chemistry and particle size, while the % ratio <Deff>/D° is a measure of the diffusion of the NPs through mucus reflective of surface chemistry characteristics alone, i.e. normalised against differences in particle size. Figure 5.23A shows the ensemble effective diffusion coefficient < Deff> versus the particle size for each of the sulfobetaine particles, while Figure 5.23B shows the zeta potential of each sulfobetaine particle versus the % ratio < Deff> to D°.

Table 5.9 shows that apart from the 60:40 BMA:sulfobetaine (P2S) particle, the increase in the proportion of sulfobetaine has essentially no effect upon particle size. Similarly, as would be predicted by the combined +ve and -ve charge within the same polymeric monomer there are no noticeable differences in zeta potential. As a result the diffusion data for the P3S, P4S, P5S particles is mainly dependent on the ratio of BMA to sulfobetaine. Since the particles are characterized by the distribution of the highly charged sulfobetaine on the surface and the lipophilic BMA in the core, any increase in the ratio of sulfobetiane indicates the increase of the highly charged sulfobetaine at the NP surface. Hence we are able to identify, essentially independently of zeta potential and particle size, the influence of charge density at the particle surface upon particle diffusivity through the mucus.

Particle diffusivities measured by both <Deff> and <Deff>/D° were greater as the ratio of the sulfobetaine increased (Table 5.9 and Figures 5.23A and 5.23B). Statistical analysis showed that % ratio <Deff>/D° was increased significantly with each increase of sulfobetaine ratio by 10%. These findings strongly support the influence of surface chemistry and in this particular case overall density of matched +ve and –ve surface charges on their ‘slippery properties’ through mucus. This is put into some perspective when the data is referenced to the P2S (60:40 ratio BMA:sulfobetaine) formulation which despite the smaller size (28 nm) resulted in an ensemble effective diffusion <Deff> of only approximately 30% of the P5S value (30:70 ratio), and with the <Deff>/D° of the P2S some x6-7 fold lower than the P5S particles.

Hence from this data it would appear, it is the increase of sulfobetaine content rather than particle size which is a dominant factor to drive mucus permeability of the particles (Figure 5.23A).

This is also a reasonable conclusion to reach when the diffusion data is viewed with respect to particle zeta potential. While all the particles were close to neutral they did display an overall net –ve value (from -2.26 to -0.57). However, comparing P4S (40:60 ratio) and zeta potential of -2.26 mv to the P2S formulation, zeta potential -2.13 mv, once again shows the importance of the overall density of matched +ve and –ve surface charges in eliciting improved mucus permeation (Figure 5.24B).

These findings are consistent with the work of Lowe et al on the anti-adherent activity of the BMA-sulfobetaine polymer [55] which involved BMA-DMAEMA polymerised at two different ratios (90:10) and (70:30) with sulfobetaine to form BMA-sulfobetaine polymers coating Poly (methyl methacrylate) discs. Both polymer ratios exhibited high antibacterial and anti-macrophage adhesion and dirt resistance but with the BMA-sulfobetaine with the ratio of 70:30 displaying a significantly higher anti-adherent properties than that of the 90:10 ratio. The impact of sulfobetaine on the anti-adherent properties of polymer films has also been reported by Li et al [39]. Li grafted poly(vinylidene fluoride) hollow membrane surfaces with various ratios of sulfobetaine polymer and found that the increased of grafting sulfobetaine from 153.2 μg/cm^2 to 244 μg/cm^2 was associated with a 90% reduction in protein adsorption from 21.4 μg/cm^2 to 2 μg/cm^2 which was further reduced when sulfobetaine coating was increased to 600 μg/cm^2.

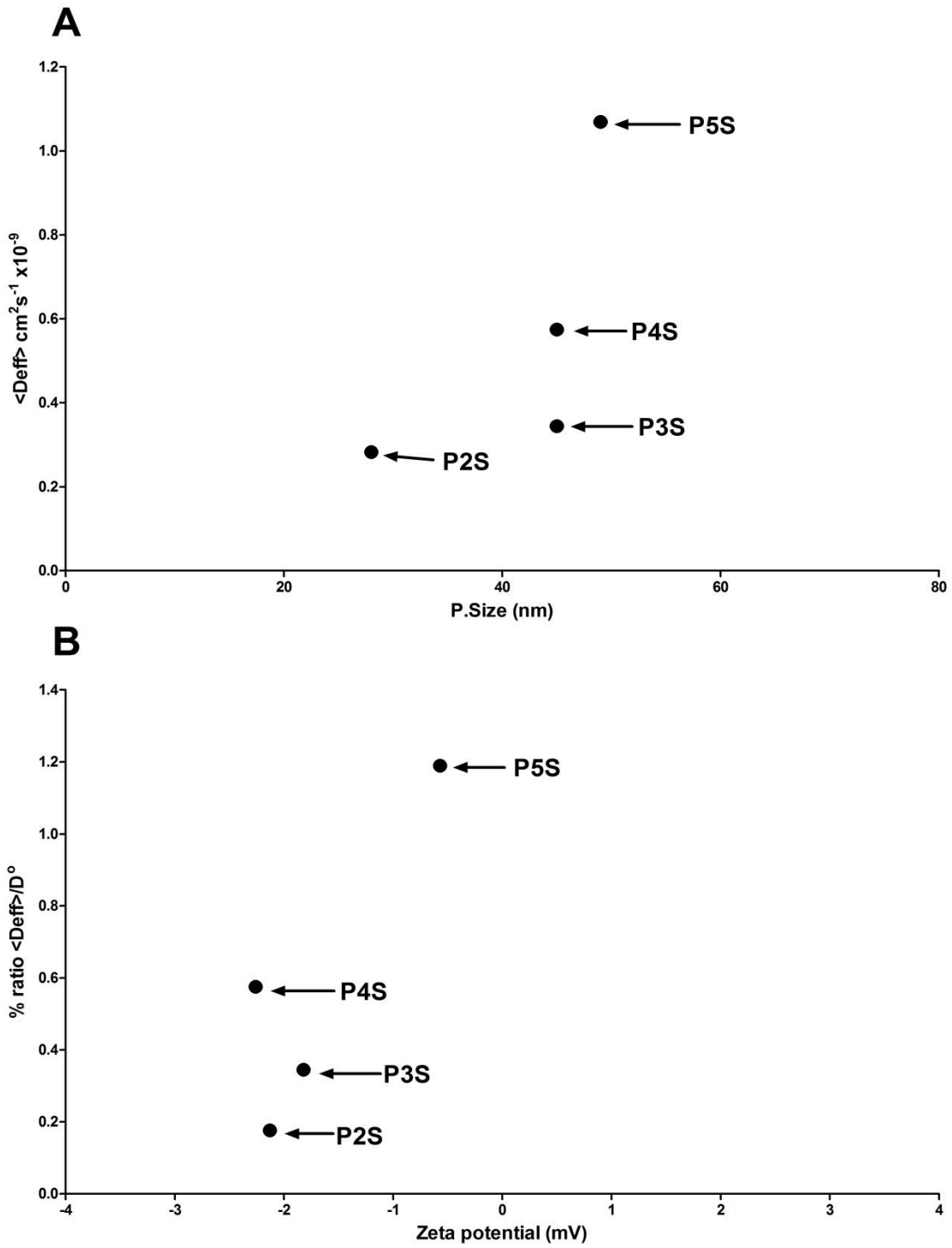

Figure 5.23: (A) Mucus diffusion <Deff> versus particle size of various sulfobetaine NPs in the "Cardiff Native Mucus" model. (B) % ratio <Deff>/D° versus zeta potential of various sulfobetaine NPs in the "Cardiff Native Mucus" model.

Table 5.9: Physicochemical characteristics and diffusion kinetics through the "Cardiff native mucus" barrier of the various sulfobetaine NPs. Statistical analysis carried out by One-way analysis of variance test (n=3).

BMA:Sulfobetaine	Code	Zeta Potential (mV) Mean (± s.d.)	Particle Size (nm) Mean (PDI)	D° (water) $cm^2. S^{-1} x10^{-9}$	<Deff> (mucus) $cm^2. S^{-1} x10^{-9}$ Mean (± s.e.m)	% Ratio <Deff> / D°	% Diffusive particles
60:40	P2S	-2.13 (±1.59)	28 (0.42)	160.50	0.2828 (±0.0768)	0.1762	35
50:50	P3S	-1.82 (±1.12)	45 (0.48)	99.87	0.3447 (±0.0683)	0.3452	44
40:60	P4S	-2.26 (±0.36)	45 (0.43)	99.87	0.5747 (±0.1019)	0.5754	54
30:70	P5S	-0.57 (±0.06)	49 (0.47)	89.88	1.0692 (±0.1861)	1.1895	70

Table 5.9 also shows for each of the formulations, the % diffusive particles within the mucus. This parameter is determined by measuring a particle's diffusion at discrete points over a1 second duration. A particle that shows a Deff at 1 second equal to or greater than 90% of the Deff at the 0.2 second point is defined as 'diffusive'. The principle relies on the probability that as the contact time between a particle and mucus increases, e.g. 0.2 second to 1 second, then the trapping by the mucus will increase. Hence, only diffusive particles possess a Deff at the longer time point of 1 second that is equal to or greater than 90% of the <Deff> at shorter period 0.2 second. Figure 5.24 illustrates this behaviour for 20 randomly selected particles from a total of 360 particles of formula P3S; these particles were tracked by the MPT technique. It can be seen that 11 (45%) of the randomly selected 20 particles showed an increase of the diffusion at the longer time point as compared to the shorter time point. For each NP species, the percent of diffusive particles was measured for 360 particles. On this basis, for P3S formula, 45% of particles were identified as the proportion of the diffusive particles.

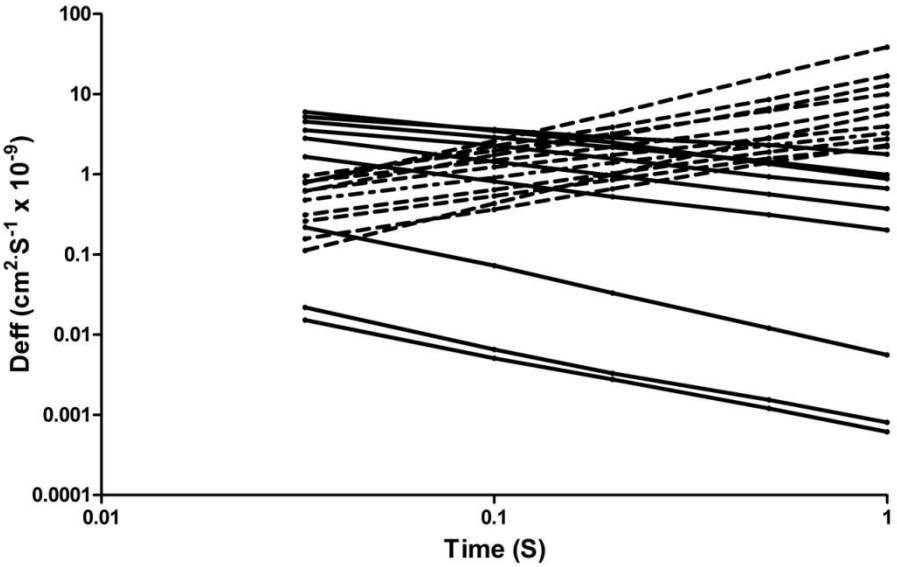

Figure 5.24: Deff for each of 20 randomly individual particles Selected from P3S. The online source random.org was used to randomly select the particles.

Table 5.9 shows a gradual increase in the % of diffusive particles as the sulfobetaine content increases. That is, the percent of diffusive particles increase by 1.2 times with each 10% increase in the ratio of sulfobetaine. For example, percent of diffusive particles was increased from 44% to 54% and from 54% to 70% when sulfobetaine ratio was increased from 50% 60 60% and from 60% to 70% respectively. In general, all the sulfobetaine particles showed a high % diffusive particles as compared with the respective data obtained from all other particles analysed by consortium partners (Chapter Four), this includes PEG-PLGA hydrophilic particles which is known to readily permeate mucus and which displayed a % diffusive particles of 32% (Chapter Four) lower than any of the sulfobetaine particles reported here.

The mathematical correlation of the increase in the particle diffusivity with the increase in sulfobetaine content is consistent with the hypothesis of this study which is the direct correlation between the diffusion behaviour of NPs and the ratio of sulfobetaine at the NPs shell. Figure 5.25 summarizes the effect of the increase of the sulfobetaine ratio on particle behaviour in the mucus. Specifically, the gradual increase of sulfobetaine ratio to the BMA is associated with an increased covering of the lipophilic BMA core by the densely charged sulfobetaine. The P2S particle has a ratio of 60:40 (BMA:Sulfobetaine) which makes the lipophilic core (BMA) relatively large compared to the content of the sulfobetaine (40%) which is insufficient to prevent some contact of BMA with the mucus lipophilic components and hence the introduction of hydrophobic-hydrophobic interactions. With the gradual increase of sulfobetaine to 50% (P3S), the exposed area of BMA is reduced such that a BMA interaction with the mucus components is reduced. It is also notable that with the relatively greater sulfobetaine content, the charge density at the surface of particles increases. As a result of the above, the <Deff>, %<Deff>/D°

and the % diffusive particles increase in gradual manner with the increase of sulfobetaine ratio.

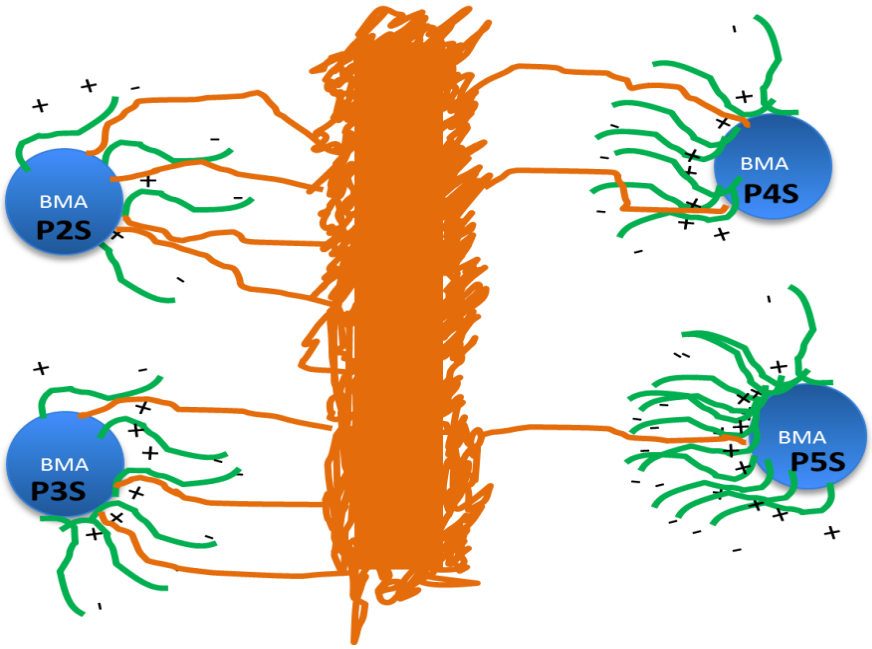

Figure 5.25: Effect of charge density on the surface of sulfobetaine NPs and the exposed area of the BMA core on the particles' interaction with mucus.

Figure 5.26 shows the heterogeneity of particle diffusion through mucus. Specifically, for each sulfobetaine NP species, it shows the ranking of 360 particles (all the same formulation) based on their diffusion in mucus (Deff), with the fastest particles in the 90 percentile, the definition of which is the Deff value below which 90% of the Deff values within the particle population occur. The correlation of the increase in the diffusivities of particles with the increase of sulfobetaine ratios is again consistent within this particular set of data. The Deff values associated with 50 percentile for each sulfobetaine NP formulation displayed a relatively high diffusion through the mucus (> $2x10^{-9}$ cm^2s^{-1}) as compared to the data obtained for NPs in Chapter Four and encouragingly the formulations showed a low degree of heterogeneity (ratio of Deff for 90% vs Deff for 10%).

In particular it is noteworthy that the heterogeneity decreases as the sulfobetaine ratio increases, i.e. particles with a more complete shell of sulfobetaine covering the lipophilic BMA core. In other words, the highest ratio of sulfobetaine is the more compact distribution of sulfobetaine at the surface of particles which makes the surface distribution of sulfobetaine uniform and facilitates good particle diffusion. This may be realised by considering the difference between the fastest 90 percentile and slowest 10 percentile is only 28-fold for the P5S (Figure 5.26D). Accordingly, difference in diffusion between the fastest 90% and slowest 10% for P4S (Figure 5.26C) and P3S (Figure 5.26B) were 1090 and 1731 times respectively. For P2S (Figure 5.26A) where the lipophilic BMA ratio (60%) is higher than the hydrophilic sulfobetaine ratio (40%), the difference between the fastest 90% and slowest 10% was much higher (4755 times) than other sulfobetaine NPs.

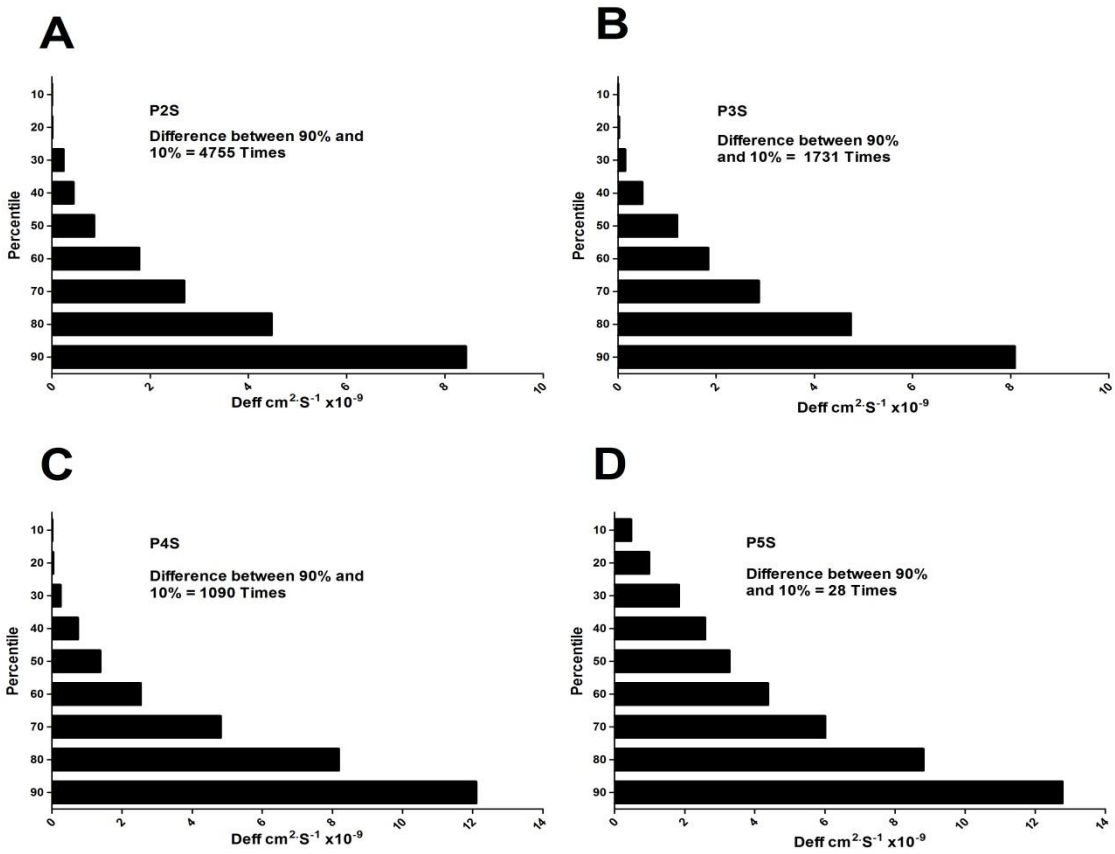

Figure 5.26: Heterogeneity of particle movement through mucus. For each particle type, an effective diffusion coefficient (Deff) was calculated for each of 360 individual particles over a time interval of 1 sec. The data was ranked into percentiles from the 90th through to 10th percentile, where the 90th percentile is the Deff value below which 90% of the Deff observations may be found. (A) P2S, (B) P3S, (C) P4S and (D) P5S.

3.e Comparison of Sulfobetiane NPs Diffusion through the "Cardiff Native Mucus" Model with other Nano-Strategies.

The main aim of synthesizing this novel zwitterionic sulfobetaine NPs is to produce viral like NPs with densely charged surface but with net neutral charge and with proper physicochemical properties for clinical uses. However, all the above-mentioned properties is a pathway to reach to the main aim of this work which is producing highly mucus permeable NPs. Previous section showed the comparison of diffusivities of the various synthesized sulfobetaine NPs through the mucus. It was shown that sulfobetaine ratio is the critical factor for the diffusion of particles through the "Cardiff native

mucus" model barrier. In this section, sulfobetaine NPs are compared with all other NPs representing various strategies to overcome the mucus barrier (chapter three).

Figure 5.27A shows the <Deff> versus particle size of the various sulfobetaine NPs marked in red as compared with all other NPs which have shown high diffusivities in Chapters three (SMEDD systems and PEG-PLGA NPs). Figure 5.27B illustrates the %<Deff>/D° versus the zeta potential of the same groups of particles in figure 5.27A. For better clarification of the data of <Deff> versus particle size and %<Deff>/D° versus zeta potential, figure 5.28 A and B show these values presented in histogram where more attention was given to the particles having high diffusion through the mucus barrier (sulfobetaine NPs, SMEDD systems and PEG-PLGA NPs).

Figure 5.27A and 5.28A show that all the sulfobetaine NPs exhibited high <Deff>(s) as compared to other particles. In specific, P5S and P4S showed superior diffusions coefficients through the mucus barrier as compared with other particles specifically the known highly mucus permeable PEG-PLGA NP. Only SMEDD system A in which a combination of SMEDD system and mucolytic agent was used, showed higher <Deff> than P4S but not P5S. Accordingly, P2S and P3S were within the fastest 6 particles among the 113 particles that were tested for their diffusion through the "Cardiff native mucus" model.

Regarding the comparison based on %<Deff>/D°, figure 5.27B and 5.28B demonstrates that P5S showed the highest %<Deff>/D° among all the tested particles made the particle with compacted sulfobetaine surface as the particle with best surface chemistry. This sulfobetaine particle showed double the %<Deff>/D° value of PEG-PLGA NP. P4S also showed higher diffusivity than that of PEG-PLGA and mucus permeability comparable to that of SMEDD systems. P3S ranked within the fastest 10 particles for its

%<Deff>/D°. Even the slowest sulfobetaine NP (P2S) showed a comparatively high %<Deff>/D° as compared with other strategies.

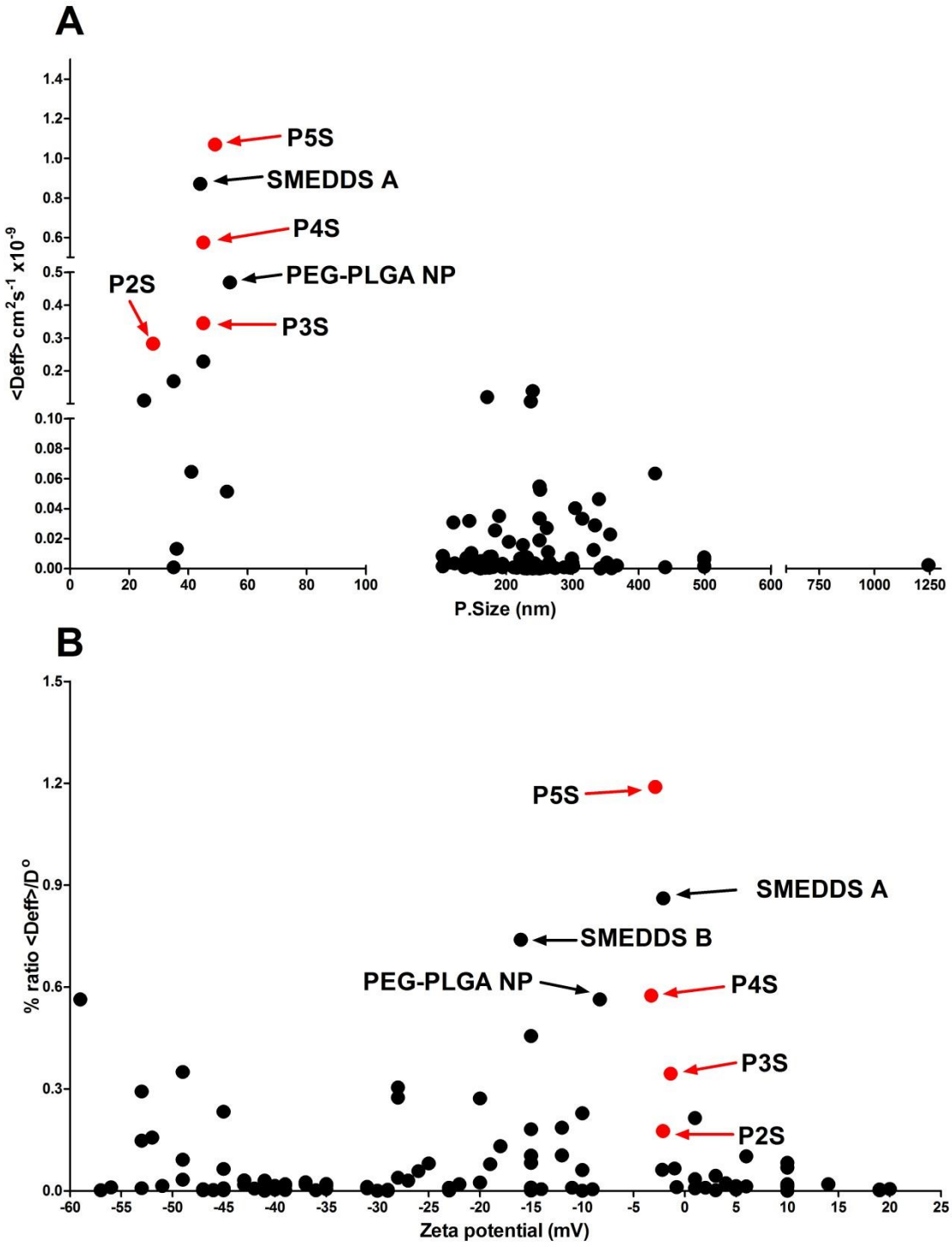

Figure 5.27: Comparison of diffusivities of sulfobetaine NPs (defined by PXS abbreviation) as compared to 113 other NPs comprising various surface chemistries and permeation strategies. (A) Mucus diffusion <Deff> versus particle size. (B) % ratio <Deff>/D° versus zeta potential.

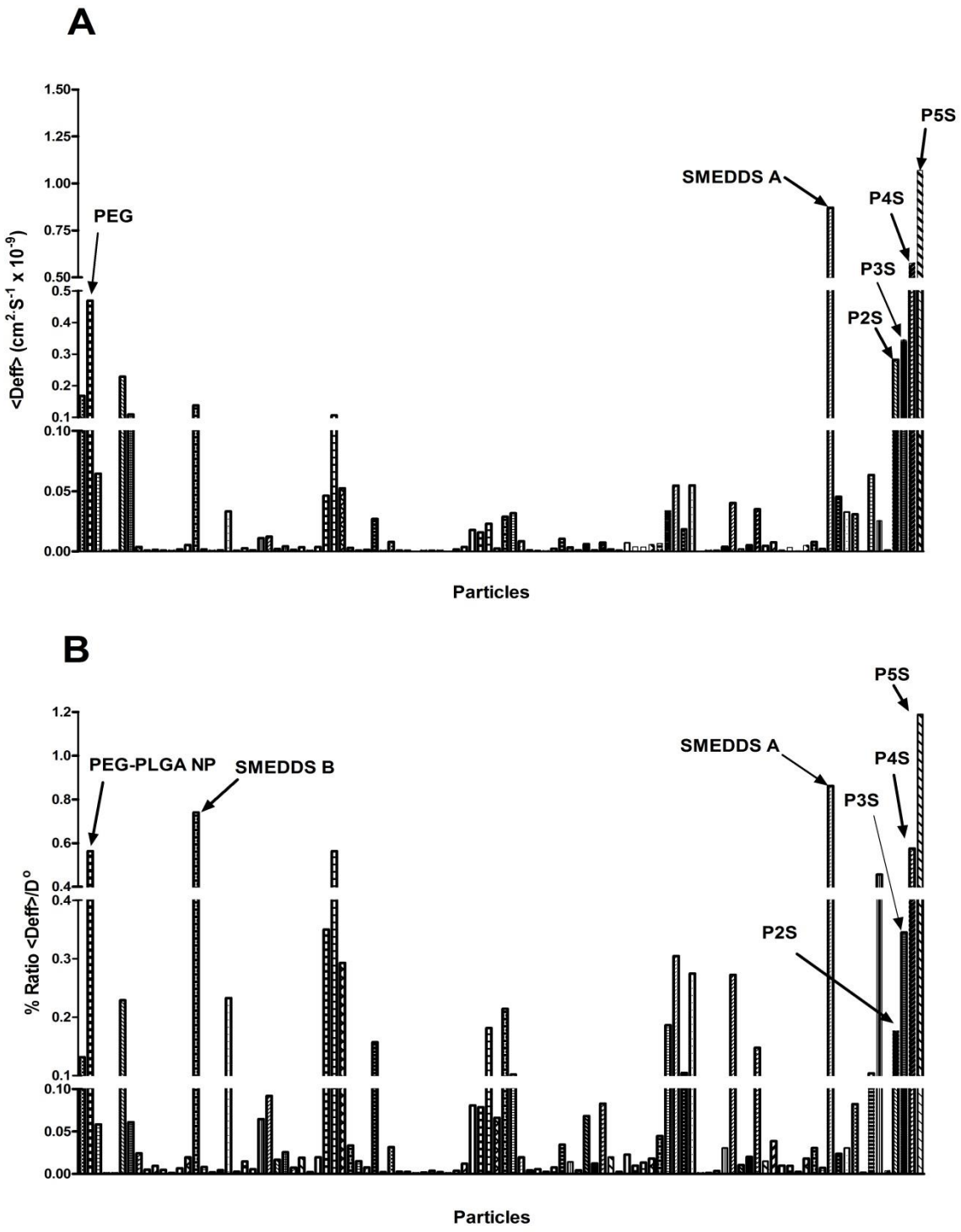

Figure 5.28: Histogram **c**omparison of diffusivities of sulfobetaine NPs (defined by PXS abbreviation) as compared to 113 other NPs comprising various surface chemistries and permeation strategies. (A) <Deff> of various sulfobetaine NPs. (B) % ratio <Deff>/D° of various sulfobetaine NPs.

The superior mucus permeability results for sulfobetaine particles are not surprising and in accordance with the hypothesis and with the previous studies which have shown a very strong anti-adherent properties to proteins (introduction part of this chapter). Since mucin is simply a protein, then sulfobetaine at the shell of particles should not adhere to the mucin fibres and let particles to slip through the mucus network. The anti-adherent properties of sulfobetaine to the proteins (mucin) can be explained depending on two distinctive physicochemical properties of sulfobetaine.

Firstly, sulfobetaine moiety at the terminal position has a unique chemical characteristic. This is related to the quaternary amino and sulfonate groups which are characterized by the disability of protonation at any pH [105]. Unlike carboxybetiane in which carboxylate group can be protonated at certain pH, sulfobetaine will never lose its negative or positive charges [115]. This makes sulfobetaine moiety to be fully charged with the oppositely charges on nthe surface at any pH in mucus. Hence, mucus components have no chance to form H bonds to sulfobetaine particles. H bonding is one of the main mucus pathway to trap hydrophilic particles that come in contact with mucus [116]. Also, the retaining of the positive and negative charges by the sulfonate and quaternary amine groups at any pH value will prevent the electrostatic interaction of the negatively charged mucin to the particles due to the repulsion by the negatively charged sulfonate group. The third pathway through which mucus can trap particles is the lipophilic interaction to the lipophilic core which is also diminished by the covering of the BMA lipophilic core with the sulfobetaine shell.

Secondly, the anti-protein characteristic of some polymers is widely attributed to the hydration capability of these polymers [117]. As example, the tendency of PEGylated polymer to be hydrated is the reason for the non-specific protein-repulsion properties of PEG polymer and is known as water barrier theory [118]. According to this theory, the

water layer surrounding ethylene glycol molecules is thermodynamically stable and serves as a barrier that sterically prevents any interaction of protein molecules to the hydrated PEG polymer [119]. On the same basis, the efficient resistance to the protein adsorption to the eye lenses by the phosphorylcholine coating layer was explained on the high capacity of phosphorylcholine to hold water molecules which makes it very efficient protein-barrier [38].

Wu and Chen studied the water holding capacity of sulfobetaine and PEG polymer using low-field NMR [120]. This study showed that while each ethylene glycol molecule holds one water molecule, on the other hand, each sulfobetaine moiety holds up to 8 water molecules indicating 8 times higher efficiency to form steric water layer to resist protein adsorption as compared to PEG. For this reason, a monolayer formed by self-assembly of zwitterionic molecules (phosphorylcholine) exerted an efficient protein resistance layer on gold surface [121] as compared with protein resistance properties of PEG layer which showed a limited protein resistance layer when ethylene glycol molecules were self-assembled on gold surface [122]. For self-assembled PEGylated layer, only the 6 units ethylene glycol has shown sufficient protein resistance properties in comparison with 2 and 4 units ethylene glycol. This is in agreement with the water holding capacity of the zwitterionic polymer and PEG polymer.

From the abovementioned, the higher water holding capacity of sulfobetaine and diminished probability of sulfobetiane to form H bonds with the mucin are reasonable reasons for the high mucus permeability of these sulfobetaine NPs as compared with the known muco-diffusive PEG NPs. The only site within these novel NPs that can bind the mucus is the lipophilic BMA core. Ensuring a non-exposed BMA surface will ensure a lack of mucus interaction and slippery behaviour of these particles when they come in contact with mucus. For this reason, sulfobetaine NPs could be very promising NPs to

be investigated for *in vivo* studies and for the oral delivery of protein and peptides to permeate through the intestinal mucus barrier.

4 SUMMARY AND CONCLUSION

In this study, RAFT technique was used to synthesize novel zwitterionic sulfobetaine co-polymers in which BMA is served as the lipophilic block polymer and sulfobetaine served as the hydrophilic block polymer. Various serial ratios of the zwitterionic BMA-Sulfobetaine co-polymers were synthesized with controlled molecular weight. Then zwitterionic sulfobetaine NPs were formulated in which the BMA block polymer became the lipophilic core and the hydrophilic sulfobetaine the shell of these particles. The stability of these particles was studied to ensure the stability of these particles to exert their biological action. Also, re-suspendability after freeze drying of these particles was studied to assess the stability of these particles for the long storage term. The capacity of these particles to encapsulate big hydrophobic molecules exemplified by Lumogen red was examined in this chapter. Lastly, the diffusivity of these novel particles through the intestinal mucus barrier was studied.

It was shown that by using proper techniques, it was possible to produce NPs possessing densely charged surface with an overall net neutral charge and excellent stability at physiological pH (biological fluid). Moreover, in contrast to the currently available neutrally charged surface NPs, these novel sulfobetaine NPs exhibited relatively small particle size (ca 50 nm) that were stable to be used to for mucus delivery. Also, these particles were re-suspended successfully after freeze drying with reproducing of their original particle sizes and zeta potential. The encapsulation efficiency for Lumogen red was dependent on the ratio of each block polymer with relatively high encapsulation efficiency for particles with highest BMA ratio (P2S). Moreover, the techniques involved in the synthesis of these particles are relatively simple and at lower costs than other techniques involved in the synthesis of other “BIO-Inert” NPs such as PEGylated NPs. Lastly, these sulfobetaine NPs were found to be highly diffusive through the

intestinal mucus barrier as compared with other particles synthesized by the partners in the consortium.

Conclusions obtained from this study can be summarized as follows:

- Trithiocarbonate was found to be a suitable CTA agent for the control polymerization of BMA and copolymerization of BMA-DMAEMA.
- Particles with neutral surface charge, still can be very stable and having small particle size (<50 nm) if the oppositely charged groups are arranged on the same monomer (polybetaine polymer). This is unlikely to be obtained when neutrally charged NPs are prepared from polyampholyte polymer in which the opposite groups are on different monomers.
- Moreover, the loading capacity and *in vitro* release of the lipophilic molecule was detected to be directly correlated to the size of the lipophilic core in shell-core NPs.
- The betaine shell on NP core can form muco-inert surface that can highly minimize the interaction of NPs with the mucus components leading to highly diffusive NPs.

5. References

[1] K. Pal, A.K. Banthia, D.K. Majumdar, Polymeric Hydrogels: Characterization and Biomedical Applications, Des. Monomers Polym. 12 (2009) 197–220. doi:10.1163/156855509X436030.

[2] P. Kratochvil, U.W. Suter, Definitions of terms relating to individual macromolecules, their assemblies, and dilute polymer solutions (Recommendations 1988), Pure Appl. Chem. 61 (1989) 211–241. doi:10.1351 /pac198961020211.

[3] George Odian, Radical Chain polymerization, in: Princ. Polym., John Wiley & Sons, Inc., Hoboken, New Jersey., 2009: pp. 199–350. doi:10.1016/B978-1-85617-803-7.50022-5.

[4] M. Uchida, N. Tada, Micro-, meso- to macroscopic modeling of deformation behavior of semi-crystalline polymer, Int. J. Plast. 49 (2013) 164–184. doi:10. 1016/j.ijplas. 2013.03.007.

[5] C. Priya, K. Ankita, polymer: a boon to controlled drug delivery system, Int. Res. J. Pharm. 4 (2013) 28–34. doi:10.7897/2230-8407.04405.

[6] R.H. Marchessault, Principles of polymer morphology, J. Polym. Sci. Polym. Lett. Ed. 20 (1982) 279–280. doi:10.1002/pol.1982.130200506.

[7] P.J. Flory, Fundamental principles of condensation polymerization., Chem. Rev. 39 (1946) 137–197. doi:10.1021/cr60122a003.

[8] K. Fukukawa, M. Ueda, Sequence Control in One-Step Polycondensation, Polym. Sci. A Compr. Ref. 10 Vol. Set. 5 (2012) 71–93. doi:10.1016/B978-0-444-53349-4.00134-5.

[9] T. Ohishi, T. Suzuki, T. Niiyama, K. Mikami, A. Yokoyama, K. Katagiri, et al., Synthesis of linear and cyclic aromatic peptides with fixed conformation owing to intramolecular hydrogen bonding by condensation polymerization method, Tetrahedron Lett. 52 (2011) 7067–7070. doi:10.1016/j.tetlet.2011.10.071.

[10] U. Appala Naidu, S. Dinda, Development of ketonic resin by polymerization reaction: A critical review, Polymer (Guildf). 61 (2015) 204–212. doi:10.1016 /j. polymer.2015.02.013.

[11] A.D. Jenkins, A. Ledwith, Reactivity, mechanism and structure in polymer chemistry., John Wiley & Sons., london, 1974.

[12] P.J. Flory, The Mechanism of Vinyl Polymerizations 1, J. Am. Chem. Soc. 59 (1937) 241–253. doi:10.1021/ja01281a007.

[13] S. Russo, Initiation, propagation and termination in free radical copolymerization, Makromol. Chemie. Macromol. Symp. 10-11 (1987) 395–414. doi:10.1002/masy.19870100120.

[14] J.C. Bevington, Initiation of polymerization: Azo compounds and peroxides, Makromol. Chemie. Macromol. Symp. 10-11 (1987) 89–107. doi:10.1002 /masy .19870100106.

[15] W. a. Braunecker, K. Matyjaszewski, Controlled/living radical polymerization: Features, developments, and perspectives, Prog. Polym. Sci. 32 (2007) 93–146. doi:10.1016/j.progpolymsci.2006.11.002.

[16] J.P.A. Heuts, Theory of Radical Reactions, in: K. Matyjaszewski, T.P. Davis (Eds.), Handb. Radic. Polym., John Wiley & Sons, Inc., Hoboken, 2002: pp. 1–76. doi:10.1002/0471220450.ch1.

[17] D. Braun, Origins and development of initiation of free radical polymerization processes, Int. J. Polym. Sci. 2009 (2009). doi:10.1155/2009/893234.

[18] M. Szwarc, "Living" Polymers, Nature. 178 (1956) 1168–1169. doi:10.1038 /1781168a0.

[19] Y.Y. J. Cao, J. He, C. Li, Nitroxide Mediated Radical Polymerization of Styrene in Emulsion, Polymer (Guildf). (2001) 75–80.

[20] J. Xia, S.G. Gaynor, K. Matyjaszewski, Controlled/"Living" Radical Polymerization. Atom Transfer Radical Polymerization of Acrylates at Ambient Temperature, Macromolecules. 31 (1998) 5958–5959.

[21] A. Goto, T. Fukuda, Kinetics of living radical polymerization, Prog. Polym. Sci. 29 (2004) 329–385. doi:10.1016/j.progpolymsci.2004.01.002.

[22] G. Moad, The Emergence of RAFT Polymerization, Aust. J. Chem. 59 (2006) 661–662. doi:10.1071/CH05072.

[23] S.G. Gaynor, J. Wang, K. Matyjaszewski, Controlled Radical Polymerization by Degenerative Transfer: Effect of the Structure of the Transfer Agent, Macromolecules. 28 (1995) 8051–8056. doi:10.1021/ma00110a050.

[24] S.H.T. Tam Phuong Le, Graeme Moad, Ezio Rizzardo, Polymerization with living characteristics, US7714075 B1, 2010.

[25] J. Chiefari, Y.K.B. Chong, F. Ercole, J. Krstina, J. Jeffery, T.P.T. Le, et al., Living Free-Radical Polymerization by Reversible Addition - Fragmentation Chain Transfer : The RAFT Process, Macromolecules. 31 (1998) 5559–5562. doi:S0024-9297(98)00495-1.

[26] J. Chiefari, R.T. a Mayadunne, C.L. Moad, G. Moad, E. Rizzardo, A. Postma, et al., Thiocarbonylthio compounds (S=C(Z)S-R) in free radical polymerization with reversible addition-fragmentation chain transfer (RAFT polymerization).

Effect of the activating Group Z, Macromolecules. 36 (2003) 2273–2283. doi:10. 1021/ma020883+.

[27] G. Moad, E. Rizzardo, S.H. Thang, Living radical polymerization by the RAFT process, Aust. J. Chem. 58 (2005) 379–410. doi:10.1071/CH05072.

[28] G. Moad, E. Rizzardo, S.H. Thang, Living Radical Polymerization by the RAFT Process—A First Update, Aust. J. Chem. 59 (2006) 669. doi:10.1071/CH06250.

[29] G. Moad, E. Rizzardo, S.H. Thang, Living radical polymerization by the RAFT process A second update, Aust. J. Chem. 62 (2009) 1402–1472. doi:10 .1071 /CH09311.

[30] A.B. Lowe, C.L. McCormick, Stimuli responsive water soluble and amphiphilic (co)polymers, ACS Symp. Ser. 780 (2001) 1–13. doi:10.1021/bk-2001-0780. ch001.

[31] W.H. Kuo, M.J. Wang, H.W. Chien, T.C. Wei, C. Lee, W.B. Tsai, Surface modification with poly(sulfobetaine methacrylate-co-acrylic acid) to reduce fibrinogen adsorption, platelet adhesion, and plasma coagulation, Biomacromolecules. 12 (2011) 4348–4356. doi:10.1021/bm2013185.

[32] N. Tarannum, M. Singh, Advances in Synthesis and Applications of Sulfo and Carbo Analogues of Polybetaines: A Review, Rev. Adv. Sci. Eng. 2 (2013) 90–111. doi:10.1166/rase.2013.1036.

[33] V.M. Monroy Soto, J.C. Galin, Poly(sulphopropylbetaines): 1. Synthesis and characterization, Polymer (Guildf). 25 (1984) 121–128. doi:10.1016/0032-3861 (84)90276-3.

[34] A.B. Lowe, N.C. Billingham, S.P. Armes, Synthesis of polybetaines with narrow molecular mass distribution and controlled architecture, Chem. Commun. (1996) 1555. doi:10.1039/cc9960001555.

[35] D.N. Schulz, D.G. Peiffer, P.K. Agarwal, J. Larabee, J.J. Kaladas, L. Soni, et al., Phase behaviour and solution properties of sulphobetaine polymers, Polymer (Guildf). 27 (1986) 1734–1742. doi:10.1016/0032-3861(86)90269-7.

[36] M.A.R. Malcolm B. Huglin, Properties of poly[N-2-(methyacryloyloxy)ethyl-N,N-dimethyl-N-3-sulfopropylammonium betaine] in dilute solution, Makro-mol.Chem. Phys. 192 (1991) 2433–2445. doi:10.1002 /macp.1991.021921021.

[37] X. Peng, L. Zhao, G. Du, X. Wei, J. Guo, X. Wang, et al., Charge tunable zwitterionic polyampholyte layers formed in cyclic olefin copolymer micro-channels through photochemical graft polymerization, ACS Appl. Mater. Interfaces. 5 (2013) 1017–1023. doi:10.1021/am3027019.

[38] L. Xu, P. Ma, B. Yuan, Q. Chen, S. Lin, X. Chen, et al., Anti-biofouling contact lenses bearing surface-immobilized layers of zwitterionic polymer by one-step modification, RSC Adv. 4 (2014) 15030–15035. doi:10.1039/c3ra47119e.

[39] Q. Li, H.-H. Lin, X.-L. Wang, Preparation of Sulfobetaine-Grafted PVDF Hollow Fiber Membranes with a Stably Anti-Protein-Fouling Performance, Membranes (Basel). 4 (2014) 181–199. doi:10.3390/membranes4020181.

[40] Y. Chang, W. Chang, Y. Shih, T. Wei, G. Hsiue, Zwitterionic Sulfobetaine-Grafted Poly (vinylidene fluoride) Membrane with Highly Effective Blood Compatibility via Atmospheric Plasma-Induced Surface Copolymerization, ACS Appl. Mater. Interfaces. 3 (2011) 1228–1237. doi:10.1021/la0015258.

[41] E.G. Detlef Ballschuh, Roland Ohme, Horst Seibt, Sulfobetaine-substituted α-sulfonylcarboxylic acids from diallylammonium salts and a process for the preparation thereof, EP 0434175 A1, 1992.

[42] S.F.G. David J. Heiler, Treatment of contact lenses with an aqueous solution including sulfobetaine compounds, CA 2245174 C, 2002.

[43] D.C. Turner, J.C. Heaton, D.G. Vanderlaan, R.B. Steffen, J.M. Wood, L.L. Copper, et al., Method of coating of contact lenses, EP2059384B1, 2013.

[44] D.S. Yanshi Zhang, Gary William Yeager, Hongyi Zhou, Polyarylether compositions bearing zwitterion functionalities, US20100044314 A1, 2010.

[45] M.W.M. Kenneth W. Lemke, Quaternary aminehydroxypropane sulfobetaines, US4526968 A, 1985.

[46] A.D. Shmuel A. Ben-Sasson, Sulfobetaines for therapy, A2, WO 2009136396, 2009.

[47] K.M. Xiu, N.N. Zhao, W.T. Yang, F.J. Xu, Versatile functionalization of gene vectors via different types of zwitterionic betaine species for serum-tolerant transfection, Acta Biomater. 9 (2013) 7439–7448. doi:10.1016 /j.actbio.2013.04 .010.

[48] F. Dai, P. Wang, Y. Wang, L. Tang, J. Yang, W. Liu, et al., Double thermoresponsive polybetaine-based ABA triblock copolymers with capability to condense DNA, Polymer (Guildf). 49 (2008) 5322–5328. doi:10.1016/j. polymer. 2008.09.060.

[49] J.T. Sun, Z.Q. Yu, C.Y. Hong, C.Y. Pan, Biocompatible zwitterionic sulfobetaine copolymer-coated mesoporous silica nanoparticles for temperature-responsive drug release, Macromol. Rapid Commun. 33 (2012) 811–818. doi:10.1002 /marc. 201100876.

[50] R. Ghosh Chaudhuri, S. Paria, Core/shell nanoparticles: Classes, properties, synthesis mechanisms, characterization, and applications, Chem. Rev. 112 (2012) 2373–2433. doi:10.1021/cr100449n.

[51] M.A. Nash, J.J. Lai, A.S. Hoffman, P. Yager, P.S. Stayton, “Smart” diblock copolymers as templates for magnetic-core gold-shell nanoparticle synthesis, Nano Lett. 10 (2010) 85–91. doi:10.1021/nl902865v.

[52] D.J. Keddie, A guide to the synthesis of block copolymers using reversible-addition fragmentation chain transfer (RAFT) polymerization., Chem. Soc. Rev. 43 (2013) 496–505. doi:10.1039/c3cs60290g.

[53] B. Ebeling, P. Vana, RAFT-polymers with single and multiple trithiocarbonate groups as uniform gold-nanoparticle coatings, Macromolecules. 46 (2013) 4862–4871. doi:10.1021/ma4008626.

[54] J. Pretula, K. Kaluzynski, B. Wisniewski, R. Szymanski, T. Loontjens, S. Penczek, Formation of poly(ethylene phosphates) in polycondensation of H3PO4 with ethylene glycol. Kinetic and mechanistic study, J. Polym. Sci. Part a-Polymer Chem. 46 (2008) 830–843. doi:10.1002/pola.

[55] A.B. Lowe, M. Vamvakaki, M. a. Wassall, L. Wong, N.C. Billingham, S.P. Armes, et al., Well-defined sulfobetaine-based statistical copolymers as potential antibioadherent coatings, J. Biomed. Mater. Res. 52 (2000) 88–94. doi:10.1002/1097-4636(200010)52.

[56] Z. Tuzar, H. Pospisil, J. Plestil, a. B. Lowe, F.L. Baines, N.C. Billingham, et al., Micelles of hydrophilic-hydrophobic poly(sulfobetaine)-based block copolymers, Macromolecules. 30 (1997) 2509–2512. doi:10.1021/ma9615617.

[57] K.S. Yadav, K.K. Sawant, Modified nanoprecipitation method for preparation of cytarabine-loaded PLGA nanoparticles., AAPS PharmSciTech. 11 (2010) 1456–1465. doi:10.1208/s12249-010-9519-4.

[58] M. Sameti, G. Bohr, M.N. V Ravi Kumar, C. Kneuer, U. Bakowsky, M. Nacken, et al., Stabilisation by freeze-drying of cationically modified silica nanoparticles for gene delivery, Int. J. Pharm. 266 (2003) 51–60. doi:10.1016/S0378-5173(03)00380-6.

[59] F. Danhier, N. Lecouturier, B. Vroman, C. Jérôme, J. Marchand-Brynaert, O. Feron, et al., Paclitaxel-loaded PEGylated PLGA-based nanoparticles: In vitro and in vivo evaluation, J. Control. Release. 133 (2009) 11–17. doi:10.1016 /j. jconrel.2008.09.086.

[60] W. Chen, S. Hu, Suitable carriers for encapsulation and distribution of endostar: comparison of endostar-loaded particulate carriers., Int. J. Nanomedicine. 6 (2011) 1535–1541. doi:10.2147/IJN.S21881.

[61] V. Sreelola, A.K. Sailaja, M. Pharmacy, Preparation and characterisation of ibuprofen loaded polymeric nanoparticles by solvent evaporation technique, Int. J. Pharm. Pharm. Sci. 6 (2014) 416–421.

[62] A.W. York, S.E. Kirkland, C.L. McCormick, Advances in the synthesis of amphiphilic block copolymers via RAFT polymerization: Stimuli-responsive drug and gene delivery, Adv. Drug Deliv. Rev. 60 (2008) 1018–1036. doi:10. 1016/j.addr.2008.02.006.

[63] A.E. Smith, X. Xu, C.L. McCormick, Stimuli-responsive amphiphilic (co)polymers via RAFT polymerization, Prog. Polym. Sci. 35 (2010) 45–93. doi:10.1016/j.progpolymsci.2009.11.005.

[64] H. Willcock, R.K. O'Reilly, End group removal and modification of RAFT polymers, Polym. Chem. 1 (2010) 149–157. doi:10.1039/b9py00340a.

[65] W. Li, M. Nakayama, J. Akimoto, T. Okano, Effect of block compositions of amphiphilic block copolymers on the physicochemical properties of polymeric micelles, Polymer (Guildf). 52 (2011) 3783–3790. doi:10.1016/j. polymer. 2011. 06.026.

[66] G. Gaucher, M.-H. Dufresne, V.P. Sant, N. Kang, D. Maysinger, J.-C. Leroux, Block copolymer micelles: preparation, characterization and application in drug delivery., J. Control. Release. 109 (2005) 169–188. doi:10.1016/j. jconrel .2005 .09.034.

[67] V. Strehmel, A. Laschewsky, H. Wetzel, E. Görnitz, Free Radical Polymerization of n -Butyl Methacrylate in Ionic Liquids, Macromolecules. 39 (2006) 923–930. doi:10.1021/ma0516945.

[68] C. Yang, Y.L. Cheng, RAFT synthesis of poly(N-isopropylacrylamide) and poly(methacrylic acid) homopolymers and block copolymers: Kinetics and characterization, J. Appl. Polym. Sci. 102 (2006) 1191–1201. doi:10.1002 /app. 24415.

[69] Y.I. Puzin, R.K. Yumagulova, V. a. Kraikin, Radical polymerization of methyl methacrylate and styrene in the presence of ferrocene, Eur. Polym. J. 37 (2001) 1801–1812. doi:10.1016/S0014-3057(01)00038-6.

[70] K. Davis, K. Matyjaszewski, Investigation of the ATRP of n-butyl methacrylate using the /n,n,n',n",n" pentamethyldiethylenetriamine catalyst system, Chinese J. Polym. 22 (2004) 195–204.

[71] C. Granel, P. Dubois, R. Jérôme, P. Teyssié, Controlled Radical Polymerization of Methacrylic Monomers in the Presence of a Bis(ortho-chelated) Arylnickel(II) Complex and Different Activated Alkyl Halides, Macromolecules. 29 (1996) 8576–8582. doi:10.1021/ma9608380.

[72] K. Nakabayashi, H. Mori, Recent progress in controlled radical polymerization of N-vinyl monomers, Eur. Polym. J. 49 (2013) 2808–2838. doi:10.1016/j.eurpoly mj.2013.07.006.

[73] J. Pretula, K. Kaluzynski, B. Wisniewski, R. Szymanski, T. Loontjens, S. Penczek, Formation of poly(ethylene phosphates) in polycondensation of H3PO4 with ethylene glycol. Kinetic and mechanistic study, J. Polym. Sci. Part a-Polymer Chem. 46 (2008) 830–843. doi:10.1002/pola.

[74] G. Moad, E. Rizzardo, S.H. Thang, Reversible Addition Fragmentation Chain Transfer (RAFT) Polymerization, Mater. Matters. 5 (2010) 2. http://www. sigma-

aldrich.com/technical-documents/articles/material-matters /reversible-addition. html#sthash.2qQSTEIK.dpuf.

[75] G. Moad, Y.K. Chong, A. Postma, E. Rizzardo, S.H. Thang, Advances in RAFT polymerization: The synthesis of polymers with defined end-groups, Polymer (Guildf). 46 (2005) 8458–8468. doi:10.1016/j.polymer.2004.12.061.

[76] M.W.M. Fijten, R.M. Paulus, U.S. Schubert, Systematic parallel investigation of RAFT polymerizations for eight different (meth)acrylates: A basis for the designed synthesis of block and random copolymers, J. Polym. Sci. Part A Polym. Chem. 43 (2005) 3831–3839. doi:10.1002/pola.20868.

[77] X. Zhou, P. Ni, Z. Yu, F. Zhang, Latices of Poly(fluoroalkyl mathacrylate)-b-Poly(butyl methacrylate) Copolymers Prepared via Reversible Addition–Fragmentation Chain Transfer Polymerization, J. Polym. Sci. Part A Polym. Chem. 45 (2007) 471–484. doi:10.1002/pola.

[78] R. Rojas, N.K. Harris, K. Piotrowska, J. Kohn, Evaluation of automated synthesis for chain and step-growth polymerizations: Can robots replace the chemists?, J. Polym. Sci. Part A Polym. Chem. 47 (2009) 49–58. doi:10.1002/pola.23119.

[79] S.M. Henry, A.J. Convertine, D.S.W. Benoit, A.S. Hoffman, P.S. Stayton, End-functionalized polymers and junction-functionalized diblock copolymers via RAFT chain extension with maleimido monomers, Bioconjug. Chem. 20 (2009) 1122–1128. doi:10.1021/bc800426d.

[80] Z. Jia, C. Liu, J. Huang, Synthesis of (ABCB)n type ternary amphiphilic multiblock copolymer via poly(ethylene oxide) macro-chain transfer agent, Polymer (Guildf). 47 (2006) 7615–7620. doi:10.1016/j.polymer.2006.09.009.

[81] Y.-Z. You, C.-Y. Hong, C.-Y. Pan, A novel strategy for synthesis of multiblock copolymers., Chem. Commun. (Camb). (2002) 2800–2801.

[82] M. Abdulkarim, N. Agulló, B. Cattoz, P. Griffiths, A. Bernkop-Schnürch, S.G. Borros, et al., Nanoparticle diffusion within intestinal mucus: Three-dimensional response analysis dissecting the impact of particle surface charge, size and heterogeneity across polyelectrolyte, pegylated and viral particles, Eur. J. Pharm. Biopharm. 97 (2015) 230–238. doi:10.1016/j.ejpb.2015.01.023.

[83] G. Natus, E.J. Goethals, Sulfoalkylation of dimethylsulfoxide with propane sultone, Bull. Des Sociétés Chim. Belges. 74 (1965) 450–452. doi:10.1002/bscb .19650740908.

[84] V. Bütün, C.E. Bennett, M. Vamvakaki, A.B. Lowe, N.C. Billingham, S.P. Armes, Selective betainisation of tertiary amine methacrylate block copolymers, J. Mater. Chem. 7 (1997) 1693–1695. doi:10.1039/a703566g.

[85] J.P. Rao, K.E. Geckeler, Polymer nanoparticles: Preparation techniques and size-control parameters, Prog. Polym. Sci. 36 (2011) 887–913. doi:10.1016/j .pro gpolymsci.2011.01.001.

[86] W. Lin, Z. Wang, S. Chen, Zwitterionic polymers for targeted drug delivery, in: Youqing Shen (Ed.), Funct. Polym. Nanomedicine, Royal Society of Chemistry, london, 2013: pp. 227–244. doi:10.1039/9781849737388-00227.

[87] C. Vauthier, K. Bouchemal, Methods for the Preparation and Manufacture of Polymeric Nanoparticles, Pharm. Res. 26 (2009) 1025–1058. doi:10.1007/s11095-008-9800-3.

[88] S. Galindo-rodriguez, E. Alle, H. Fessi, E. Doelker, Physicochemical Parameters Associated with Nanoparticle Formation in the Salting-out , Nanoprecipitation Methods, Pharm. Res. 21 (2004) 1428–1439. doi:10.1023/B:PHAM.00000 36917 .75634.be.

[89] A.J. Coupe, S.S. Davis, I.R. Wilding, Variation in gastrointestinal transit of pharmaceutical dosage forms in healthy subjects, Pharm. Res. 8 (1991) 360–364. doi:10.1023/A:1015849700421.

[90] S.A. Galindo-Rodriguez, E. Allemann, H. Fessi, E. Doelker, Polymeric nanoparticles for oral delivery of drugs and vaccines: a critical evaluation of in vivo studies., Crit. Rev. Ther. Drug Carrier Syst. 22 (2005) 419–464. doi:10.1615/CritRevTherDrugCarrierSyst.v22.i5.10.

[91] A.B. Lowe, N.C. Billingham, S.P. Armes, Synthesis and Properties of Low-Polydispersity Poly (sulfopropylbetaine)s and Their Block Copolymers, Macromolecules. 32 (1999) 2141–2148. doi:10.1021/ma980543h.

[92] K. Letchford, H. Burt, A review of the formation and classification of amphiphilic block copolymer nanoparticulate structures: micelles, nanospheres, nanocapsules and polymersomes, Eur. J. Pharm. Biopharm. 65 (2007) 259–269. doi:10.1016/j.ejpb.2006.11.009.

[93] T. Riley, S. Stolnik, C.R. Heald, C.D. Xiong, M.C. Garnett, L. Illum, et al., Physicochemical Evaluation of Nanoparticles Assembled from Poly (lactic acid) - Poly (ethylene glycol) (PLA - PEG) Block Copolymers as Drug Delivery Vehicles, (2001) 3168–3174.

[94] C. Heald, S. Stolnik, K. Kujawinski, Poly (lactic acid)-poly (ethylene oxide)(PLA-PEG) nanoparticles: NMR studies of the central solidlike PLA core and the liquid PEG corona, Langmuir. (2002) 3669–3675.

[95] S. Hornig, T. Heinze, C.R. Becer, U.S. Schubert, Synthetic polymeric nanoparticles by nanoprecipitation, J. Mater. Chem. 19 (2009) 3838–3840. doi:10.1039/b906556n.

[96] E. Muro, T. Pons, N. Lequeux, A. Fragola, N. Sanson, Z. Lenkei, et al., Small and stable sulfobetaine zwitterionic quantum dots for functional live-cell imaging, J. Am. Chem. Soc. 132 (2010) 4556–4557. doi:10.1021/ja1005493.

[97] J. a Pedro, J.R. Mora, M. Silva, H.D. Fiedler, C. a Bunton, F. Nome, Surface charge of zwitterionic sulfobetaine micelles with 2-naphthol as a fluorescent probe., Langmuir. 28 (2012) 17623–31. doi:10.1021/la303880m.

[98] J.P. Priebe, M.L. Satnami, D.W. Tondo, B.S. Souza, J.M. Priebe, G. a. Micke, et al., The chameleon-like nature of zwitterionic micelles: The intrinsic relationship of anion and cation binding in sulfobetaine micelles, J. Phys. Chem. B. 112 (2008) 14373–14378. doi:10.1021/jp801337n.

[99] A. Laschewsky, Structures and synthesis of zwitterionic polymers, Polymers (Basel). 6 (2014) 1544–1601. doi:10.3390/polym6051544.

[100] T.S.J. Kashi, S. Eskandarion, M. Esfandyari-Manesh, S.M.A. Marashi, N. Samadi, S.M. Fatemi, et al., Improved drug loading and antibacterial activity of minocycline-loaded PLGA nanoparticles prepared by solid/oil/water ion pairing method, Int. J. Nanomedicine. 7 (2012) 221–234. doi:10.2147/IJN.S27709.

[101] B. Gupta, B.K. Poudel, S. Pathak, J.W. Tak, H.H. Lee, J.-H. Jeong, et al., Effects of Formulation Variables on the Particle Size and Drug Encapsulation of Imatinib-Loaded Solid Lipid Nanoparticles., AAPS PharmSciTech. (2015) 1–11. doi:10.1208/s12249-015-0384-z.

[102] K.S. Chu, A.N. Schorzman, M.C. Finniss, C.J. Bowerman, L. Peng, J.C. Luft, et al., Nanoparticle drug loading as a design parameter to improve docetaxel pharmacokinetics and efficacy, Biomaterials. 34 (2013) 8424–8429. doi:10.1016/ j.biomaterials.2013.07.038.

[103] W. Abdelwahed, G. Degobert, S. Stainmesse, H. Fessi, Freeze-drying of nanoparticles: Formulation, process and storage considerations, Adv. Drug Deliv. Rev. 58 (2006) 1688–1713. doi:10.1016/j.addr.2006.09.017.

[104] F. De Jaeghere, E. Allémann, J.C. Leroux, W. Stevels, J. Feijen, E. Doelker, et al., Formulation and lyoprotection of poly(lactic acid-co-ethylene oxide) nanoparticles: influence on physical stability and in vitro cell uptake., Pharm. Res. 16 (1999) 859–66. doi:10.1023/A:1018826103261.

[105] chemicalize.org, ChemAxon, (1999). http://www.chemicali ze.org/structure/#!mol=CC%28C%29%5BC%40H%5D1C%28%3DO%29N%5BC% 40H%5D%28C%28%3DO%29NCC%28%3DO%29N%5BC%40H%5D%28C%28%3DO%29N%5BC%40%40H%5D%28C%28%3DO%29N1C%29Cc2ccccc2%29CC%28%3DO%29O%29CCCNC%28%3DN%29N&source=fp (accessed June 9, 2015).

[106] N.I. Lebovka, Aggregation of Charged Colloidal Particles, in: Martin Müller (Ed.), Polyelectrolyte Complexes Dispersed Solid State I Princ. Theory, Springer Berlin Heidelberg, Berlin, 2012: pp. 57–96. doi:http://dx.doi.org /10.1007/ 12_ 2012_171.

[107] G.I. Guerrero-García, P. González-Mozuelos, M. Olvera De La Cruz, Large counterions boost the solubility and renormalized charge of suspended nanoparticles, ACS Nano. 7 (2013) 9714–9723. doi:10.1021/nn404477b.

[108] K. Trofymchuk, A. Reisch, I. Shulov, Y. Mély, A.S. Klymchenko, Tuning the color and photostability of perylene diimides inside polymer nanoparticles: towards biodegradable substitutes of quantum dots, Nanoscale. 6 (2014) 12934–12942. doi:10.1039/C4NR03718A.

[109] C. Gómez-Gaete, N. Tsapis, M. Besnard, A. Bochot, E. Fattal, Encapsulation of dexamethasone into biodegradable polymeric nanoparticles, Int. J. Pharm. 331 (2007) 153–159. doi:10.1016/j.ijpharm.2006.11.028.

[110] T.C. Johnstone, S.J. Lippard, The effect of ligand lipophilicity on the nanoparticle encapsulation of Pt(IV) prodrugs, Inorg. Chem. 52 (2013) 9915–9920. doi:10.1021/ic4010642.

[111] D.C. Buehler, M.D. Marsden, S. Shen, D.B. Toso, X. Wu, J. a Loo, et al., Bioengineered Vaults: Self-Assembling Protein Shell-Lipophilic Core Nanoparticles for Drug Delivery., ACS Nano. (2014) 7723–7732. doi:10.1021/nn5002694.

[112] A. Lamprecht, Y. Bouligand, J.P. Benoit, New lipid nanocapsules exhibit sustained release properties for amiodarone, J. Control. Release. 84 (2002) 59–68. doi:10.1016/S0168-3659(02)00258-4.

[113] P. Pietzonka, B. Rothen-Rutishauser, P. Langguth, H. Wunderli-Allenspach, E. Walter, H.P. Merkle, Transfer of lipophilic markers from PLGA and polystyrene nanoparticles to Caco-2 monolayers mimics particle uptake, Pharm. Res. 19 (2002) 595–601. doi:10.1023/A:1015393710253.

[114] P. Saarinen-Savolainen, T. Järvinen, H. Taipale, A. Urtti, Method for evaluating drug release from liposomes in sink conditions, Int. J. Pharm. 159 (1997) 27–33. doi:10.1016/S0378-5173(97)00264-0.

[115] E.E.L. Kathmann, L. a White, C.L. Mccormick, Water-Soluble Polymers. 73. Electrolyte- and pH-Responsive Zwitterionic Copolymers of 4-[(2-Acrylamido-2-methylpropyl)- dimethylammonio]butanoate with 3-[(2-Acrylamido-2-methylpropyl) dimethylammonio]propanesulfonate, Macromolecules. 30 (1997) 5297–5304.

[116] J. Cleary, L. Bromberg, E. Magner, Adhesion of polyether-modified poly(acrylic acid) to Mucin, Langmuir. 20 (2004) 9755–9762. doi:10.1021/la048993s.

[117] S.. Jeon, J.. Andrade, Protein—surface interactions in the presence of polyethylene oxide, J. Colloid Interface Sci. 142 (1991) 159–166. doi:10.1016/0021-9797(91)90044-9.

[118] R. Liu, Y. Li, Z. Zhang, X. Zhang, Drug carriers based on highly protein-resistant materials for prolonged in vivo circulation time, Regen. Biomater. 2 (2015) 125–133. doi:10.1093/rb/rbv003.

[119] E. Ostuni, R.G. Chapman, R.E. Holmlin, S. Takayama, G.M. Whitesides, A survey of structure-property relationships of surfaces that resist the adsorption of protein, Langmuir. 17 (2001) 5605–5620. doi:10.1021/la010384m.

[120] J. Wu, S. Chen, Investigation of the hydration of nonfouling material poly(ethylene glycol) by low-field nuclear magnetic resonance, Langmuir. 28 (2012) 2137–2144. doi:10.1021/la203827h.

[121] S. Chen, J. Zheng, L. Li, S. Jiang, Strong resistance of phosphorylcholine self-assembled monolayers to protein adsorption: Insights into nonfouling properties of zwitterionic materials, J. Am. Chem. Soc. 127 (2005) 14473–14478. doi:10. 1021/ja054169u.

[122] L. Li, S. Chen, J. Zheng, B.D. Ratner, S. Jiang, Protein Adsorption on Oligo (ethylene glycol) -Terminated Alkanethiolate Self-Assembled Monolayers : The Molecular Basis for Nonfouling Behavior, Surf. Sci. (2005) 2934–2941. doi: 10. 1021/jp0473321.

CHAPTER SIX

GENERAL CONCLUSIVE DISCUSSION AND FUTURE WORK

1 General Conclusive Discussion

Oral delivery of certain types of therapeutic agents like peptides and proteins is very limited due to the environmental and enzymatic degradation. These therapeutic agents need to be protected from the GIT environment to be delivered in effective therapeutic level. This issue was found to be possible through the incorporation of these therapeutic agents into suitable nano-delivery systems which provides enzymatic protection and sustained drug release to improve their bioavailability. For intestinal mucosal delivery, NPs need to permeate through the mucus layer covering the mucosa.

All studies that have been carried out showed that mucus permeation is the limiting step for NPs to be absorbed through the intestinal mucosa. Some promising results have been obtained in terms of in vitro NPs permeation and *in vivo* drug bioavailability. However, nano-delivery through intestinal mucus is still one of the most challenging tasks in the world of drug delivery due to many reasons such as the trapping of the majority of NPs in the intestinal mucus and selecting of the improper techniques to measure NPs permeation through mucus barrier.

The ultimate aim of the Alexander European consortium was to synthesize muco-diffusive NP that can be used to for oral delivery of certain peptides such as insulin. For this reason, this thesis aimed to synthesize novel NPs that can highly diffuse through the intestinal mucus barrier. This was achieved step by step through the preparation of the elements enabling by the end to obtain novel highly permeable NPs through the intestinal mucus barrier. These elements were: the suitable pig intestinal mucus barrier model, the proper technique to measure NPs diffusion through the mucus and understanding the factors affecting NPs diffusion through the intestinal mucus barrier.

In the second chapter, two pig intestinal mucus models were introduced, one is native and collected from the pig intestine with no further processing steps; ”Cardiff native mucus”, while the other was squeezed from the pig intestine followed by washing steps “Consortium mucus gel” model. These mucus models were studied biophysically to identify their structural and physical properties. Thus, the water content, pH and rheological properties of each mucus model were examined; also, AFM imaging was used to study the structural properties of each model. These biophysical tests were used to identify differences between each model and to use these differences to interpret the diffusion of NPs through the both mucus models.

The MPT technique was exploited to study particles diffusion through the both pig intestinal mucus models. To do so, the MPT technique was validated to ensure that the diffusion data is valid for all the tested particles. Hence, carefully selected NPs in which Lumogen red dye was encapsulated were used so as to validate the fluorescent dye, the fluorescent microscopy, the mucus and the tracking software so as to limit any error associated with the measurement of particles diffusion through the mucus by this technique. The diffusion of particles through the two mucus models were studied by the MPT technique to identify the best mucus model that can used to study the diffusion of other NPs.

In chapter three, the diffusion coefficients of various NPs representing different nano-strategies to overcome the mucus barrier were tested. These nano-strategies included slippery surface PEG NPs, slippery surface polymer mixture, slippery PEC NPs, SMEDD systems, mucolytic NPs and thiomer NPs. These NPs were synthesized and fluorescently labelled by the partners in the Alexander consortium. The diffusivities of all these NPs were compared through both mucus models. Particles were ranked depending on their diffusivities through the mucus barrier, to identify the promising

muco-diffusive nano-strategy. Also, the nano-strategy that was not covered adequately by the partners in the Alexander consortium was identified for further studies.

In chapter four, determined by the outcomes of Chapter three where the PEC nano-strategy was found to not be studied properly by our partners, this PEC NP strategy was studied and compared with other slippery surface nano-strategies. PEC NPs were synthesized in which chitosan and PAA polymers were the source of the positively and negatively charged polymer respectively. Chitosan and PAA were mixed at serial ratios to produce densely surface charge particles with zeta potential ranging from highly negative to neutral up to highly positive charges and with various particle sizes. The diffusivity through the mucus was increased as the surface charge of these particles approached neutrality; oppositely, the diffusivity through mucus was decreased as the charge of these particles was increased either positively or negatively. However, even with the promising diffusivities of these particles through mucus barrier, the low stability of these particles limited the use of these particles. Hence, developing particles with neutral surface charge and high stability was the next aim in the thesis.

In chapter five, novel NPs with densely surface charge but with overall neutral zeta potential and with very small particle sizes were synthesized. To achieve this goal, the reversible addition fragmentation chain transfer (RAFT) technique was used to synthesize co-polymers with lipophilic and zwitterionic hydrophilic block. NPs were made from these polymers in which the lipophilic core was the butyl methyl methacrylate (BMA) and the hydrophilic shell was the hydrophilic slufobetaine polymer. These novel small particles (< 50 nm) were highly charged with overall neutral zeta potential and very stable. These physicochemical properties should enable these particles to be highly muco-diffusive and stable enough to exert their biological activity.

Following the synthesis of these novel NPs, the diffusivity of these sulfobetaine particles through the mucus was studied. These particles were found to be highly diffusive through the intestinal mucus when they were compared with other strategies that were adopted by the other partners in the Alexander consortium. The ability of sulfobetaine NP to cross mucus barrier will allow more ready access to the underlying epithelial surface for the absorption of material released from the NP as cargo. With this discovery, the main aim of this thesis was achieved through the obtaining of these novel zwitterionic muco-diffusive NPs.

2 Future Works

- **Sulfobetaine NPs**

Besides the promising *in vitro* diffusion data through mucus barrier, these sulfobetaine NPs are inexpensive, biocompatible and easy to prepare. Hence, these NPs could be exploited for wider therapeutic applications for which further studies are required. These further studies and exploitations can be summarized as follows:

(i) In vivo and toxicity studies could be performed in the future to prove the suitability of these NPs to improve the bioavailability of orally administered peptide with low bioavailability such as insulin and to correlate the in vivo and in vitro data to prove the concept of the mucus permeability of these NPs.

(ii) Chemical modification of these NPs could be done by altering the size or the type of the lipophilic core or the zwitterionic hydrophilic shell. For example, BMA could be replaced by another lipophilic block polymer. Further studies could be performed to investigate the effect of new chemical

entities on the physicochemical properties and diffusion behaviour of these sulfobetaine NPs.

(iii) Further chemical and physical analytical studies such as scanning electron microscopy and differential scanning microscopy are required in the future for better understanding and explanation of the formation of sulfobetaine NPs.

(iv) Due, to the densely charged nature, Sulfobetaine NPs could have long circulating properties following intravenous, intramuscular, sub-cutaneous or intra-dermal administration. Hence, further pharmacokinetic studies could be done in the future to study the suitability of these NPs for other clinical applications and pharmaceutical devices.

(v) Following the high diffusion data through the mucus biopolymer barrier, the permeation of these NPs through the biopolymer barrier of bacterial biofilms is a promising area to be studied in the future.

- **MPT Technique**

(i) Further studies are required in the future for better understanding of the process involved in the measurement of NPs diffusion through the mucus barrier by the MPT technique. Factors such as changing the mucus preparation steps and time of the addition of NPs suspension into mucus sample could reveal better explanation about the process of NPs mixing with, penetration across and diffusion through the mucus barrier.

(ii) MPT technique could be exploited in the future to study NPs permeation through the biopolymer bacterial biofilm.

APPENDIX A

AFM IMAGES OF THE PIG INTESTINAL "CARDIFF NATIVE MUCUS" MODEL AND THE "CONSORTIUM MUCUS GEL" MODEL

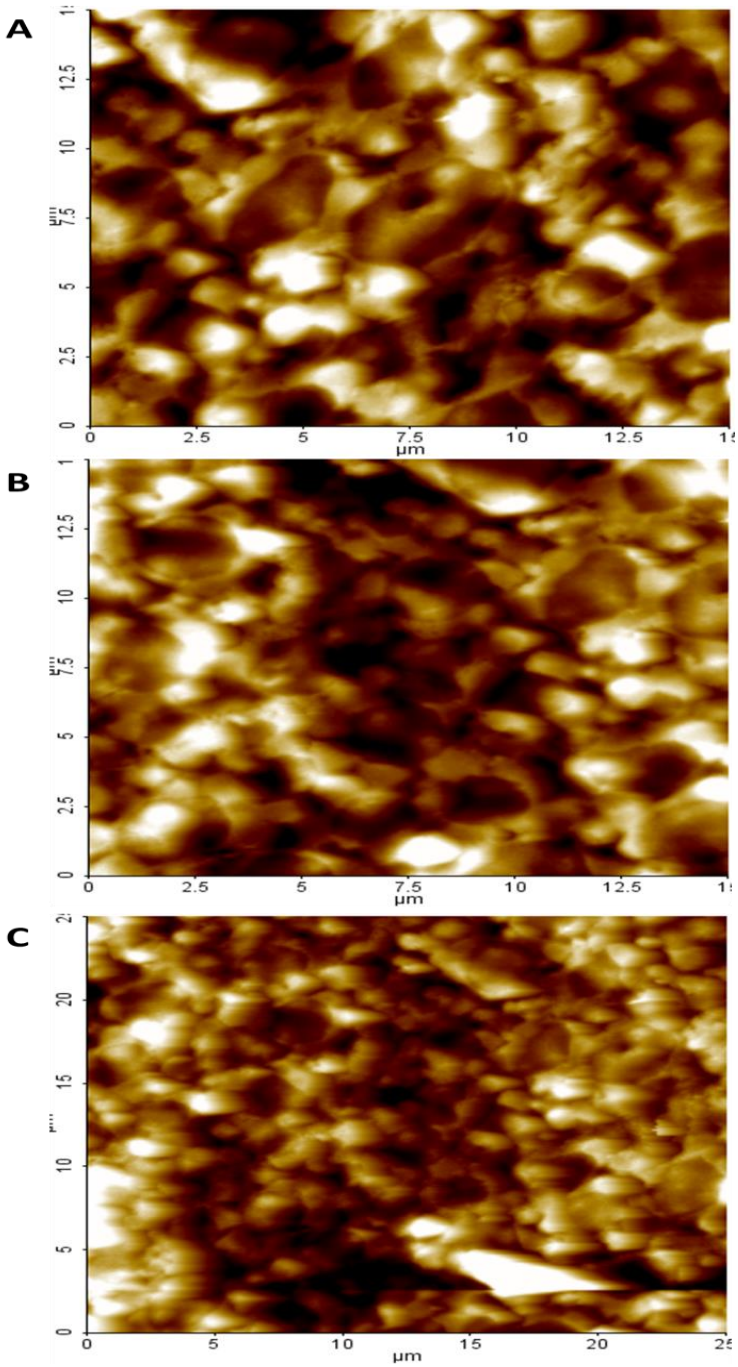

Figure A.1: AFM imaging of the surface morphology from different scanned areas within the "Cardiff native mucus" model. (A) Medium scale (15x15 µm) AFM image of one area within the mucus sample, (B) Medium scale (15x15 µm) AFM image of another area imaged within the mucus sample, (C) Large scale (25x25 µm) AFM image of another different area imaged within the mucus sample.

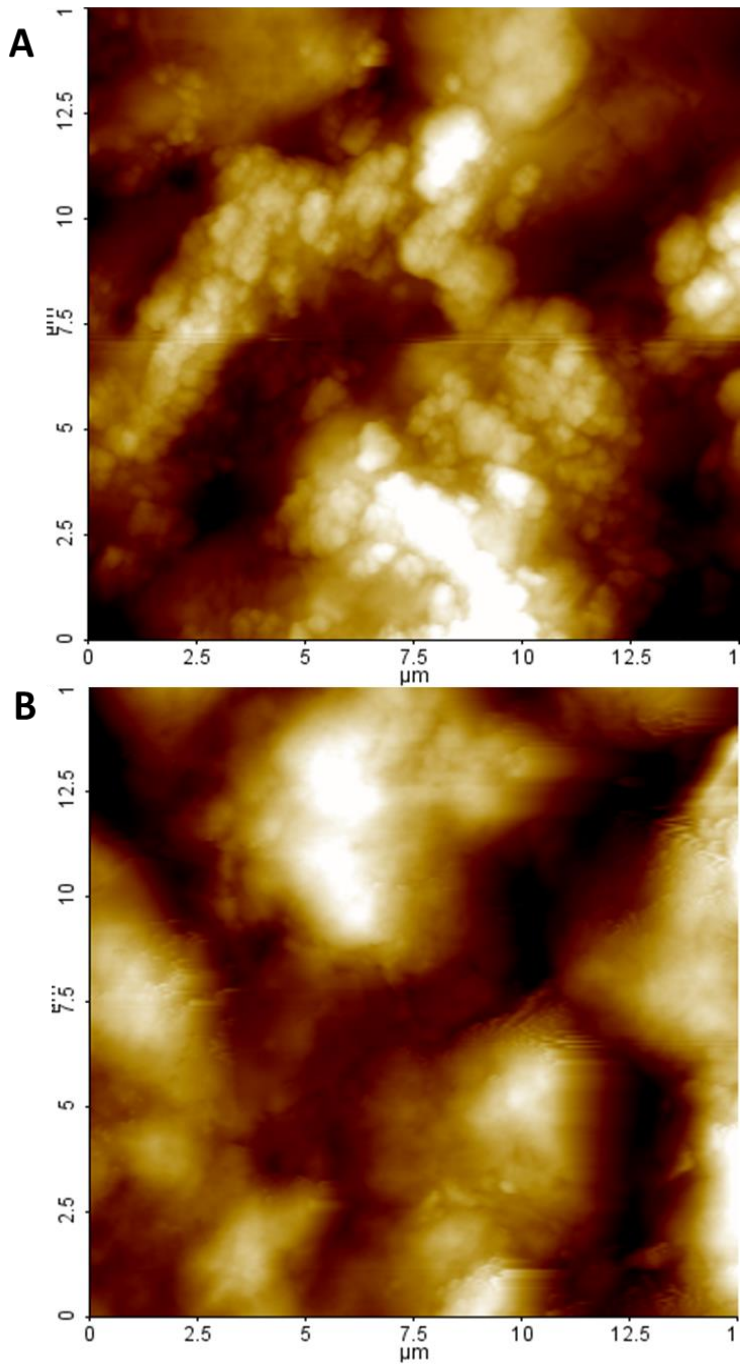

Figure A.2: AFM imaging of the surface morphology from different scanned areas within the "Consortium mucus gel" model. (A) Medium scale (15x15 µm) AFM image of one site within the mucus sample showing 5 and 2.5 micron pores, (B) Medium scale (15x15 µm) AFM image of another site imaged within the mucus sample showing 5 and 7.5 micron pores.

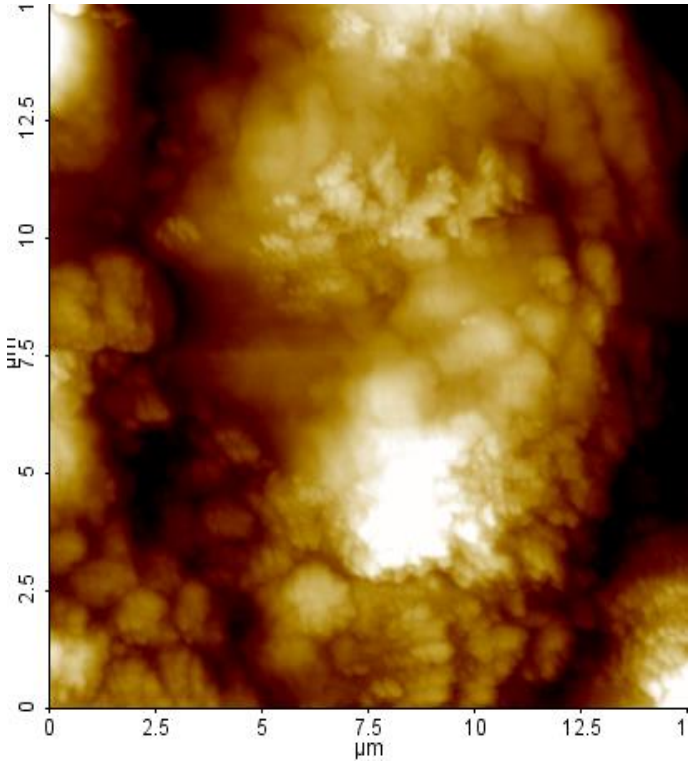

Figure A.3: AFM imaging of the surface morphology of the "Consortium mucus gel" model at medium scale of (15x15 µm) showing a (5 x 5) micron aggregated cluster of mucin fibres.

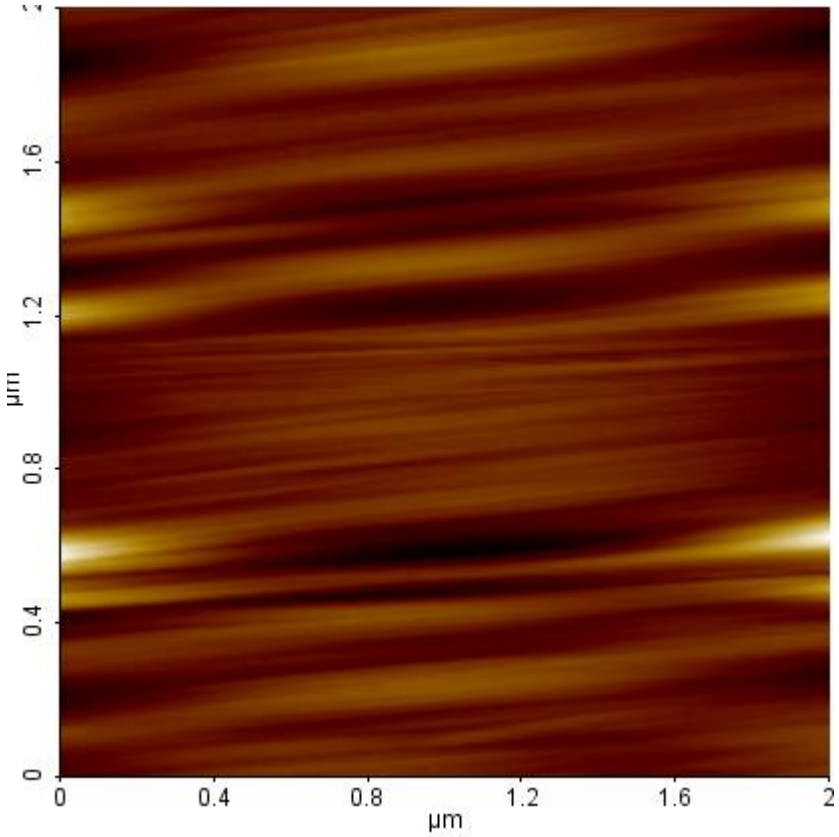

Figure A.4: AFM imaging of the surface morphology of the "Consortium mucus gel" model at small scale of (2x2 µm) showing the mucin fibres bundling into thick cables.

APPENDIX B

DIFFUSION OF NPS REPRESENTING NANO-STRATEGIES ADOPTED BY THE ALEXANDER PARTNERS THROUGH THE "CONSORTIUM MUCUS GEL" MODEL (PROCESSED INTESTINAL MUCUS BARRIER)

Table B.1: Particles' composition, physical characteristics and diffusion behavior of various PEGylated NPs in the "Consortium mucus gel" model.

Partner	NP Code	Compositions	Zeta Potential (mV) Mean (± s.d.)	Particle Size (nm) Mean (PDI)	D° (water) $cm^2. S^{-1} x10^{-9}$	<Deff> (mucus) $cm^2. S^{-1} x10^{-9}$ Mean (± s.e.m)	% of Deff to D°	Ranking Fastest to slowest
Nanomi	PLGA-15% PEG (5000)	PLGA coated with 15% methoxy PEG (MW: 5000).	-18	35	127.8	0.00702 (±0.00167)	0.0055	29
	PLGA-15% PEG (6000)	PLGA coated with 15% PEG (MW: 6000).	-8.3	54	83.22	0.01396 (±0.00477)	0.0168	9
	PLGA-10% PEG (5000)	PLGA coated with 10% methoxy PEG (MW: 5000).	-26	41	110.7	0.00561 (±0.00113)	0.0051	31
Nevara	G-15% PEG (2000)	Lipophilic polymer coated with 15% PEG (MW: 2000) (Lyophilized NP)	-45	178	25.21	0.00100 (±0.00013)	0.0040	38
	G-15% PEG (6000)	Lipophilic polymer coated with 15% PEG (MW: 6000) (Lyophilized NP)	-47	230	19.54	0.00026 (±0.00005)	0.0013	71
AUTH	RG502H-PEG2000	Acidic PLGA (50:50) coated with 25% methoxy PEG (MW:2000)	-20	300	15.01	0.00023 (±0.00004)	0.0015	67
	RG502H-PEG5000	Acidic PLGA (50:50) coated with 25% methoxy PEG (MW:5000)	-14	287	15.64	0.00038 (±0.00007)	0.0025	55
	RG752H-PEG2000	Acidic PLGA (75:25) coated with 25% methoxy PEG (MW:2000)	-11	301	14.91	0.00047 (±0.00009)	0.0032	48
	RG752H-PEG5000	Acidic PLGA (75:25) coated with 25% methoxy PEG (MW:5000)	-9	261	17.21	0.00031 (±0.00006)	0.0018	64
	PEC- 22.5% PEG	(70:30) Negatively charged polymer+ Positively charged polymer conjugated to 75% PEG (Total ratio of PEG is 22.5%)	-28	250	17.98	0.00088 (±0.00015)	0.0049	33

LEK	PEC- 52.5% PEG	(30:70) Negatively charged polymer+ Positively charged polymer conjugated to 75% PEG (Total ratio of PEG is 52.5%)	-12	250	17.98	0.00306 (±0.00039)	0.0170	8
	PEC- 15.0% PEG	(70:30) Negatively charged polymer+ Positively charged polymer conjugated to 50% PEG (Total ratio of PEG is 15%)	-27	250	17.98	0.00035 (±0.00009)	0.0020	60
	PEC- 35.0% PEG	(30:70) Negatively charged polymer+ Positively charged polymer conjugated to 50% PEG (Total ratio of PEG is 35%)	-15	250	17.98	0.00287 (±0.00052)	0.0160	10
Evonik	Mix 3	PLGA-PEG		120	37.45	0.00305 (±0.00057)	0.00814	21
	Mix 4	PLGA-PEG		342	13.13	0.00066 (±0.00011)	0.00502	32
	Mix 10	PLGA-PEG		424	10.58	0.00464 (±0.00171)	0.04386	1
	Mix 18	PLGA-PEG		183	24.56	0.00471 (±0.00088)	0.01916	7
	Mix 19	PLGA-PEG		171	26.28	0.00516 (±0.00118)	0.01962	6

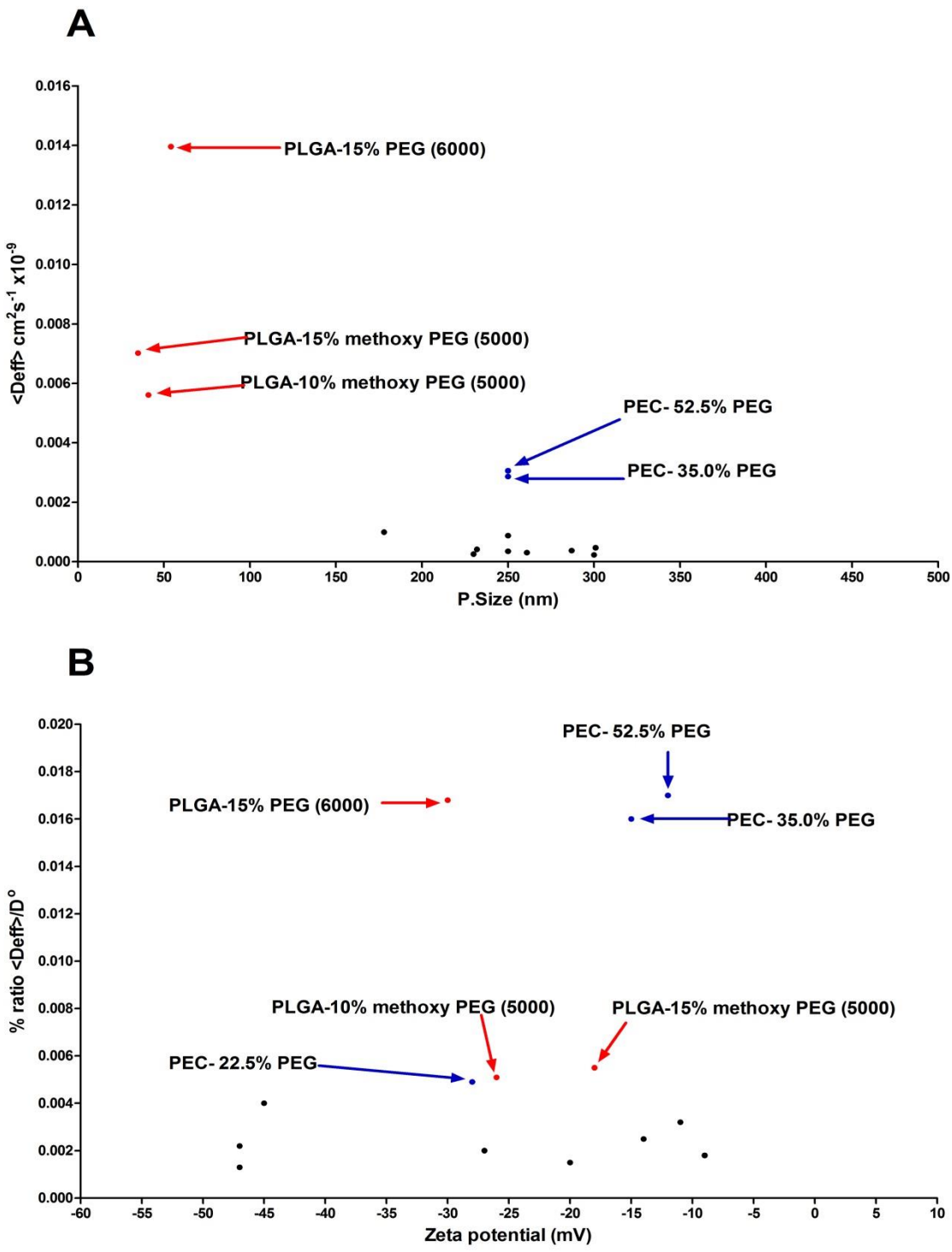

Figure B.1: (A) Mucus diffusion <Deff> versus particle size of PEGylated NPs in the "Consortium mucus gel" model. (B) % ratio <Deff>/D° versus zeta potential of PEGylated NPs in the "Consortium mucus gel" model.

Table B.2: Particles' composition, physical characteristics and diffusion behavior of slippery polymer mixture NPs in the "Consortium mucus gel" model.

Partner	NP Code	Compositions	Zeta Potential (mV) Mean (± s.d.)	Particle Size (nm) Mean (PDI)	D° (water) $cm^2. S^{-1} x10^{-9}$	<Deff> (mucus) $cm^2. S^{-1} x10^{-9}$ Mean (± s.e.m)	% of Deff to D°	Ranking Fastest to slowest
Nevara	NPA-L-L	Gantrez NP	-53	217	20.71	0.00110 (±0.00018)	0.0053	30
	1% D-M-L-L	Lipophilic polymer coated with 1% D-mannosamine hydrochloride	-40	242 (0.11)	18.56	0.00083 (±0.00014)	0.0045	35
	2.5% D-M-L-L	Lipophilic polymer coated with 2.5% D-mannosamine hydrochloride	-35	271 (0.12)	16.56	0.00064 (±0.00016)	0.0039	39
	5% D-M-L-L	Lipophilic polymer coated with 5% D-mannosamine hydrochloride	-45	263 (0.12)	17.09	0.00545 (±0.00098)	0.0319	2
	7.5% D-M-L-L	Lipophilic polymer coated with 7.5% D-mannosamine hydrochloride	-49	332 (0.13)	13.54	0.00151 (±0.00025)	0.0111	16
	10% D-M-L-L	Lipophilic polymer coated with 10% D-mannosamine hydrochloride	-39	367 (0.12)	12.25	0.00265 (±0.00050)	0.0216	3
	1% CO-DM L-L	Lipophilic polymer copolymerized with 1% D-mannosamine hydrochloride	-37	265 (0.12)	16.96	0.00041 (±0.00009)	0.0024	56
	2.5% CO-DM-L-L	Lipophilic polymer copolymerized with 2.5% D-mannosamine hydrochloride	-31	249 (0.13)	18.05	0.00058 (±0.00009)	0.0032	47
	5% CO-DM L-L	Lipophilic polymer copolymerized with 5% D-mannosamine hydrochloride	-37	242 (0.12)	18.57	0.00161 (±0.00024)	0.0087	20
	7.5% CO-DM L-L	Lipophilic polymer copolymerized with 7.5% D-mannosamine hydrochloride	-45	254 (0.12)	17.69	0.00028 (±0.00005)	0.0016	66
	10% CO-DM L-L	Lipophilic polymer copolymerized with 10% D-mannosamine hydrochloride	-39	243 (0.14)	18.49	0.00052 (±0.00009)	0.0028	51
	1% LMPEC-L-L	Lipophilic polymer coated with 1% low methoxylated pectin	-49	340 (0.21)	13.22	0.00280 (±0.00072)	0.0212	4

	5% LMPEC-L-L	Lipophilic polymer coated with 5% low methoxylated pectin	-59	237 (0.23)	18.96	0.00203 (±0.00032)	0.0107	17
	5% LMPEC-L-L- 0.5 BSA	Lipophilic polymer coated 5% low methoxylated pectin loaded with 0.5% BSA	-47	174 (0.22)	25.83	0.00029 (±0.00001)	0.0011	76
	5% LMPEC-L-L- 1 BSA	Lipophilic polymer coated with 5% low methoxylated pectin loaded with 1% BSA	-43	161 (0.24)	28.00	0.00134 (±0.00008)	0.0048	34
	5% LMPEC-L-L- 1.5 BSA	Lipophilic polymer coated with 5% low methoxylated pectin and loaded with 1.5% BSA	-41	174 (0.24)	25.90	0.00147 (±0.00008)	0.0057	28
	5% LMPEC-L-L- 2 BSA	Lipophilic polymer coated with 5% low methoxylated pectin and loaded with 2% BSA	-42	163 (0.25)	27.62	0.00112 (±0.00007)	0.0041	37
	10% LMPEC-L-L	Lipophilic polymer coated with 10% low methoxylated pectin	-53	251 (0.23)	17.90	0.00116 (±0.00021)	0.0065	27
	1% Co-LMPEC-L-L	Lipophilic polymer copolymerized with 1% low methoxylated pectin	-49	221 (0.24)	20.34	0.00231 (±0.00032)	0.0114	15
	5% Co-LMPEC-L-L	Lipophilic polymer copolymerized with 5% low methoxylated pectin	-35	221 (0.23)	20.34	0.00072 (±0.00012)	0.0036	42
	10% Co-LMPEC-L-L	Lipophilic polymer copolymerized with 10% low methoxylated pectin	-39	175 (0.22)	25.68	0.00034 (±0.00008)	0.0013	70
	1% HMPEC-L-L	Lipophilic polymer coated with 1% high methoxylated pectin	-45	239 (0.24)	18.80	0.00079 (±0.00016)	0.0042	36
	5% HMPEC-L-L	Lipophilic polymer coated with 5% high methoxylated pectin	-52	261 (0.23)	17.22	0.00039 (±0.00009)	0.0023	57
	10% HMPEC-L-L	Lipophilic polymer coated with 10% high methoxylated pectin	-46	274 (0.25)	16.40	0.00020 (±0.00003)	0.0012	73
	1% Co-HMPEC-L-L	Lipophilic polymer copolymerized with 1% high methoxylated pectin	-43	178 (0.23)	25.25	0.00164 (±0.00033)	0.0065	26
	5% Co-HMPEC-L-L	Lipophilic polymer copolymerized with 5% high methoxylated pectin	-47	157 (0.24)	28.63	0.00040 (±0.00007)	0.0014	69

	10% Co-HM PEC-L-L	Lipophilic polymer copolymerized with 10% high methoxylated pectin	-36	168 (0.23)	26.75	0.00040 (±0.00008)	0.0015	68
	CO-TH- SD	Lipophilic polymer copolymerized with thiamine (spray dried NP)	-29	231 (0.21)	19.46	0.00006 (±0.00001)	0.0003	80
	OA-SD -L	Lipophilic polymer copolymerized with octadecyl- amine (spray dried NP)	-57	227 (0.22)	19.80	0.00023 (±0.00007)	0.0012	75
	NIC- SD	Lipophilic polymer copolymerized with nicotin- amide (spray dried NP)	-40	297 (0.25)	15.13	0.00049 (±0.00008)	0.0032	46
	HPCD-SD	Lipophilic polymer copolymerized with 2-hydroxypropyl-beta-cyclodextin (spray dried NP)	-57	245 (0.23)	18.34	0.00047 (±0.00011)	0.0026	53
	TH- SD	Lipophilic polymer coated with thiamine NP	-41	240 (0.12)	18.75	0.00019 (±0.00005)	0.0010	77

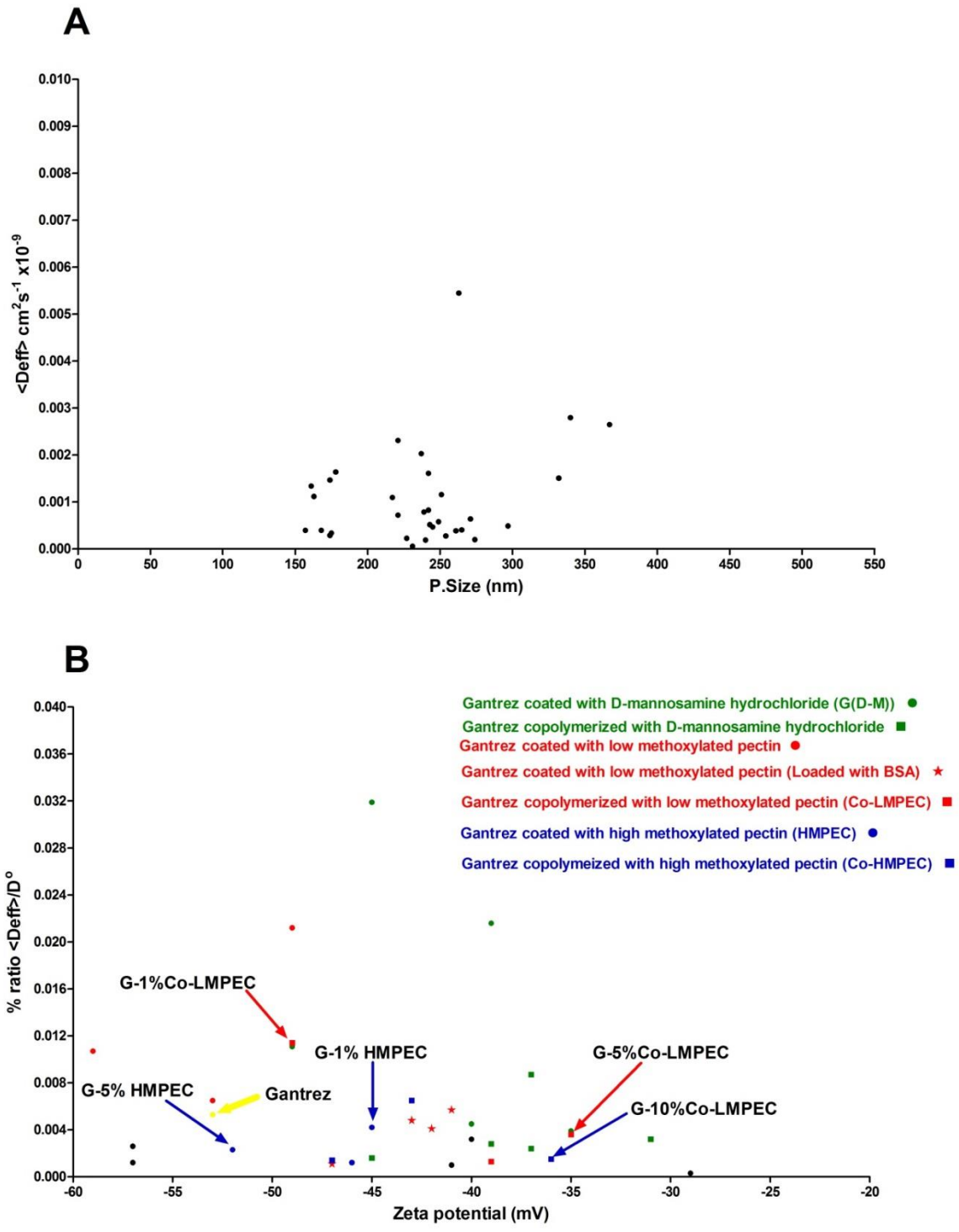

Figure B.2: (A) Mucus diffusion <Deff> versus particle size of slippery polymeric mixture NPs in the "Consortium mucus gel" model. (B) % ratio <Deff>/D° versus zeta potential of various slippery polymeric mixture NPs in the "Consortium mucus gel" model.

Table B.3: Particles' composition, physical characteristics and diffusion behavior of PEC NPs in the "Consortium mucus gel" model.

Partner	NP Code	Compositions	Zeta Potential (mV) Mean (± s.d.)	Particle Size (nm) Mean (PDI)	D° (water) $cm^2. S^{-1} x10^{-9}$	<Deff> (mucus) $cm^2. S^{-1} x10^{-9}$ Mean (± s.e.m)	% of Deff to D°	Ranking Fastest to slowest
Lek	L1009	(90:10) Unknown (+) charged polymer + (-) Alginate	16	250	17.98	0.00031 (±0.00006)	0.0017	65
	L1010	(30:70) Unknown (+) charged polymer + (-) chondroitin 4-sulfate	-22	250	17.98	0.00022 (±0.00005)	0.0012	72
	L1011	(40:60) Unknown (+) charged polymer + (-) chondroitin 4-sulfate	-18	250	17.98	0.00037 (±0.00010)	0.0019	62

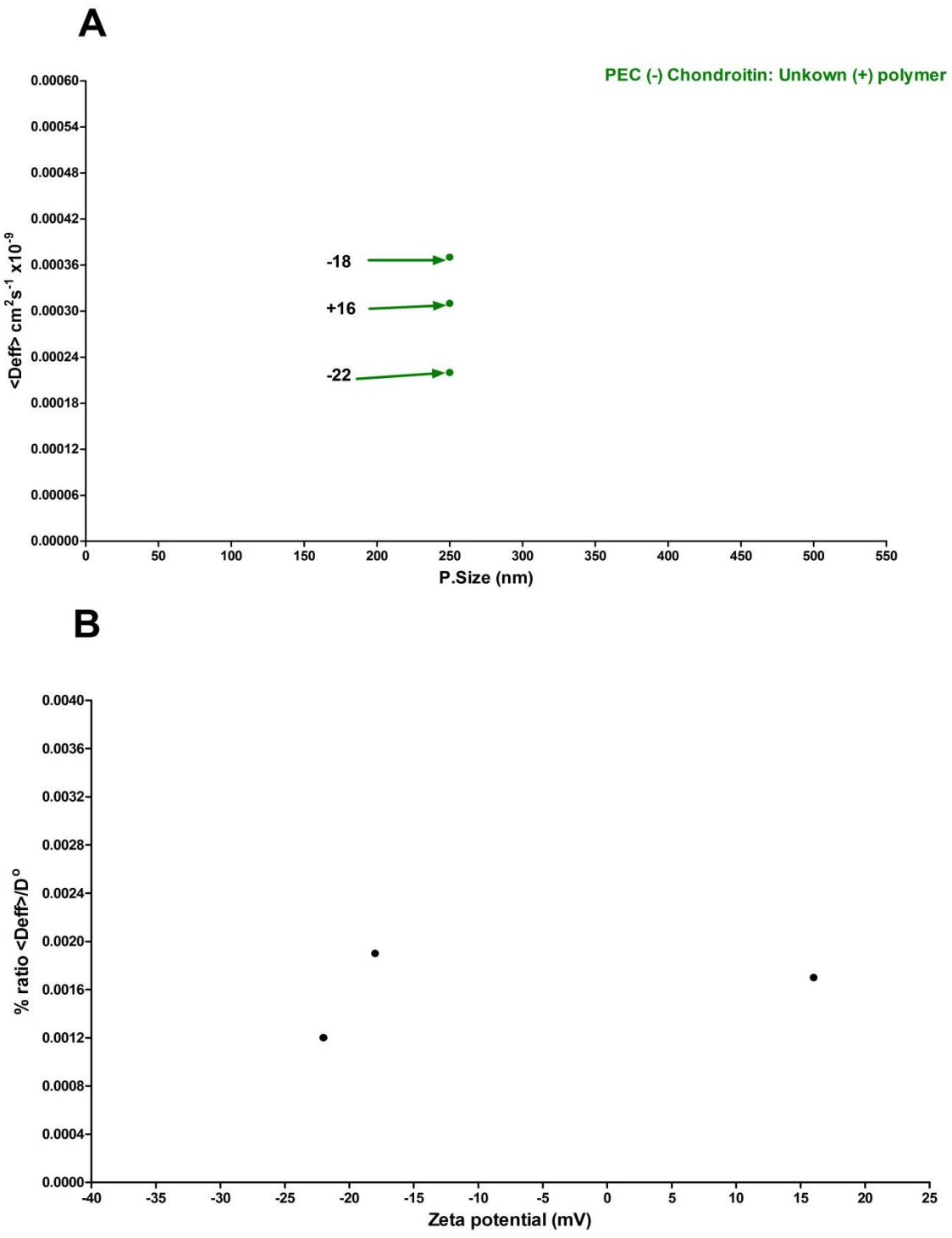

Figure B.3: (A) Mucus diffusion <Deff> versus particle size of PEC NPs in the "Consortium mucus gel" model. (B) % ratio <Deff>/D° versus zeta potential of PEC NPs in the "Consortium mucus gel" model.

Table B.4: Particles' composition, physical characteristics and diffusion behavior of NPs loaded with mucolytic agent in the "Consortium mucus gel" model.

Partner	NP Code	Compositions	Zeta Potential (mV) Mean	Particle Size (nm) Mean (PDI)	D° (water) $cm^2. S^{-1} x10^{-9}$	<Deff> (mucus) $cm^2. S^{-1} x10^{-9}$ Mean (± s.e.m)	% of Deff to D°	Ranking Fastest to slowest
Insbruck	PAA-PAP	PAA NP loaded with 25% Papaine (proteolytic agent)	-27	352 (0.26)	12.77	0.00034 (±0.00006)	0.0026	52
	PAA-BRO	PAA NP loaded with 25% Bromelaine (proteolytic agent)	-20	304 (0.29)	14.78	0.00099 (±0.00018)	0.0067	25
Sagetis	CSTGA360/-CD3	Chitosan-thioglycolic acid+ unknown (-) charged Poly(β-amino ester)s (PBAEs) (disulfide breaking agent).	NA	NA	NA	NA	NA	NA
	CSNAC177/ CD3	Chitosan-NAC+ unknown (-) charged Poly(β-amino ester)s (PBAEs) (disulfide breaking agent).	NA	NA	NA	NA	NA	NA
	CSGSH188/ CD3	Chitosan-Glutathione + unknown (-) charged Poly(β-amino ester)s (PBAEs) (disulfide breaking agent).	NA	NA	NA	NA	NA	NA
Nevara	0.3P-NPA-L-L	Muco-adhesive NP loaded with papain (0.3 %) (lyophilized NP)	-45	315 (0.19)	14.27	0.00150 (±0.00031)	0.0105	18
	0.3P-NPB-L-L	Muco-adhesive NP loaded with papain (0.3 %) (spray dried NP)	-46	216 (0.24)	20.80	0.00045 (±0.00007)	0.0022	59
	20NAC-NPA-L-L	Muco-adhesive NP loaded with NAC (5 %) (lyophilized NP)	-51	145 (0.32)	30.95	0.00037 (±0.00002)	0.0012	74
	200NAC-NPA-L-L	Muco-adhesive NP loaded with NAC (50 %) (lyophilized NP)	-53	189 (0.18)	23.77	0.00047 (±0.00003)	0.0020	61
	20NAC-NPB-L-L	Muco-adhesive NP loaded with NAC (5 %) (spray dried NP)	-28	231 (0.20)	19.49	0.00075 (±0.00004)	0.0038	40
	200NAC-NPB-L-L	Muco-adhesive NP loaded with NAC (50 %) (spray dried NP)	-23	440 (0.30)	10.21	0.00075 (±0.00004)	0.0073	22

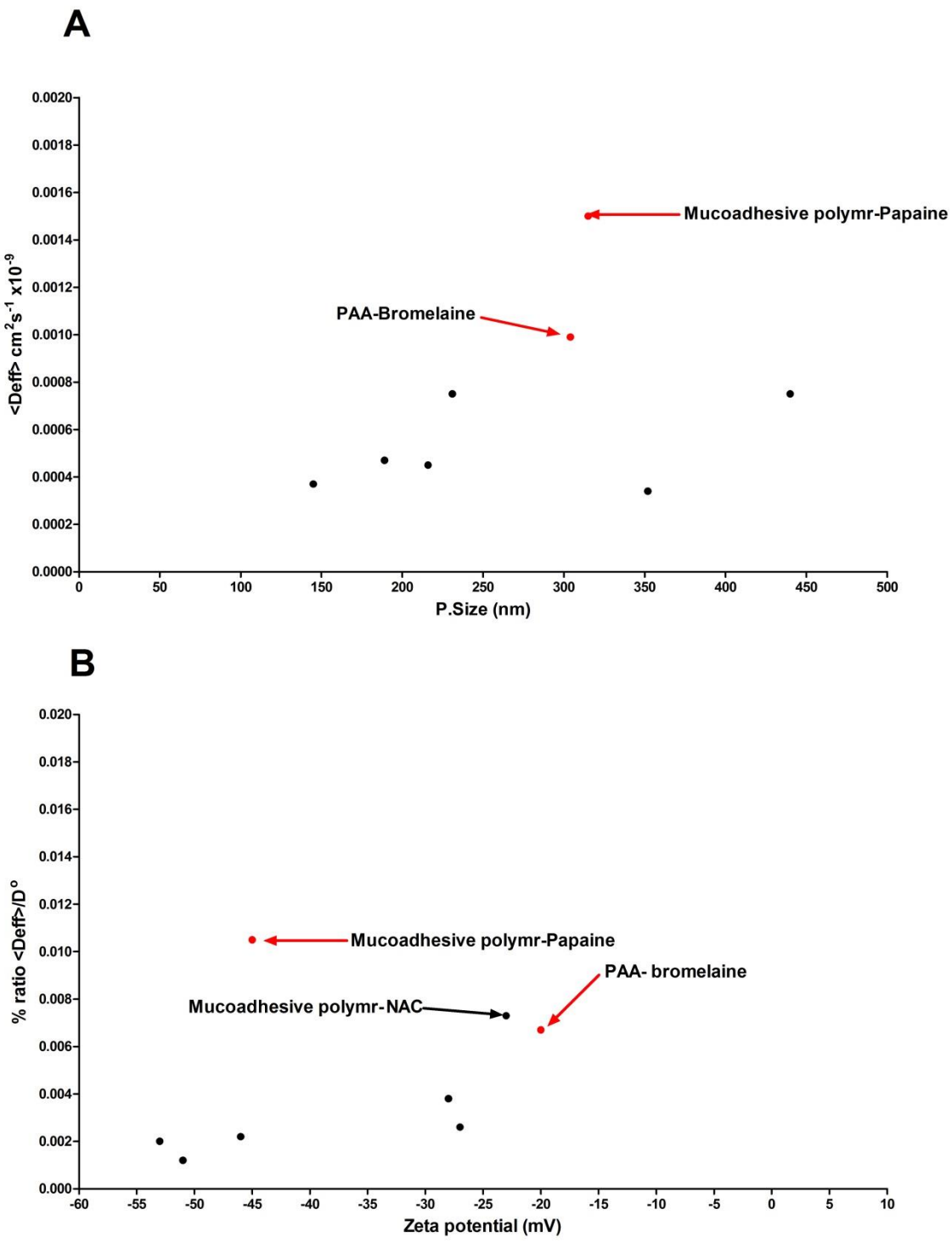

Figure B.4: (A) Mucus diffusion <Deff> versus particle size of NPs loaded with mucolytic agent in the "Consortium mucus gel" model. (B) % ratio <Deff>/D° versus zeta potential of NPs loaded with mucolytic agent in the "Consortium mucus gel" model.

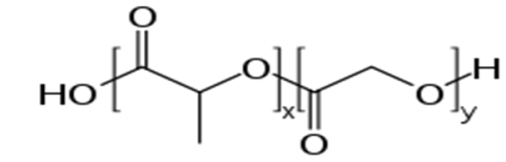

PLGA Polymer

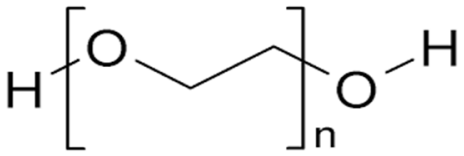

PEG Polymer

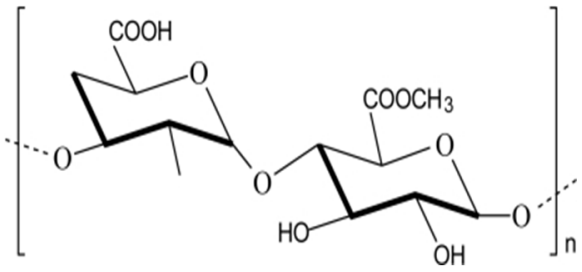

Pectin Polymer

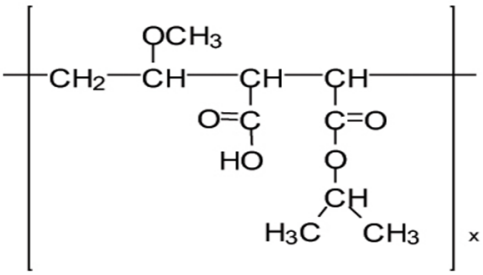

Gantrez Polymer

Figure B.5: Structures of main polymers used by the partners in chapter 3.

APPENDIX C

KINETIC STUDIES ON THE DIFFUSION OF SMEDD SYSTEMS LOADED WITH THIOL AND NAC AGENTS THROUGH THE PIG INTESTINAL "CARDIFF NATIVE MUCUS" MODEL

SMEDD systems that were studied in this work are as follows: SMEDD system loaded with TBA-dodecylamine was given the symbol SMEDD A, while the SMEDD system loaded with the other thiol agent (TGA-octylamine) was given the symbol SMEDD B. Accordingly, the SMEDD system loaded with NAC was given the symbol SMEDD NAC. Lastly, the blank SMEED system which was not loaded with any thiol or mucolytic agents was given the symbol SMEDD C.

Table C.1: Zeta potential, particle size, Diffusion coefficient in water and mucus, % ratio of <Deff>/D^o and percentage (%) of diffusive particles of various SMEDDS preparations.

SMEDDS	Zeta potential (mV) Mean (± s.d.)	Particle size (nm) Mean (PDI)	D^o (water) $cm^2.S^{-1} \times 10^{-9}$	<Deff> (mucus) $cm^2.S^{-1} \times 10^{-9}$ Mean (± s.e.m)	% Ratio <Deff>/D^o	% Diffusive particles
A	-2.1 (± 0.5)	44.42 (0.04)	101.18	0.87123 (± 0.1223)	0.8611	59
B	-2.2 (± 0.4)	53.39 (0.04)	82.28	0.05135 (± 0.0089)	0.0624	35
C	-0.8 (± 0.9)	36.91 (0.05)	122.12	0.01318 (± 0.0003)	0.0108	16
NAC	-7.1 (± 0.2)	43.89 (0.23)	102.41	0.24624 (± 0.0376)	0.2405	40

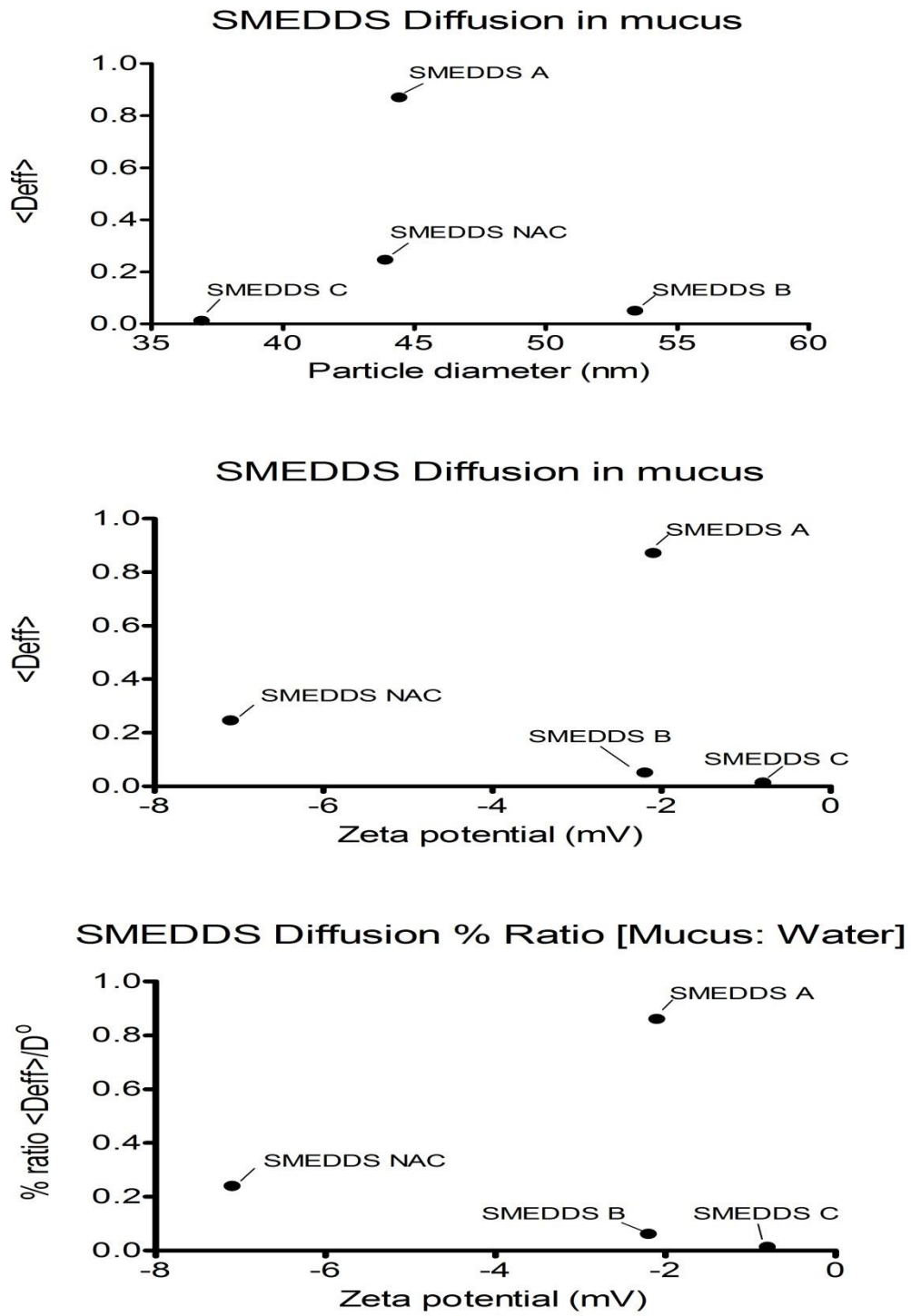

Figure C.1: Correlation of particle size and surface charge of various SMEDDS to their mucus diffusion. (A) Correlation of particle size of various SMEDDS versus <Deff>. (B) Correlation of zeta potential of various SMEDDS versus <Deff>. (c) Correlation of zeta potential of various SMEDDS versus the % ratio of <Deff>/D°. Particle size of NPs is expressed in nm, Zeta potential is expressed in mV and Deff is measured in cm^2. $s^{-1} * 10^9$.

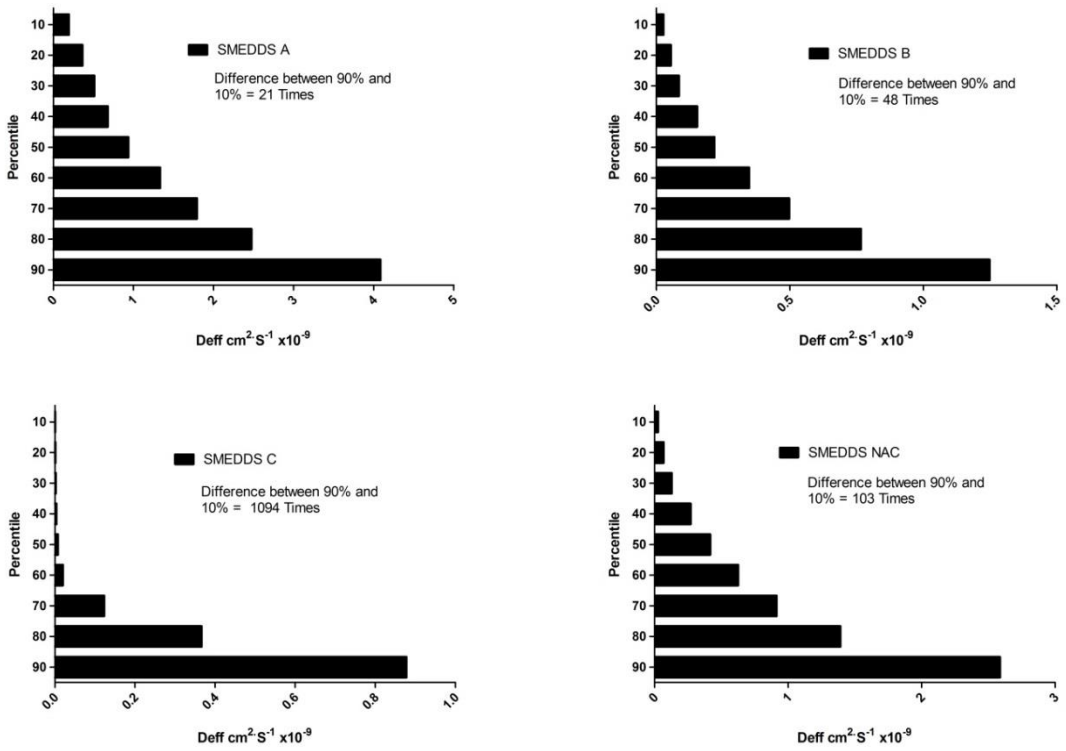

Figure C.2: Comparison of average Deff of SMEDDS A, SMEDDS B, SMEDDS C and SMEDDS NAC at a time scale of 1 sec in mucus of subclasses from the fastest to the slowest percentile. Figure presents data of 3 experiments each with n ≥ 120 particles.

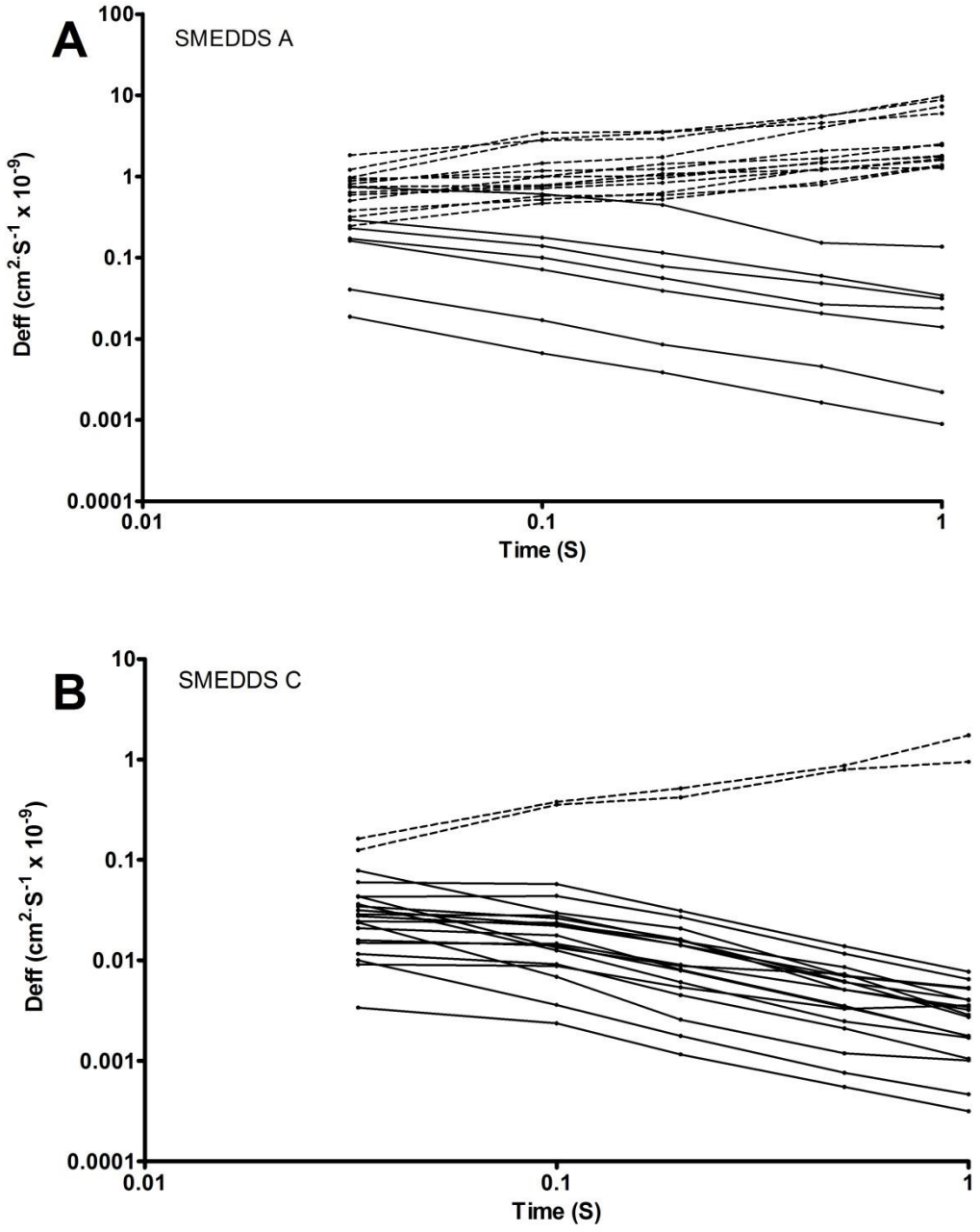

Figure C.3: Effective diffusivities Deff versus time scale of 20 randomly selected particles selected by (random.org). (A) SMEDDS A: high ratio of particles shows diffusivities. (B) SMEDDS C: Some particles are diffusive vs major restricted particles.

APPENDIX D

KINETIC STUDIES ON THE DIFFUSION OF PEC NPS SYNTHESIZED BY SAGETIS GROUP THROUGH THE NATIVE PIG INTESTINAL MUCUS MODEL

Five PEC NPs were synthesized by Sagetis group to be studied for their kinetics of diffusivity through the native pig intestinal mucus model. PAA and unknown novel peptide agent were used as the source of the positively and negatively charged polymers. Moreover, these PEC NPs were loaded with the mucolytic agent (papaine). These PEC NPs were symbolised as follows: RDPB0, RDPB0.17,RDPB0.33,RDPB0.67,RDPB1.33.

Table D.1: Zeta potential, particle size, Diffusion coefficient in water and mucus, % ratio of <Deff>/D^o and percentage (%) of diffusive particles of various PEC NPs.

RDPB	Zeta potential (mV) Mean (±s.d.)	Particle size (nm) Mean (PDI)	D^o (water) $cm^2.S^{-1}$ x 10^{-9}	<Deff> (mucus) $cm^2.S^{-1}$ x 10^{-9} Mean (±s.e.m)	% Ratio <Deff>/D^o	% Diffusive particles
0	20.2	143	31.4	0.0283 (+0.0081)	0.0900	21
0.17	19.3	134	33.4	0.3281 (±0.0683)	0.9823	61
0.33	19.6	138	32.6	0.0546 (±0.0093)	0.1675	34
0.67	18.1	213	21.1	0.0099 (±0.0024)	0.0471	2
1.33	13.4	368	12.2	0.0145 (±0.0048)	0.1188	24

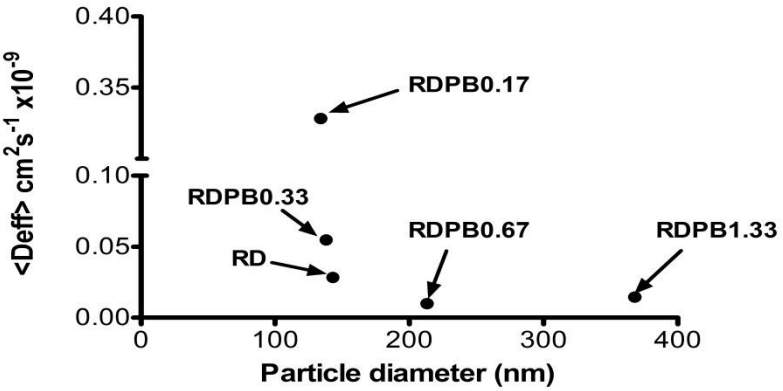

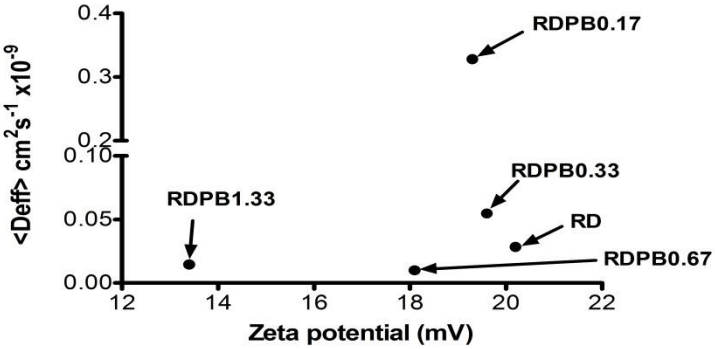

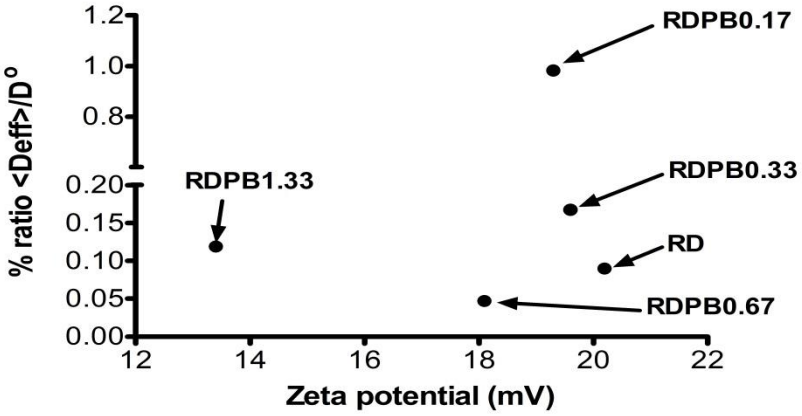

Figure D.1: Correlation of particle size and surface charge of various RDPB to their mucus diffusion. (A) Correlation of particle size of various RDPB versus <Deff>. (B) Correlation of zeta potential of various SMEDDS versus <Deff>. (c) Correlation of zeta potential of various RDPB versus the % ratio of <Deff>/D°. Particle size of NPs is expressed in nm, Zeta potential is expressed in mV and Deff is measured in cm^2. s^{-1} $*10^9$.

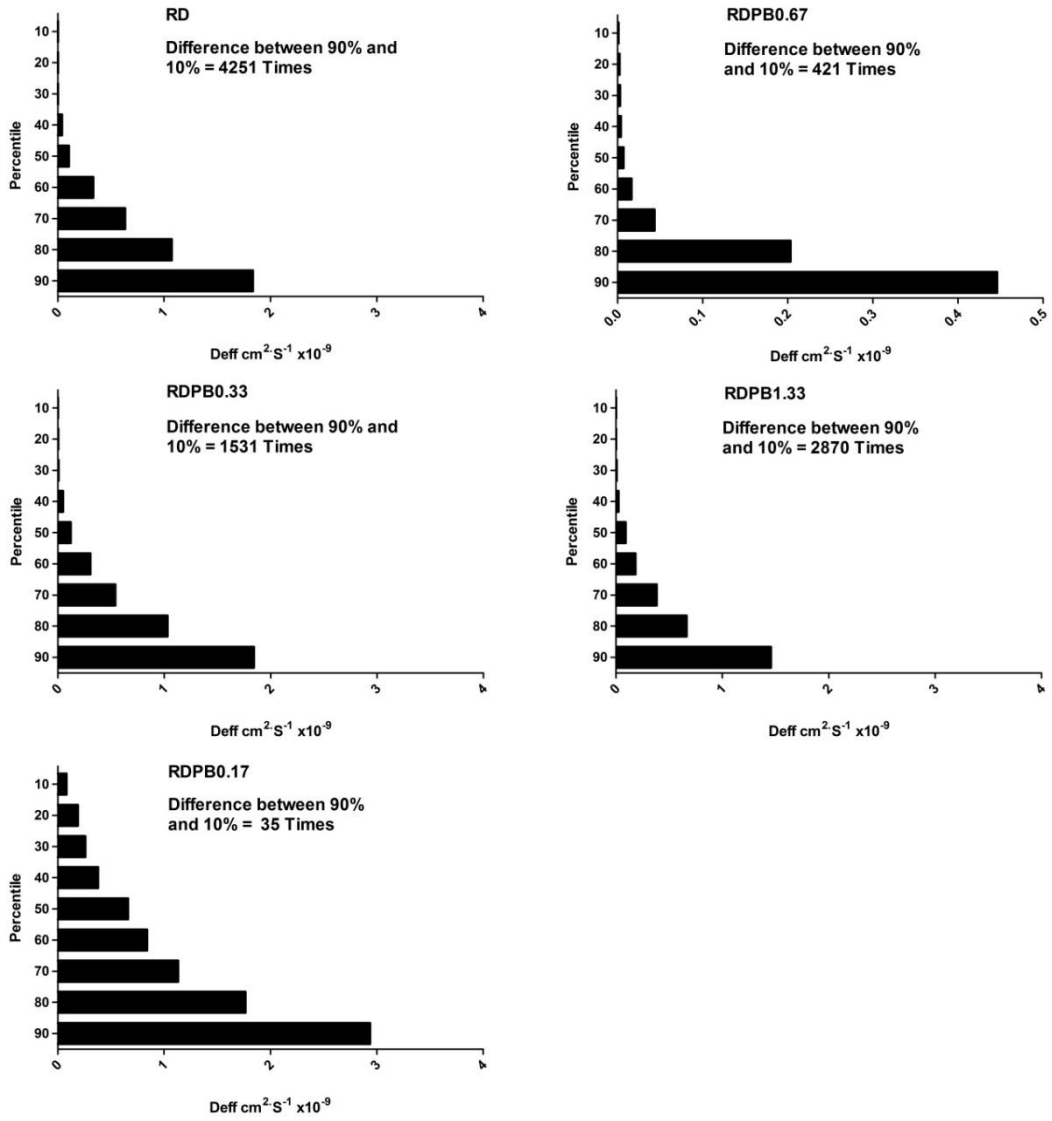

Figure D.2: Comparison of average Deff of RD, RDPB0.17, RDPB0.33, RDPB0.67 and RDPB1.33 at a time scale of 1 sec in mucus of subclasses from the fastest to the slowest percentile. Figure presents data of 3 experiments each with $n \geq 120$ particles.

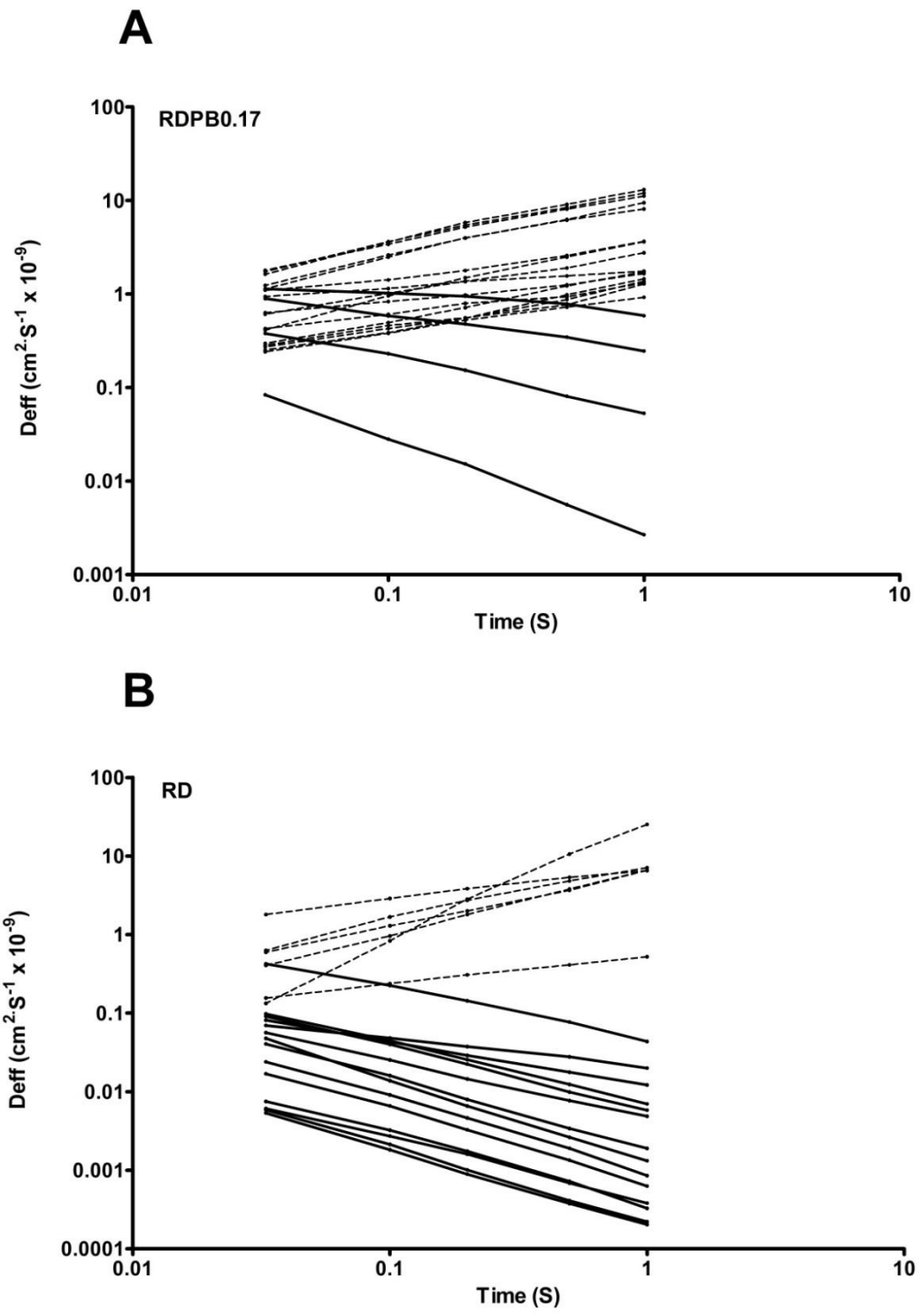

Figure D.3: Effective diffusivities Deff versus time scale of 20 randomly selected particles selected by (random.org). (A) RDPB0.17: high ratio of particles shows diffusivities. (B) RD: Some particles show diffusivity vs major restricted particles.

APPENDIX E

DIFFUSION BEHAVIOUR OF (PAA:CHITOSAN) PEC NPs, PLGA, PEG-PLGA AND AD5 THROUGH THE "CONSORTIUM MUCUS GEL" MODEL (CHAPTER FOUR)

Table E.1: Diffusion coefficient measurements of various polyelectrolyte NPs, PLGA, PEG-PLGA and AD5 in gel-mucus and water obtained by using Epifluorescence microscopy and by Einstein-stokes equation.

Nature of NPs	PAA:Chitosan Mass ratio	Code	Zeta Potential (mV) Mean (± s.d.)	Particle Size (nm) Mean (PDI)	D° (water) $cm^2. S^{-1} x10^{-9}$	<Deff> (mucus) $cm^2. S^{-1} x10^{-9}$ Mean (± s.e.m)		% Ratio <Deff> / D°
Negatively charged Polyelectrolyte	5:1	F1	-29.1 (±3.6)	104 (0.14)	43.21	0.00131	(0.00022)	0.0030
	4:1	F2	-30.6 (±4.4)	149 (0.10)	30.16	0.00211	(0.00038)	0.0070
	3:1	F3	-25.0 (±4.0)	204 (0.21)	22.03	0.00334	(0.00057)	0.0152
	2:1	F4	-18.9 (±1.3)	225 (0.13)	19.97	0.00255	(0.00053)	0.0128
	1:1	F5	-15.4 (±0.8)	357 (0.21)	12.59	0.00198	(0.00033)	0.0157
	1:1*	F6	-15.2 (±1.2)	365 (0.21)	12.31	0.00192	(0.00036)	0.01557
Neutral Polyelectrolyte	1:2.2	F7	-0.5 (±1.9)	1244 (0.32)	3.61	0.00024	(0.00005)	0.0067
	1:2.2*	F8	+1.1 (±2.4)	334 (0.19)	13.46	0.00268	(0.00045)	0.0199
Positively charged Polyelectrolyte	1:3	F9	+6.0 (±1.1)	144 (0.18)	31.21	0.00319	(0.00054)	0.0102
	1:4	F10	+14.3 (±0.3)	104 (0.09)	43.21	0.00154	(0.00027)	0.0036
	1:5	F11	+19.2 (±0.5)	180 (0.17)	24.97	0.00082	(0.00014)	0.0033
	1:6	F12	+19.5 (±0.9)	293 (0.17)	15.34	0.00048	(0.00009)	0.0031
	1:8	F13	+19.2 (±0.6)	359 (0.11)	12.52	0.00041	(0.00007)	0.0033
	1:8*	F14	+19.5 (±2.3)	373 (0.23)	11.92	0.00039	(0.00007)	0.00328
Lipophilic	PLGA	-	-29.2 (±2.1)	161 (0.03)	27.91	0.00021	(0.00005)	0.0008
Hydrophillic	PEG-PLGA	-	-8.3 (±1.2)	54 (0.03)	83.22	0.01396	(0.00425)	0.0168
Capsid Virus	AD5	-	-0.5 (±2.3)	146 (0.18)	30.78	0.00449	(0.00090)	0.01458

* indicates NPs sonicated after fabrication prior to diffusion measurement.

APPENDIX F

^{1}H-NMR SPECTRUM OF THE MONOMERS AND CTA USED TO SYNTHESIZE THE POLYMERS AND CO-POLYMERS IN CHAPTER FIVE (BMA, DMAEMA, 2-CYANO-2-PROPYL DODECYL TRITHIOCARBONATE)

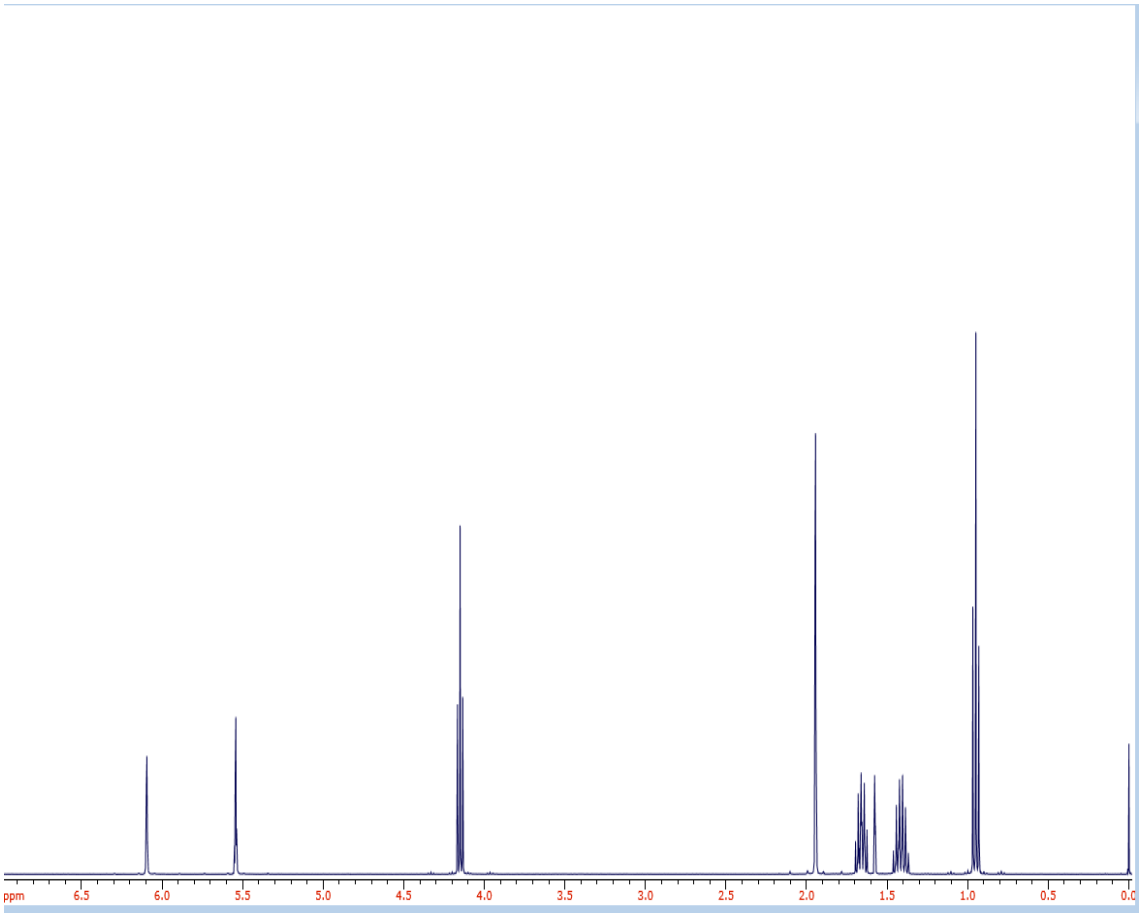

Figure F.1: ^{1}H-NMR spectrum of the BMA monomer (Solvent: CDCL3).

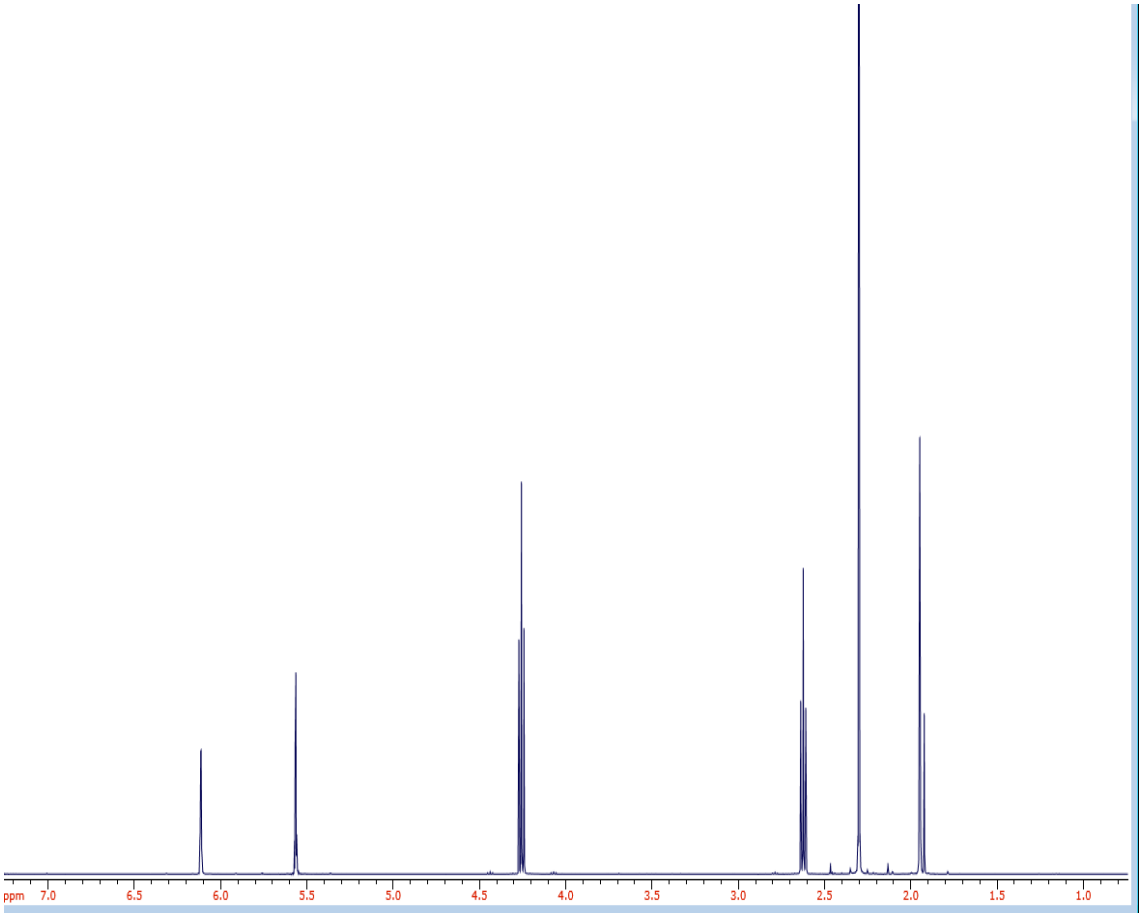

Figure F.2: ^{1}H-NMR spectrum of the DMAEMA monomer (Solvent CDCL3).

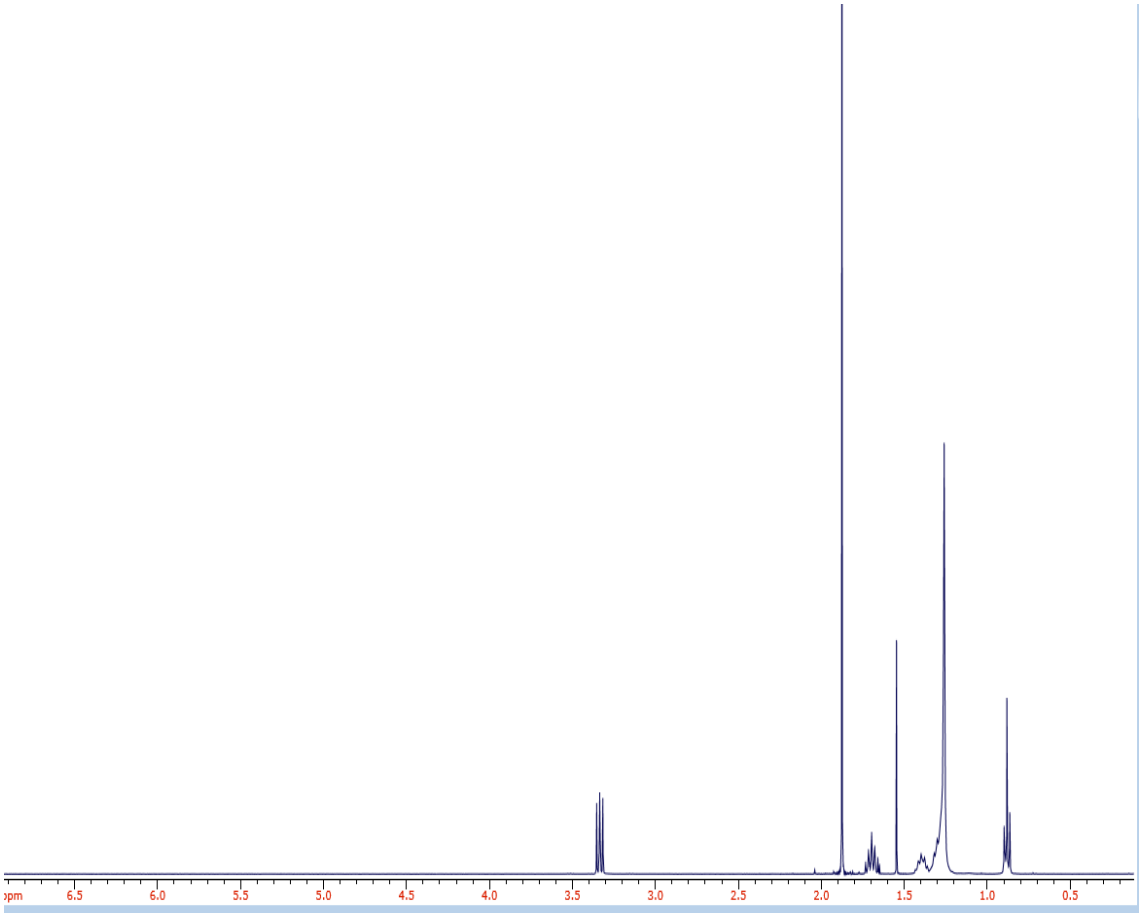

Figure F.3: ^{1}H-NMR spectrum of the 2-Cyano-2-propyl dodecyl trithiocarbonate (Solvent: CDCL3).